Nºd`ordre: 3854

THÈSE

Manuscrit provisoire

L'UNIVERSITÉ BORDEAUX-1

ÉCOLE DOCTORALE DES SCIENCES CHIMIQUES

Par **MUHAMMAD MUMTAZ**

Pour obtenir le grade de

DOCTEUR

SPÉCIALITÉ **: POLYMÈRE**

****

SYNTHESIS OF POLY(3,4-ETHYLENEDIOXYTHIOPHENE), POLYANILINE AND THEIR METAL-COMPOSITE NANO-OBJECTS BY DISPERSION POLYMERIZATION

****

Date de soutenance: 26 octobre 2009

Jury :

M. Claude CHEVROT, Professeur, Université de Cergy-Pontoise	*Rapporteur*
M. David MECERREYES, Research Head, CIDETEC, Espagne	*Rapporteur*
M. Jaroslav STEJSKAL, Professeur, IMC, Czech Republic	*Examinateur*
M. Georges HADZIIOANNOU, Professeur, Université Bordeaux 1	*Examinateur*
M. Henry CRAMAIL, Professeur, Université Bordeaux 1	*Directeur de thèse*
M. Eric CLOUTET, Chargé de Recherche, CNRS, LCPO	*Invité*

PUBLICATIONS

- **M. Mumtaz, C. Labrugere, E. Cloutet, H. Cramail, *"Water-borne dispersions of PEDOT using PNVP-based reactive stabilizers"*** *Macromolecules* (submitted)

- **M. Mumtaz, C. Labrugere, E. Cloutet, H. Cramail, *"Synthesis of PEDOT- and PANI-metal composites particles in aqueous dispersion media"*** *Chemistry of Materials* (submitted)

- **M. Mumtaz, C. Labrugere, E. Cloutet, H. Cramail, *"Synthesis of polyaniline nano-objects using poly(vinyl alcohol), poly(ethylene oxide), and poly[(N-vinyl pyrrolidone)-co-(vinyl alcohol)] based reactive Stabilizers"*** *Langmuir*, **2009** (accepted)

- **E. Cloutet, M. Mumtaz, H. Cramail**, ***Synthesis of PEDOT latexes by dispersion polymerization in aqueous media.*** *Materials Science & Engineering, C: Materials for Biological Applications* **2009**), 29, 377-382

- **M. Mumtaz, E. Ibarboure, C. Labrugere, E. Cloutet, H. Cramail**, ***"Synthesis of PEDOT Nano-objects Using Poly(vinyl alcohol)-Based Reactive Stabilizers in Aqueous Dispersion"*** *Macromolecules*, **2008**, 41, 8964-8970

- **M. Mumtaz, S. Lecommandoux, E. Cloutet, H. Cramail, *"Synthesis of Calibrated Poly(3,4-ethylenedioxythiophene) Latexes in Aqueous Dispersant Media"*** *Langmuir*, **2008**, 24, 11911-11920.

- **M. Mumtaz; A. de Cuendias,; J.-L. Putaux,; Cloutet, Eric; H. Cramail, *"Synthesis of PEDOT nanoparticles and vesicles by dispersion polymerization in alcoholic media"*** *Macromolecular Rapid Communications.* ***2006****, 27, 1446-1453.*

CONFERENCES

- **M. Mumtaz, E. Cloutet, H. Cramail, *"Synthesis of PEDOT nano-objects by dispersion polymerization in aqueous media (poster)"*** *International conference ELECMOL'08, December 8–12,* ***2008*** *(Grenoble – HMMNT/Minatec, France)*

- **M. Mumtaz, E. Cloutet, H. Cramail, *"Synthesis of π-congugated polylers latexes (poster)"*** *The 1st Aquitaine Conference on Polymers, October 16-19,* ***2007****,(Arcachon, France)*

Acknowledgements

Firstly, I would like to thank Prof. Yves GANANOU and Prof. Henri CRAMAIL to allow me to work as a PhD student in LCPO. I am really grateful to Prof. Henri CRAMAIL and Dr. Eric CLOUTET for giving me the chance to do my PhD under their very watchful eye and very kind supervision in LCPO. They always encouraged me and gave lot of suggestions whenever I presented my before them. They were very helpful and gave me lot of freedom while doing my research work and helped me whenever it was needed. They gave me a plenty of their precious time for discussions during research, writing publications and thesis.

I am indeed thankful to my other colleagues in LCPO particularly Rachid MATMOUR, Anne de CUENDIAS, Cécile BOUILHAC for their initial support to handle the instruments etc at the beginning of my PhD work. I would like to thankful to my collaborators without whom my research would have been considerably more difficult: Christine Labrugere for XPS analysis discussions about them; Emmanuel IBARBOURE, Jean-Luc PUTAUX and Sabrina LACOMME for their help in AFM and TEM analysis respectively; Sebastian LECOMMANOUX for SANS and important discussions about DLS results and Nicolas GUIDOLIN for teaching how to use DLS and GPC instruments.

I am grateful to Catherine ROULINAT, Corine GONCALVES de CARVALHO, Bernadette GUILLABERT and Nicole GABRIEL for their help in administrative works. I cannot forget their ever smiling faces. They treat me like their family member whenever I visited them and feel them like my mother.

Without a doubt, the best part of my D.Phil was being able to spend my days working alongside, so many great people like Rachid MATMOUR (Expert in anionic polymerization); Anne de CUENDIAS (Conducting polymers); Yougang LI and Suresh Kumar (Expert in RAFT and ATRP and I never forget the time when we use to go to have a cup of coffee every afternoon) etc.

I am equally thankful to all members of LCPO for their lot of help and moral support.

I really grateful to the Pakistani student community in Bordeaux with home I passed excellent time during my PhD studies. I cannot forget the time we passed together during trips, dinner and lunch parties, EID celebrations and other occasions. I am also thankful for their services and contribution for preparing some delicious Pakistani food on the day of my thesis defense

Finally, of course, thanks to my mother, father, wife (Misbah Batool), sister, brothers and friends for lot of their moral supports and prayers.

Dedications

I feel pleasure to dedicate this thesis to my dear and sweet parents and wife as without their help, moral support and prayers it was not possible to achieve this goal.

Muhammad Mumtaz

List of abbreviations

AFM : Atomic Force Microscopy

$AlCl_3$: Aluminum chloride

AIBN : Azo bis-isobutyro Nitrile

AsF_5 : Arsenic pentafluoride

BEDOT : Bis(ethylenedioxythiophene)

Br_2 : Bromine

BF_3 : Boron trifloride

n-BuLi : n-butyl lithium

$CuBr_2$: Copper(II) bromide

$CuCl_2$: Copper(II) chloride

CB : Conduction Band

CMRP : Cobalt Mediated controlled Radical Polymerization

Cu^{2+} : Cupric ion

DBSA : Dodecylbenzene sulfonic acid

DLVO : Derjaguin and Landau, Verwey and Overbeek

DLS : Dynamic Light Scattering

DMSO : Dimethyl sulfoxide

DMF : *N*,*N'*-dimethylformamide

DMAEMA : 2-(dimethylamino)ethyl methacrylate

DPMK : Diphenyl methyl potassium

DPTS : 4-(dimethylamino)pyridinium 4-toluenesulfonate

$\overline{DP}_n$: Average degree of polymerization

DSC : Differential Scanning Calorimetry

EA : Electronic Affinity

EAP : Electrically Active Polymer

EDOT : ethylenedioxythiophene

EHEC : Ethylhydroxycellulose

Fe^{2+}: Ferrous ion

Fe^{3+} : Ferric ion

$FeCl_3$: Ferric chloride

$Fe(OTs)_3$: Iron (*p*-toluenesulfonate)

GPC : Gel Permeation Chromatography

HBr : Hydrobromic acid

HCSA : Camphorsulfonic acid

HFIP : 1,1,1,3,3,3-hexafluoro-2-propanol

H_2O_2 : Hydrogen peroxide

H_2SO_4 : Sulfuric acid

HOMO : Highest Occupied Molecular Orbital

HCl : Hydrochloric acid

I_2 : Iodine

IR : Infra Red

IP : Ionization potential

ITO : Indium tin oxide

$KMnO_4$: Potassium permanganate

LUMO : Lowest Unoccupied Molecular Orbital

$\overline{M}_n$ **:** Number average molecular weight

$\overline{M}_w$ **:** Mass average molecular weight

NMP : *N*-methyl pyrrolidone

$(NH_4)_2S_2O_8$: Ammonium persulfate

OCPs : Organic Conducting Polymers

OEGMA : Oligo(ethylene oxide) methacrylate

PAA : Poly(acrylic acid)

PEO : Poly(ethylene oxide)

PNVP : Poly(*N*-vinylpyrrolidone)

PS : Polystyrene

PPP : Poly(*para*-phenylene)

PT : Polythiophene

PPy : Polypyrrole

PU : Polyurethane

PANI : Polyaniline

PEDOT : Poly(3,4-ethylenedioxythiophene)

PIL : Polymeric Ionic Liquid

PPV : Poly(*p*-phenylenevinylene)

PLED : Polymer Light Emitting Diode

PSS : Poly(styrenesulfonate)

PTEB : poly[2-(3thienyl)-ethoxy-4-butylsulfonate]

PTSA : *p*-toluenesulfonic acid

PVA : Poly(vinyl alcohol)

PVA-*mod*-Py : Py-*modified*-poly(vinyl alcohol)

PVME : Poly(vinyl methyl ether)

PNVP-*b*-PVA-*mod*-Py : Pyrrole-*modified*-poly[(N-vinylpyrrolidone)-*block*-(vinyl alcohol)]

PNVP-*co*-PVA-*mod*-Py : Pyrrole-*modified*-poly[(N-vinylpyrrolidone)-*co*-(vinyl alcohol)]

SDS : Sodium dodecylsulfonate

SEM : Scanning Electron Microscopy

$SnCl_4$: Tin tetrachloride

$SbCl_5$: Antimony pentachloride

T : Temperature

TGA : Thermo Gravimetric Analysis

THF: Tetrahydrofuran

TEM : Transmission Electron Microscopy

$TiCl_4$: Titanium tetrachloride

UV : Ultra Violet

UPS : UV Photoelectron Spectroscopy

VB : Valence Band

V-70 : 2,2´-azobis(4-methoxy-2,4-dimethylvaleronitrile)

XANES : X-ray Near Edge structure Spectroscopy

XPS : X-ray Photoelectron Spectroscopy

Table of contents

Chapter II: Synthesis of PEDOT nano-objects using poly(ethyleneoxide) based reactive stabilizers

Chapter III: Synthesis of PEDOT nano-objects using poly(vinyl alcohol), poly(N-vinylpyrrolidone)-b-poly(vinyl alcohol) and poly(N-vinylpyrrolidone)-co-poly(vinyl alcohol) based reactive stabilizers

Chapter IV: Synthesis of Polyaniline nano-objects using PVA, PEO, and PNVP-co-PVA based reactive Stabilizers

General Introduction

As is well-known, most organic polymers are electrically insulating. Since the first discovery in 1977, that chemical doping with iodine converts electrically insulating polyacetylene into a highly conducting material with a conductivity those to that of metals, conducting polymers have been a hot research area for many academic institutions. The impact of the field was recognized in 2000 by the awarding of the Nobel Prize in chemistry to three discoverers of conducting polymers: MacDiarmid, Heeger and Shirakawa. Electron-conducting polymers are able to transfer electrical charges to the same extent as an electrical conductor or semiconductor. Early versions of conducting polymers, mostly based on oxidatively doped polyacetylenes (PAcs), faced intrinsic obstacles that prevented their industrial commercialization. The material degrade readily in air, and no good methods are available for making easily processable PAc polymers. These obstacles led to the investigation of various polymer backbone structures in the search for stable, processable, high-conductivity conjugated polymers. Over the years, several promising polymers have emerged as potential alternatives to PAc for commercial applications, such as polypyrroles, polyanilines and polythiophenes. One main criteria required for most applications is not only a metal-like electrical property, but the combination of electrical conductivity and polymeric properties such as flexibility, low density, and ease of structural modification that suffice for many commercial applications.

Due to their molecular characteristics, the majority of these materials are infusible and practically insoluble in common organic solvents. This lack of solubility was, for a long time, an important drawback impeding a precise characterization of these polymers and the

establishment of their structure-properties relationship. In order to overcome this drawback, many research groups enhanced the solubility of conjugated polymers by introducing flexible side chains such as alkyl groups and poly(ethylene oxide) (PEO) onto the polymer backbone. Another strategy is based on the preparation of blends with insulator polymers bearing polar functions such as quaternary sulfonate or ammonium salts; PEDOT/PSS being one important example for solar cell applications. Blends and composites of polymers offer certain combinations of desired properties that cannot be obtained from the individual components.

Another route to ease the processability of conjugated polymers is to synthesize them under the form of colloidal particles in aqueous media which is the main subject of this Ph.D. In this research work, poly(3,4-ethylenedioxythiophene) (PEDOT), polyaniline (PANI) and polypyrrole (PPy) were chosen due to their high stability and interesting optical and electrical properties. These conducting polymers have potential applications in the field of organic light emitting devices, anti-static coating, rechargeable batteries, super capacitors etc. The dispersion polymerizations of EDOT, aniline and pyrrole were performed in the presence of specific reactive stabilizers to prevent the bulk precipitation of the conducting polymer chains and keep them in the form of stable latex particles. One main objective of this work is thus to control the morphology of the conducting polymer obtained under the shape of core-shell nano-objects (particles, rods, vesicles, etc.).

The first chapter of this manuscript reviews literature data concerning the principal families of conducting polymers, their electronic structure and the mechanism of electrical conduction. Different routes for the synthesis of PPy, PANI and PEDOT, their structures as well as their stability are specifically discussed. In a second part of this chapter, the main methods for the synthesis of polymer colloids and the mechanism of their stabilization are described. Data dealing with the synthesis of conducting polymer colloids are finally presented.

The second chapter of the manuscript describes the EDOT dispersion polymerization in the presence of monofunctional α-ended PEO reactive stabilizer in methanol/water mixtures. Ammonium persulfate or iron *p*-toluenesulfonate hexahydrate have been used as oxidants. The effect of PEO end group (EDOT, pyrrole, thiophene and fluorene) on the formation of PEDOT nano-objects and the control of their size and morphology has been investigated.

In order to see the effect of multiple reactive sites along the stabilizer chains, dispersion polymerization of EDOT was then performed in the presence of pyrrole modified poly(vinyl alcohol) (PVA-*mod*-Py) as reactive stabilizers having pyrrole moieties functionalized along the polymer backbone. In the first part of the third chapter, the effect of substitution degree and molecular weight of the stabilizers on the formation and morphology of PEDOT particles is discussed. In a second part, the dispersion polymerization of EDOT was performed in the presence of pyrrole modified poly(*N*-vinylpyrrolidone-*co*-vinyl alcohol) (PNVP-*co*-PVA-*mod*-Py) and PNVP-*b*-PVA-*mod*-Py used as reactive stabilizers, with similar objectives as previous experiments. Indeed, the objective of the use of PNVP-based reactive stabilizers was to increase the PEDOT conductivity and ease the film forming properties.

With the goal to extend this methodology to other conducting polymers, the dispersion polymerizations of aniline in the presence of α,ω-aniline-poly(ethylene oxide) (α,ω-An-PEO), PVA-*mod*-An and the above mentioned described reactive stabilizers were performed in aqueous media. The fourth chapter thus describes the effects of the nature, molecular weight, concentration and number of reactive moieties of the reactive stabilizer on the size, morphology and conductivity of the PANI nano-objects formed.

Finally, in order to improve the conductivity and opto-electronic properties of the conductive polymer particles, the synthesis of PEDOT- and PANI-metal nanocomposites using the corresponding metal salts as co-oxidants has been also performed by dispersion techniques. The effects of several parameters such as the addition time of the co-oxidant, the nature of the stabilizer on final nanocomposites morphology have been studied and is discussed in a fifth chapter.

Finally, all the experimental methods for the synthesis and characterization of the various reactive stabilizers and conductive polymer are described in a last chapter.

Chapter I

Literature Review

Table of contents

I. Semiconductor conjugated polymers

I.1. Characteristics of Conjugated polymers

I.1.1. Main families of conjugated polymers

A polymeric material that possesses the electronic, magnetic, electrical and optical properties of a metal while retaining the processibility and mechanical properties usually associated with a conventional organic polymer is called a conducting polymer. Since, the discovery by MacDiarmid and co-workers in 1977 [1] that polyacetylene can gain conductivity of metal by doping with either Br_2, I_2, or AsF_5, conducting polymers have been a hot research area for many academic institutions. Following these observations, many aromatic conjugated polymers were studied such as poly(*para*-phenylene) (PPP),[2] polythiophene (PT),[3] polypyrrole (PPy),[4] polyaniline (PANI),[5,6] etc. (Figure I.1). This research has supported the industrial development of conducting polymer products and provided the fundamental understanding of the chemistry, physics and materials science of these materials. The impact of the field was recognized in 2000 by the awarding of the Nobel Prize of chemistry to three discoverers of conducting polymers: MacDiarmid, Heeger and Shirakawa. Currently, many conjugated polymers resulting from these parental structures have been synthesized, such as poly(3,4-ethylenedioxythiophene)[7-10] (PEDOT) marketed by the Bayer company since the 80s. This polymer shows a high conductivity (300 S/cm), a quasi-transparency in the form of film and a very high stability in oxidized state.[8-11] It is characterized by a dark blue colour in a neutral state and a sky blue colour in an oxidized state, which make it an excellent material for electro-chromic devices. Another capital development in the search of conjugated polymers was the discovery in 1990, by Friend and co-workers, of the electroluminescence properties of poly(*p*-phenylenevinylene) (PPV) at the undoped state.[12] The electroluminescent diodes carried out from this polymer, present an emission in the green. This breakthrough was followed in 1991, by the manufacture of the first blue PLED, made up of poly(9,9'-di-*n*-hexylfluorene).[13]

The synthesis of polyacetylene, achieved by passing acetylene vapour over toluene or *n*-hexadecane containing a soluble Ziegla-Natta catalyst, requires the rigorous exclusion of oxygen and moisture.[14] Moreover, the as-made polymer rapidly oxidises in air, whilst the conductivity of iodine-doped polyacetylene decreased to half its initial value in little over a day under ambient conditions.[15] In stark contrast, polypyrrole and polyaniline can be

synthesised electrochemically in air to form free-standing films[16,17,18] or chemically in aqueous solution using oxidants such as $FeCl_3$ and $(NH_4)_2S_2O_8$ to form bulk powders.[19,20,21]

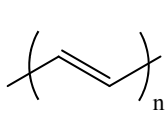

trans-polyacetylene

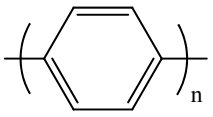

poly(*p ara*-phenylene)

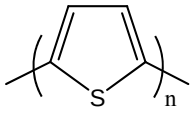

polythiophene

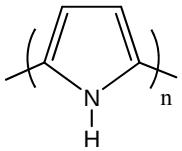

polypyrrole

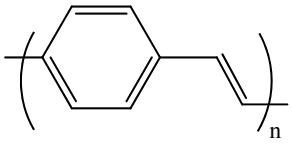

poly(*p*-phenylenevinylene)

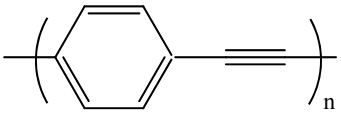

poly(*p*-phenylene ethynylene)

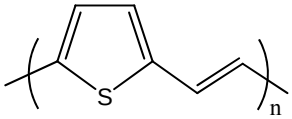

poly(thienylenevinylene)

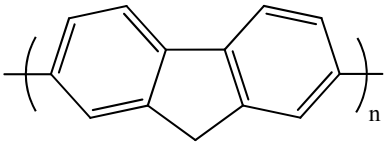

polyfluorene

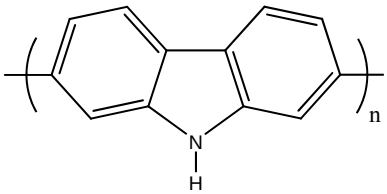

polycarbazole

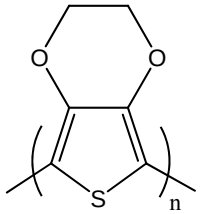

poly(3,4-ethylenedioxythiophene)

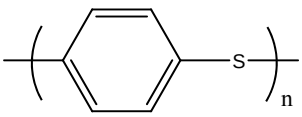

poly(phenylenesulfide)

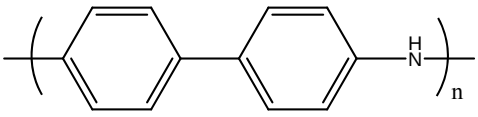

poly(diphenylamine)

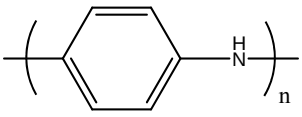

polyaniline

Figure I.1: Chemical Structures of principal families of conjugated polymers.

Moreover, both polyaniline and polypyrrole possess relatively high conductivities and exhibit reasonable air stability (see Sections I.2 and I.3). Hence in recent years, research has focused less on polyacetylene and more on these latter organic conducting polymers (OCPs), as well as more recently, synthesised electroactive polymers such poly(3,4-ethylenedioxythiophene), which offer enhanced stability (see Section I.4).

I.1.2 Electronic Structure of Conjugated polymers

The majority of conjugated polymers consist of a regular alternating single and double bonds which permit the delocalization of the electrons along the polymer skeleton. The recovery of π orbital leading to the electronic delocalization is influenced by the geometry of the system. This recovery is maximum when π-conjugated system is planar and any deviation from planarity resulted in a reduction of conjugation. The electronic structure of these systems depends on their different levels of molecular orbitals and particularly the value of their HOMO and LUMO. The HOMO (Highest Occupied Molecular Orbital) represents together the highest occupied energy levels and the LUMO (lowest unoccupied Molecular Orbital) represents the lowest unoccupied energy levels. This energy difference corresponds to a π - π* transition in simple molecules and band gap in the polymers. The HOMO and LUMO levels of a conjugated polymer depend on the degree of conjugation, i. e. the number of monomer units (Figure I.2). When the number of repetitive units becomes very high, it passes

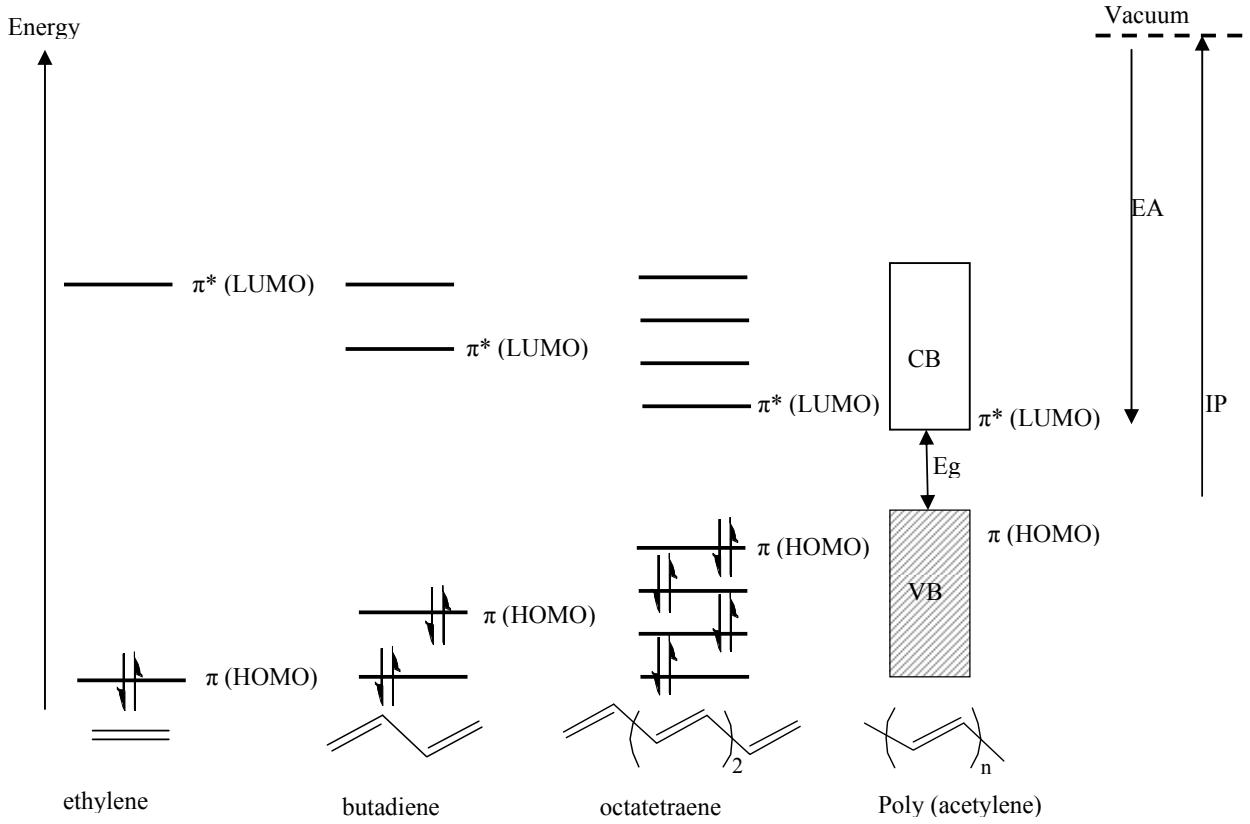

Figure I.2: Diagrams of the molecular orbitals (π levels) as a function of the number of monomer units.

a series of discrete levels to a situation where the energy levels are grouped into two bands, the valence band (VB) and the conduction band (CB). All HOMO group together form the VB

and all LUMO combine to form the conduction bond (CB), the energy difference between these two levels is called band gap or forbidden band. It is characterized by its value Eg (energy gap) which determines the opto-electronic properties of conjugated polymers. It can be determined for a neutral species from the onset of absorption in the solid-state (film) UV–vis spectrum. This "gap" can also be described as the difference between the ionization potential (IP: energy required to transfer an electron from the highest state HOMO) and the electronic affinity (EA: energy required for the injection of an electron in the lowest state LUMO).

According to this model, it is thus possible to highlight the electronic structure of a material and hence, to make a qualitative distinction between insulators and semiconductors.

- The intrinsic semiconductors have a forbidden band ranging between 0 and approximately 2 to 3 eV. When the charge carriers are not subjected to thermal (T = 0°C), optical or electrical excitation, their valence band is completely filled and their conduction band is empty.

- The insulators have a similar structure of bands as that of the semiconductors but the band gap is too high (higher than 4 eV) to allow the passage of one electron from the valence band to the conduction band. The majority of conjugated polymers are at the border between insulators and semiconductors (Table I.1).

Conjugated polymers	Forbidden Band (eV)
trans-polyacetylene (PA)	1,4-1,5[22,23]
polythiophene (PT)	2,0-2,1[24,25]
poly(*p*-phenylene) (PPP)	2,7[26]
poly(*p*-phenylenevinylene) (PPV)	2,5[27]
polypyrrole (PPy)	3,2[28]
poly(3,4-ethylenedioxythiophene) (PEDOT)	1,6[29,30]

Table I.1: Band gap values of certain conjugated polymers

The conjugated nature of neutral conducting polymers allows them to have two electronically extreme states;

i) which are equivalent in thermodynamic stability point of view and called as a system with degenerated ground state structure. It is the case of the trans-polycetylene (Figure I-3). It is the only existing conducting polymer which has degenerated resonance state.

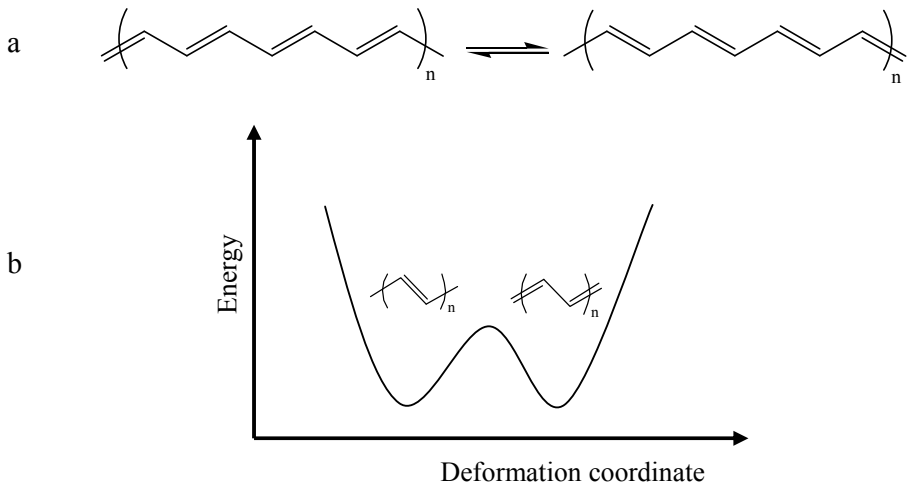

Figure I-3: (a) mesomeric forms of trans-polyacetylene and (b) Sketch of the potential energy curve for polyacetylene showing two energetically equivalent structures (degenerated ground state)

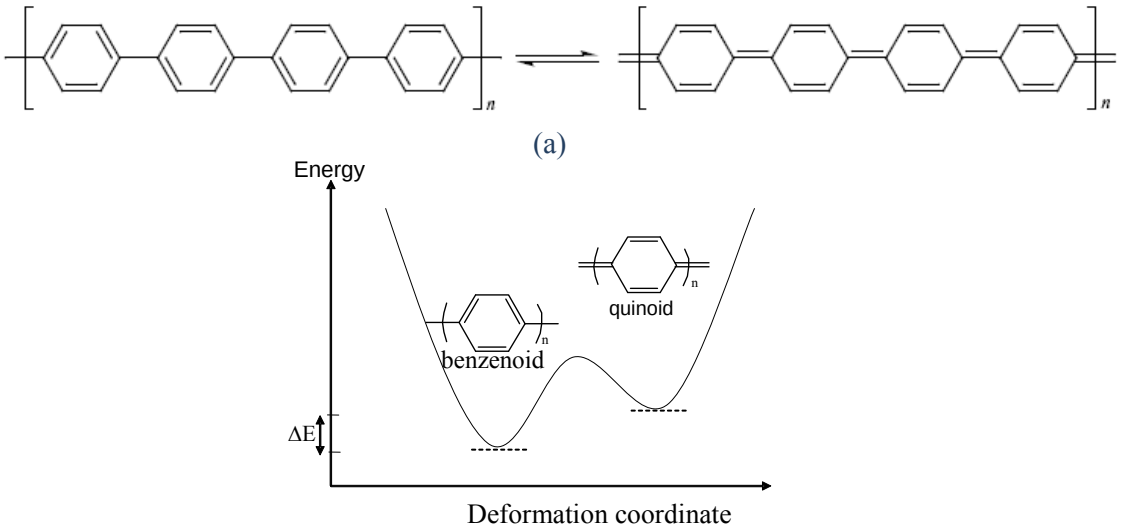

Figure I-4: (a) mesomeric forms of poly (p-phenylene) and (b) Sketch of the potential energy curve for poly (p-phenylene) showing inequivalent structures ((nondegenerated ground state)

ii) the energy difference exits between two resonance forms and is called as a system with non degenerated ground state structure. The majority of the conjugated polymers present two resonance forms; benzenoid and quinoid forms, which are not energetically equivalent, the quinoid structure being substantially higher in energy (Figure I-4).

I.1.3. Doping of conducting polymers

To combine the mechanical properties of polymers to the conducting properties of metals, one can introduce a load into the structure of semiconductor polymer by a process known as doping. This process consists of oxidation-reduction reaction in which the introduction of donor (doping of the type n) or acceptor impurities (doping of the type p) into the material is mainly carried out by chemical or electrochemical ways. It is however important to note that contrary to conducting polymers, the semiconductors do not always present a reversible and easily controllable doping. In the case of a chemical doping for example, of the type p (or type n), the neutral conjugated polymer is transformed into a poly(cation) (or poly(anion)) by action of an oxidant (or reducing agent). In same time, a counter-ion is associated to it in order to maintain the overall electro-neutrality of the system, as illustrated in the following examples.

- p-type doping:

$$(\pi\text{-polymer})_n + 3/2\ ny(I_2) \rightarrow [(\pi\text{-polymer})^{+y}\,(I_3^-)_y]_n \qquad \textbf{Eq. I.1}$$

- n-type doping

$$(\pi\text{-polymer})_n + [Na^+(C_{10}H_8)^{-\bullet}]_y \rightarrow [(Na^+)_y\,(\pi\text{-polymer})^{-y}]_n + (C_{10}H_8)^0 \qquad \textbf{Eq. I.2}$$

The introduction of charges during the process of doping modifies the alternation of single and double bonds locally, thus positioning the charge carriers on the chain. In the forbidden band, new localised electronic states with holes (radical cations) or electrons appears. The quasi-particles thus formed can be classified in two categories according to whether the fundamental state of the polymeric chain is degenerated or not.

Soliton is a term used by physicists in various connections. From chemist's point of view, a soliton is positive, negative or neutral radical-like site and corresponds to conformational "kink" in the simple conjugated system of polyacetylene separating two "semi-infinite" conjugated chains. The soliton is mobile in the chain and is thought to be the charge carrier in polyacetylene. (Figure I-5)

As a result of the degenerated ground states of *trans*-polyacetylene, charges formed during doping readily separate (because there is no increase in distortion energy). The charge carrier, called a soliton, is relatively stable as a result of the degeneracy and the energy required creating and moving such a defect is relatively small. Calculations suggest that solitons are delocalized over 15 carbon atoms.[31]

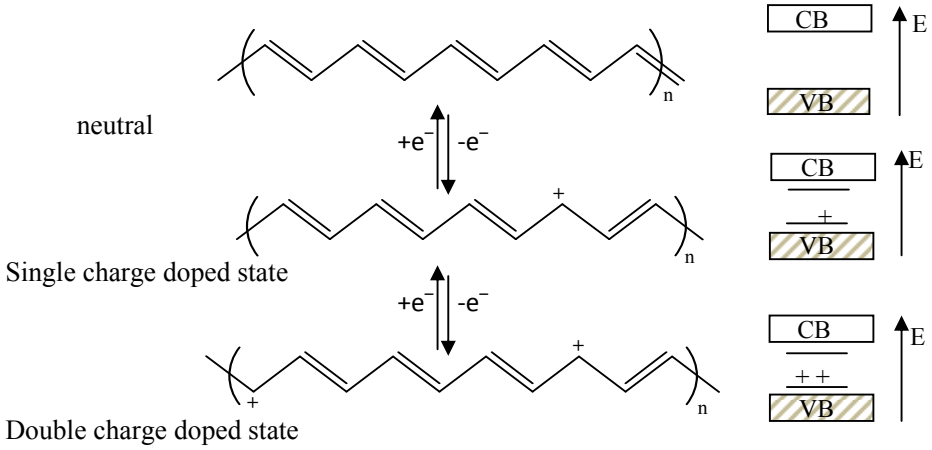

Figure I-5: Doping of polyacetylene

Polarons and **Bipolarons**. By polaron in connection with conducting polymers, we mean radical ion (positive or negative) introduced by oxidizing or reducing a conducting polymer molecule. The charge accompanied by bond distortion is mobile not only along the polymer chain but also in neighboring chain by the hopping mechanism. Hence these radical ions deserve recognition as an independent species. Polaron are supposed to be present in conjugated polymers having generally ring structures as monomer moieties, e.g., in polythiophene (Figure I-6.). Removal (or introducing) of second electron from (or inside)

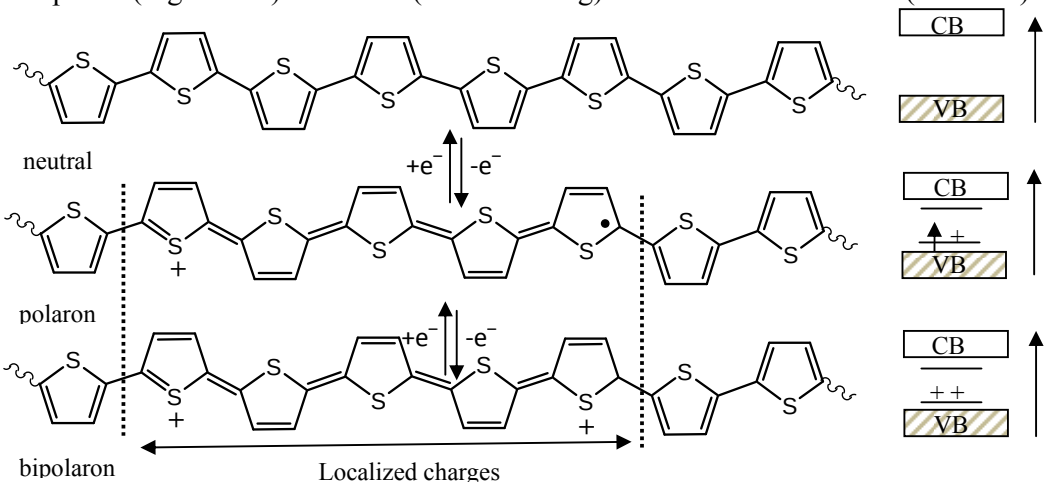

Figure I-6: p-doping of polythiophene

conjugated polymer gives a dicationic (or anionic) species with no unpaired electrons, called a **bipolaron**. Bipolaron can also be formed by the dimerization of two polarons due to their radical nature. The two ions in a bipolaron need to be isolated from each other to minimize unfavorable interactions; recent work suggests that at least five rings are needed to stabilize a dicationic species.[32,33] The conversion between neutral, polaronic, and bipolaronic species is reversible, using either chemical or electrochemical means to oxidize or reduce the polymer. PANI and other conjugated polymers possessing strongly basic functionalities undergo a more complex chemical doping mechanism[34,35] (Figure I-7). While the leucoemeraldine form can undergo oxidative doping, leading to radical cation (polaron) formation, the emeraldine base form of PANI can also undergo protonation by acid–base chemistry to yield the emeraldine salt (bipolaron) form. Internal charge redistribution in the emeraldine salt also yields the polaron form.

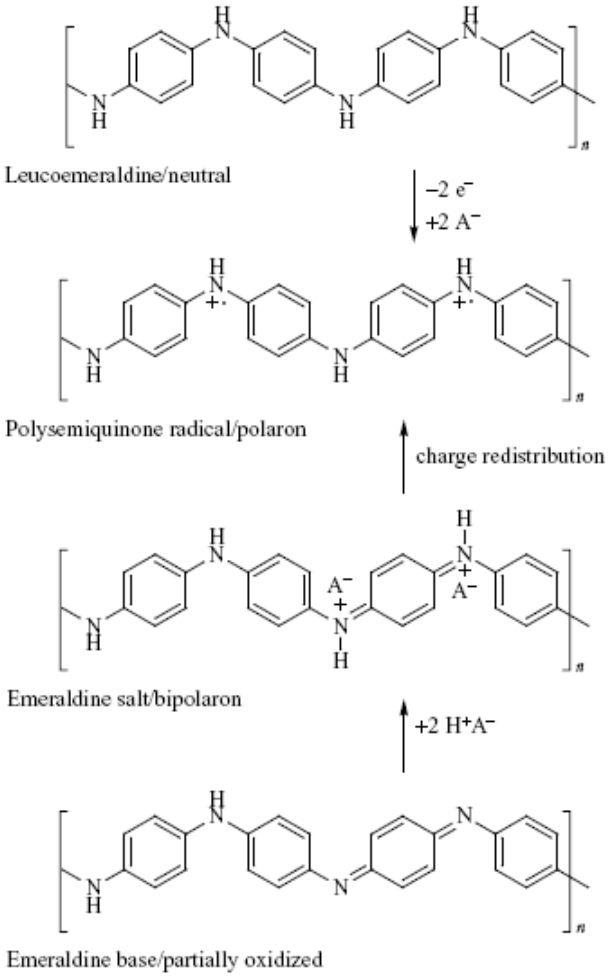

Figure 1.7: Chemical doping of polyaniline.

Finally, the charge carriers allow electronic transport within these materials. With strong rate of doping, there is a collection of the polaronic and/or bipolaronic states, so that the defects charges can move along the polymeric chains.

I.1.4. Electrical Conductivities of Conjugated Polymers

While conductivity in conjugated polymers is typically at least one order of magnitude lower than that of the best metals, the ability to switch conjugated polymers from insulating to conducting and the ease of processability of many conjugated polymers has led to some unique applications.

The electrical conductivity, σ, of a conjugated polymer is equal to the inverse of its specific resistivity, ρ, which is a measure of the ability of the conjugated polymer to conduct an electrical charge. Electrical conductivity is determined by measuring the resistance, R, to charge transport through a known volume, where L is the length over which resistance is being measured and A is the cross-sectional area through which the current passes:

$$\sigma = 1/\rho = L/(R \cdot A) \qquad \textbf{Eq. I.3}$$

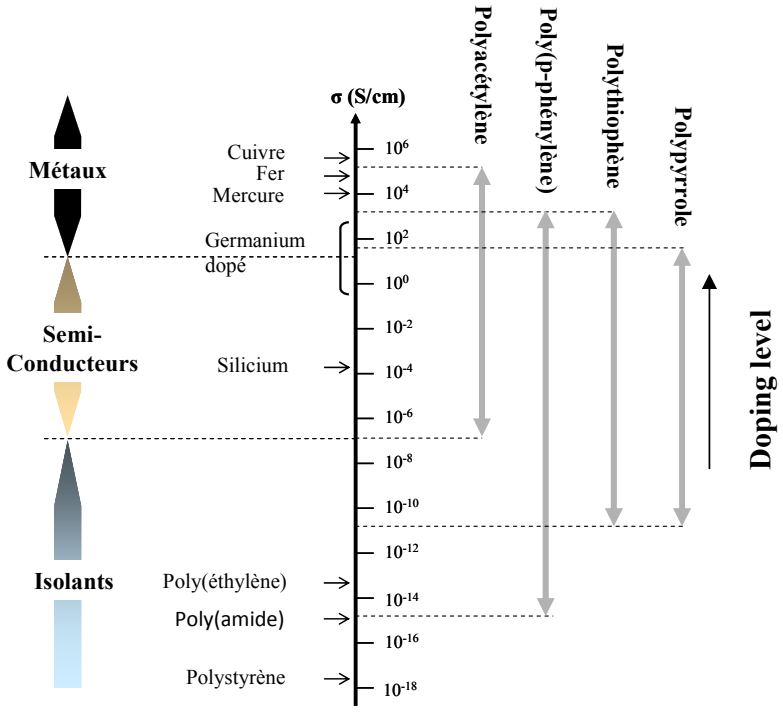

Figure I.8: Electronic conductivity of conjugated polymers with different degrees of doping

Typically, electrical conductivity of conjugated polymers is measured in units of S/cm. Both two- and four-point probe techniques are used to measure σ in films and pressed pellets[36]. Conductivities as high as 10^5 S/cm have been reported for several conjugated polymers. Values vary depending on synthetic procedures, fabrication techniques, and measurement methods. Conjugated polymers are typically only partially crystalline;[37–39] amorphous conjugated polymers have been also reported.[40–42] Therefore, disorder plays a significant role in their electrical conductivities, and the conductivity arises from the metal–insulator transition.[43] As an example, polyaniline with the highest conductivity reported so far shows temperature dependence of conductivity.[44] Thus, electrical conductivity is limited by the disorder-induced localization of the electrons rather than by the intrinsic conductivity of the delocalized charges on the polymer backbone. Conductivities of principal polymers together in their neutral state and various rates of doping are given in the Figure 1.8 and are compared with those of the reference materials.

From the above discussion it is clear that conducting polymers are alternative source of semiconducting materials which can be used to replace relatively expensive and environmentally dangerous inorganic semiconducting materials. They are excellent candidates for electroluminescent devices, rechargeable batteries, sensors, electrochromic windows, photovoltaic devices, photodiodes etc. due to their interesting opto-electronic properties. Among conducting polymers, polyaniline, polypyrrole and poly(3,4-ethylenedioxythiophene) possess relatively high conductivities and exhibit reasonable air stability (see Sections 1.2-1.4). Hence in recent years research has focused more on these latter OCPs.

I.2 Polypyrrole

Among the conducting polymers, polypyrrole has attracted great attention because of its high electrical conductivity and good environmental stability. The first reported polymerization of pyrrole was in 1916.[45] Polypyrrole was prepared by the chemical oxidation of pyrrole using hydrogen peroxide. An amorphous black powder known as “pyrrole black” was obtained, which was insoluble in common organic solvents. One of the advantages of polypyrrole (PPy) is the low oxidation potential of pyrrole relative to other electrically active polymers (EAP) precursors, facilitating oxidative polymerization.

As mentioned earlier, polypyrrole (PPy) is one of the most studied OCPs due to its ease of synthesis, relatively high conductivity and reasonable environmental stability. Moreover, pyrrole does not present the same toxicity problems as the monomers for other conducting polymers, such as aniline.[46] PPy has been considered as the key material to many potential applications such as electronic devices, electrodes for rechargeable batteries and supercapacitors, solid electrolytes for capacitors, electromagnetic shielding materials, sensors, corrosion protecting materials, actuators, electrochromic devices or membranes. Polypyrrole can be easily synthesized both by electrochemical and chemical oxidative polymerization.

I.2.1 ***Electrochemical Synthesis***

The first electrochemical synthesis of PPy was reported as early as 1968 by Dall'Olio et al., who deposited thin PPy films onto platinum electrodes and reported conductivities as high as 7.5 S cm^{-1}.[47] This early work was improved upon by subsequent research efforts, notably by Kanazawa and Diaz, leading to electrochemical production of thin films with conductivities as high as 100 S cm^{-1} routinely being reported.[48,49,50] The mechanism by which the electrochemical polymerization proceeds, begins with the oxidation of a pyrrole monomer to a resonance stabilized radical cation.[51,52] The latter combines with a second such species to form a bipyrrole intermediate, which undergoes deprotonation to form an aromatic pyrrole dimer. Oxidation of this dimer then allows to react further with other monomeric, oligomeric or polymeric species. Early in the reaction, it is most likely that coupling will occur with a monomer radical cation, (Figure I-9) as the polymerization only starts when the oxidation potential is sufficiently high to oxidize the monomers. However, at later stages coupling is more likely to occur between oligomer radical cations, since the dimers, trimers and oligomers are progressively easier to oxidize than the monomer.[51,52] As a result, PPy is always obtained in its oxidized state rather than its neutral form. A similar mechanism has been proposed for other pyrrole derivatives, as well as thiophenes.[53,54]

The exact properties of the electrochemically synthesised PPy films will depend on such preparation conditions as the monomer concentration, nature of the counter-ion[55] electrodes[56] current density, solvent etc.[57-59]

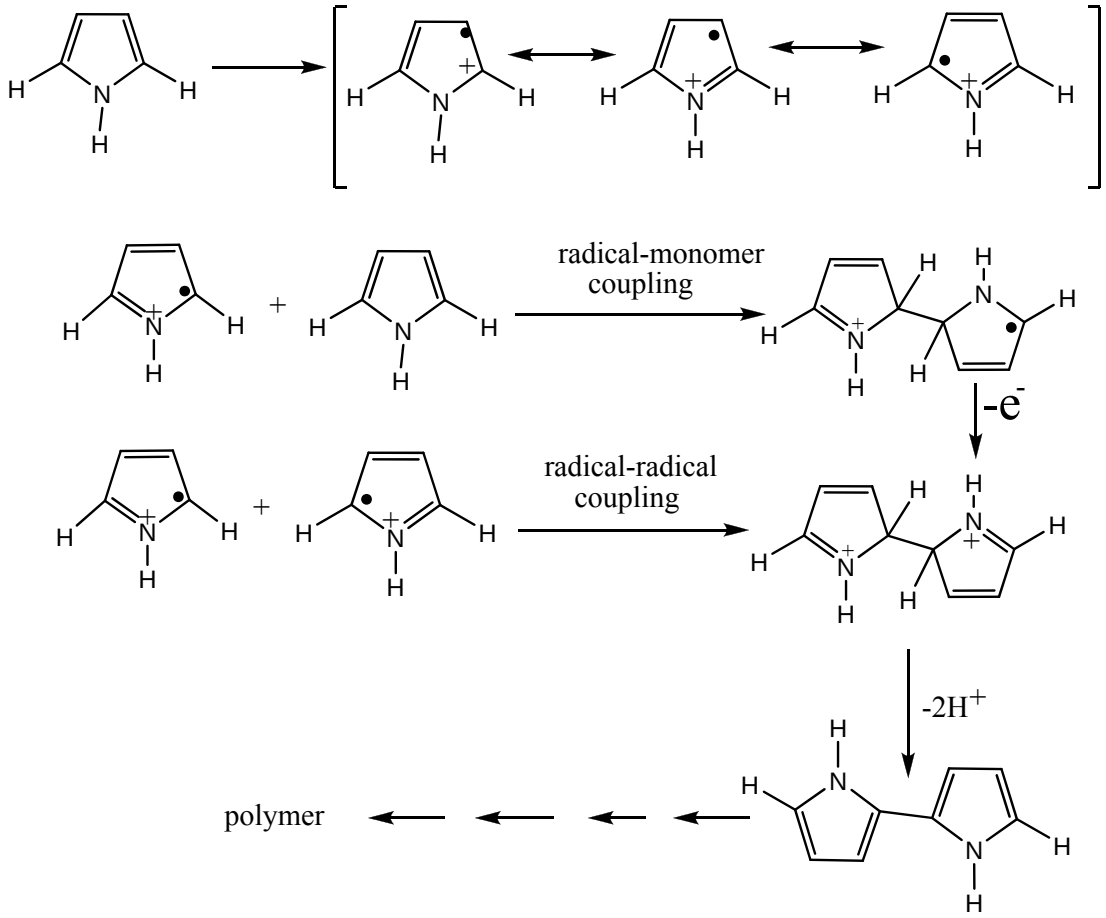

Figure I-9: Schematic representation of the electrochemical oxidation of pyrrole to PPy

I.2.2. Chemical Synthesis

Although electrochemical synthesis of OCPs can be carried out at neutral pH, and allows a wide range of counter-ions to be incorporated with good control over the oxidation potential, it is restricted by the geometric area of the electrode onto which the OCP is deposited. In order to synthesize larger quantities of OCPs, chemical synthesis is necessary. The first such synthesis was carried out as early as 1916, in which pyrrole was exposed to hydrogen peroxide in acidic media.[45] Unfortunately, since OCPs were not appreciated until many decades later, no conductivity measurements were reported. Following the work of Cristofini and co-workers [60] in the 1970's, it was only in the early 1980's that the chemical synthesis of PPy was re-visited. Over the last two decades, synthesis conditions have been optimized to allow the chemical preparation of PPy powders with conductivities of the order of 10^2 S cm^{-1}. The two most important methods by which PPy can be synthesized chemically are either in solution[61] or by chemical vapour deposition.[62-65] In the latter case, pyrrole vapour

is introduced into a vessel containing the chemical oxidant either in solution or more commonly incorporated into a solid substrate.

However, chemical polymerization in solution is far more common. A wide range of oxidants have been investigated for the chemical polymerization of pyrrole, with salts of Fe^{3+} and Cu^{2+} being particularly effective.[20,21,60,66-69] Although less common, the use of oxidants such as $(NH_4)_2S_2O_8$ has also been reported.[70,71] However, since persulfate is a stronger oxidant than the aforementioned metal salts,[72] faster rates of polymerization have been observed, as well as over-oxidation of the PPy backbone, invariably resulting in diminished conductivities.[73,74] The kinetics and mechanism of the persulfate mediated polymerization, however, have not been reported in great detail. A catalytic oxidant system has also been reported using Fe^{2+}, Fe^{3+}, or Cu^{2+}-H_2O_2; the advantage here is that only a small amount of transition metal is required.[75,76]

The mechanism of pyrrole polymerization in water using $FeCl_3$ is believed to be similar to that proposed by Genies et al.[54] for the electrochemical polymerization. This similarity was noted by Bjorklund whilst observing the formation of chemically synthesized PPy colloids using visible absorption spectroscopy[73] and was later confirmed by Wei *et al*.[77] Again, the polymerization begins with oxidation of the pyrrole monomer to the radical cation, followed by combination to form the bipyrrole intermediate, and then further reaction with other monomer, dimer, oligomeric or polymeric radical cations (see Figure I-10).

Assuming a doping level of 33% in the final chloride-doped PPy, the theoretical molar ratio of $FeCl_3$/pyrrole required is 2.33/1.[21] It follows that since $FeCl_3$ is only a one electron acceptor, two moles are required to polymerise one mole of pyrrole to produce one mole of neutral, undoped PPy, followed by a further 0.33 moles per pyrrole residue to oxidize and dope the polymer.

Among the problems associated with oxidative polymerization is the abundance of possible side reactions. Oxidation of the simple, unsubstituted heterocycles results in poorly soluble, poorly processable materials, so structural modifications are typically used to

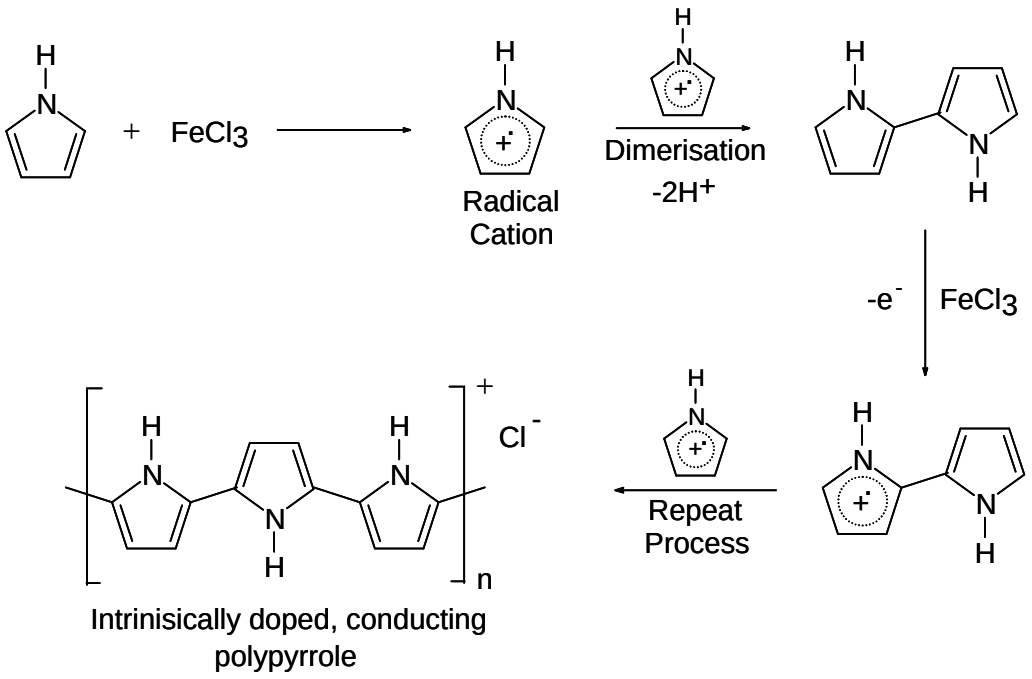

Figure I-10. Schematic representation of the chemical oxidation of pyrrole to PPy using $FeCl_3$ as the oxidant.

improve polymer properties. Often, the strong oxidation conditions required to effect polymerization cause over-oxidation and decomposition. While coupling at a carbon adjacent to the heteroatom is favored, as it is the most electron-rich site, coupling is also possible at other unsubstituted carbons, and irregular polymer backbones can be formed as shown in Figure I-11 for oxidative polymerization of pyrrole.

Coupling of heterocycles occurs predominantly through the 2- and 5-positions (α,α-coupling), but some coupling also occurs at the 3- and 4-positions to give a small amount of α,β and β,β-couplings. The mixture of couplings induces larger twist angles, reducing conjugation and yielding poor electronic properties. Multiple couplings on the same heterocyclic molecule can also occur, resulting in cross-linked polymers. Coupling at β-positions during polymerization can be avoided by blocking the 3- and 4-positions of the heterocycle. If symmetrical substitution is used, problems associated with regioirregularity can be avoided

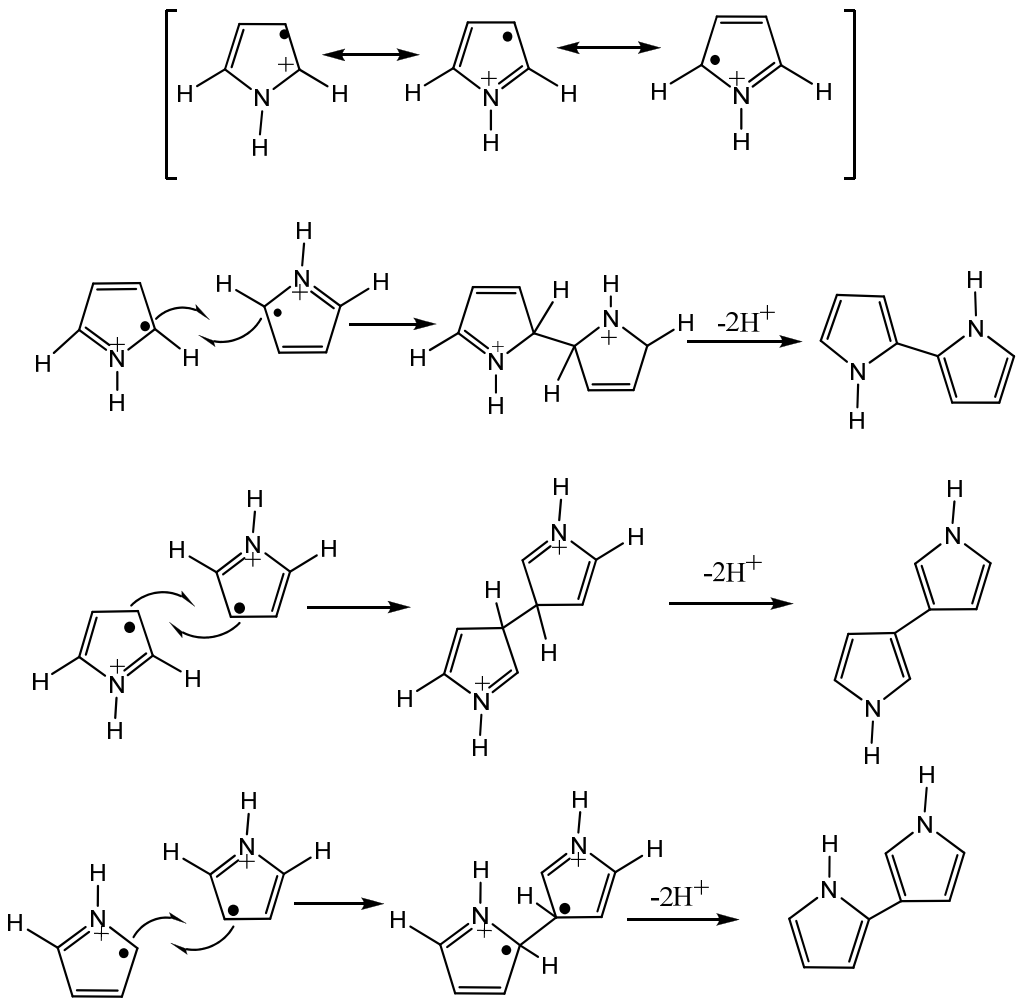

Figure I-11: Coupling pathways during oxidative polymerization of pyrrole.

I.2.3. Structure and Stability

In an early study by Gardini, treatment of PPy with acidified $KMnO_4$ yielded α,α' pyrrole dicarboxylic acid as the major decomposition product. Hence it was suggested that PPy consisted primarily of α,α' linked pyrrole residues.[78] However, later XPS studies of the C 1s core-line spectrum of PPy and related polymers suggested that up to one third of pyrrole rings may in fact be α,β-linked.[79] In particular, it was found that a more-ordered C 1s peak was obtained after using 3,4-dimethylpyrrole as monomer, thus preventing any α,β-linkages from being formed. Analysis of the N 1s peak in PPy was also carried out, demonstrating that there were several different nitrogen species present, including a N^+ species at high dopant

levels.[79,80] In view of these observations, it is obvious that the structure shown for PPy earlier in Figure I-10 is somewhat idealized. Further evidence for the deviation from the idealized structure can be found in microanalytical data reported for PPy, since C and H values for PPy are often in excess of those expected.[20,78,81] The presence of oxygen-based counter-ions was suggested by Pfluger et al[80] whereas Diaz and co-workers have proposed the presence of carbonyl moieties along the PPy backbone[82]

As mentioned earlier, doped and conductive PPy is relatively air stable.[83] The most straightforward, yet sensitive, way to monitor oxidative degradation in an OCP is simply by measuring its conductivity regularly over time. The conductivity of polyacetylene, for example, decreased by a factor of two in air at 80°C within 1 h, whereas the same conductivity decay took nearly a week with toluenesulfonate-doped PPy.[83] Furthermore, polyacetylene has been shown to be intrinsically unstable, with decreased conductivities being observed even under inert conditions. PPy, on the other hand, maintained its conductivity in the absence of water and oxygen, and can therefore be considered intrinsically stable. Samuelson and Druy carried out accelerated ageing tests on toluenesulfonate-doped PPy; from their kinetic data they predicted a one-order of magnitude loss in conductivity for every three years exposure to air in ambient conditions.[84] This prediction is in relatively good agreement with long-term, ambient temperature ageing tests carried out by Lascelles.[85]
In terms of providing both higher conductivity and better conductivity stability, it has been demonstrated that aromatic sulfonate anions are the most suitable dopant.[86] It was postulated that this improvement is due to the aromatic, and hence planar, nature of the dopant species, which causes increased anisotropy and order in the conducting polymer backbone, thereby facilitating more efficient conduction.[87]

I.3. Polyaniline

Like PPY, polyaniline (PANI) has become one of the most studied conducting polymers due to the fact that it can be readily synthesized, possesses good conductivity and conductivity stability, and also exhibits interesting redox properties. Polyaniline is an example of a conjugated polymer that can be tailored for specific applications through doping process. Since its conductive properties were rediscovered in the early 1980s, polyaniline has been used for many other applications like lightweight battery electrodes,[88] electromagnetic

shielding devices,[89,90] and anticorrosion coatings.[91,92] However, like PPY, it suffers from poor processability, being soluble only in concentrated acids in its conducting form.

I.3.1. Electrochemical Synthesis

Initial investigations into the electrochemical polymerization of aniline demonstrated that PANI could be formed under an applied potential in acidic media.[93-95] However, these experiments resulted in powdery residues with poor adhesion to the electrode at which they were deposited. Subsequent improvements have resulted in PANI films which can be readily removed from the electrode as free-standing films.[17,18,96-98] Typical electrochemical syntheses are carried out using either dilute HCl or H_2SO_4 as the polymerization medium. An interesting feature of PANI is that it can be easily switched from its conducting to insulating form depending on its chemical environment (see Section 1.3.3). Electrochemically synthesised PANI films can be cycled between these states by varying the applied potential. Conductivities have been reported in the range of 10^{-8} – 10^{2} S cm^{-1}, depending on preparation conditions and the final oxidation state of the PANI.[97,98]

The first investigations into the electrochemical polymerization mechanism of aniline were carried out by Yasui as early as 1935.[99] It was proposed that the polymerization proceeded via a *p*-aminodiphenylamine intermediate species. Further work was carried out by Mohilner et al., who proposed that the initial, and rate determining step of the polymerization was the protonation of the aniline monomer at the nitrogen atom, followed by oxidation to form an aniline radical cation species.[100] It is now generally accepted that this is indeed the initial step, but that it is not rate determining.[101-104] Breitenbach and Heckner reported that this radical cation species was a nitrenium cation [$(C_6H_5NH^+)^{\cdot}$], and that it reacted with another aniline monomer to form the dimeric *p*-aminodiphenylamine.[102-104] Genies et al. have since reported that the rate determining step is in fact formation of this dimer.[101]

I.3.2. Chemical Synthesis

A wide range of chemical oxidants have been employed to carry out the polymerization of aniline to produce conducting PANI. These include potassium dichromate[105] potassium iodate[106] hydrogen peroxide[107] potassium or copper perchlorate[108] and, most commonly, ammonium persulfate.[109-111] If the oxidant concentration is too high,

over-oxidation and degradation can occur.[105,112] For example, in the case of ammonium persulfate, Armes and Miller clearly showed that below an initial persulfate/aniline molar ratio of ~1.25, the conductivity and degree of oxidation of the resulting PANI were constant. However, at higher oxidant/monomer molar ratios an increase in over-oxidation of the PANI and concomitant decrease in conductivity were observed.[113]

I.3.3 Structure and Stability

It was nearly a century ago that Green and Woodhead first proposed that 'aniline blacks' were made up of octamers of eight aniline units joined head-to-tail through the para position on the aromatic ring.[114,115] The parent species was named leucoemeraldine, and four further structures were proposed covering the possible oxidation states of the nitrogen atoms in the octamer (see Figure I-12). In the fully reduced form of leucoemeraldine, the nitrogens are all secondary amines. Oxidation of 2, 4, 6, or 8 of these amines to imine groups leads to the protoemeraldine, emeraldine, nigraniline and pernigraniline forms, respectively. The fully oxidized (pernigraniline) and fully reduced (leucoemeraldine) forms of PANI are both electrically insulating. For efficient conduction to take place, the polymer backbone must be in its half-oxidized emeraldine state as well as being protonated (see Figure I-13). When the polymer is in this emeraldine form, the oxidized imine nitrogens can be readily protonated by acids to yield the conducting emeraldine salt.

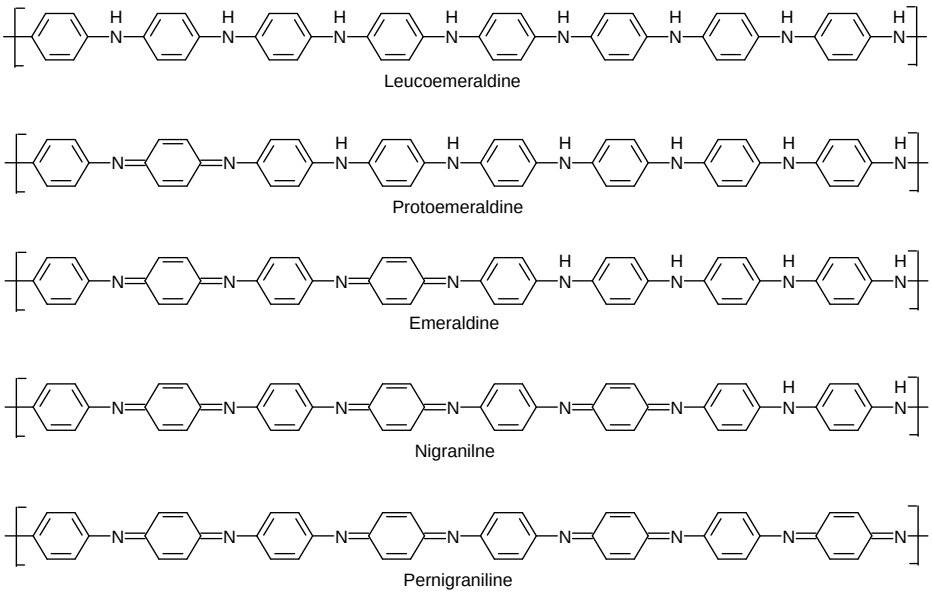

Figure I-12. Structures of the various oxidation states of 'aniline blacks' as proposed by Green and Woodhead.

PANI synthesized using ammonium persulfate in 1.2 M HCl is obtained directly in the conductive emeraldine salt form as a dark-green precipitate with chloride as the dopant anion. XPS studies of doped conductive PANI confirmed the presence of three nitrogen species in the polymer.[116-118] Deconvolution of the N 1s peak resulted in three peaks centred at 398, 399 and 401 eV which were assigned to imine, amine and protonated imine nitrogen species, respectively.

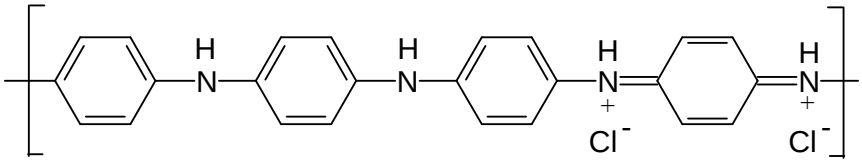

Figure I-13. Structure of the conductive, protonated emeraldine base form of polyaniline.

As mentioned earlier in Section 1.2.3, PPY has been demonstrated to be much more air stable than polyacetylene. Moreover, in the complete absence of O_2 and water, its electrical conductivity remains constant, suggesting intrinsic stability. In the case of PANI, it has been proposed that water vapour actually plays a role in the conduction mechanism. MacDiarmid and co-workers demonstrated that the conductivity at room temperature of chloride-doped PANI could be increased by a factor of two when placed in the presence of water vapour.[119] However, Neoh *et al*. proposed that the considerable decrease in conductivity observed when chloride-doped PANI is heated above 100°C is not due to the loss of adsorbed water alone.[120] The thermal stability of PANI was investigated by Kulkarni *et al*., and it was found that the non-conductive emeraldine base form was highly heat-stable, exhibiting significant weight loss only after heating above 420°C.[121] The thermal stability of the doped, conductive form of PANI was found to be somewhat lower, with significant weight loss occurring at around 200°C, depending on the counter-ion. Interestingly, similarly to PPY, the effect of temperature on the decay in conductivity depended on the nature of the counter-ion, with stability decreasing in the order $CH_3SO_3^- > HSO_4^- > Cl^-$.

I.4. Poly(3,4-ethylenedioxythiophene) (PEDOT)

Poly(3,4-ethylenedioxythiophene) [PEDOT] is a relatively new conducting polymer which was developed by scientists at the Bayer AG research laboratories in Germany in conjunction with AGFA in the late 1980's.[9,122] PEDOT possesses the structure shown in Figure I-14. It was initially developed to give a soluble conducting polymer that lacked the

presence of undesirable α,α'- and α,β-couplings, which were believed to contribute significantly to the insolubility of related conducting polymers such as polythiophene. Unfortunately, conventional chemical or electrochemical polymerization of the 3,4-ethylenedioxythiophene (EDOT) monomer also led to an insoluble conducting polymer. However, in contrast to PPY, which possesses a band gap of approximately 3.2 eV and is black in colour,[123] PEDOT's band gap is only approximately 1.4 – 1.5 eV.[124] Depending on the extent of doping, oxidation and film thickness, PEDOT films can range in appearance from almost transparent with a sky-blue tint, to intensely blue-black.[11] As a result, much of the research on PEDOT has centered on its use in low colour anti-static coatings and electrochromic devices. [9,122,125-129]

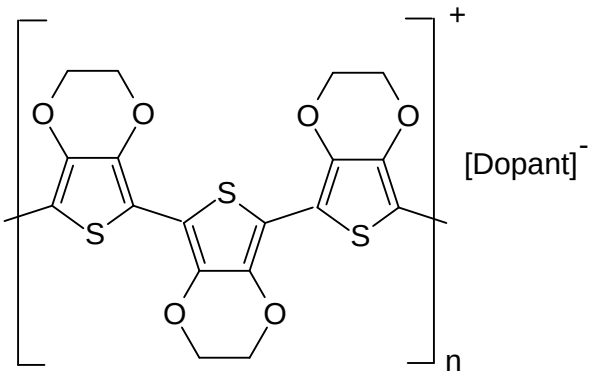

Figure I-14. Structure of doped, conductive poly(3,4-ethylenedioxythiophene).

I.4.1. Electrochemical Synthesis

The electrochemical polymerization of EDOT was first reported by Jonas and co-workers in 1992. These workers carried out the electropolymerization in aqueous or acetonitrile solutions, leading to near-transparent films with conductivities up to 200 S/cm.[9,11,125] Notably, the higher conductivities were obtained in acetonitrile, rather than water. Inganäs and co-workers reported similar results, producing perchlorate-doped PEDOT electrochemically with conductivities as high as 210 S/cm.[124] One of the inherent difficulties in polymerizing EDOT is its low solubility in water, hence the use of acetonitrile. However, this issue was addressed by Sakmeche *et al*. when they demonstrated that EDOT could be electropolymerized in aqueous SDS solutions.[130,131] Not only did the SDS micellar solution aid the solubility of EDOT, but it was also claimed to lower its oxidation potential. Moreover, it was claimed that the PEDOT films electrodeposited in this way were actually smoother than

the analogous films prepared in acetonitrile; however, no SEM evidence was provided to support this. Wernet and co-workers showed that EDOT could be electrochemically polymerized in polyelectrolyte solutions to produce PEDOT films with excellent mechanical properties which exhibited thermoplastic behaviour.[132] Polyanions such as sulfated-poly(β-hydroxyether) and sulfated-poly(butadiene) were incorporated as dopants, yielding conductivities as high as 390 S cm^{-1}. Similar thermoplastic behavior could not be obtained using small molecule dopants such as perchlorate or tosylate anions.

I.4.2. Chemical Synthesis

The chemical polymerization of EDOT can be carried out using similar methods and oxidants as those employed to polymerize pyrrole. The earliest reported syntheses were carried out in acetonitrile and employed various ferric salts as the oxidant.[9,124,125,129] These polymerizations resulted in dark blue powders, which were insoluble in all solvents, with typical conductivities of 5 – 10 S cm^{-1}. Corradi and Armes demonstrated that EDOT could be polymerized in water, despite its limited solubility, using $FeCl_3$.[133] They found that using the theoretical oxidant/monomer molar ratio of 2.33 at room temperature gave relatively low yields of PEDOT, with conductivities of about 4 S cm^{-1}. Yields could be dramatically increased by increasing the reaction temperature, but this resulted in a reduction in conductivity of several orders of magnitude, presumably due to over-oxidation. The use of cerium salts was also investigated, but the PEDOT synthesized in this way was found to be contaminated with up to 20 wt% of an unidentified incombustible cerium residue.
More recently, Kudoh *et al*. showed that the low solubility of EDOT in water could be overcome by carrying out an emulsion polymerization employing an anionic surfactant.[134] By adding Fe(III) salts to an emulsion of EDOT stabilized by sodium alkylnaphthalenesulfonate, PEDOT was obtained in far higher yields over a given time than in control reactions carried out without surfactant. Moreover, PEDOT synthesized in the presence of surfactant had conductivities of nearly 100 S cm^{-1}, which is two orders of magnitude higher than that prepared in the absence of surfactant.

The chemical polymerization methods described for PEDOT produce only insoluble powders. However, De Leeuw *et al*. reported a novel chemical polymerization method which resulted in PEDOT films with conductivities as high as 300 S cm^{-1}.[135] EDOT monomer was dissolved in *n*-butanol, along with $Fe(OTs)_3$ as an oxidant and imidazole, and this solution

was then film-casted. A highly conductive, insoluble PEDOT film was formed after heating to 110°C for 5 minutes. Imidazole is a base and it inhibits the polymerization at room temperature, thus making this protocol ideal for applying surface coatings, followed by thermally-induced polymerization.

Recently, Kirchmeyer *et al.*[136] proposed the detailed mechanism of oxidative polymerization of EDOT (Figure I-15). They obtained a set of kinetic parameters that fully explains the polymerization rate and stoichiometry. Additionally it gives some insight into some new preparative aspects of EDOT chemistry. The reaction starts with the slowest, rate determining step, the EDOT oxidation to the radical cation (reaction rate constant k_1 = 0.16 L /mol /h) followed by the dimerization of the free radicals ($k_2 = 10^9$ L/ mol/h). End group oxidation of oligomers, beginning with dimers, is faster than the monomer oxidation (k_5 = 3.000 L /mol/ h as proposed for all chain lengths) and leads, after recombination of two radical cationic end groups, to higher oligomers with the same rate constant for the recombination as with the monomer cations ($k_2 = 10^9$ L/ mol/h). At the end, oligomers or polymers, respectively, are doped by further oxidation. In Figure I-15 the paramagnetic polaron state as the first step of doping and intermediate to the highly conductive, diamagnetic bipolaron state is shown. This state is stabilised by the charge balancing counter ion. A recent publication suggests a chain growth mechanism for the oxidative synthesis of aqueous PEDOT microdispersions.[137]

Acidification significantly enhances the reaction rate. The effects of protons have mechanistic aspects to be dealt with more precisely. Protic acids and a variety of Lewis acids catalyse an equilibrium reaction of EDOT to the corresponding dimeric and trimeric compounds without further oxidation or reaction (Figure 1-16).[138]

Use of effective catalysts like BF_3, $AlCl_3$, $TiCl_4$, $SnCl_4$, $SbCl_5$, etc. yields the desired dimer in the range of 25 to 50 wt.%, accompanied by about 5 to 15 wt.% of the stereoisomeric trimeric compounds. Similar results were obtained with some strong protic acids, of which trifluoro acetic acid and sulfuric acid, for example, are very effective. The EDOT-dimer can be easily oxidised to bis-(3,4-ethylenedioxythiophene) (BEDOT) using quinones like chloranil or 2,3-dichloro-4,5-dicyano-1,4-benzoquinone.[139] The smooth formation in acceptable yields can be utilised for a new and very simple access to BEDOT.

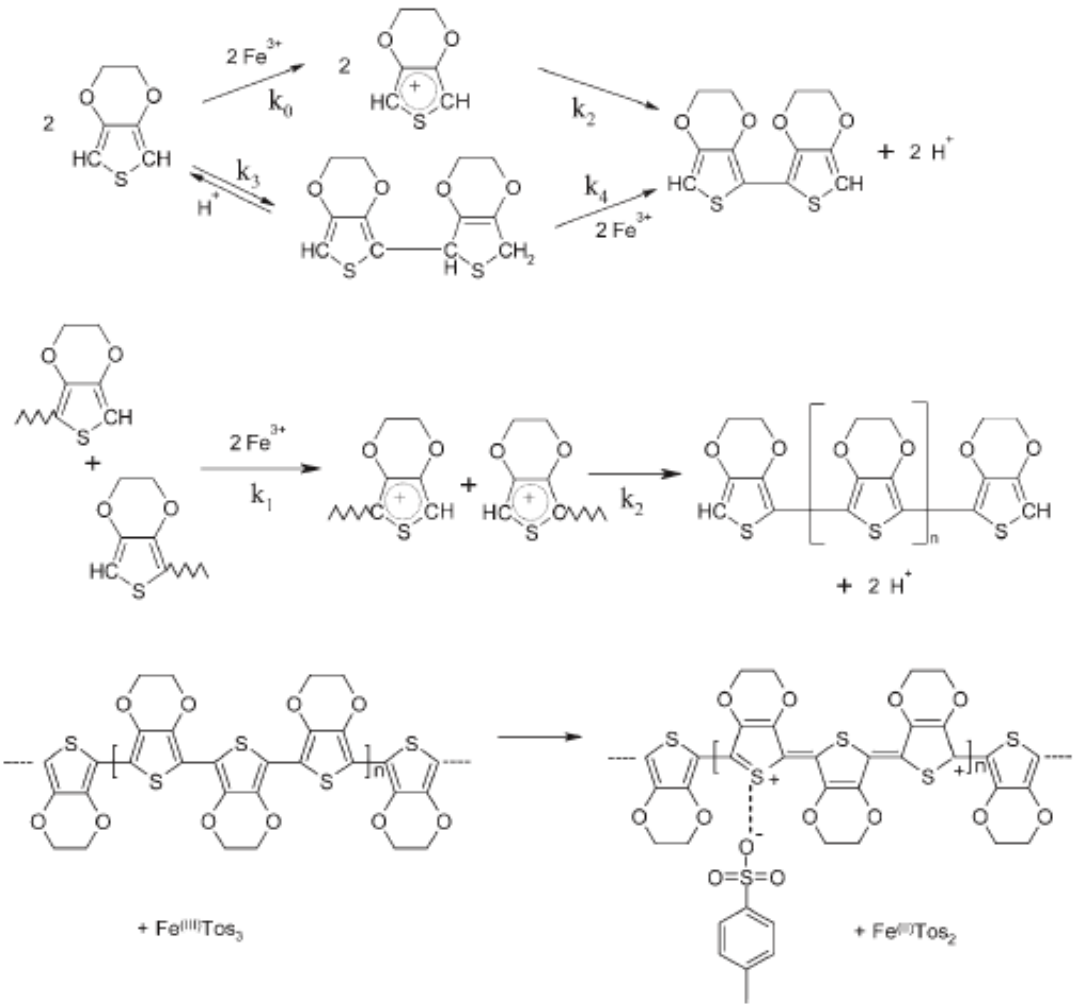

Figure I-15: Proposed reaction mechanism for EDOT oxidation to conductivePEDOT-tosylate.

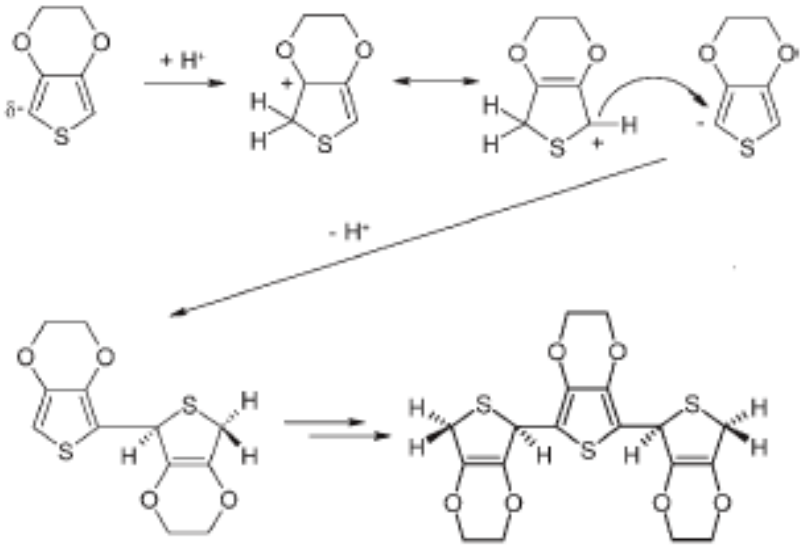

Figure 1-16: Reaction products of EDOT di- and trimerisation (only R-isomer of dimer and R,S-isomer of trimer are shown).

Various X-ray structures of PEDOT salts have been reported including the perchlorate,[140] p-toluene sulfonate[141] and hexafluoro phosphate.[142] PEDOT chains are stacked with repeating distance of 6.8 Å respectively, a distance of 3.4 Å resembling the high tendency of thiophenes towards π-stacking. The doping counter ions are incorporated between the π-stacks leading to a structure resembling the structure of *'Lasagne'* (Figure I-17), where the distance between the stacked layers is determined by the counter ion size.

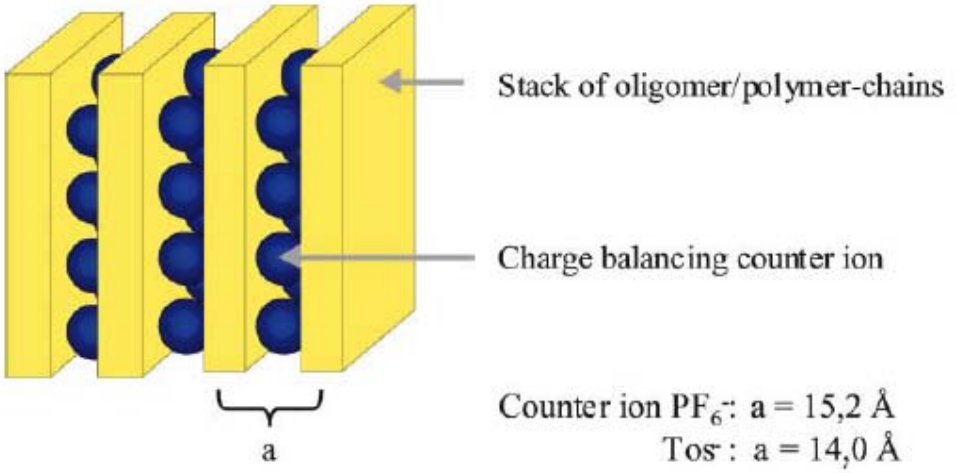

Figure 1.17: PEDOT stacks; a 5 counter ion-dependent layer distance between stacks.

I.4.3. Structure and Stability

Relatively little has been published on the structure of PEDOT. The bulk polymer was shown to have an amorphous, fibrillar structure in a combined SEM and X-ray diffraction study.[143] Semi-empirical modelling of the PEDOT structure was carried out by Granström and Inganäs.[144] The results were much as expected, with the monomer units bonded in a trans 'head-to-head' fashion in order to minimise steric congestion between the adjacent alkoxy substituents. In a subsequent combined XPS and UV photoelectron spectroscopy (UPS) study, Inganäs and co-workers found good agreement between the calculated and measured electronic structures.[145] It was shown that the C 1s peak in the XPS spectra broadened after the polymer was oxidized into its doped form. The narrow O 1s and S 2p peaks contained additional features due to the two dopants used (OTs^- and PSS^-).

Probably the most notable characteristic of PEDOT is its environmental stability.[11,127,143] This can be primarily attributed to the 3,4-disubstituted thiophene ring. In other heterocyclic conducting polymers such as PPY, these positions are prone to aerial

oxidation leading to carbonyl formation and consequently lower conductivities. In PEDOT, this degradation cannot occur. In addition, α,β-crosslinking is prevented (see Figure I-18).

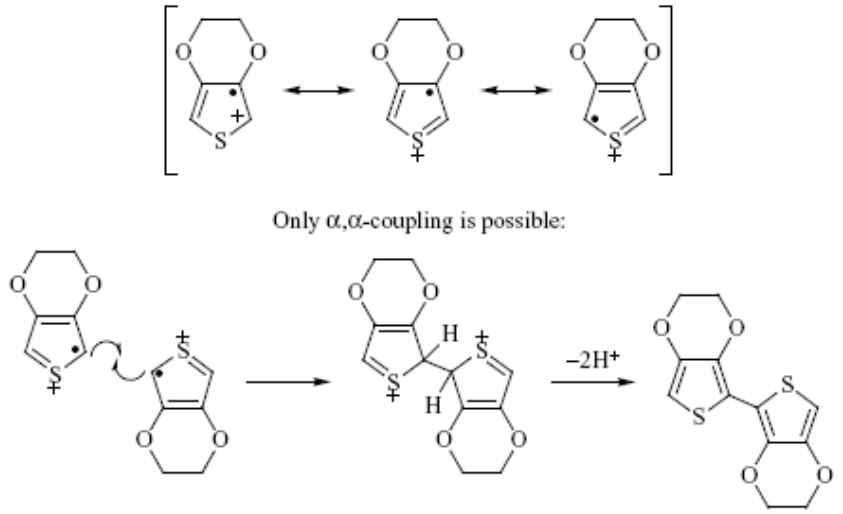

Figure I-18: Coupling pathways during oxidative polymerization of EDOT.

Pei *et al*. carried out stability studies on electrochemically prepared perchlorate-doped PEDOT films.[124] They found that there was no significant loss in conductivity after 60 h at 110ºC, and thus PEDOT outperformed polythiophene and PPY in comparative studies. Similar results were achieved by Rannou and Nechtschein in accelerated ageing tests carried out at high temperatures on tosylate-doped PEDOT thin films.[146] Jonas and Heywang carried out tests on PEDOT and PPY in saturated water vapour at 100ºC.[126] While the conductivity of PEDOT showed no change over 24 h, that of PPY decreased by several orders of magnitude under these conditions. An interesting XPS and x-ray near edge structure spectroscopy (XANES) study carried out by Winter *et al*. examined the changes that occurred in $FeCl_4^-$-doped PEDOT on heating to 150ºC.[147] Although the 3,4-disubstitution of the backbone makes PEDOT more resilient to oxidation, it was clearly demonstrated that other oxidative side-reactions could clearly reduce its conductivity. On heating in air, the sulfur atoms became oxidized, and in some cases became cleaved from the polymer altogether. Evidence was also found for the formation of covalent C-Cl bonds, suggesting decomposition of the dopant species and further polymer degradation.

Because of their molecular characteristics, the majority of these materials are infusible and practically insoluble in common organic solvents. This insolubility was a long time an important obstacle with the good characterization of these polymers like to the establishment of the relations between their structure and their properties. Moreover, the difficulties to

process conjugated polymers are still preventing their common use and large scale development. In order to overcome this drawback, many research groups enhanced the solubility of conjugated polymers by introducing flexible side chains like alkyl groups[148-150] and poly(ethyleneoxide)[151] or the incorporation of polar functions like the quaternary sulfonates[152,153] or ammoniums, to the rigid backbone, by preparing blends and composites with other insulator polymers[154,155] Blends and composites of polymers offer certain combinations of desired properties that cannot be obtained from the individual components. Another route to ease the processability of conjugated polymers is to synthesize them under the form of colloidal particles which is the subject of this Ph.D work. Conducting polymer colloids typically consist of a colloidal suspension of conducting polymer particles or conducting polymer-coated particles (latex, metal, silica, etc) in an aqueous medium; the dimensions of the dispersed particles are in the 10 nm–10 μm range. These materials are normally prepared via dispersion polymerization.[156,157]

II. Colloidal dispersions of organic conducting polymers (OCPs)

A colloidal system can be defined as a dispersed phase within a continuous phase, such that at least one of the dimensions of the dispersed phase is between 1 nm and 1 μm.[158] The precise physical nature of the colloidal system depends on the constituent phases, which may be solid, liquid or gas. The specific colloids discussed herein are *polymer colloids* (commonly called *latexes*), in which solid polymer particles are dispersed within a liquid medium.

II.1 General Principals of Colloidal Stability[159]

When a piece of material in the bulk state, immersed in a fluid medium, is subdivided into many colloidal particles, there is an accompanying change in the free energy of the system, $\Delta G°$, which is defined in Equation I.4.

$$\Delta G° = \gamma_{sl} \Delta A_{sl} \qquad (I.4)$$

γ_{sl} is the solid/liquid interfacial tension or free energy, and ΔA_{sl} is the increase in interfacial surface area arising from the subdivision of the bulk material. If $\Delta G°$ is negative, the colloid is said to be lyophilic (where lyo- refers to the dispersion medium), and is thermodynamically stable. Conversely, if $\Delta G°$ is positive the colloid is referred to as lyophobic, and is thermodynamically unstable. Lyophobic colloids can, however, be made kinetically stable if

there is a sufficiently high energy barrier which prevents re-aggregation of the colloidal particles, as shown in Figure I-19.

If the energy barrier, E_{act}, is absent (as depicted in the lower curve in Figure I-19) or is low relative to the thermal energy of the particles, kT, then spontaneous aggregation back to the bulk state occurs by means of attractive van der Waals forces, in order to minimize A_{sl} and hence the free energy of the system. The two principal methods for stabilizing lyophobic polymer colloids in order to provide a sufficient energy barrier against aggregation are charge and steric stabilization.

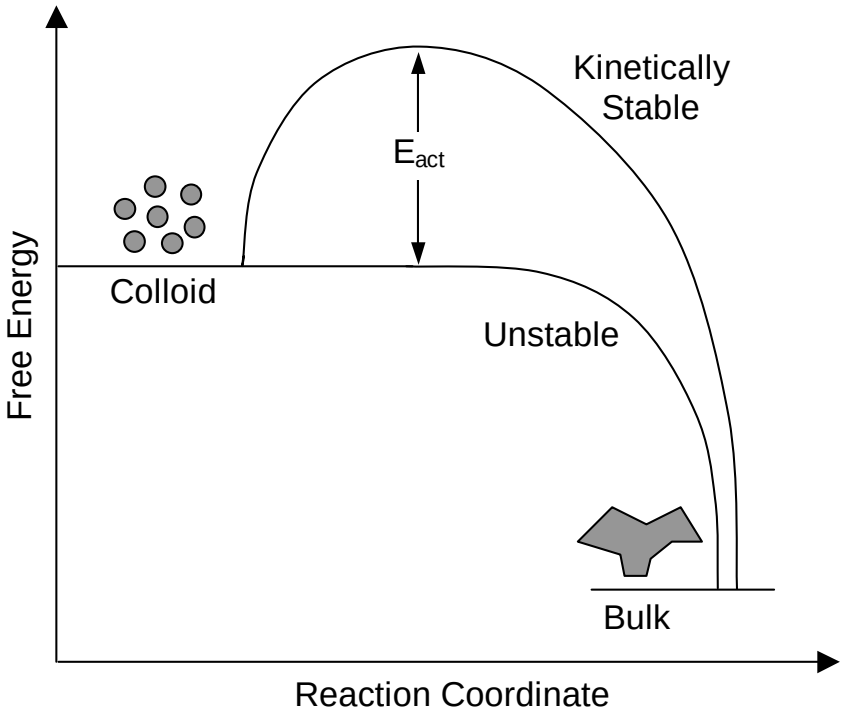

Figure I-19: Kinetic stability of a lyophobic colloid.

II.1.1. Charge Stabilization[158,159]

In order for colloidal particles to be charge stabilized, they must possess a degree of surface charge. In polymer colloids, the origin of this surface charge could be, for example, sulfate chain ends or adsorbed ionic surfactant. In order to preserve overall charge neutrality, there are an equal number of oppositely charged ions in the vicinity of the surface ions. The result is an *electrical double layer*, consisting of surface bound ions and a diffuse layer of moving counterions in the solvent. The interaction of these double layers between particles is energetically unfavourable and gives rise to repulsive forces. The combination of these repulsive forces and the attractive van der Waals forces, which act over similar distances, gives rise to a complex set of energy curves, the rationalization of which is known as 'DLVO' theory (named after Derjaguin and Landau, Verwey and Overbeek).[160,161] A further energy term, known as Born repulsion, must also be considered, which is a result of overlapping electron clouds when the particles come within very close contact at near atomic separations. A typical potential energy diagram is shown schematically in Figure I-20 where V_A and V_R represent the attractive and repulsive energy terms, respectively, and V_T represents the sum of these energy terms.

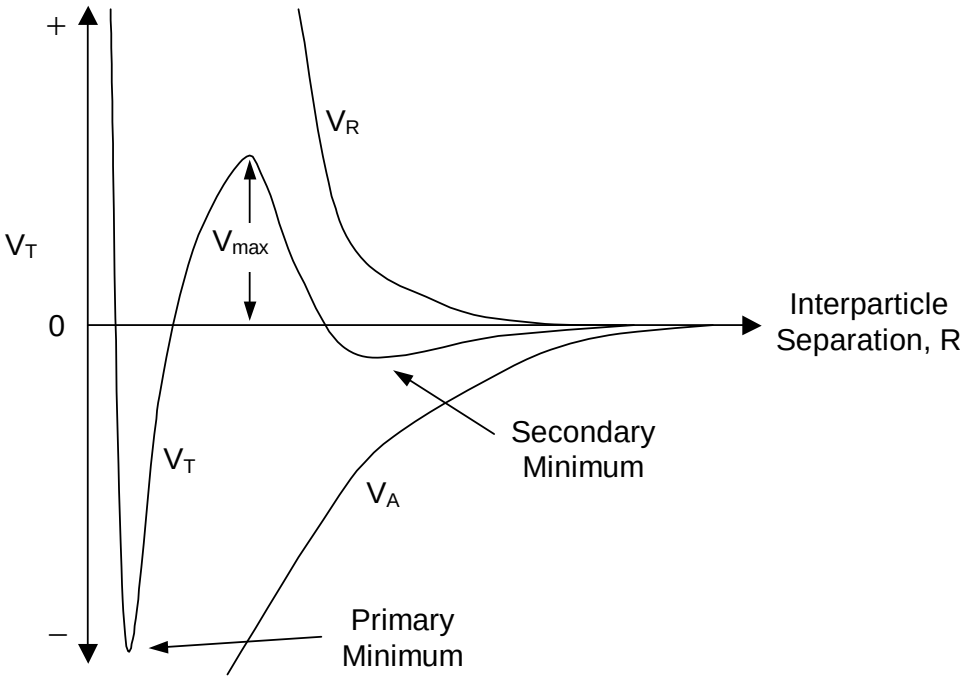

Figure I-20: Total interaction free energy curve [$V_T(R) = V_A + V_R$] between two charges stabilized particles, one located at the origin and the other at a distance R.

It should be noted that the energy barrier, $V_{(max)}$ is the same as E_{act} in Figure I-19. There are two energy minima: (i) the primary minimum which results from the combination of the Van der Waals attraction (very strong at short distances) and the Born repulsion, and (ii) the secondary minimum which is usually quite shallow, if it exists at all. The primary minimum is usually so deep that the energy barrier for particle separation is considered to be infinite. This type of particle aggregation is called *coagulation*, and is generally considered to be irreversible. However, provided that $V_{(max)}$ is sufficiently large relative to kT then the dispersion will remain stable. The secondary minimum, on the other hand, is much shallower. When this is comparable to kT, it gives rise to a loose, reversible type of particle aggregation known as *flocculation*. It should be pointed out, however, that in much of the colloid science literature, the terms aggregation, coagulation and flocculation are often used interchangeably.
In order for charge stabilization to be effective, aqueous or highly polar solvents are required, with relatively high dielectric constants, to enable effective double layer formation. Charge stability, however, is relatively easily compromised by the addition of small amounts of electrolyte, which causes compression of the diffuse regions of the double layer, thus reducing repulsive forces and allowing closer approach of the particles. If the particle separation is reduced sufficiently, the ever-present attractive Van der Waals forces will dominate. Finally, charge stabilization can only be used at relatively low solids concentrations (≤ 10 %), since at higher concentrations, compression of the double layers leads to a lower kinetic barrier towards coagulation.

II.1.2. Steric Stabilization [158,159,162]

Steric stabilization refers to the mechanism by which particle aggregation is prevented due to physically adsorbed or chemically grafted polymers at the surface of the colloidal particles. It has been found that amphiphilic block or graft copolymers are best suited for use as steric stabilizers. Such polymers consist of at least two blocks, one of which is soluble in the dispersion medium, and one which is not. The insoluble block(s) act as an anchor and adsorb onto the lyophobic particle surface. This leaves the soluble block(s) tethered to the particle surface, but solvated in the dispersion medium, to act as the stabilizing moiety. It follows that there are many different possibilities for steric stabilizer architectures, since the relative number, order, type and length of the blocks can be varied. This is not to say that homopolymers cannot be used as steric stabilizers, but they are generally less effective than amphiphilic block or graft copolymers for reasons to be discussed later.

Three important criteria must be fulfilled if steric stabilization is to be effective. Firstly, there must be efficient anchoring of the stabilizing polymer to the particle surface in order to prevent desorption. This anchoring may be via physical adsorption or, even better, chemical adsorption (grafting). Secondly, the stabilizer should completely cover the particle surface, as bare patches would allow the close approach of other particles. Thirdly, the steric layer should be relatively thick in order to prevent close approach of other particles. If these criteria are fulfilled, the stability of the particles towards aggregation is determined by thermodynamic factors, principally arising from the solvency of the stabilizing moieties in the dispersion medium.

As two particles approach each other, the outermost segments of the two layers of stabilizing polymer start to overlap, a situation known as interpenetration. This increase in the local concentration of polymer segments results in a local increase in osmotic pressure, which causes solvent to enter the overlap region from the surrounding medium, leading to repulsive forces between the two particles. The free energy change which occurs when the stabilizing polymer chains interpenetrate is influenced by such factors as temperature and solvent composition. The temperature at which this free energy change is zero is called the θ-temperature, and such a solvent is known as a θ-solvent. Under these conditions, the solvency is such that the polymer segments neither attract nor repel each other, and no preference is displayed for either polymer-polymer or polymer-solvent interactions. However, for steric stabilisation to be effective, the polymer chains must repel each other, i.e. the solvent should be a better-than-θ-solvent. As the solvency is reduced to a worse-than-θ-solvent then polymer chains will begin to attract each other, and this mutual attraction of steric stabilizer layers between particles will lead to flocculation.

Whether a dispersion is stable or not does not merely depend on the solvency of the stabilising moieties as in the simplistic explanation given above. The changes in enthalpy and entropy that occur during the particle collision must also be considered. When two particles collide, there is an accompanying change in the free energy of flocculation, ΔG_f. According to the Gibbs-Helmholtz equation, this can be separated into enthalpic (ΔH_f) and entropic (ΔS_f) terms as shown in Equation I.5.

$$\Delta G_f = \Delta H_f - T\Delta S_f \qquad \text{Eq.(I.5)}$$

For sterically stabilized particles to remain stable, flocculation must be energetically unfavourable, i.e. ΔG_f must be positive. There are clearly various combinations of the signs and magnitudes of ΔH_f and ΔS_f which would result in a positive free energy change, these are summarized in Table I-2

ΔH_f	ΔS_f	ΔG_f	Stabilisation Type	Flocculation
+	+	+	Enthalpic	On heating
−	−	+	Entropic	On cooling
+	−	+	Combined enthalpic-entropic	Not accessible

Table I-2. Thermodynamic factors affecting the stability of sterically-stabilized particles.

In principle, a dispersion exhibiting combined enthalpic-entropic stabilization cannot be flocculated at any accessible temperature. However, in practice variations in temperature and/or pressure may lead to a solely enthalpically or entropically stabilized dispersion, where upon the dispersion stability will become susceptible to temperature changes.

The entropic mode of stabilization is predominately observed in non-aqueous (or perhaps more accurately, non-polar) dispersion media at room temperature and pressure. Exclusion of solvent molecules during the overlap, or mixing, of the steric stabilizer layers and the concomitant local increase in polymer segment concentration leads to an unfavourable decrease in ΔS_f. This dominates the unfavourable negative change in ΔH_f, which is a result of the usually endothermic enthalpy of mixing ($\Delta H_{mix} > 0$) found for most polymers in non-polar media.[163] Clearly, though, this entropy term can be reduced by lowering the temperature and in principle, entropically stabilized dispersions can be flocculated on cooling.

Dispersions in aqueous media differ in their behaviour due to strong specific interactions, such as hydrogen bonding, which occur between the solvent and the stabilizing polymer. On overlap and mixing of the steric stabilizer layers, bound solvent molecules must be released. This leads to an unfavourable increase in ΔS_f, but is dominated at room temperature and pressure by a favourable increase in ΔH_f which opposes flocculation. Thus these dispersions are enthalpically stabilized. In these cases, the entropy term can be increased by raising the temperature and hence enthalpically stabilized dispersions can be flocculated on heating.

Thus, broadly speaking, the entropic stabilization mechanism is dominant in non-aqueous media, whilst the enthalpic mechanism is more common in aqueous solvents.

However, this is only a very general statement, and enthalpically-stabilized non-aqueous dispersions and entropically-stabilized aqueous dispersions are known.[164]

Unlike the DLVO theory for charge stabilization, no *ab initio* quantitative theory exists for steric stabilization. This is because any such rationalization would have to be based on theories of the behaviour of polymers in solution, and these are semi-quantitative at best. Furthermore, to determine the distance dependence of a steric stabilizer layer, the conformation of the surface-anchored polymer in solution is required, which cannot be accurately predicted.

However, some rationalization of the distance dependence of steric stabilization is possible, and three domains of interaction can be identified. If we consider the close approach of two particles, the particle surfaces can be considered to be flat, and each covered in a steric stabilizer of thickness L. If the distance between the particles, d, is greater than 2L, then no interaction between the stabilizer layers can occur and there is no change in free energy. This is called the *non-interpenetrational domain*. However, if $L < d < 2L$, then interpenetration of the stabilizer layers occurs, with the accompanying expulsion of solvent molecules in order to accommodate the increased local concentration of polymer segments within this *interpenetrational domain*. If the particles are in a worse-than-θ-solvent, polymer-polymer mixing will result in a favourable decrease in free energy and the particles will remain attracted to each other. If $d < L$, the stabilizer layers not only interpenetrate, but are actually compressed by the surface of the other particle. This is known as the *interpenetrational-and-compression domain*. The free energy change which arises in this situation is a result of not only the change in polymer-solvent interaction, but also an elastic component associated with the compression of the steric stabilizer layer. Compression of the stabiliser layer reduces the configurational entropy of the polymer chains and invariably results in separation of the particles, irrespective of the solvent.

The free energy changes for both the interpenetrational and the interpenetrational-and-compression domains in a better-than-θ-solvent are positive. Furthermore, the elastic component for the interpenetrational-and-compression domain is also positive (regardless of the solvent). Thus repulsion is favoured at all stages of close approach, and these repulsive forces are large enough relative to the attractive van der Waals forces to ensure that no minimum is observed in the potential energy diagram (see Figure I-21) As a result, in good

solvents, sterically stabilized particles are both kinetically *and* thermodynamically stable. This is in contrast to charge stabilized particles, which can only exhibit kinetic stability.

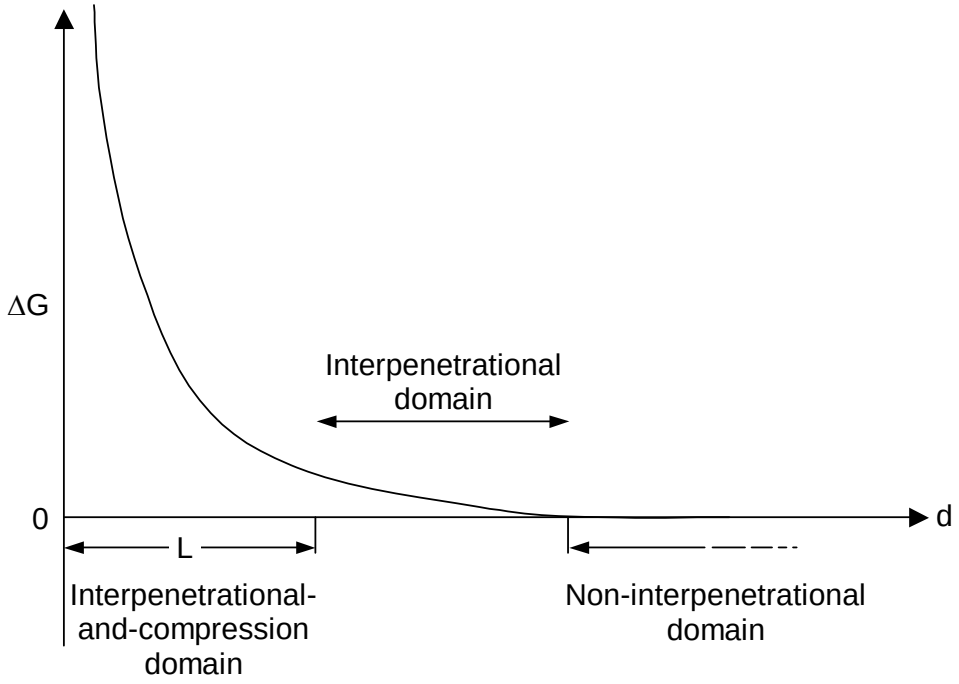

Figure1.21: Free energy curve for a collision between two sterically-stabilized particles in a better than θ-solvent for the steric stabiliser.

However, in worse than θ-solvents, a minimum is observed in the potential energy diagram (see Figure I-22) on entering into the interpenetrational domain. This is because the stabilizer chains prefer to interact with each other rather than interact with solvent, leading to particle flocculation. Therefore, it is this preferred interaction of steric stabilizer layers in worse-than-θ-solvents that causes the flocculation of many sterically stabilized dispersions. Only for thin steric stabilizer layers or very large particles is the ever present van der Waals attraction term sufficiently strong to cause aggregation. The relative unimportance of the van der Waals attraction in inducing the aggregation of many sterically stabilized dispersions is in stark contrast with its dominant role in causing the coagulation of charge stabilized dispersions. It is worth noting, however, that if better-than-θ-conditions are imposed either by adding a good solvent or by changing the temperature, the polymer will expand upon resolvation, leading to particle re-dispersion.

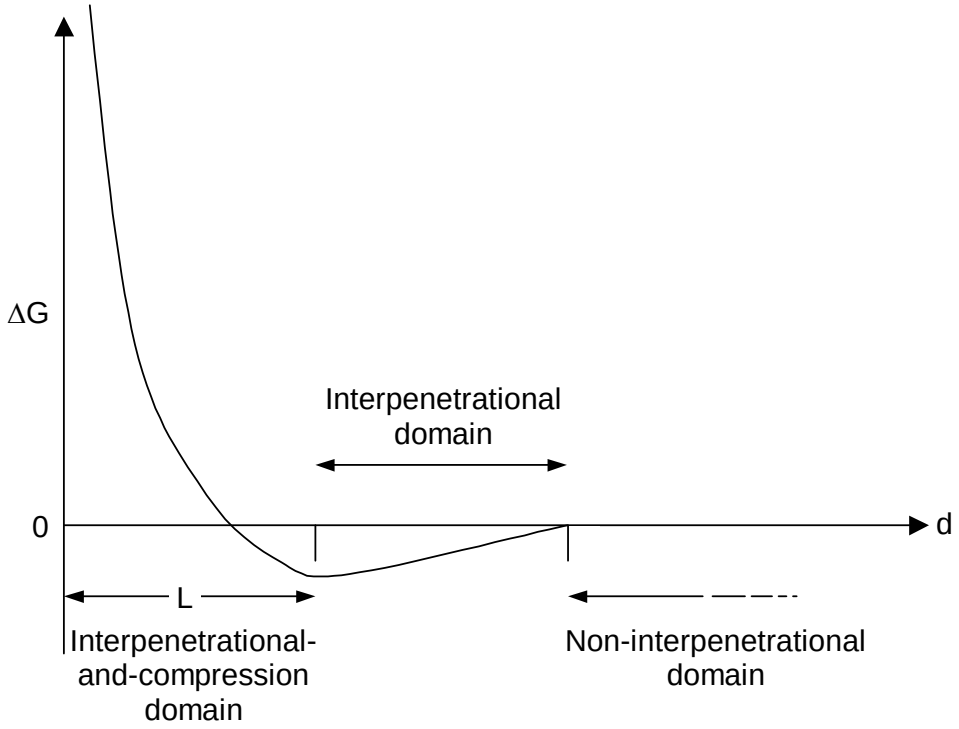

Figure I-22: Free energy curve for a collision between two sterically-stabilized particles in a worse than θ-solvent for the steric stabilizer.

Steric stabilization has several advantages over charge stabilization. Firstly, sterically stabilised colloids in aqueous media are relatively insensitive to the presence of electrolyte, providing of course that the stabilizing polymer is non-ionic. Secondly, as it is not dependent on surface charge, steric stabilization can be highly effective in both aqueous and non-aqueous media. Thirdly, unlike charge stabilized dispersions, sterically stabilized particles can be stable at relatively high solid concentrations (> 50 %). A fourth advantage is that sterically stabilized systems often display good freeze-thaw properties, an attribute which is useful in industrial applications such as latex paints. And finally, unlike charge stabilized particles, there is no potential energy minimum in which irreversible aggregation can occur, and so under suitable conditions sterically stabilized particles may be reversibly flocculated.

II.2. Synthesis of Polymer latexes

There are several different methods for the synthesis of latexes. The choice of which method to use is dictated by the desired particle size, choice of solvent media, and the relative solubilities of the initiator, monomer and polymer with respect to the solvent and to each

other. An in-depth discussion of all these methods is beyond the scope of this work, but the two most important methods (emulsion and dispersion) will be discussed briefly.

II.2.1. Emulsion Polymerization[165]

The main components of an emulsion polymerization, typically carried out in water, are a water-insoluble monomer, a surfactant (also referred to as an emulsifier), and a water-soluble initiator. If shear is applied (i.e. if the system is stirred) an emulsion of micrometer-sized, surfactant-stabilized monomer droplets is obtained. The majority of the monomer will be within these droplets, but a small amount will also be solubilised within surfactant micelles. Generation of free-radicals, typically from persulfate initiators, takes place in the aqueous phase. The mechanism by which the polymerization proceeds is quite complex and has been studied in great depth.[166-168]

Polymerization begins with entry of the radicals into the micelles; this stage is known as micellar nucleation. As polymer particles begin to grow within the micelles, they adsorb more surfactant, thus depleting the amount of surfactant in solution to below the critical micellar concentration. At this point, micellar nucleation ceases, and polymerization occurs only within the nascent monomer-swollen polymer particles. The monomer diffuses from the monomer droplets into the polymer particles, where polymerization continues until the monomer droplets are depleted and eventually disappear. The final polymer particles are typically spherical, between 50 – 500 nm in diameter, and can be of narrow particle size distribution. The particle surface is covered with adsorbed surfactant, which provides the basis for colloidal stabilization. Control of the final particle size, and particle size distribution, can be achieved through variation of reaction parameters such as the relative monomer, initiator and surfactant concentrations, temperature, and even the degree of shear within the system.

Another very useful form of emulsion polymerization is *surfactant-free* emulsion polymerization. It has been shown that by using an excess of persulfate initiator, sulfate-terminated oligomers are generated *in situ* and effectively act as the surfactant species.[169,170] These are subsequently incorporated into the polymer particles. Since the latexes are stabilized by chemically-bound sulfate groups the latexes are easier to purify without loss of colloid stability and retain their stability over a wider range of conditions than the corresponding latexes prepared using added surfactant.[165]

Emulsion polymerization is the most common method of producing latexes on an industrial scale, with vinyl monomers such as styrene, butadiene, vinyl acetate and methyl methacrylate being polymerized for use in paints, adhesives, rubber formulations and paper coatings. The principal advantages of the emulsion process are that polymers of very high molecular weight can be synthesized, and that reactions can be carried through to relatively high conversion.[168] Moreover, emulsion polymerizations are favoured for use on an industrial scale for several practical reasons: firstly, the heat generated by the exothermic free-radical polymerization process can be readily absorbed and dissipated by the aqueous phase. Secondly, since the process is water- rather than solvent-based, safety and environmental hazards, not to mention cost, are significantly reduced.

II.2.2. Dispersion Polymerization [165,171]

In a dispersion polymerization, the monomer, stabilizer and initiator are all soluble in the dispersion medium, resulting in a homogeneous solution at the onset of the reaction. It is within this homogeneous phase that polymerization is initiated. To fulfill the criteria of a dispersion polymerization, however, the newly formed polymer must be *insoluble* in the reaction medium. The growing polymer chains precipitate from solution as some critical chain length is exceeded, which will depend upon the solvency of the medium and the nature of the polymer, and then aggregate to form small particles. These primary particles will be swollen by monomer, and will continue to grow in size due to further polymerization of occluded monomer and also from coalescence with other polymer chains/particles.

Such a polymerization in the absence of any suitable stabilizer would result in coagulation and precipitation. However, the presence of a suitable polymeric stabilizer results in the formation of stable polymer colloids. Dispersion polymerizations can lead to the formation of spherical particles of relatively narrow particle size distribution which are typically 0.1 to 10 μm in diameter. Effective stabilizers for dispersion polymerization tend to be block- or graft-copolymers which exhibit high solubility in the reaction medium and an affinity for the polymer particles. For example, methacrylic polymers with oligostearic grafts have been found to be useful stabilizers for the dispersion polymerization of hydrophobic monomers in hydrocarbons.[181] Suitable homopolymers may also be used, such as poly(*N*-vinylpyrrolidone) or poly(vinyl alcohol) in polar organic solvents, which typically become chemically grafted to the growing polymer chains during polymerisation.[172,173]

Perhaps the most well-documented examples of dispersion polymerization are for styrene and methyl methacrylate in hydrocarbons or lower alcohols. For example, Ober[174] and Almog[175] have reported on the dispersion polymerization of styrene and methyl methacrylate in alcohol, alcohol-ether and alcohol-water mixtures. Other groups have carried out detailed studies on the effects of various reaction parameters on the size of the resultant particles.[172,176] The final particle size (and particle size distribution) in dispersion polymerization depends on many factors, such as monomer and initiator concentration, temperature, the nature and concentration of stabilizer, and the solvency of the polymerization medium. Since these early studies, various developments and applications have been investigated, such as the synthesis of porous particles,[177] coloured particles[178] and surface-functionalized particles.[179] Dispersion polymerization, however, is not used on an industrial scale to the same extent as emulsion polymerization. This is primarily due to the safety and environmental factors that must be considered, as well as the increased cost, when using organic solvent- rather than water-based systems on an industrial scale

II.3. Sterically Stabilized Conducting Polymer colloids

Since 1986, there have been many reports on dispersions of sterically-stabilized conducting polymer particles. Typically, aqueous polymerizations are carried out in the presence of a water-soluble polymer, which becomes physically adsorbed onto nascent conducting polymer particles precipitating from solution. Thus, the precipitation polymerization becomes a dispersion polymerization (see Figure I-.23).

Various commercially available water-soluble polymers have been employed as steric stabilizers, including cellulosics,[180-184] poly(vinyl alcohol),[185-189] poly(methyl vinyl ether)[190,191] and poly(*N*-vinylpyrrolidone).[185,188,192] Particle sizes are typically 100 – 300 nm and, despite the presence of an insulating layer of stabilizing polymer, pressed pellet conductivities are often more than 1 S cm^{-1}).

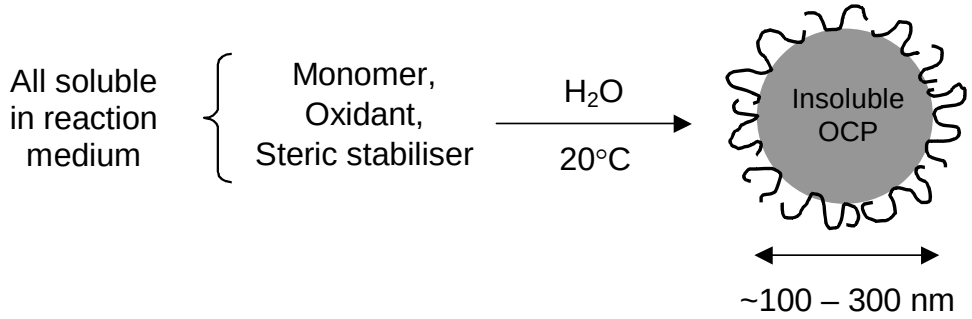

FigureI-23: Schematic formation of sterically-stabilised conducting polymer particles by aqueous dispersion polymerisation.

II.3.1. PANI dispersions

PANI, like other conducting polymers, are insoluble or only partially soluble in most common organic solvents (viz. alcohols, chloroform, benzene, xylene, DMF, DMSO, etc.) and therefore, is difficult to process, hindering commercial utilization of this polymer. Therefore, the objective of bringing this untractable polymer in an easily processable form has initiated a lot of investigations that give rise to hybrid materials named as composites with interesting properties. The latter are successful combination of polyanilines with different processable insulating polymers so their complementary properties can be taken together.

Among different techniques for the synthesis of conducting composites, the dispersion polymerization, following a steric stabilization mechanism is a widely accepted route that lead, after drying, to microstructured composites, composed of electrically-conducting particles of sub-micrometer size dispersed in an insulating polymer matrix.

In dispersion polymerization, macroscopic precipitation of the polymer is prevented (in contrast to precipitation polymerization) and sub-micrometer dispersion particles are obtained. Poly(*N*-vinylpyrrolidone) [193,194], poly(styrenesulfonic acid) [185,196], poly(ethylene oxide) [197-200] poly(methyl vinylether) [201,191], cellulose ethers, namely methylcellulose [202,182], hydroxylpropylcellulose [203] and ethyl(hydroxyethyl)cellulose [204], poly(acrylic acid) [205,206] and poly(vinyl alcohol) [207-214] have all been employed for the stabilization of PANI colloids produced in aniline dispersion polymerization. The preparation of spherical PANI particles of a good uniformity has also been described, when colloidal silica was used for the steric stabilization [215, 216]

The most effective stabilizers employed for forming PANI colloids, however, are *reactive* stabilizers, which become chemically grafted to the particle surface. A range of such stabilizers have been reported in the literature. In some cases the stabilizers have been formed by chemical modification of existing polymers[217] or by anionic polymerisation.[218] A commonly used method involves the free radical polymerization of 4-aminostyrene with water soluble co-monomers such as 1-vinylimidazole,[219] 2-vinyl pyridine[220] or *N*-vinylpyrrolidone[221] thus giving a stabilizer with pendant aniline groups. These groups participate in the subsequent aniline polymerization, leading to the copolymer stabilizer becoming chemically grafted to the growing PANI particles.

Polyaniline particles of spherical, rice-grain, or needlelike morphology have been described. DeArmitt et al.[221] observed that the particle morphology (spherical or rice-grain) depends on the oxidant nature. Thus $(NH_4)_2S_2O_8$ oxidant produces spherical particles while KIO_3 leads to the formation of "rice-grain"-shaped particles. Vincent *et al*.[199] tested the effect of the stabilizer architecture; stabilization by poly(ethylene oxide) yielded needle-like PANI particles, while graft-copolymer stabilizer based on poly(ethylene oxide) produced PANI spheres. Nagaoka *et al*.[222,223] reported that needle-like structure was produced when poly(vinyl alcohol) was used for the steric stabilization, while a sodium polystyrenesulfonate, produced spherical PANI particles. The deviations from the spherical shape after polymerization temperature increase have been reported for PANI dispersion stabilized with colloidal silica [224] and hydroxypropylcellulose (Figure I-24).[205]

A similar change in particle shape could also be obtained at 0ºC by the acceleration of PANI formation via addition of *p*-phenylenediamine to increase the rate of polymerization (Figure 1.25). Chattopadhyay *et al*.[204] found that the morphology of PANI particles stabilized by methylcellulose could be controlled by the composition of the ethanol-water mixture.
Generally, the behaviour of these systems is now well understood and Gospodinova and Janca[225] have claimed that, by judicious control of reaction conditions, PANI dispersions can be prepared with particle size distributions at least as narrow as, but in most cases narrower than, commercially available uniform polystyrene latex standards.

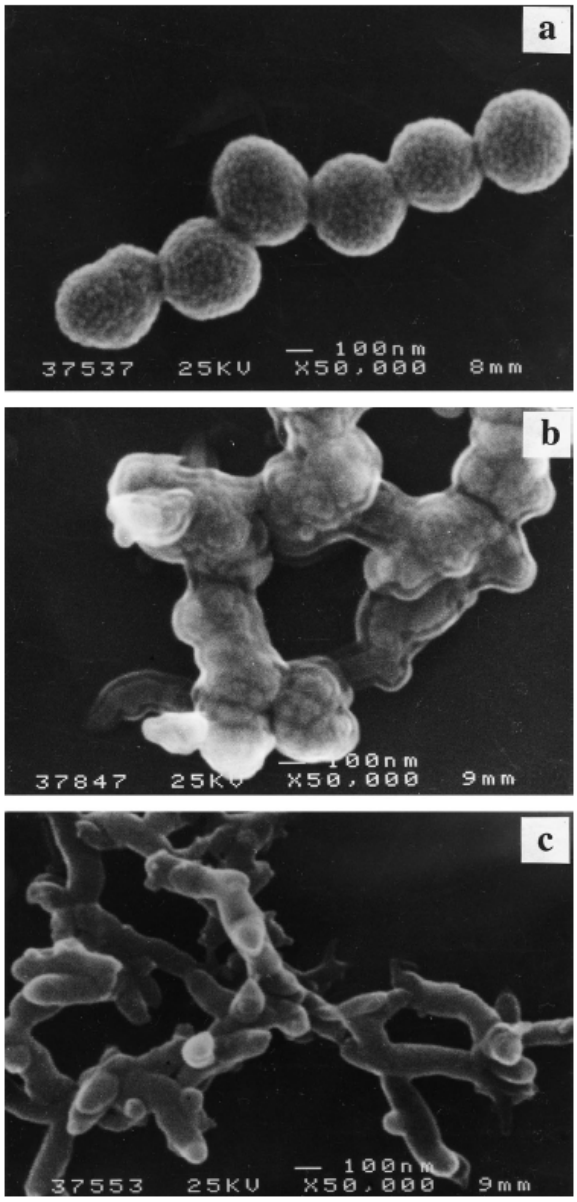

Figure I-24: Particles formed in dispersion polymerization of anilinehydrochloride at (a) 0°C; (b) 20°C; and (c) 40°C.[203]

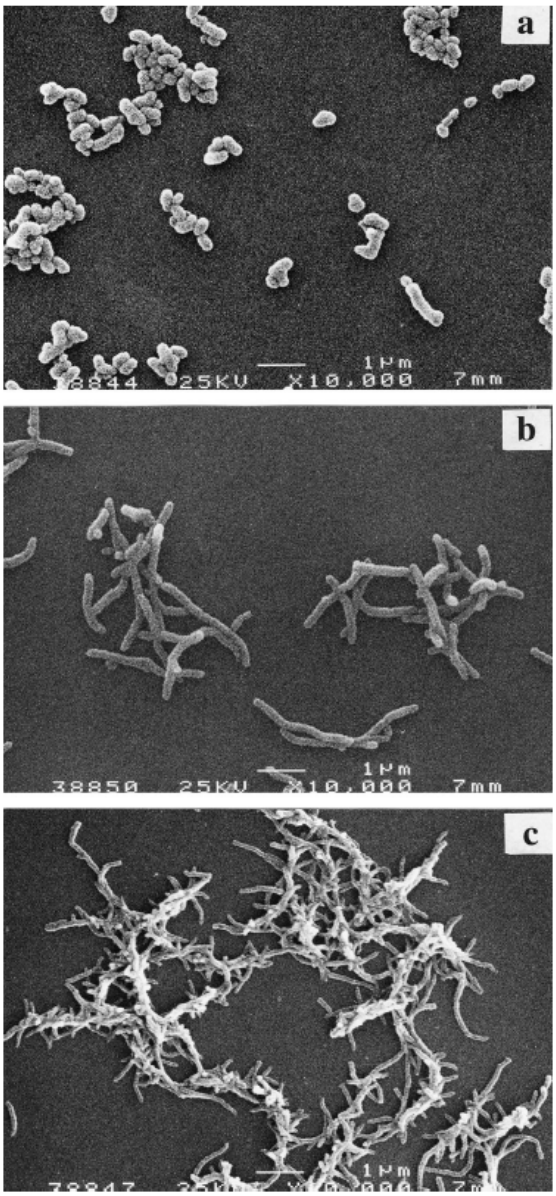

Figure I-25: Products of the dispersion polymerization of aniline hydrochloride (0.2 M) accelerated by addition of (a) 2.3×10^{-5} M; (b) 2.3×10^{-4} M; and (c)2.3×10^{-3} M *p*-phenylenediamine dihydrochloride at 0°C.[203]

The majority of PANI colloids are produced via chemical oxidation. However, there has also been a limited amount of research on the electrochemical production of such particles. Wallace and co-workers[226,227] have developed a technique utilizing an electrochemical flow cell to synthesize PANI or PPY colloids. This approach is based on the fact that electropolymerization is initiated in solution, rather than at the electrode surface, and that the use of steric stabilizers hinders the deposition of the conducting polymer on the

anode. The potential advantages of such a method over chemical routes include: (i) greater quantitative control over the oxidation process and (ii) wider range of counterions that can be incorporated into the polymer at the synthesis stage. This latter advantage was used to synthesize *chiral* PANI particles. By polymerizing aniline in an electrochemical cell in the presence of (1R)-(-)-camphorsulfonic acid [(-)-HCSA] or (+)-HCSA and using PEO as a steric stabilizer, Wallace *et al*.[228,229] obtained a PANI dispersion that exhibited optical activity depending upon which enantiomer of HCSA was used as the dopant species.

Stable PANI dispersions can also be prepared using ultrafine colloidal silica particles as a stabilizer. Silica of 7 and 22 nm diameter has been used for the synthesis of PANI colloids by Gill *et al*.[230-232] The resulting dispersion of sub-micrometer size had a distinct raspberry morphology. Stejstkal *et al*[224] also prepared PANI-silica particles under various conditions. It was found that polymerizations carried out between 0°C produced stable spherical particles of reasonably narrow polydispersity (see Figure I-26). However, at room temperature, the formation of PANI became too fast and only ill-defined, polydisperse particles were formed.

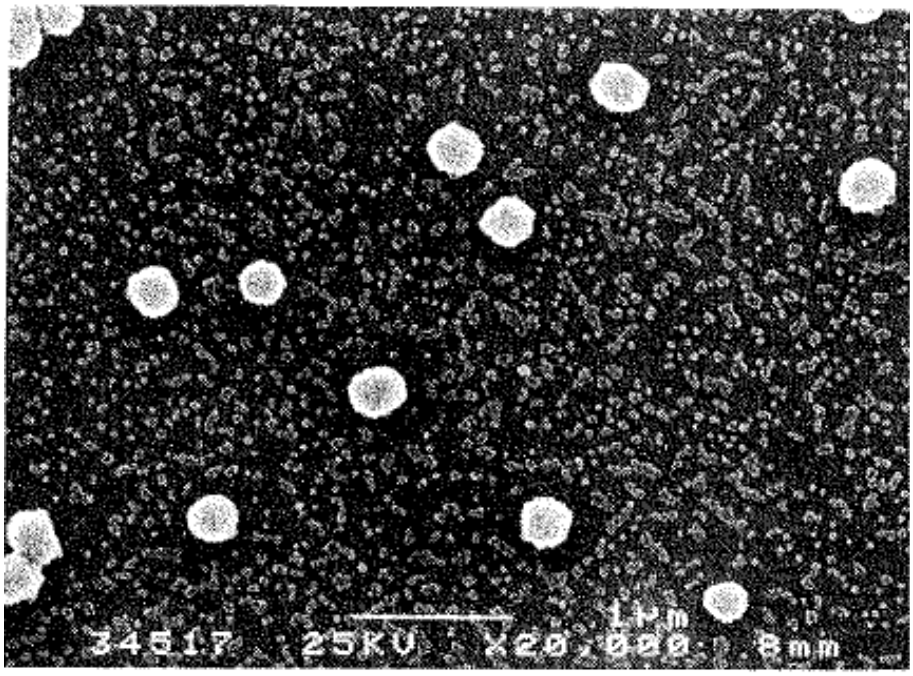

Figure I-26: Polyaniline particles stabilized with a particulate stabilizer, ultrafine nanocolloidal silica. Free silica is visible on the background.[224]

When the concentration of silica was sufficiently high, the composite particles in the diameter range of 300-600 nm wee obtained. The raspberry morphology is well seen especially when silica particles of larger diameter have been used.

An alternative route to forming colloidal dispersions of conducting polymers involves coating sterically-stabilized latex particles with an ultrathin overlayer of conducting polymer, thus forming composite particles with a *core-shell* morphology. The advantage of this approach is that far less conducting polymer is required to obtain particles with useful electrical properties. Moreover, the intractable conducting polymer is now the *minor* component, typically only 5 to 20 % by mass.

Beadle *et al*.[233] polymerized aniline in the presence of commercially available chlorinated copolymer latex particles of 200 nm size. The featureless morphology of the film produced latex changed to distinctly globular as the concentration of the PANI increased. Barthet *et al*.[234,235] coated PS latexes with PANI. However, surface coverages of only 60% could be achieved in this case, and the PANI overlayers appeared far rougher by SEM than their relatively smooth PPY counterparts at equivalent loadings. Disc centrifuge measurements clearly showed that the degree of particle flocculation increased with conducting polymer loading for both PPY-PS and PANI-PS latexes[234,236] This would be expected as thicker PANI overlayers would disrupt the stabilization imparted by the PNVP steric stabilizer on the latex surface.

II.3.2. Polypyrrole dispersions

Unlike in polyaniline case, where particles generally deviate from spherical morphology, usually spherical particles are obtained during dispersion polymerization of pyrrole. Many water soluble stabilizers like poly(vinyl alcohols),[185,186,237] poly(styrenesulfonate),[238] ethyl(hydroxyethyl)cellulose,[239] poly(ethylene oxide),[240-243] poly(methyl vinyl ether), [244,245] poly(vinylpyrrolidone),[185] etc., tailor-made reactive stabilizers,[246] polymer latexes,[247] surfactants[248] and silica particles[249] have been extensively used for the synthesis of polypyrrole dispersions.

II.3.2.1. Polypyrrole dispersions stabilized by polymer steric stabilizers

In the case of PVA stabilizer, the rate of addition of pyrrole affects the particle size; slower feed-rate leads to the formation of larger particles [185]. It was reported that the addition of an aqueous solution of initiator to a stirred solution of pyrrole and stabilizer led to non-spherical particles and varying the water/ethanol ratio did not lead to any systematic trends in particle size variations. Saunders *et al*.[237] prepared PPy/PVA particles having size about 145 nm. The conductivity of PPy/PVA is two orders of magnitude lower than that reported by Armes *et al*.[186] for a similar material. The use of PVA with a higher nominal molecular weight in the present work (cf. Armes *et al*.[186]) and the relatively poor air stability[186] of PPy doped with chloride would be factors contributing to the conductivity differences observed between the different groups. Adsorption of PVA with a higher molecular weight should result in a thicker non-conducting sheath about the PPy particles and decreased conductivity.

Pickup and Qi [238] reported that the presence of PSS in the reaction medium allows the size of chemically synthesized PPy/PSS particles to be controlled by varying the concentration of the Fe(III) oxidant (the higher the concentration, the smaller the resulting polymer particles) (see Figure I-27).

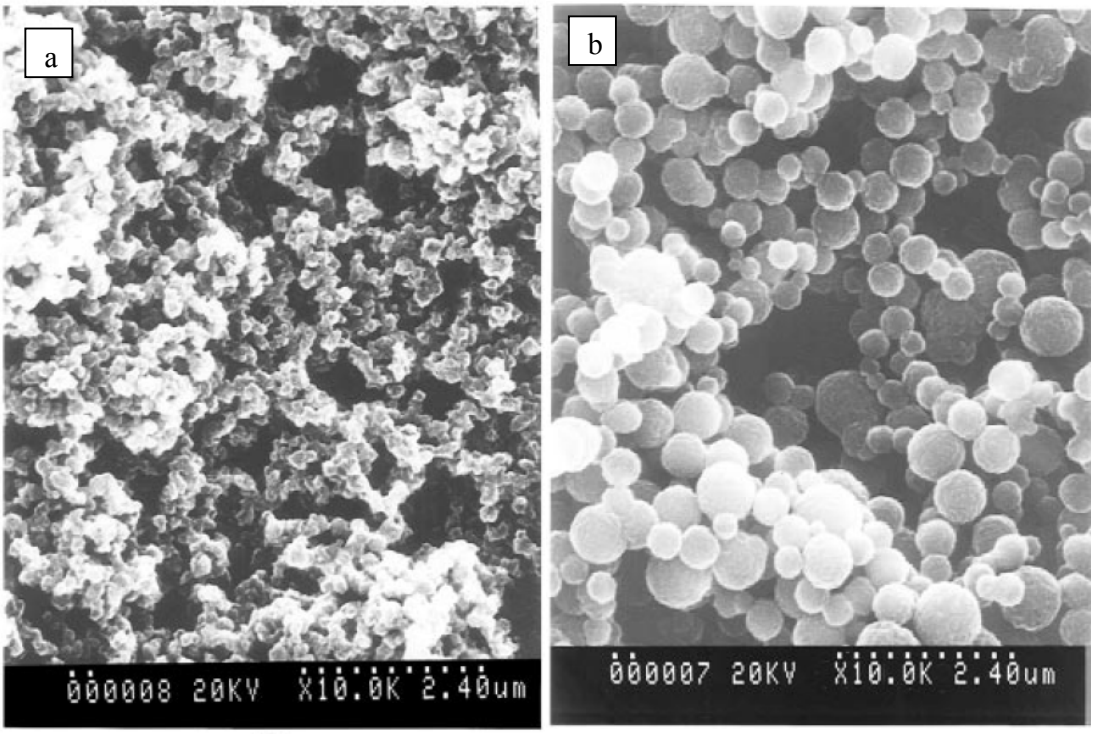

Figure I-27: Scanning electron micrographs of PPy/PSS samples prepared using different concentrations of the oxidant (a) 0.15 moles and (b), 0.05 moles of $FeCl_3$.[238]

Mandal and Mandal[239] found that in aqueous ethanol solution small and large particles (about a factor of ten larger) are formed during oxidative polymerization of pyrrole in the presence of ethylhydroxycellulose (EHEC) when $FeCl_3$ is used. But only large particles were obtained, when ammonium persulfate (APS) was employed as an oxidant. However, in pure water, small particles were not found, irrespective of the oxidant used. Additionally the particle size was found to decrease with an increase in molecular weight of the EHEC for the same stabilizer concentration.

Although PEO has been reported to stabilize the dispersions in many cases,[240-243] this polymer and its block copolymers have been found inefficient in some cases probably due to their low adsorption affinity; unless a very high molar mass PEO was used. Cawdery *et al*.[243] prepared PPy stable dispersions using high molecular weight PEO ($M>10^5$). The size of the particles ranges from 445±45 nm to 350±40 when the molecular weight of the stabilizer increases from 3×10^5 to 4×10^6 g/mol which is significantly higher than those produced using PVA or PNVP as stabilizer. With the latter stabilizer, the particle size is typically in the range 70-150 nm. Clearly, these data reflect the much weaker adsorption affinity for PEO on PPy surface. In case of PVA or PNVP, there is a possibility of hydrogen bonding between N–H of the pyrrole moieties on the PPy surface and C=O of pyrrolidone or acetate moieties of the stabilizer chains. They further showed that charge-stabilized PPy particles could be obtained by removing the adsorbed poly(ethylene oxide) stabilizer layer from particles by repeated centrifugation/redispersion cycles, providing the particles were redispersed in a solvent of high dielectric constant (e.g. water, methanol) where interfacial charge may be maintained. Moreover, the particles could then be redispersed in a medium of low dielectric constant using the stabilizer of choice.

Mandal *et al*. synthesized [244] PPy particles at room temperature by oxidative polymerization using $FeCl_3$ oxidant in the presence of poly(vinyl methyl ether) (PVME) as a stabilizer, and ethanol or aqueous ethanol as the dispersion medium. With water as dispersion medium, lower temperatures are required to ensure a steric stabilization. PPy prepared in 50% ethanol or in water exhibits high specific conductivity, about 10 S cm^{-1}, while PPy prepared in ethanol under similar conditions has conductivity two to four decades lower, depending on the temperature and the $FeCl_3$ concentration used in the preparation. Transmission electron micrographs of PPy reveal that the particles are spherical but polydisperse. Pich *et al*.[245] reported the synthesis of PPy dispersions in the presence of PVME and cross-linked PVME

microgels using $FeCl_3$ as an oxidant and water or aqueous ethanol as a dispesion media. They found that the architecture of the polymeric stabilizer in the reaction medium has a strong influence on the morphology of particles formed during oxidative polymerization of pyrrole. In the case where uncross-linked PVME was used as a stabilizer, small spherical particles in the range of 50–100 nm were formed in both aqueous ethanol and water. On the other hand, when cross-linked PVME microgels were used in the same reaction procedure, large PPy fibrils were formed (see Figure I-28). Needle-like particles were formed due to the porous structure of microgels, which play a template role in the pyrrole polymerization process. They predict that the dimensions of the PPy fibrils can be controlled by changing the pore size of the microgel particles and adjusting the polymerization rate.

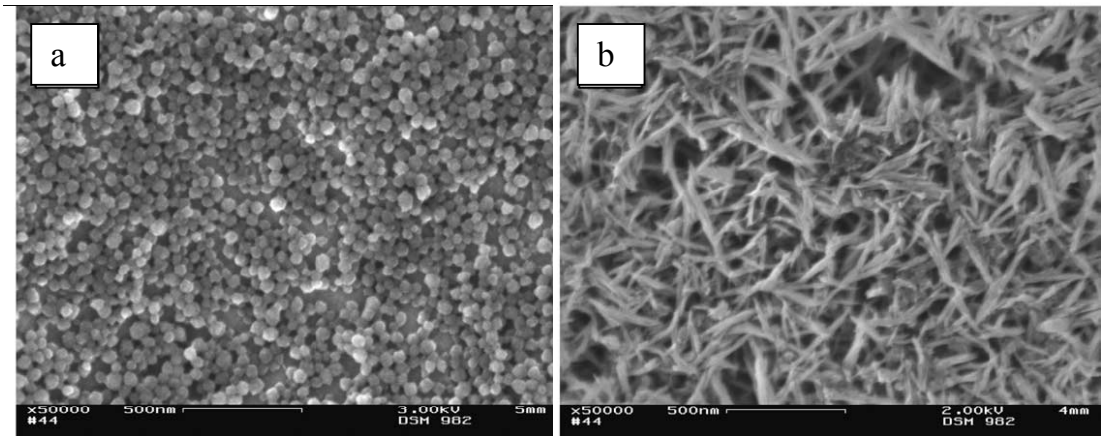

Figure I-28: SEM images of PPy dispersions prepared using (a) un-crosslinked PVME and (b) crosslinked PVME microgel in similar reaction conditions.[245]

II.3.2.2. Polypyrrole dispersion stabilized by tailor-made reactive polymeric stabilizers

All of these examples utilize commercially available polymers as steric stabilizers. However, there have also been examples of the use of tailor-made polymers for stabilization, such as the use of a poly(2-vinyl pyridine-co-*n*-butyl methacrylate) random copolymer by Armes and Aldissi[250]to stabilise PPy particles. Another study by Beadle *et al.*[251] used a poly(2-(dimethylamino)ethyl methacrylate-b-*n*-butyl methacrylate) block copolymer stabilizer of narrow molecular weight distribution to give PPy colloids with surprisingly high stabilizer contents of 54 wt%.

The more useful tool to prepare stable PPy dispersion is the use of reactive polymeric stabilizers. Ishizu and co-workers[252] utilised a PVA stabiliser with pendant pyrrole groups to

create PPY colloids with a very narrow particle size distribution. A different approach was used by Simmons *et al*.[253], who prepared a series of reactive stabilizers by the statistical free radical copolymerisation of 2-(dimethylamino)ethyl methacrylate (DMAEMA) with various (bi)thiophene comonomers. These authors found that in the presence of a suitable oxidant such as $FeCl_3$, the pendant (bi)thiophene groups became oxidized. The activated groups then acted as initiation sites for the subsequent pyrrole polymerization, thus leading to chemical grafting of the stabiliser onto the nascent PPy particles. Spherical PPy particles of 100 nm diameter were prepared (See Figure I-29). The particles size could be reduced to 50-60 nm using an oligo(ethylene oxide) methacrylate-based co-polymer stabilizer. In order to verify that the (bi)thiophene moieties were essential, DMAEMA homopolymer was employed as a stabilizer and there was no colloid formation observed.

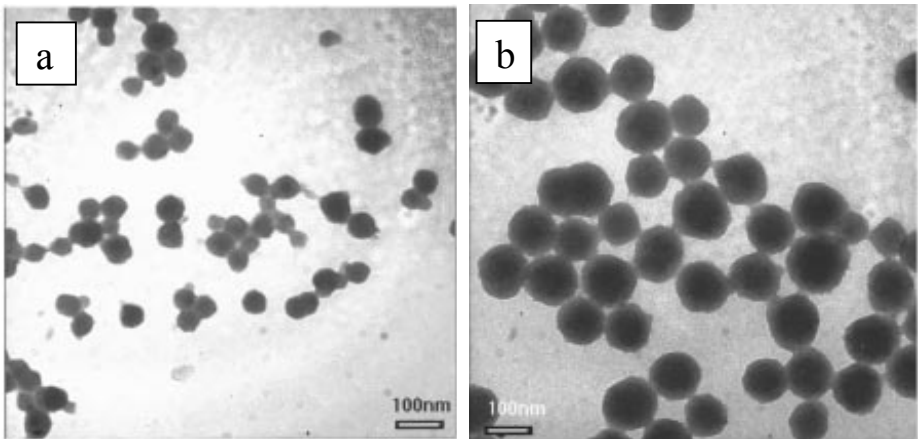

Figure I-29: Typical transmission electron micrographs of polypyrrole particles synthesized using the following stabilizer-oxidant combinations: (a) a OEGMA-3VT stabilizer with $FeCl_3$.(b) a DMAEMA-3VT stabilizer with $FeCl_3$.[253]

II.3.2.3. Polypyrrole dispersions stabilized by colloidal silica particles

PPy nanocomposites can also be prepared by using ultrafine silica colloidal particles. Since their discovery in 1993, Armes and various co-workers have published extensively on the subject of PPy-silica colloidal nanocomposites.[254-256] It was found that when pyrrole was chemically polymerized in the presence of an ultrafine (~20 nm diameter) silica sol, the silica particles became coated with the nascent PPy and, above a certain minimum silica concentration, aggregated to form colloidally stable dispersions of PPy-silica particles with a distinctive 'raspberry' morphology (see Figure I-30). These nanocomposites were typically about 100 - 300 nm in diameter, with relatively narrow particle size distributions. Pressed-pellet conductivities as high as 4 S cm^{-1} were reported, despite the presence of up to 30 wt%

electrically insulating silica. The characteristics of the nanocomposite particles could be controlled by varying synthesis parameters such as the initial silica concentration, an increase in which leading to a reduction of particle diameter. The choice of oxidant was also shown to be very important – using $FeCl_3$ led to particles with diameters of 160–230 nm and PPy contents of up to 70 wt%, whereas using $(NH_4)_2S_2O_8$ led to smaller particles of 110 – 180 nm with lower PPy contents of between 37 – 55 wt%.

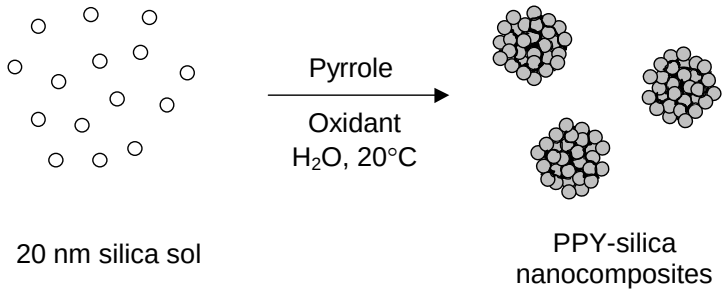

Figure I-30: Schematic formation of colloidal PPy-silica nanocomposites from the original silica sol.

II.3.2.4. Polypyrrole coated sterically-stabilized particles

An alternative route to forming colloidal dispersions of conducting polymers involves coating sterically-stabilised latex particles with an ultrathin overlayer of conducting polymer, thus forming composite particles with a *core-shell* morphology. The advantage of this approach is that far less conducting polymer is required to obtain particles with useful electrical properties. Moreover, the intractable conducting polymer is now the *minor* component, typically only 5 to 20 % by mass.

In 1987, Yassar *et al*.[257] reported the chemical synthesis of PPy in the presence of a 130 nm diameter sulfonated PS latex which was claimed to result in core-shell particles. Similar results were achieved by Liu *et al*.[258] in which 250 - 350 nm styrene-butadiene latexes were coated with PPy using the H_2O_2-HBr-Fe^{3+} oxidant system. However, in these early papers, the particles were not extensively characterized and the proposed core-shell morphology was not proven. Furthermore, little mention was made of the colloidal stability of the latexes after coating. Workers at DSM Research in the Netherlands[259,260] showed that a 60-100 nm diameter sterically stabilized polyurethane latex could be coated with PPY in aqueous

media and the particles still retained a reasonable degree of colloidal stability. Solid state conductivities were in the range 10^{-5}-10^{1} S cm^{-1} depending on the conducting polymer loading. Non-ionic stabilizers such as PEO were reported to be essential to prevent latex flocculation at the high Fe^{3+} concentrations required for the OCP formation. Using dielectric constant data in conjunction with TEM images, it was shown that the PPy was at the surface of the particles. In spite of the encapsulation of the low T_g latex core by an outer layer of high T_g conducting polymer, these particles have been shown to exhibit good film-forming properties and are marketed by DSM in the fields of anti-corrosion and anti-static coatings under the trade name of Conquest®. Subsequent work on the morphology of the PPy overlayer coated onto 710 nm poly(butyl methacrylate) latex revealed a smooth shell at low PPy loadings, but increasing roughness as the conducting polymer loading was increased.[261] These particles exhibited a sharply defined percolation threshold at only 0.25 wt%.

In recent years, Armes and co-workers have carried out a great deal of research on the coating of micrometer-sized polystyrene (PS) latexes with conducting polymers. Using a modified DSM protocol, Lascelles and Armes [262,263] coated a 1.8 μm diameter poly(*N*-vinyl pyrrolidone) [PNVP]-stabilised PS latex with PPy. The PPy loading could be varied over a wide range simply by varying the initial PS latex concentration. Conductivities as high as 2 S cm^{-1} were achieved for composites containing as little as 5.1 wt% PPy. Extensive surface characterization of these particles confirm that the PPY form a homogeneously encapsulating layer over the underlying PS latex, with surface coverages of 95-100% as determined by XPS.[264,265] Disc centrifuge measurements clearly showed that the degree of particle flocculation increased with conducting polymer loading for PPY-PS latexes.[264] This would be expected as thicker OCP overlayers would disrupt the stabilization imparted by the PNVP steric stabilizer on the latex surface.

Attempts to coat submicrometer-sized PS latexes with PPY were less successful. Cairns *et al*.[266,267] found that PPY deposition onto a 140 nm PEO-stabilized PS latex did not result in the anticipated 'core-shell' particles. Instead, a combined SEM, TEM, XPS and DCP study showed that the PPy was deposited as 10-20 nm nanoparticles onto the PS latex, leading to weak heteroflocculation. It is likely that this unexpected outcome was caused by one or more of the following three factors: (1) the PPy grain size is around 10 nm[268] which is larger than the target PPy overlayer thickness of 5 nm; (2) the PEO steric stabilizer may have too low molecular weight; (3) the PS particles were prepared via emulsion polymerization using an anionic initiator [$(NH_4)_2S_2O_8$], which may lead to a relatively hydrophilic latex surface

limiting coating with PPy.[269] It is noteworthy that several characteristics of this PPY-PS system are shared by the PPy-PU latexes described by DSM. Moreover, DCP analyses of these two dispersions are remarkably similar.[270] This suggests that DSM's PPy-PU particles may in fact also be heteroflocculated, rather than genuine discrete core-shell particles.

II.3.2.5. Polypyrrole dispersion prepared using surfactants

Small molecule surfactants have also been employed as stabilizers. The first reported example was by DeArmitt and Armes[271]in 1993, in which PPy dispersions stabilized by an anionic surfactant, sodium dodecylbenzenesulfonate, were prepared.

II.3.3. PEDOT dispersions

The first example of dispersion polymerization of EDOT is the so-called BAYTRON-P synthesis developed at Bayer AG.[126] In this method, EDOT is chemically polymerized using $Na_2S_2O_8$ in an aqueous solution containing poly(4-styrene sulfonate sodium salt) [PSS] at room temperature. This results in a dark blue, aqueous PEDOT/PSS dispersion (see Figure I-31), which is commercially available from Bayer as a solution with PEDOT and PSS contents of 0.5 and 0.8 wt%, respectively.[272]

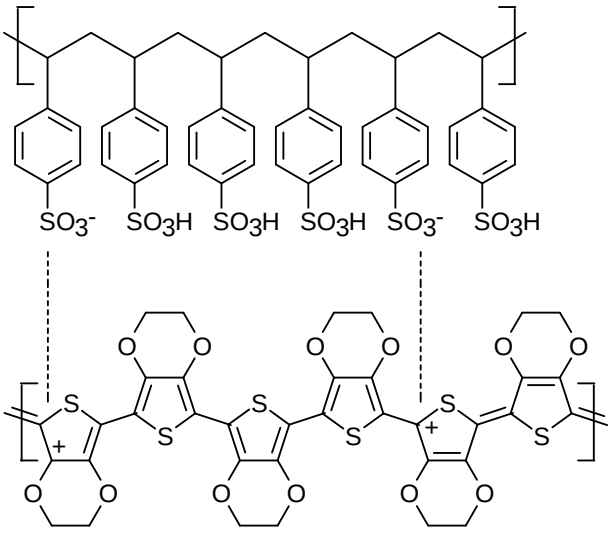

Figure I-31: Schematic representation of PEDOT/PSS structure.

The solution can be used to coat a substrate and, after drying, results in a durable, insoluble, conductive film which is transparent with a slight blue tint. This makes the

PEDOT/PSS system ideal for imparting anti-static properties onto insulating substrates such as plastic or glass, and currently more than 10^8 m^2 of photographic film are coated in this way every year.[9] Kim *et al*.[273] studied the effect of different solvents (H_2O, THF, DMF and DMSO) on the conductivity of the PEDOT/PSS films and reported that the conductivity increases from 0.8 S/cm in water to 80 S/cm in DMSO. The increase in conductivity of PEDOT/PSS films by the addition of N-methyl pyrrolidone (NMP) and DMSO was also reported by Louwet[274] and Sun *et al*.[275] respectively. However, it has been described that in organic light emitting devices (OLEDs) the ITO/PEDOT:PSS is not stable due the etching of ITO as a consequence of the strong acidic nature of PSS.[276] The degraded surface can act as a defect site and lead to deterioration of the device performance, especially its long term stability.[277]

Recently, Sun and Hagner[278] developed a polyelectrolyte-based preparative route to composited nanowires based on PEDOT conducting polymer, involving chemical polymerization of EDOT monomer using $FeCl_3$ as an oxidant in the presence of a poly(acrylic acid) (PAA). This polymerization process leads to water-dispersible, wire-like nanocomposites, namely, nanowires which are about 20 nm in diameter and several hundred nanometers in length (Figure I-32)

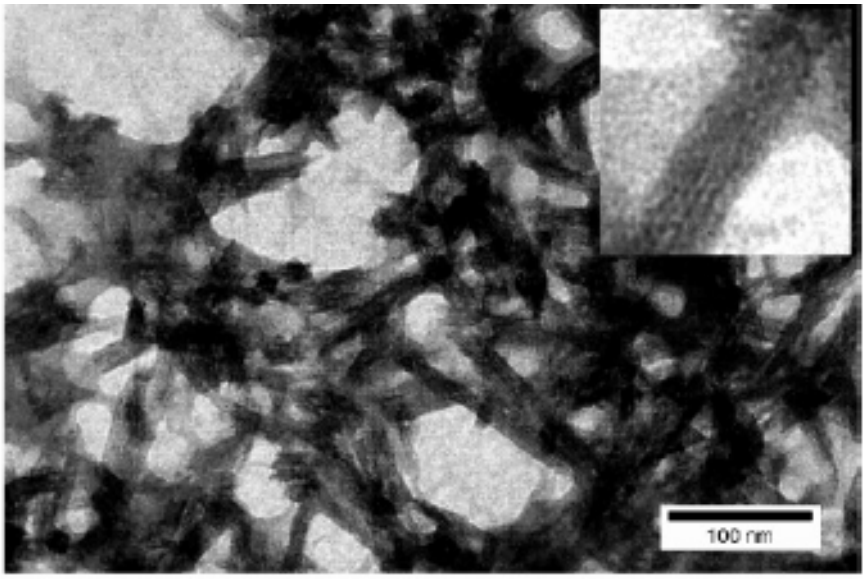

Figure I-32: TEM image of the PEDOT nanowires produced prepared in the presence of PAA.[278]

There are some reports on the synthesis of PEDOT nanparticles in the presence of surfactants. [279-281] Im *et al.* have prepared PEDOT particles in micellar solution templates using sodium dodecylbenzene sulfonic acid (DBSA) as a surfactant and $FeCl_3$ /$Na_2S_2O_8$ as an oxidant in aqueous media.[280] However, in this case, PEDOT particles were poorly defined and showed tendency to form aggregates (Figure I-33). Saunders and co-workers[279] synthesized PEDOT particles with narrow size distribution using short chain alcohol ethoxylate surfactants. More recently, Dai *et al*.[281] prepared PEDOT nanoparticles using conductive poly[2-(3-thienyl)-ethoxy-4-butylsulfonate] (PTEB) as surfactant for the emulsion polymerization of PEDOT. These particles show large size distribution (Figure I-34).

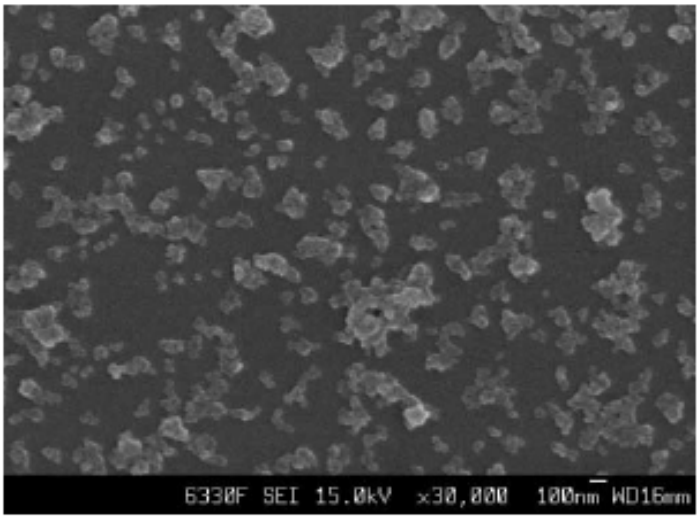

Figure.I-33: SEM image of PEDOT particles prepared from APS–DBSA system (DBSA conc. 0.044 M).[280]

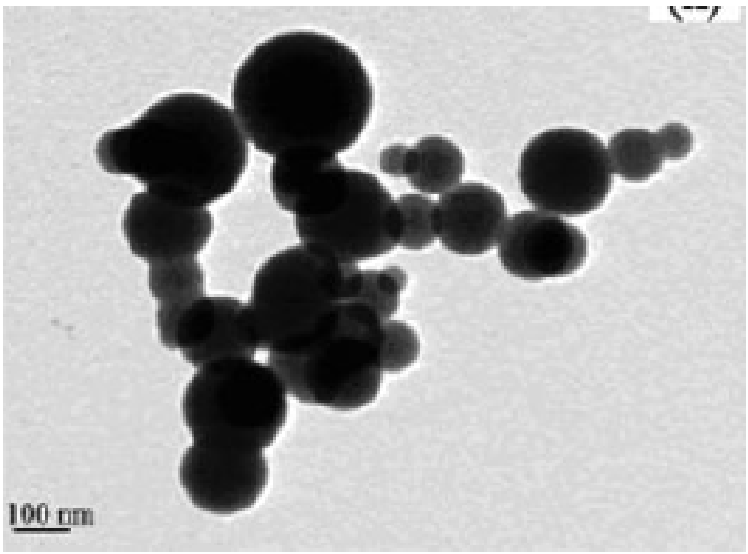

Figure I-34: PEDOT particles prepared using10 wt % of H-PTEB to EDOT.[281]

In their attempt to prepare PEDOT dispersions in organic media, Marcilla *et al*.[282] first polymerized EDOT in aqueous media in the presence of a polymeric ionic liquid (PIL), poly(1-vinyl-3-ethylimidazolium bromide). By addition of bispentafluoroethanesulfonimide lithium salt, the PIL stabilizer becomes hydrophobic and precipitates in water and traps the conducting polymer microparticles inside. The dispersion of the recovered powders in organic solvents leads to organic conducting dispersions. The authors mentioned nothing about the morphology of the PEDOT particles. On the other hand, Müllen *et al*.[283] reported the synthesis of PEDOT nanoparticles by emulsion system consisting of cyclohexane as the continuous phase and acetonitrile as the dispersed one in the presence of polyisoprene-block-poly(methyl methacrylate) copolymer as emulsifiers.

In another approach, the syntheses of PEDOT-coated polystyrene particles and PEDOT-coated silica particles have been reported by Khan *et al*.[284]and Han *et al*.[285] respectively. Recently, Zhang *et al*.[286]described the synthesis of PEDOT nanotubes using aluminum oxide templates. To our knowledge, the synthesis of well-defined PEDOT nano-objects using steric and reactive stabilizer has never been described in the literature and thus would be one of our objectives in this PhD.

II-3.4. Polythiophenes and poly(3-hexylthiophene) dispersions

There are very few examples of dispersion polymerization of thiophene and 3-hexylthiophene. Recently, Jung *et al*.[287] described the synthesis of core-shell poly(styrene/thiophene) latex particles by the oxidative polymerization of thiophene monomers during the emulsifier-free emulsion polymerization of styrene monomers using the different polymerization rate of each monomer. Growing and pre-existing poly(St/NaSS) latex particles provide polymerization loci for the growing oligomers of thiophene to polymerize with monomers or other oligomers. To confirm core-shell morphology of the resulting particles, they were exposed to a chloroform ($CHCl_3$) solution for 15–20 hrs to remove the polystyrene cores. The crumpled poly(thiophene) shells corroborates the core-shell morphology of the resulting latex particles (See Figure I-35).

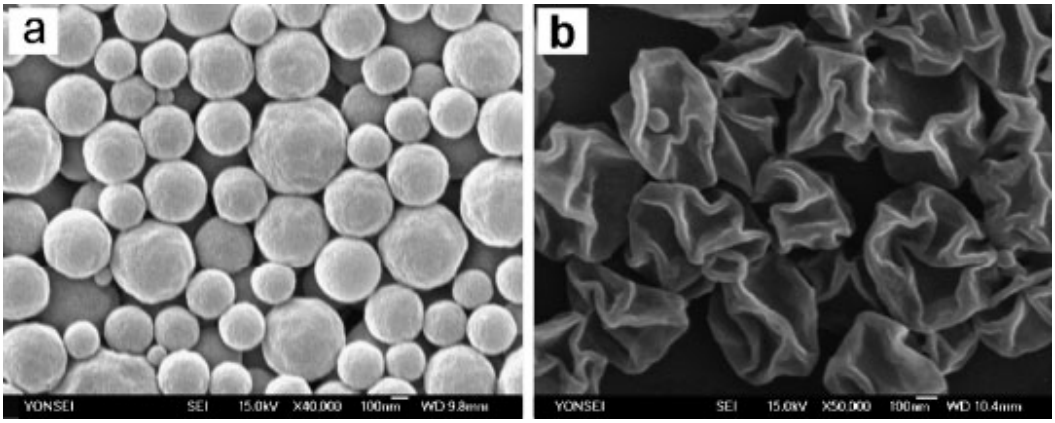

Figure I-35: SEM images of (a) core-shell poly(styrene/thiophene) latex particles (b) crumpled polythiophene shell layer of poly(styrene/thiophene) latex particles.[287]

Karim *et al*.[288] on the other hand, demonstrated a novel route to synthesize a new morphology, micrometer particle sizes of buckyballshaped giant spherical conducting polythiophene, by the *in-situ* gamma radiolysis chemical oxidative polymerization of thiophene (see Figure I-36). Different structural characterizations including electron microscope images and spectroscopy analysis data clearly indicated the formation of spherical conducting polythiophene particles.

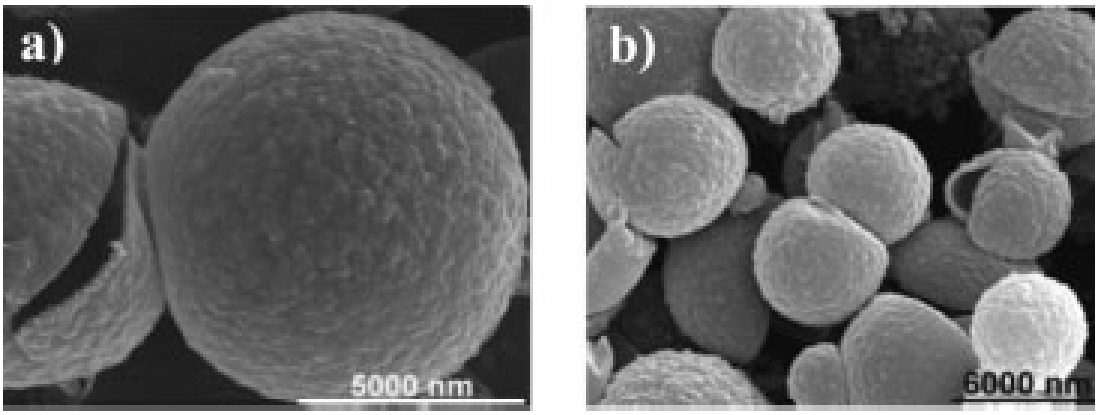

Figure I-36: FE-SEM images of (a) single, (b) groups of giant spherical conducting polythiophene synthesized by the in-situ gamma radiation-induced chemical polymerization method.[288]

Stable colloidal dispersion of poly(3-hexylthiophene) have been successfully obtained by Takeuchi and Kobashi by simple precipitation technique with selected poor solvent like 1-methyl-2-pyrrolidinone (NMP) and 1,1,1,3,3,3-hexafluoro-2-propanol (HFIP). These particles have size between 20 – 40 nm. The dispersions prepared in HFIP were more stable and lightly doped form (doped by HFIP) than prepared in NMP.

III. Conclusion

This literature review was to identify main semiconductor polymers, focusing on their main synthetic routes, their molecular structure, stability and new applications as materials in opto-electronics. This study revealed that the conduction properties are closely related to the molecular structure of the polymer chains. Because of their interesting optical and semiconducting properties, these conjugated organic polymers have potential application in electrochromics, supercapacitors, antistatic and electro-static coatings, light-emitting devices, photovoltaics, sensors etc. Among conducting polymers, PANI, PPy and PEDOT have attracted special attention because of their reasonable environmental stability. These semiconducting polymers can be easily prepared by both chemical and electrochemical methods. Unfortunately, like most of the conjugated polymers, they are insoluble in common organic solvents, therefore difficult to process, thus preventing their common use and large scale development. In order to overcome this drawback, many research groups enhanced the processability of conjugated polymers by synthesizing them under the form of sterically stabilized particles.

References

(1) Shirakawa, H.; Louis, E. J.; MacDiarmid, A. G.; Chiang, C. K.; Heeger, A. *J. Chem Commun.* **1977**, 578.

(2) Ivory, D. M.; Miller, G. G.; Sowa, J. M.; Shacklette, L. W.; Chance, R. R.; Baughman, R. H. *J. Chem. Phys.* **1979**, 71, 1506.

(3) Tourillon, G.; Garnier, F. *Electroanal. Chem. Interfacial. Electrochem.* **1982**, 135, 173.

(4) Diaz, A. F.; Kanazawa, K. K. *J. Chem. Soc., Chem. Commun.* **1979**, 635.

(5) Langer, J. *Sol. Stat. Commun.* **1978**, *26*, 839.

(6) MacDiarmid, A. G.; Chiang, J.; Halpern, M.; Huang, W.; Mu, S.; Somasiri, N. L. D.; Wu, W.; Yaniger, S. I. *Mol. Cryst. Liq. Cryst.* **1985**, *121*, 173.

(7) Bayer AG. *Eur. Patent 339 340*, **1988**.

(8) Jonas, F.; Schrader, L. *Synth. Metal.* **1991**, 831, 41.

(9) Heywang, G.; Jonas, F. *Adv. Mater.* **1992**, 4, 116.

(10) Winter, C.; Reece, C.; Hormes, J.; Heywang, G.; Jonas, F. *Chem. Phys.* **1995**, 194, 207.

(11) Dietrich, M.; Heinze, J.; Heywang, G.; Jonas, F. *J. Electroanal. Chem* **1994**, 369, 87.

(12) Burroughes, J. H.; Bradley, D. D. C.; Brown, A. R.; Marks, R. N.; Mackay, K.; Friend, R. H.; Burn, P. L.; Holmes, A. B. *Nature* **1990**, 347, 539.

(13) Ohmori, Y.; Uchida, M.; Muro, K.; Yoshino, K. *Jpn J. Appl. Phys.* **1991**, 30(12B), L1941.

(14)Shirakawa, H.; Ikeda, S. *Polym. J.* **1971**, *2*, 231.

(15) Chien, J. C. W., *Polyacetylene: Chemistry, Physics and Material Science*, Academic Press, London, Chapter 9, **1984**.

(16)Diaz, A. F.; Kanazawa, K. K.; Gardini, G. P. *J. Chem. Soc., Chem. Commun*. **1979**, 635.

(17) Genies, E. M.; Tsintavis, C. *J. Electroanal. Chem.* **1985**, *195*, 109.

(18) Stilwell, D. E.; Park, S. *J. Electrochem. Soc*. **1988**, *135*, 2491.

(19) Chiang, J.; MacDiarmid, A. G. *Synth. Met.* **1986**, *13*, 193.

(20) Myers, R. E. *J. Electr. Mater.* **1986**, *2*, 61.

(21) Armes, S. P. *Synth. Met.* **1987**, *20*, 365.

(22) Burroughes, J. H.; Friend, R. H., The semiconductor device physics of polyacetylene. In *Conjugated Polym.*, Eds.Silbey, R., Ed. Kluwer Academic Press, Dordrecht: **1991**; p 555.

(23) Greenham, N. C.; Moratti, S. C.; Bradley, D. D. C.; Friend, R. H.; Holmes, A. B. *Nature* **1993**, 365, 628.

(24) Chung, T. C.; Kaufman, J. H.; Heeger, A. J.; et al. *Physical Review B Condensed Matter* **1984**, 30, 702.

(25) Sato, M.; Tanaka, S.; Kaeriyama, K. *Synth. Metal.* **1986**, 14, 279.

(26) Grem, G.; Leditzky, G.; Ullrich, B.; Leising, G. *Synth. Metal.* **1992**, 51, 383.

(27) Friend, R. H.; Gymer, R. W.; Holmes, A. B.; Burroughes, J. H.; Markes, R. N.; Taliani, C.; Bradley, D. D. C.; Dos Santos, D. A.; Brédas, J. L.; Löglund, M.; Salanek, W. R. *Nature* **1999**, 397, 121.

(28) Brédas, J. L., In *Handbook of Conducting Polymers*, Eds.*Dekker, M.*, Ed. *New York*, **1986**; Vol. 2, p 859.

(29) Q. Pei; Zuccarello, G.; Ahlskog, M.; Inganäs, O. *Polymer* **1994**, 35, 1347.

(30) Akoudad, S.; Roncali, J. *Synth. Met.* **1998**, 93, 111-114.

(31) Bredas, J. L.; Chance, R. R.; Silbey, R. *Phys. Rev. B* **1982**, 26, 5843

(32) Irvin, D. J.; Dudis, D. S.; Reynolds, J. R. *Polym. Prepr.* **1997**, 38, 318

(33) Irvin, D. J. *Modification of the Electronic Properties of Conjugated Polymers*, PhD dissertation, University of Florida, **1998**.

(34) MacDiarmid, A. G.; Chiang, J.-C.; Richter, A. E.; Somaisiri, N. L. D.; Epstein, A. J. ; in L. Alcacer, ed., *Conducting Polymers*, Reidel, Dordrecht, Holland, **1987**, p. 105.

(35) Iroh, J. O.;. Rajagopalan, R. R. *J. Appl. Polym. Sci.* **2000**, 76, 1503

(36). Wang, C. L.; Martino, F. *Phys. Rev. B,* **1986**, 34, 5540.

(37) Winokur, M. J.; Spiegel, D.; Kim, Y.; Hotta, S.; Heeger, A. J. *Synth. Met.* **1989**, 28, C419.

(38) Chen, S.-A. ; Ni, J.-M. *Macromolecules,* **1992**, 25, 6081.

(39) Curtis, M. D. *Macromolecules,* **2001**, 34, 7905.

(40) Ruiz, J. P.; Dharia, J. R.; Reynolds, J. R. *Macromolecules,* **1992**, 25, 849.

(41) Nicolini, C.; Maccioni, E.; Ram, M. K. *Thin Solid Films* **1997**, 303, 27.

(42) Nishio, S.; Matsuzaki, A.; Sato, H. *Synth. Met.* **1997**, 84, 367.

(43) Reghu, M.; Cao, Y.; Moses, D.; Heeger, A. J. *Phys. Rev. B* **1993**, 47, 1758.

(44) Park, Y. W.; Choi, E. S.; Suh, D. S. *Synth. Met.* **1998**, 96, 81.

(45) Angeli, A. *Gazz. Chim. Ital.* **1916**, 46, 279.

(46) Lenga, R. E., *The Sigma-Aldrich Library of Chemical Safety Data*, Sigma-Aldrich Corp., 2nd Edition **1988**.

(47) Dall'Olio, A.; Dascola, G.; Varacca, V.; Bocchi, V. *C. R. Acad. Sci. Ser.* **1968**, *C267*, 433.

(48) Diaz, A. F.; Kanazawa, K. K.; Gardini, G. P. *J. Chem. Soc., Chem. Commun*. **1979**, 635.

(49) Kanazawa, K. K.; Diaz, A. F.; Geiss, R. H.; Gill, W. D.; Kwak, J. F.; Logan, J. A.; Rabolt, J. F.; Street, G. B. *J. Chem. Soc., Chem. Commun*. **1979**, 854.

(50) Kanazawa, K. K.; Diaz, A. F.; Gill, W. D.; Grant, P. M.; Street. G. B.; Gardini, G. P.; Kwak, J. F. *Synth. Met.* **1979**, *1*, 329.

(51) Diaz, A. F.; Crowley, J.; Bargon, J.; Gardini, G. P., Torrance, J. B. *J. Electroanal. Chem.* **1981**, *121*, 355.

(52) Genies, E. M.; Bidan, G.; Diaz, A. F. *J. Electroanal. Chem.* **1983**, *149*, 101.

(53) Koßmehl, G.; Chatzitheodorou, G. *Makromol. Chem., Rapid. Commun.* **1981**, *2*, 551.

(54) *Handbook of Conducting Polymers*; Skotheim, T. A., Ed. Marcel Dekker, New York, p.81,1st Edition **1986**.

(55) Yamaura, M.; Sato, K.; Hagiwara, T. *Synth. Met.* **1990**, *39*, 43.

(56) Cheung, K. M.; Bloor, D.; Stevens, G. C. *Polymer*, **1988**, *29*, 1709.

(57) Kanazawa, K. K.; Diaz, A. F.; Krounbi, M. T.; Street, G. B. *Synth. Met.* **1981**, *4*, 119.

(58) Maddison, D. S.; Unsworth, J. *Synth. Met*. **1989**, *30*, 47.

(59) Genies, E. M.; Marchesiello, M.; Bidan, G. *Electrochimica Acta*. 1992, 37, 1015.

(60) Hautiere-Cristofini, F.; Kuffer, D.; Yu, L. T. *C. R. Acad. Sci. Paris. Ser.* **1973**, *C277*, 1323.

(61) Rapi, S.; Bocchi, V.; Gardini, G. P. *Synth. Met.* **1988**, *24*, 217.

(62) Ojio, T.; Miyata, S. *Polymer J.* **1986**, *18*, 95.

(63) Mohammadi, A.; Lundstrom, I.; Salaneck, W. R.; Inganas, O. *Chemtronics* **1986**, *1*, 171.

(64) Mohammadi, A.; Lundstrom, I.; Salaneck, W. R.; Inganas, O. *Synth. Met.* **1987**, *21*, 169.

(65) Asano, M.; Inoue, M.; Takai, Y.; Mizutani, T.; Ieda, M. *Jap. J. Appl. Phys.* **1989**, *28*, 713.

(66) Machida, S.; Miyata, S.; Techagumpuch, A. *Synth. Met.* **1989**, *31*, 311.

(67) Zhang, J.; She, Y.; Lu, B.; Zhou, Y.; Fu, K. *Chinese J. Polym. Sci.* **1993**, *11*, 337.

(68) Chao, T. H.; March, J. *J. Polym. Sci. A: Polym. Chem.* **1988**, *26*, 743.

(69) Bocchi, V.; Gardini, G.P. *J. Chem. Soc. Chem. Commun*. **1986**, 148.

(70) Khulbe, K. C.; Mann, R. S.; Khulbe, C. P. *J. Polym. Sci.: Polym. Chem. Ed.* **1982**, *20*, 1089.

(71) Ayad, M. M. *J. Appl. Polym. Sci.* **1994**, *53*, 1331.

(72) *CRC Handbook of Chemistry and Physics*, Weast, R. C., Ed. CRC Press Inc., Florida, 66th Edition **1986**.

(73) Bjorklund, R. B. *J. Chem. Soc., Faraday Trans.* **1987**, *83*, 1507.

(74) Maeda, S.; Armes, S. P. *J. Mater. Chem*. **1994**, *4*, 935.

(75) Moon, D. K.; Osakada, K.; Maruyama, T.; Yamamoto, T. *Makromol. Chem.* **1992**, *193*, 1723.

(76) Liu, C. F.; Moon, D. K.; Maruyama, T.; Yamamoto, T. *Polymer J.* **1993**, *25*, 775.

(77) Wei, Y.; Tian, J.; Yang, D. *Makromol. Chem., Rapid Commun.* **1991**, *12*, 617.

(78) Gardini, G. P. *Adv. Heterocyclic. Chem.* **1973**, *15*, 67.

(79) Pfluger, P.; Street, G. B. *J. Chem. Phys.* **1984**, *80*, 544.

(80) Pfluger, P.; Krounbi, M.; Street, G. B.; Weiser, G. *J. Chem. Phys.* **1983**, *78*, 3212.

(81) *Handbook of Conducting Polymers*; Skotheim, T. A., ed. Marcel Dekker, New York, Ch.8 ,1st Edition (1986).

(82) Diaz, A. F.; Castillo, J. I.; Logan, J. A.; Lee, W. *J. Electroanal. Chem.* **1981**, *129*, 115.

(83) Munstedt, H. *Polymer* **1988**, *29*, 296.

(84) Samuelson, L. A.; Druy, M. A. *Macromolecules* **1986**, *19*, 824.

(85) Lascelles, S. F. *D.Phil. Thesis*, University of Sussex, **1997**.

Plenum, New York, Ch.8, **1982**.

(86) Thieblemont, J. C.; Planche, M. F.; Petrescu, C.; Bouvier, J. M.; Bidan, G. *Synth. Met.* **1993**, *59*, 81.

(87) Mitchell, G. R.; Davis, F. J.; Legge, C. H. *Synth. Met*. **1988**, *26*, 247.

(88) Desilvestro, J.; Scheifele, W.; Hass, O. J. Electrochem. Soc. **1992**, 139, 2727.

(89) Joo, J.; Epstein, A. J. Appl. Phys. Lett. **1994**, 65, 2278.

(90) Trivedi, D. C.; Dhawan, S. K. Synth. Met. **1993**, 59, 267.

(91) Lu, V. K.; Elsenbaumer, R. L. ; Wessling, B. Synth. Met. **1995**, 71, 2163.

(92) Fahlman, M; Jasty, S.; Epstein, A. J. Synth. Met. **1997**, 85, 1323.

(93) Gilchrist, L. *J. Phys. Chem*. **1904**, *8*, 539.

(94) Letheby, H. *J. Chem. Soc*. **1862**, *15*, 161.

(95) Diaz, A. F.; Logan, J. A. *J. Electroanal. Chem*. **1980**, *111*, 111.

(96) Huang, W.; Humphrey, B. D.; MacDiarmid, A. G. *J. Chem. Soc.; Faraday Trans.* **1986**, *82*, 2385.

(97) Watanabe, A.; Mori, K.; Iwabuchi, A.; Iwasaki, Y.; Nakamura, Y. *Macromolecules*, **1989**, *22*, 3521.

(98) Oyama, N.; Ohsaka, T. *Synth. Met*. **1987**, *18*, 375.

(99) Yasui, T. *Bull. Chem. Soc. Jpn*. **1935**, *10*, 305.

(100) Mohilner, D. M.; Adams, R. H.; Argersinger, W. J. *J. Am. Chem. Soc*. **1962**, *84*, 3618.

(101) Genies, E. M.; Lapkowski, M. *J. Electroanal. Chem*. **1987**, *236*, 199.

(102) Breitenbach, M.; Heckner, K. H. *J. Electroanal. Chem*. **1971**, *29*, 306.

(103) Breitenbach, M.; Heckner, K. H. *J. Electroanal. Chem*. **1971**, *33*, 45.

(104) Breitenbach, M.; Heckner, K. H. *J. Electroanal. Chem*. **1973**, *43*, 267.

(105) Travers, J. P.; Chroboczek, J.; Devreux, F.; Genoud, F.; Nechtschein, M.; Syed, A. A.; Genies, E. M.; Tsintavis, C. *Mol. Cryst. Liq. Cryst*. **1985**, *121*, 195.

(106) Pron, A.; Genoud, F.; Menardo, C.; Nechtschein, M. *Synth. Met*. **1988**, *24*, 193.

(107) Moon, D. K.; Osakada, K.; Maruyama, T.; Yamamoto, T. *Makromol. Chem*. **1992**, *193*, 1723.

(108) Inoue, M.; Brown, F.; Munoz, I. C.; Munoz, F. O. *Polymer Bulletin* **1991**, *26*, 403.

(109) Neoh, K. G.; Kang, E. T.; Tan, K. L. *Polymer*, **1993**, *34*, 3921.

(110) Kang, E. T.; Neoh, K. G.; Woo, Y. L.; Tan, K. L.; Huan, C. H. A.; Wee, A. T. S. *Synth. Met*. **1993**, *53*, 333.

(111) Syed, A.; Dinesan, M. K. *Synth. Met*. **1990**, *36*, 209.

(112) Genies, E. M.; Sayed, A. M.; Tsintavis, C. *Mol. Cryst. Liq. Cryst*. **1985**, *121*, 181.

(113) Armes, S. P.; Miller, J. F. *Synth. Met*. **1988**, *22*, 385.

(114) Green, A. G.; Woodhead, A. E. *J. Chem. Soc*. **1910**, *97*, 2388.

(115) Green, A. G.; Woodhead, A. E. *J. Chem. Soc*. **1912**, *101*, 1117.

(116) Kang, E. T.; Neoh, K. G.; Tan. K. L. *Polymer. J*. **1989**, *21*, 873.

(117) Kang, E. T.; Neoh, K. G.; Khor, S. H.; Tan, K. L.; Tan, B. T. G. *J. Chem. Soc., Chem. Commun.* **1989**, 695.

(118) Kang, E. T.; Neoh, K. G.; Tan, K. L. *Adv. Polym. Sci*. **1993**, *106*, 135.

(119) Angelopoulos, M.; Ray, A.; MacDiarmid, A. G.; Epstein, A. J. *Synth. Met*. **1987**, *21*, 21.

(120) Neoh, K. G.; Kang, E. T.; Khor, S. H.; Tan, K. L. *Polymer Deg. Stab*. **1990**, *27*, 107.

(121) Kulkarni, V. G.; Campbell, L. D.; Mathew, W. R. *Synth. Met*. **1989**, *30*, 321.

(122) Groenendaal, L.; Jonas, F.; Freitag, D.; Pielartzik, H.; Reynolds, J. R. *Adv. Mat*. **2000**, *12*, 481.

(123) *Handbook of Conducting Polymers*; Skotheim, T. A., ed. Marcel Dekker, New York, p.79, Vol.2, 1st Edition (1986).

(124) Pei, Q.; Zuccarello, G.; Ahlskog, M.; Inganäs, O. *Polymer* **1994**, *35*, 1347.

(125) Jonas, F.; Morrison, J. T. *Synth. Met*. **1997**, *85*, 1397.

(126) Jonas, F.; Heywang, G. *Electrochimica Acta*. **1994**, *39*, 1345.

(127) Sapp, S. A.; Sotzing, G. A.; Reddinger, J. L.; Reynolds, J. R. *Adv. Mat*. **1996**, *8*, 808.

(128) Chang, Y.; Lee, K.; Kiebooms, R.; Aleshin, A.; Heeger, A. J. *Synth. Met*. **1999**, *105*, 203.

(129) Jonas, F.; Krafft, W.; Muys, B. *Macromol. Symp*. **1995**, *100*, 169.

(130) Sakmeche, N.; Aaron, J. J.; Fall, M.; Aeiyach, S.; Jouini, M.; Lacroix, J. C.; Lacaze, P. C. *Chem. Commun*. **1996**, 2723.

(131) Sakmeche, N.; Bazzaoui, E. A.; Fall, M.; Aeiyach, S.; Jouini, M.; Lacroix, J. C.; Aaron, J. J.; Lacaze, P. C. *Synth. Met*. **1997**, *84*, 191.

(132) Yamato, H.; Kai, K.; Ohwa, M.; Asakura, T.; Koshiba, T.; Wernet, W. *Synth. Met*. **1996**, *83*, 125.

(133) Corradi, R.; Armes, S. P. *Synth. Met*. **1997**, *84*, 453.

(134) Kudoh, Y.; Akami, K.; Matsuya, Y. *Synth. Met*. **1998**, *98*, 65.

(135) De Leeuw, D. M.; Kraakman, P. A.; Bongaerts, P. F. G.; Mutsaers, C. M. J.; Klaassen, D. B. M. *Synth. Met*. **1994**, *66*, 263.

(136) Kirchmeyer, S.; Reuter, K. *J. Mater. Chem*., **2005,** 15, 2077.

(137) Groenendaal, L.; Louwet, F.; Adriaensens, P.; Carleer, R.; Vanderzande, D.; Gelan, J. *Polym. Mater. Sci. Eng*., **2002**, 86, 52.

(138) Reuter, K.; Nikanorov, V. A.; Bazhenov, V. M. EP 1 375 560 (H.C. Starck GmbH), Prior: 2002-06-28.

(139) Reuter, K. EP 1 428 827 A1 (H.C. StarckGmbH), Prior: 2002-12-10.

(140) Granström M.; Inganäs, O. *Polymer*, **1995,** 36, 15, 2867.

(141) Aasmundtveit, K. E.; Samuelsen, E. J.; Petterson, L. A. A.; Inganä s, O.; Johansson, T.; Feidenhans'l, R. *Synth. Met*., **1999,** 101, 561.

(142) Niu, L.; Kvarnström, C.; Fröberg, K.; Ivaska, A. *Synth. Met*., **2001**, 122, 425.

(143) Kiebooms, R.; Aleshin, A.; Hutchison, K.; Wudl, F. *J. Phys. Chem. B.* **1997**, *101*, 11037.

(144) Granström, M.; Inganäs, O. *Polymer* **1995**, *36*, 2867.

(145) Xing, K. Z.; Fahlman, M.; Chen, X. W.; Inganäs, O.; Salaneck, W. R. *Synth. Met*. **1997**, *89*, 161.

(146) Rannou, P.; Nechtschein, M. *Synth. Met.* **1999**, *101*, 474.

(147) Winter, I.; Reese, C.; Hormes, J.; Heywang, G.; Jonas, F. *Chem. Phys.* **1995**, *194*, 207.

(148) Hotta, S.; Rughooputh, S. D. D. V.; Heeger, A. J.; Wudl, F. *Macromolecules* **1987**, 20, 212.

(149) Elsenbaumer, R. L.; Jen, K. Y.; Oboodi, R. *Synth. Metal.* **1986**, 15, 169.

(150) Fukuda, M.; Sawada, K.; Yoshino, K. *J. Polym. Sci. Part A: Polym. Chem.* **1993**, 31, 2465.

(151) Levesque, I.; Leclerc, M. *Chem. Mater* **1996**, 8, 2843.

(152) Patil, A. O.; Ikenoue, Y.; Wudl, F.; Heeger, A. J. *J. Am. Chem. Soc.* **1987**, 109, 1858.

(153) Stéphan, O.; Schottland, P.; Le Gall, P.-Y.; Chevrot, C. *J. Chim. Phys.* **1998**, 95, 1168.

(154) Anad, J.; Palaniappan, S.; Sathyanarayana, D. N. *Prog. Polym. Sci.* **1998**.23, 993

(155) Gangopadhyay, R.; De, A. *Chem. Mater.* **2000**, 12, 608

(156) Mrkic, J.; Saunder, B. R. *J. Colloid. Interface Sci*. **2000**, 222, 75

(157) Eisazadeh, H.; Spinks, G.; Wallace, G. G. *Polymer* **1994,** 35, 3801

(158) Shaw, D. J. *Introduction to Colloid and Surface Chemistry*, Butterworth-Heinemann, Oxford, 4th Edn, Ch.1, **1992**.

(159) Fitch, R. M. *Polymer Colloids: A Comprehensive Introduction*, Academic Press, London, Ch.7, **1997**.

(160) Deryagin, B. V.; Landau, L. *Acta Phys. Chim. URSS* **1941**, *14*, 633.

(161) Verwey, E. J. W.; Overbeek, J. Th. G. *Theory of the Stability of Lyophobic Colloids*, Elsevier*, Amsterdam*, **1948**.

(162) Hunter, R. J. *Foundations of Colloid Science: Volume I*, Oxford University Press, Oxford, Ch.8, **1987**.

(163) Cowie, J. M. G. *Polymers: Chemistry and Physics of Modern Materials*, Stanley Thornes Ltd., Cheltenham, 2nd Edn, Ch.8, p.175, **1991**.

(164) Napper, D. H. *Polymeric Stabilization of Colloidal Dispersions*, Academic Press, London, Ch.7, p.150, **1983**.

(165) Kumar, D.; Butler, G. B. *J. Macromol. Sci: Rev. Macromol. Chem. Phys.* **1997**, *C37*, 303.

(166) Harkins, W. D. *J. Am. Chem. Soc.* **1947**, *69*, 1428.

(167) Smith, W. V.; Ewart, R. H. *J. Chem. Phys.* **1948**, *16*, 592.

(168) Gilbert, R. G., *Emulsion Polymerization: A Mechanistic Approach*, Academic Press, London, **1995**.

(169) Kotera, A.; Furusawa, K.; Takeda, Y. *Kolloid-Z.Z. Polym.* **1970**, *239*, 677.

(170) Goodwin, J. W.; Hearn, J., Ho, C. C.; Ottewill, R. H. *Colloid Polym. Sci.* **1974**, *252*, 464.

(171) Barrett, K. E. J., *Dispersion Polymerisation in Organic Media*, Wiley, London, **1975**.

(172) Paine, A. J.; Luymes, W.; McNulty, J. *Macromolecules* **1990**, *23*, 3104.

(173) Paine, A. J.; Deslandes, Y.; Gerrior, P.; Henrissat, B. *J. Colloid. Interface. Sci.* **1990**, *138*, 170.

(174) Ober, C, K.; Lok, K. P.; Hair, M. L. *J. Polym. Sci., Polym. Lett.* **1985**, *23*, 103.

(175) Almog, Y.; Reich, S.; Levy, M. *Brit. Polym. J.* **1982**, *14*, 131.

(176) Tseng, C. M.; Lu, N. Y.; El-Aasser, M. S.; Vanderhoff, J. W. *J. Polym. Sci. A: Polym. Chem.* **1986**, *24*, 2995.

(177) Cheng, C. M.; Micale, F. J.; Vanderhoff, J. W.; El-Aasser, M. S. *J. Polym. Sci. A: Polym. Chem.* **1992**, *30*, 235.

(178) Winnik, F. M.; Ober, C. K. *Eur. Polym. J.* **1987**, *23*, 617.

(179) Dinnela, C.; Lanzarini, G.; Zannoni, M.; Laus, M. *Macromol. Rapid Commun*. **1994**, *15*, 909.

(180) Bjorklund, R. B.; Liedberg, B. *J. Chem. Soc., Chem. Commun*. **1986**, 1293.

(181) Mandal, T. K.; Mandal, B. M. *Polymer* **1995**, *36*, 1911.

(182) Chattopadhyay, D.; Mandal, B. M. *Langmuir* **1996**, *12*, 1585.

(183) Mandal, T. K.; Mandal, B. M. *J. Polym. Sci. A: Polym. Chem.* **1999**, *37*, 3723.

(184) Banerjee, P. *Eur. Polym. J*. **1998**, *34*, 841.

(185) Armes, S. P.; Vincent, B. *J. Chem. Soc., Chem. Commun.* **1987**, 288.

(186) Armes, S. P.; Miller, J. F.; Vincent, B. *J. Colloid. Interface. Sci*. **1987**, *118*, 410.

(187) Gospodinova, N.; Terlemezyan, L.; Mokreva, P., Stejskal, J.; Kratochvil, P. *Eur. Polym. J.* **1993**, *29*, 1305.

(188) Stejskal, J.; Kratochvil, P.; Helmstedt, M. *Langmuir* **1996**, *12*, 3389.

(189) Stejskal, J.; Špirková, M.; Kratochvil, P. *Acta Polymer* **1994**, *45*, 385.

(190) Digar, M. L.; Bhattacharyya, S. N.; Mandal, B. M. *J. Chem. Soc., Chem. Commun.* **1992**, 18.

(191) Banerjee, P.; Mandal, B. M. *Macromolecules* **1995**, *28*, 3940.

(192) Ghosh, P.; Siddhanta, S. K.; Chakrabarti, A. *Eur. Polym. J.* **1999**, *35*, 699.

(193). Stejskal, J.; Kratochvíl, P.; Helmstedt, M. *Langmuir*, **1996,** 12, 3389.

(194). Riede, A.; Stejskal, J.; Helmstedt, M. *Synth. Met.* **2001**, 121, 1365.

(195) Yang, S. M.; Lee, H. L. *Synth. Met*. **1999**, 102, 1226.

(196) Shannon, K.; Fernandez, J. E. *J. Chem. Soc., Chem. Commun*. **1994**,643.

(197) Tadros, P.; Armes, S. P.; Luk, S. Y. *J. Mater.chem*. **1992**, 2, 125.

(198) Eisazadeh, H.; Gilmore, K. J.; Hodgson, A. J.; Spinks, G.; Wallace, G. G. *Colloids Surf. A* **1995**, 103, 281.

(199) Vincent, B.; Waterson, J. *J. Chem. Soc., Chem. Commun*. **1990**, 683.

(200) Barisci, J. N.; Innis, P. C.; Kane-Maguire, L. A. P.; Norris, I. D.; Wallace, G. G. *Synth Met* **1997**, 84, 181.

(201) Banerjee, P.; Mandal, B. M. *Synth. Met*. **1995**, 74, 257.

(202) Ghosh, M.; Barman, A.; De, S. K.; Chaterjee, S. *Solid State Commun*. **1997**, 103, 629.

(203) Stejskal, J.; Špírková, M.; Riede, A.; Helmstedt, M.; Mokreva, P.; Prokeš, J. *Polymer,* **1999**, 40, 2487.

(204) Chattopadhyay, D.; Banerjee, S.; Chakravorthy, D.; Mandal, B. M. *Langmuir*, **1998**, 14, 1544.

(205) Yang, S. M.; Lee, H. L. *Synth. Met*. **1999**, 102, 1226.

(206) Hu, H.; J. Saniger, M.; Banuelos, J. G. *Thin solid films*, **1999**, 347, 241.

(207) Armes, S. P.; Aldissi, M.; Hawley,M.; Beery, J. G.; Gottesfeld, S. *Langmuir,* **1991**, 7, 1447.

(208) Shannon, K.; Fernandez, J. E. *J. Chem Soc. Chem Commun*. **1994**, 643.

(209) Eisazadeh, H.; Spinks, G.; Wallace, G. G. *Polym. Int*. **1995**, 37, 87.

(210) Gospodinova, N.; Mokreva, P.; Terlemezyan, L. *J. Chem. Soc. Chem Commun*, **1992**, 923.

(211) Stejskal, J.; Kratochvı´l, P.; Gospodinova, N.; Terlemezyan, L.; Mokreva, P. *Polymer*, **1992**, 33, 4857.

(212) Chakraborthy, M.; Mukerjee, D. C.; Mandal, B. M. *Langmuir,* **2000**, 16, 2482.

(213) Gangopadhyay, R.; De, A.; Ghosh, G. *Synth. Met*. **2001**, 123, 21.

(214) Mirmohseni, A.; Wallace, G. G. *Polymer*, **2003**, 44, 3523.

(215) Butterworth, M. D.; Corradi, R.; Johal, J.; Lascelles, S. F.; Maeda, S.; Armes, S. P. *J Colloid Interface Sci.* **1995**, 174, 510.

(216) Riede, A.; Helmstedt, M.; Riede, V.; Stejskal, J. *Colloid Polym Sci.* **1997**, 275, 814.

(217) Armes, S. P.; Aldissi, M.; Agnew, S.; Gottesfeld, S. *Mol. Cryst. Liq. Cryst*. **1990**, *190*, 63.

(218) Tadros, P.; Armes, S. P.; Luk, S. Y. *J. Mater. Chem.* **1992**, *2*, 125.

(219) Bay, R. F. C.; Armes, S. P.; Pickett, C. J.; Ryder, K. S. *Polymer* **1991**, *32*, 2456.

(220) Armes, S. P; Aldissi, M. *J. Chem. Soc., Chem. Commun*. **1989**, 88.

(221) DeArmitt, C.; Armes, S. P. *J. Colloid. Interface. Sci*. **1992**, *150*, 134.

(222) Nagaoka, T.; Nakao, H.; Suyama, T.; Ogura, K.; Oyama, M.; Okazaki, S. *Anal. Chem*. **1997**, 69, 1030.

(223) Nakao, H.; Nagaoka, T.; Ogura, K. *Anal. Sci*. **1997**, 13, 327.

(224) Stejskal, J.; Kratochvíl, P.; Armes, S. P.; Lascelles, S. F.; Riede, A.; Helmstedt, M.; Prokeš, J.; Křivka, I. *Macromolecules*, **1996**, 29, 6814.

(225) Gospodinova, N.; Janca, J. *Int. J. Polym. Anal. Charact.* **1998**, *4*, 323.

(226) Eisazadeh, H.; Spinks, G.; Wallace, G. G. *Polymer* **1994**, *35*, 3801.

(227) Aboutanos, V.; Barisci, J. N.; Innis, P. C.; Wallace, G. G. *Colloids Sur. A* **1998**, *137*, 295.

(228) Barisci, J. N.; Innis, P. C.; Kane-Maguire, L. A. P.; Norris, I. D.; Wallace, G. G. *Synth. Met*. **1997**, *84*, 181.

(229) Innis, P. C.; Norris, I. D.; Kane-Maguire, L. A. P.; Wallace, G. G. *Macromolecules* **1998**, *31*, 6521.

(230) Gill, M.; Mykytiuk, J.; Armes, S. P.; Edwards, J. L.; Yeates, T.; Moreland, P. J.; Mollett, C. *J. Chem. Soc., Chem. Commun*. **1992**, 108.

(231) Gill, M.; Armes, S. P.; Fairhurst, D.; Emmett, S. N.; Pigott, T.; Idzorek, G. C. *Langmuir*, **1992**, 8, 2178.

(232) Gill, M.; Baines, F. L.; Armes, S. P. *Synth. Met.* **1993**, 55-57, 1029.

(233) Beadle, P.; Armes, S. P.; Gottesfeld, S.; Mombourquette, C.; Houlton, R.; Andrews, W. D.; Agnew, S. F. *Macromolecules*, **1992**, 25, 2526.

(234) Barthet, C.; Armes, S. P.; Lascelles, S. F.; Luk, S. Y.; Stanley, H. M. E. *Langmuir* **1998**, *14*, 2032.

(235) Barthet, C.; Armes, S. P.; Chehimi, M. M.; Bilem, C.; Omastova, M. *Langmuir* **1998**, *14*, 5032.

(236) Lascelles, S. F.; Armes, S. P. *J. Mater. Chem*. **1997**, *7*, 1339.

(237) Saunders, B. R.; Saunders, J. M.; Marci**,** J.; Dunlop, E. H. *Phys. Chem. Chem. Phys*., **1999,** 1, 1563.

(238) Qi, Z.; Pickup, P. G. *Chem. Mater*. **1997**, 9, 2934.

(239) Mandal, T.K.; Mandal, B. M. *J. Polym. Sci., Part A: Polym. Chem.* **1999**, 37, 3723.

(240) Eisazadeh, H.; Spinks, G. Wallace, G. G. *Polymer*, **1994**, 35, 3801.

(241) Eisazadeh, H.; Spinks, G. Wallace, G. G. *Polym. Int.* **1995,** 37, 87.

(242) Barisci, J.N.; Hodgson, A.J.; Liu, L.; Wallace, G.G.; Harper, G. React. Funct. Polym. **1999**, 39, 269.

(243) Cawdery, N.; Obey, T. M.; Vincent, B. *J. Chem. Soc., Chem. commun.* **1988**, 1189.

(244) Digar, M.L.; Bhattacharyya, S.N.; Mandal B.M. *Polymer*, **1994**, 35, 377.

(245) Pich, A.; Lu, Y.; Adler, H-J. P.; Schmidt, T.; Arndt, K-F. *Polymer*, **2002**, 43, 5723.

(246) Simmons, M.R.; Chaloner P. A.; Armes S.P. *Langmuir* **1995**;11:4222.

(247) Yassar, A.; Roncali, J.; Garnier, F. *Polym. Commun.* **1987**, 28, 103.

(248) Kim, B.-J.; Oh, S.-G.; Han, M.-G., Im, S.-S. *Langmuir*, **2000**, 16, 5841.

(249) Gill, M.; Mykytiuk, J.; Armes, S. P.; Edwards, J. L.; Yeates, T.; Moreland, P. J.; Mollett, *C. J. Chem. Soc., Chem. Commun.***1992**, 108.

(250) Armes, S. P.; Aldissi, M. *Polymer* **1990**, *31*, 569.

(251) Beadle, P. M.; Rowan, L.; Mykytiuk, J., Billingham, N. C.; Armes, S. P. *Polymer* **1993**, *34*, 1561.

(252) Ishizu, K.; Tanaka, H.; Saito, R.; Maruyama, T.; Yamamoto, T. *Polymer* **1996**, *37*, 863.

(253) Simmons, M. R.; Chaloner, P. A.; Armes, S. P. *Langmuir,***1998,** 14*,* 611.

(254) Maeda, S.; Armes, S. P. *J. Colloid Interface Sci*. **1993**, *159*, 257.

(255) Flitton, R.; Johal, J.; Maeda, S.; Armes, S. P. *J. Colloid Interface Sci*. **1995**, *173*, 135.

(256) Lascelles, S. F.; McCarthy, G. P.; Butterworth, M. D.; Armes, S. P. *Colloid Polym. Sci*. **1998**, *276*, 893.

(257) Yassar, A.; Roncali, J.; Garnier, F. *Polym. Commun*. **1987**, *28*, 103.

(258) Liu, C.; Maruyama, T.; Yamamoto, T. *Polymer J*. **1993**, *25*, 363.

(259) Wiersma, A. E.; Steeg, L. M. A.; Jongeling, T. J. M. *Synth. Met*. **1995**, *71*, 2269.

(260) Bremer, L. G. B.; Verbong, M. W. C. G.; Webers, M. A. M.; van Doorn, M. A. M. M. *Synth. Met*. **1997**, *84*, 355.

(261) Huijs, F. M.; Vercauteren, F. F.; Ruiter, B.; Kalicharan, D.; Hadziioannou, G. *Synth. Met*. **1999**, *102*, 1151.

(262) Lascelles, S. F.; Armes, S. P. *Adv. Mater*. **1995**, *7*, 864.

(263) Lascelles, S. F.; Armes, S. P. *J. Mater. Chem*. **1997**, *7*, 1339.

(264) Lascelles, S. F.; Armes, S. P.; Zhdan, P. A.; Greaves, S. J.; Brown, A. M.; Watts, J. F.; Leadley, S. R.; Luk, S. Y. *J. Mater. Chem*. **1997**, *7*, 1349.

(265) Perruchot, C.; Chehimi, M. M.; Delamar, M.; Lascelles, S. F.; Armes, S. P. *Langmuir* **1996**, *12*, 3245.

(266) Cairns, D. B.; Armes, S. P.; Bremer, L. G. B. *Langmuir* **1999**, *15*, 8052.

(267) Cairns, D. B.; Armes, S. P.; Chehimi, M. M.; Perruchot, C.; Delamar, M. *Langmuir* **1999**, *15*, 8059.

(268) Armes, S. P.; Aldissi, M.; Hawley, M.; Beery, J. G.; Gottesfeld, S. *Langmuir* **1991**, *7*, 1447.

(269) Huang, Z.; Wang, P.; MacDiarmid, A. G.; Xia, Y.; Whitesides, G. *Langmuir* **1997**, *13*, 6480.

(270) Cairns, D. B. *D.Phil. Thesis*, University of Sussex, **1999**.

(271) DeArmitt, C.; Armes, S. P. *Langmuir* **1993**, *9*, 652.

(272) Provisional Product Information Sheet, Trial Product AI4071, Bayer AG (Sept **1995**).

(273) Kim, J. Y.; Jung, J. H.; Lee, D. E.; Joo, J. *Synth.Met*. **2002**, 126, 311.

(274). Louwet, F.;. Groenendaal, L.; Dhaen, J.; Manca, J.;. Luppen, J. V.; Verdonck, E.;. Leenders, L. *Synth Met.* **2003**, 135-136, 115.

(275) Sun, J.; Gerberich, W. W.; Francis, L. F. *Progress in Organic Coatings* **2007**, 59, 115.

(276) de Jong, M. P.; van Ijzendoorn, L. J.; de voigtM. J. A. Appl. Phys. Lett.2000, 77, 2255.

(277) Kim, W.H.; Makinen, A. J.; Nikolov, N.; Shashidhar, R.; Kim, H.; Zafafi, Z. H. Appl. Phys. Lett. 2002, 80, 3844.

(278) Sun, X.; Hagner, M. *Macromolecules*, **2007**, 40, 8537

(279) Henderson, A. M. J.; Saunders, J. M.; Markic, J.; Kent, P.; Gore, J.; Saunders, B. R. *J. Mater. Chem*. **2001**, 11, 3037.

(280) Oh, S. -G.; Im, S.-S. *Curr. Appl. Phys.* **2002**, *2*, 273.

(281) Dai, C.-A.; Chang, C.-J.; Chi, H.-Y.; Chien, H.-T.; Su, W.-F.; Chiu, W.-Y. *J. Polym. Sci. Part A, Polym. Chem.* **2008**, 46, 2536.

(282) Marcilla, R.; Ochoteco, E.; Pozo-Gonzalo, C.; Grande, H.; Pomposo, J. A.;Mecerreyes, D. *Macromol. Rapid Commun*. **2005**, 26, 1122.

(283) Müller, K.; Klapper, M.; Müllen, K. *Macromol. Rapid Commun.* **2006**, *27*, 586.

(284) Khan, M. A.; Armes, S. P. *Langmuir* **1999**, *15*, 3469.

(285) Han, M. G.; Fougler, S. H. J. *Chem. Soc., Chem. Commun.* **2004**, *19*, 2154

(286) Zhang, X.; Lee, J.-S.; Lee, G. S.; Cha, D.-K.; Kim, M. J.; Yang, D. J.; Manohar, S. K. *Macromolecules* **2006**, *39*, 470.

(287). Jung, Y. J.; Lee, J. M.; Cheong, I. W.;. Kim, J. H. *Macromol. Symp*. **2007**, *249–250*, 265.

(288) Karim, M. R.; Lee, C. J.; Kim,1 H. J.; Bhuiyan, M. T. I.,. Lee, M. S. *Macromol. Symp*. **2007**, *249–250*, 234.

Chapter II

Synthesis of PEDOT nano-objects using poly(ethyleneoxide)-based reactive stabilizers

Table of contents

I. Water-borne dispersion polymerization of EDOT in the presence of α-EDOT-PEO reactive stabilizer

In this study, we discuss the synthesis, in alcoholic media, of well-defined spherical PEDOT objects (*i.e.* core-shell nanoparticles and vesicles) in the presence of poly(ethylene oxide) end-functionalized with a (3,4-ethylenedioxythiophene) moiety, using ammonium persulfate or iron(III) p-toluenesulfonate hexahydrate as oxidizing agents.

I.1 Synthesis of α-EDOT-PEO reactive stabilizers

It is with the objective to prepare core-shell PEDOT-PEO particles in aqueous media that we first designed poly(ethylene oxide) end-capped with one 3,4-ethylenedioxythiophene (EDOT) moiety (α-EDOT-PEO), for further use as a reactive steric stabilizer. The latter was prepared by "living" anionic polymerization of ethylene oxide. The synthesis of these polymers requires prior the synthesis of EDOT molecule carrying one hydroxyl group capable of initiating the anionic polymerization of ethylene oxide.

I.1.1 Synthesis of the initiator carrying EDOT moiety

The preparation of 2-methylol-3,4-ethylenedioxythiophene (EDOT-CH_2OH) initiator involved two steps. Formylation of EDOT was first carried out with N,N-dimethylformamide in the presence of n-BuLi to give 2-formaldehyde-3,4-ethylenedioxythiophene (EDOT-CHO) in 70% yield (see Scheme II-1).

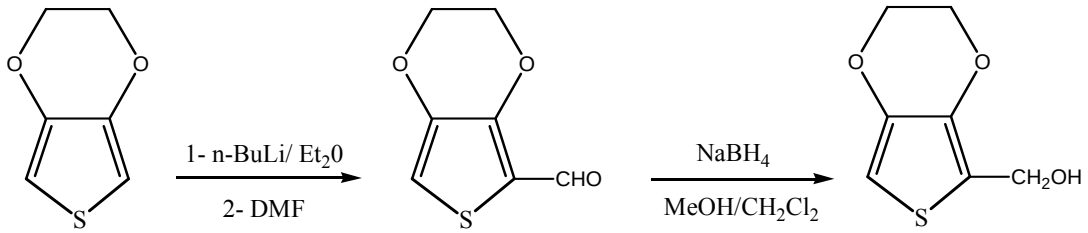

Scheme II-1: Synthesis of 2-methylol-3,4-ethylenedioxythiophene (EDOT-CH_2OH) initiator

^{1}H NMR spectrum of EDOT-CHO in $CDCl_3$ is given in Figure II-1a. It clearly shows the peaks corresponding to the EDOT structure at 4.2-4.3 ppm (a) and 6.8 ppm (b) and one signal at 9.9 ppm attributed to the aldehyde function (c).

The reduction of the aldehyde function into primary alcohol was then realized after treatment of EDOT-CHO with $NaBH_4$ to give EDOT-CH_2OH in 80% yield. ^{1}H NMR spectrum of EDOT-CH_2OH in $CDCl_3$ is shown in Figure II-1b. It proves the total derivatization of the aldehyde into alcohol with the appearance of signals located at 4.6 ppm and 1.8 ppm assigned to proton resonances of the CH_2O- and -OH groups respectively, together with the total disappearance of the signal corresponding to the resonance of the aldehyde group at 9.9 ppm.

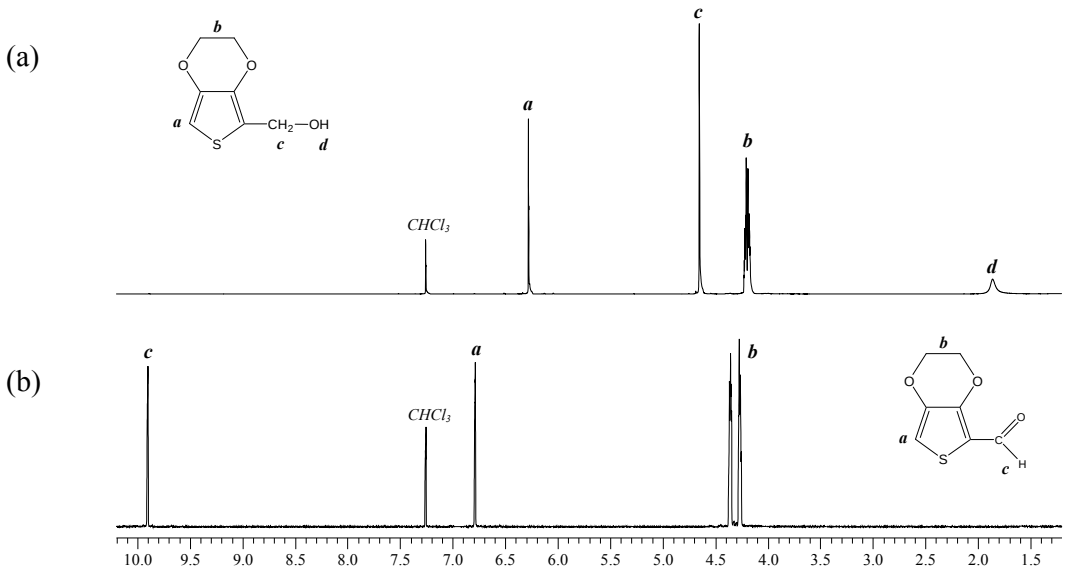

Figure II-1: ^{1}H NMR spectra of (a) EDOT-CHO in $CDCl_3$ (b) EDOT-CH_2OH in $CDCl_3$

I.1.2 Polymerization of ethylene oxide

A series of α-EDOT-PEO macromonomers of different average molecular weights were prepared from the α-EDOT-CH_2OH initiator in THF, in the presence of diphenyl methyl potassium (DPMK) (Scheme II-2).

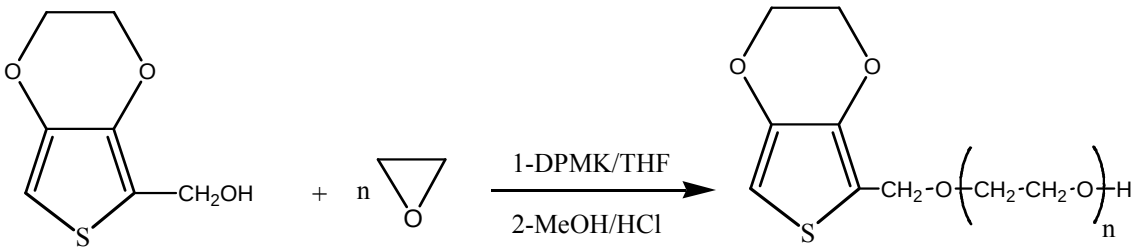

EDOT-CH_2OH α-EDOT-PEO

Scheme II-2: Synthesis of α-EDOT-PEO by EO polymerization initiated with EDOT-CH_2OH

In order to minimize the aggregation alcoholate functions, the hydroxyl groups of the initiator were partially (86%) deprotonated by DPMK. This lack of DPMK is not a problem because the exchange of protons between alcoholates groups (active species) and hydroxyl (dormant species) is significantly faster than the chains growth,[3,4] and it does not affect the controlled mechanism of the polymerization. The reactions were continued under stirring for 72 h at 45°C and then were deactivated by the addition of a MeOH / HCl mixture. Different polymers were then purified by precipitation in cold ether and analyzed by ^{1}H NMR and GPC. The characteristics of the α-EDOT-PEO samples are summarized in Table II-1

The effectiveness of the initiation of the anionic polymerization of ethylene oxide by CH_2OH-EDOT precursor does not seem complete. Indeed, the experimental $\overline{DP}_n$ measured by GPC are lower than their theoretical values, with a monomer conversions between 48 to 81%. This can be explained by a slow polymerization caused by the presence of non-reactive aggregated alcoholates. However, in all cases, the dispersity ($D = M_w/M_n$) is narrow in agreement with the living character of the polymerization and we did not try to optimize further the polymerization conditions in the context of this study.

Stabilizer	[M]/[I]	Reaction time	Theoretical $\overline{M}_n$ (at 100% conversion)	Experimental $\overline{M}_n$ GPC[a] (g/mol)	PDI
S1	46	48h	2000	1200	1.1
S2	91	72h	4000	2000	1.1
S3	136	72h	6000	4900	1.2
S4	227	72h	10000	5200	1.3
S5	454	72h	20000	9700	1.2
S6	1136	72h	50000	25000	1.2
S7	2273	72h	100000	51000	1.1

[M] = concentration of ethylene oxide, [I] = Concentration of EDOT-CH_2OH.
a) Determined in water as mobile phase and PEO as standards

Table II-1: Characteristics of α-EDOT-PEO obtained by anionic polymerization of ethylene oxide using an EDOT-CH_2OH as an initiator.

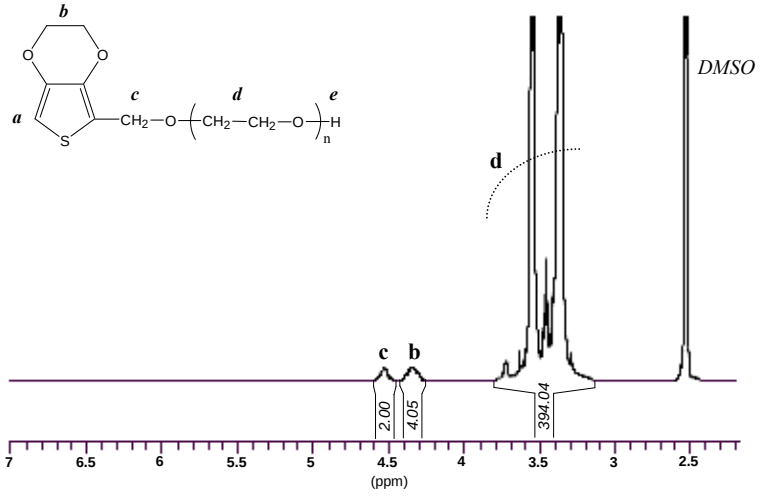

Figure II-2: ^{1}H NMR spectrum of α-EDOT-PEO in DMSO (S2, Table II-1)

The ^{1}H NMR spectrum of the α-EDOT-PEO in DMSO is shown in Figure II-2. The presence of signals at 4.53 and 4.33 ppm corresponding respectively to the protons of EDOT

C**H₂**-O and those of the ether bridge (O-C**H₂**-C**H₂**-O) of EDOT are proof of the functionality of the PEO chains. The integration of the different signals permits the determination of the degree of polymerization of the PEO chain, in agreement with GPC data.

I.2. Dispersion polymerization of EDOT

As EDOT is not soluble in pure water, we tested various solvent mixtures to obtain a homogeneous solution at the start of the polymerization, requirement for dispersion technique. It was found that EDOT and the other reactants were all soluble in a methanol/water mixture (60 % methanol/40 % water in volume fraction). A series of oxidative EDOT dispersion polymerizations were thus performed in this solvent mixture, in the presence of α-EDOT-PEO used as steric reactive stabilizers. Two oxidants were tested, namely ammonium persulfate [$(NH_4)_2S_2O_8$] and iron(III) p-toluene sulfonate hexahydrate [$Fe^{(III)}(OTs)_3$ .6(H_2O)]. The synthesis of PEDOT particles is illustrated in Scheme II-3.

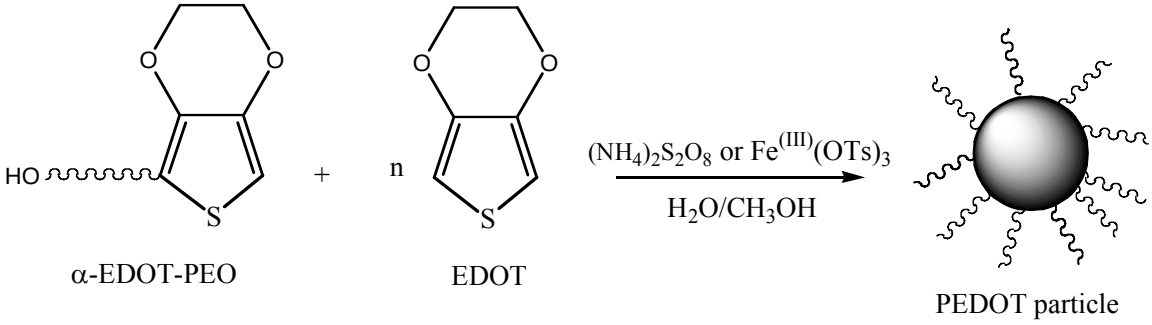

Scheme II-3: Synthesis of PEDOT nanoparticles in alcoholic media in the presence of α-EDOT-PEO using $(NH_4)_2S_2O_8$ or $Fe^{(III)}(OTs)_3$ as an oxidant.

The influence, on the PEDOT particle formation, of various parameters such as the nature of the oxidant, the molar mass and concentration of α-EDOT-PEO have been investigated. Data are given in Table II-2 and II-3

Run N°	Oxidant	α-EDOT-PEO $\overline{M}_n$ g/mol	α-EDOT-PEO [e] introduced wt.-%	T °C	Yield %	Wt % of PEO incorporated	Particle diameter (nm)	Remarks
1	$(NH_4)_2S_2O_8$	1200	50	25	30	nd	-	coagulum
2	$(NH_4)_2S_2O_8$	2000	50	25	32	nd	-	coagulum
3	$(NH4)_2S_2O_8$	5200	20	25	30	nd	100-170[a]	particles
4	$(NH_4)_2S_2O_8$	5200	50	25	35	nd	180 ± 100[c]	particles
5	$(NH_4)_2S_2O_8$	9700	50	25	30	nd	70-150[a]	particles
6[b]	$(NH_4)_2S_2O_8$	10000	50	25	31	nd	-	coagulum
7	$(NH_4)_2S_2O_8$	25000	50	25	35	75	160-500[a]	vesicles
8	$(NH_4)_2S_2O_8$	51000	50	25	32	68	80-120[a]	particles
9	$(NH_4)_2S_2O_8$	51000	50	50	30	62	500 ± 100[c]	particles
10	$(NH_4)_2S_2O_8$	51000	50	85	32	62	235 ± 70[c]	particles
11[d]	$(NH_4)_2S_2O_8$	51000[d]	50	50	25	32	175 ± 25[c]	particles

(a) Determined by TEM, (b) Commercial PEO was used as a stabilizer, (c) Determined by Malvern Zetasizer 3000 HS_A at 25°C in methanol, (d) Pure water was used as dispersant medium, (e) Versus the monomer (EDOT + α-EDOT-PEO), (nd) not determined

Table II-2: Synthesis of PEDOT nanoparticles by dispersion polymerization using $(NH_4)_2S_2O_8$ as an oxidant in water/methanol (3/2)

I.2.1. Use of Ammonium persulfate as an oxidant

The first experiments were performed using ammonium persulfate as an oxidant (at room temperature) in the presence of α-EDOT-PEO at different concentrations ranging from 20 to 50 wt.%. These conditions allowed us to prepare PEDOT-PEO latex particles (runs 3-5 and 7-10) with a relatively low yield (~30%) after three cycles of centrifugation-redispersion in the solvent mixture. A longer reaction time (72 h) and a higher reaction temperature (runs 9-10) did not result in an increase of the particle yield. This last observation argues for a low efficiency of ammonium persulfate oxidant towards EDOT polymerization. As shown in Table II-2, it is worth noting that a critical α-EDOT-PEO molecular weight ($\overline{M}_n$ =5200 g/mol) is required for the formation of a stable PEDOT latex (runs 3-5 and runs 7-10 *vs*. runs 1-2). Indeed, no particles were formed when a lower molecular weight α-EDOT-PEO was used (runs 1-2). This is in agreement with a more effective covering of the particle surface by high molecular weight stabilizer, as already mentioned in the literature.[5]

TEM images of the particles formed using 5200 g/mol (run 3), 9700 g/mol (run 5), 25000 g/mol (run 7) and 51000 g/mol (run 8) α-EDOT-PEO, respectively, are shown in Figure II-5. Loose aggregates of 20-50 nm were observed with 5200 g/mol α-EDOT-PEO sample (Figure II-3a). As the size of the aggregates strongly varied depending on the area observed and considering the particle diameter measured by DLS, the aggregation phenomenon may partly correspond to a drying artifact. Nevertheless, the shape of the constituting particles was not very well-defined. Spheroïdal objects with a diameter ranging from 50 to 100 nm and 80 to 120 nm were observed with 9700 g/mol (Figure II-3b) and 51000 g/mol (Figure II-3d) α-EDOT-PEO samples, respectively. These values are in agreement with those obtained by DLS in methanol (Table II-2). Interestingly, as shown in Figure II-3c, the PEDOT latex obtained from the 25000 g/mol α-EDOT-PEO reactive stabilizer contained vesicle-like hollow spheres. Their diameter ranged from 160 to 500 nm, with a rather regular wall thickness of 30-35 nm, independent of the particle diameter. The formation of such hollow spheres may result from a specific behavior of α-EDOT-PEO reactive stabilizer in these experimental conditions. This will be studied in the following section.

In order to prove the key role of the EDOT moiety attached to the PEO chain, EDOT dispersion polymerization was carried out in the presence of commercial hydroxy-ended PEO of comparable molecular weight (run 6). As shown in Table III-2, no stable latex could be obtained in this case, observation which points out the specific role played by α-EDOT-PEO as a reactive stabilizer towards EDOT dispersion polymerization.

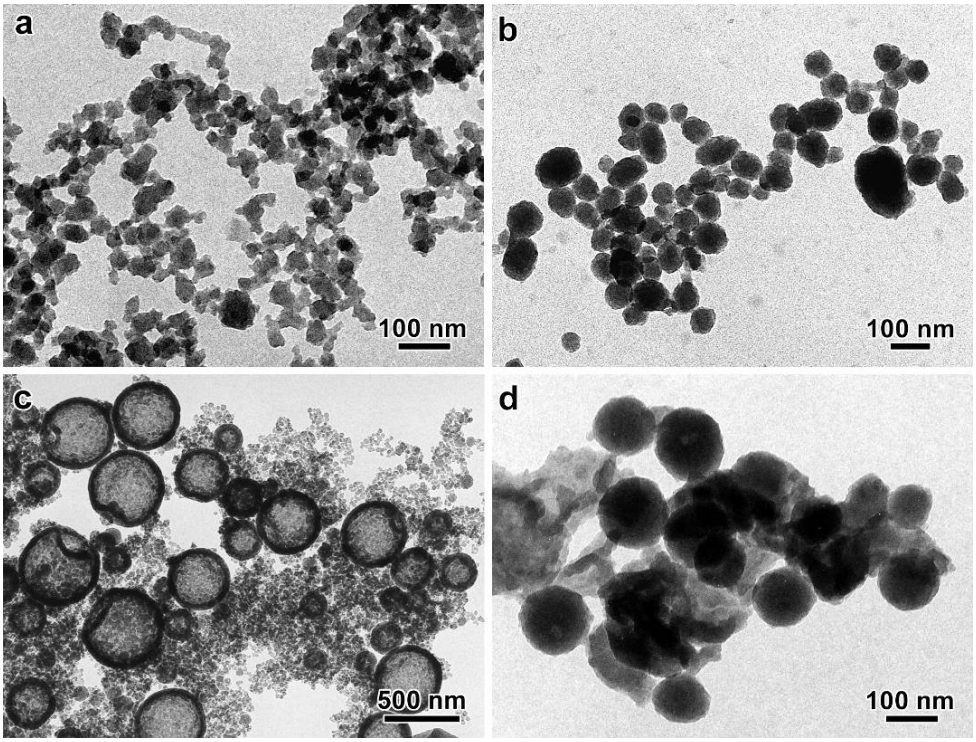

Figure II-3: TEM images of PEDOT particles prepared using PEO-based stabilizers having different molecular weight: a) 5200 g/mol ; b) 9700 g/mol ; c) 25000 g/mol ; d) 51000 g/mol in water/methanol mixture (2/3, v/v) at room temperature using ammonium persulfate as an oxidant.

Finally, EDOT polymerization was performed in pure water in similar experimental conditions. Stable PEDOT latex could be only obtained by using high molecular weight α-EDOT-PEO (run 11). Similarly to experiments implemented in methanol/water mixtures, the yield remains low in the presence of ammonium persulfate as an oxidant. With the objective of better understanding the effect of the PEO functionality type on the control of PEDOT morphology, the behavior of these end-functionalized PEOs was analyzed by DLS at different concentrations in the solvent mixture used in polymerization experiments.

I.2.2. Self-organization of α-EDOT-PEO in methanol/water mixture (2:3)

α-EDOT-PEO solutions were prepared by direct dissolution of the end-functionalized PEO in water/methanol mixture. The auto-correlation functions and their CONTIN analyses[6] obtained at 25°C for different α-EDOT-PEO samples ($\overline{M}_n$ = 9700, 25000 and 51000 g.mol^{-1}) at a concentration of 5 g/L are shown on Figure II-4.

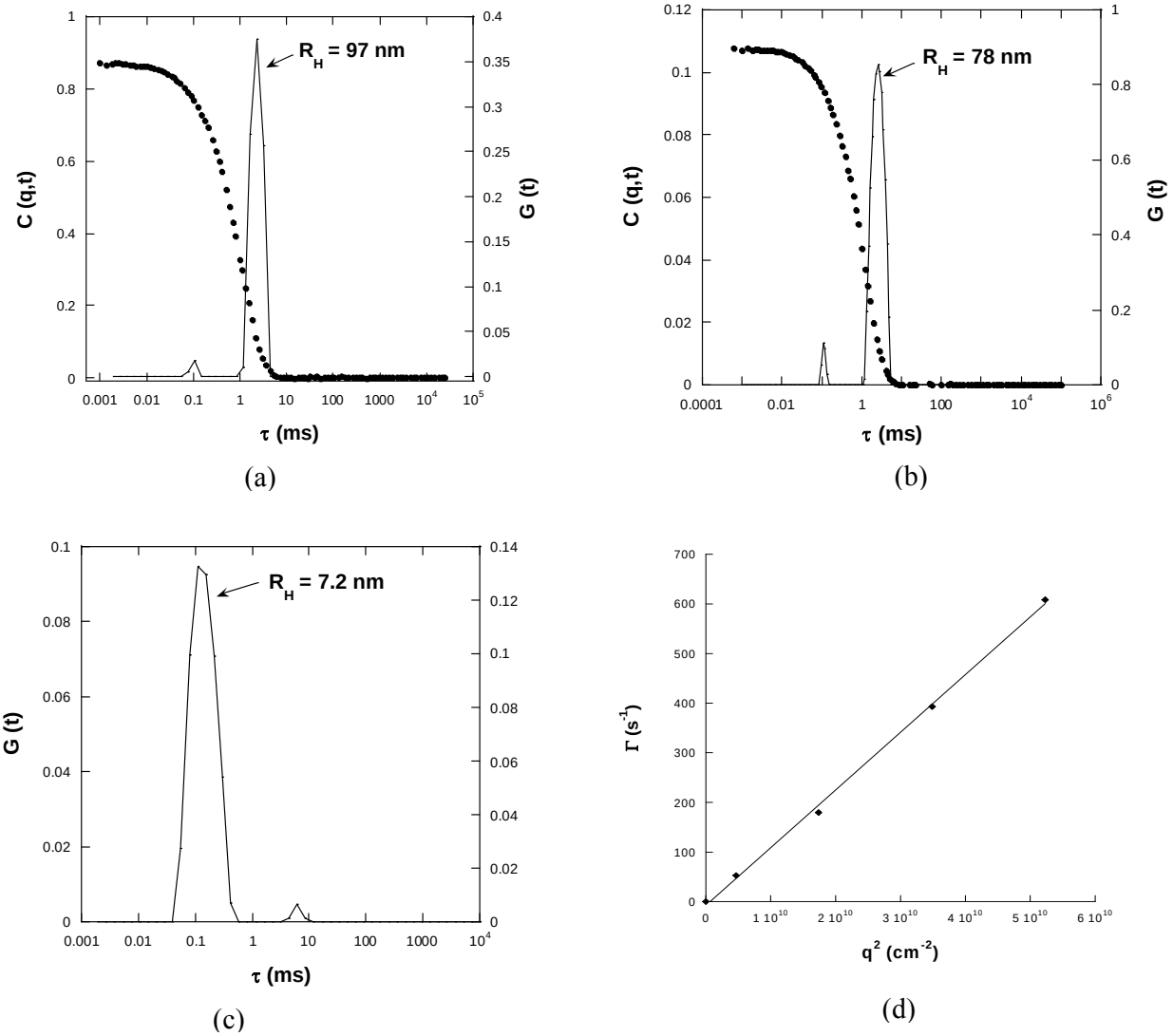

Figure II-4: Auto-correlation function C(q,t) and relaxation time distribution G(t) at 90° of α-EDOT-PEO reactive stabilizers at the concentration of 5g/L in water/methanol mixture (3:2) (a) α-EDOT-PEO ($\overline{M}_n$ = 9700 g.mol^{-1}), (b) α-EDOT-PEO ($\overline{M}_n$ = 25000 g.mol^{-1}), (c) α-EDOT-PEO ($\overline{M}_n$ = 51000 g.mol^{-1}). (d) Relaxation frequency Γ as a function of q^2 for α-EDOT-PEO (Mn = 25000 g.mol^{-1}).

In the case of the lower molecular weight α-EDOT-PEO samples ($\overline{M}_n$ = 9700 and 25000 g.mol^{-1}) (Figures II-4a and II-4b), one main population with hydrodynamic radii R_H respectively of 97 nm and 78 nm can be determined. These typical dimensions are characteristic of micellar aggregation. Concerning the highest molecular weight EDOT-PEO ($\overline{M}_n$ = 51000 g.mol^{-1}) (Figure II-4c), the scattering intensity was very low, consistent with the small size observed (R_H = 7.2 nm) that corresponds to free chains (unimers) in solution. These observations can be easily understood, as a sufficient hydrophilic to hydrophobic balance is needed to ensure enough incompatibility and self-assembly process.

The solution behavior in methanol/water mixture of EDOT-PEO ($\overline{M}_n$ = 25000 g/mol) was more systematically investigated by DLS at different concentrations and different diffusion angles. First, no significant evolution of the apparent hydrodynamic radius has been observed with concentration. In addition, the linear dependence of relaxation frequency Γ as a function of the square of the wave vector q^2 confirms that the observed micellar aggregates are spherical and homogeneous in size (Figure II-4d). Taking into account the dimension of a unimer (about 5 nm), such a morphology is not really consistent with a spherical micelle, but a vesicular structure is expected.[7, 8]

In order to further investigate the morphology of the aggregates formed, SANS of the α-EDOT-PEO sample was performed using D_2O as a solvent. Although not very well-defined, the evolution of the intensity at q^{-2} and q^{-4} suggests again a vesicular type organization (see Figure II-5).

The formation of these spherical objects was further confirmed by TEM analysis (see Figure II-6). The majority of these nanoparticles have a size around 80 nm which is very close to the value obtained by DLS analysis. From these analyses, one may anticipate that α-EDOT-PEO ($\overline{M}_n$ = 25000 g.mol^{-1}) self-assembles to form vesicular nano-objects that serve as templates of PEDOT vesicles (run 7, Table II-2).

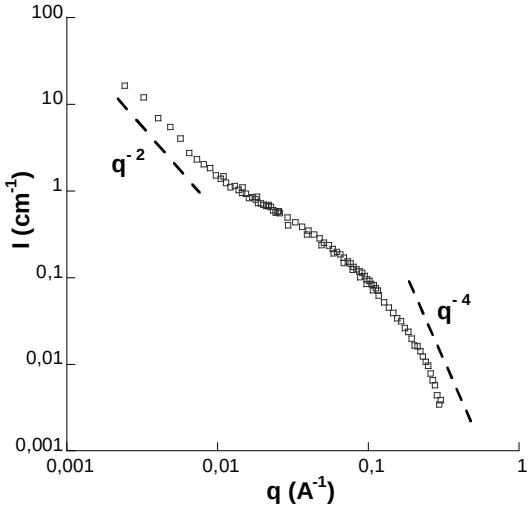

Figure II-5: SANS scattering intensity I(q) profile of α-EDOT-PEO ($\overline{M}_n$ = 25000 g.mol^{-1}) solution (20 g/L) in D_2O.

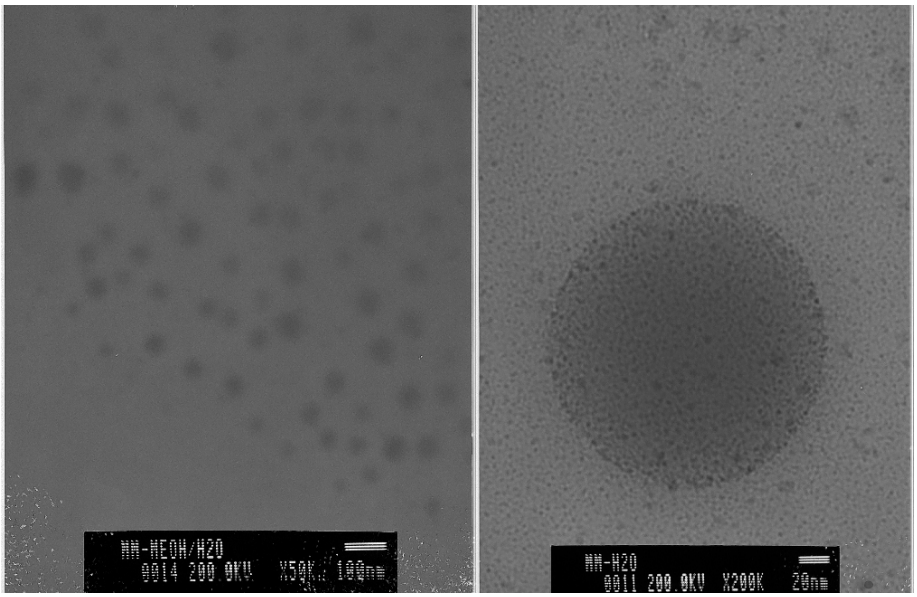

Figure II-6: Cryo-TEM images of α-EDOT-PEO ($\overline{M}_n$ = 25000 g.mol^{-1}) in water/methanol mixture (3:2).

I.2.3. Use of Iron(III) p-toluene sulfonate hexahydrate [$Fe^{(III)}(OTs)_3$ 6(H_2O)] as an oxidant

Conversely to data obtained with [$(NH_4)_2S_2O_8$] as an oxidant, use of high reaction temperature (85°C) allowed us to prepare PEDOT latex in high yield (80%) (runs 1-5, Table II-3) in the presence of $Fe^{(III)}(OTs)_3.6(H_2O)$ after 48 h reaction time (methanol/water; 3/2). In this case, the reaction temperature was found crucial since the polymerization does not take place at room temperature (run 4). The higher efficiency of $Fe^{(III)}(OTs)_3.6(H_2O)$ oxidant in comparison to [$(NH_4)_2S_2O_8$] allowed us to use lower α-EDOT-PEO reactive stabilizer concentration to obtain PEDOT latexes particles (runs1-3and 5). In accordance with literature data, a decrease of the average particle size from 280 to 200 nm was observed when the concentration of the reactive stabilizer α-EDOT-PEO increases from 10 wt% to 50 wt% (runs 1-3).[5] Such a tendency can be explained by a higher surface coverage when using higher amount of steric stabilizer (see Figure II-7).

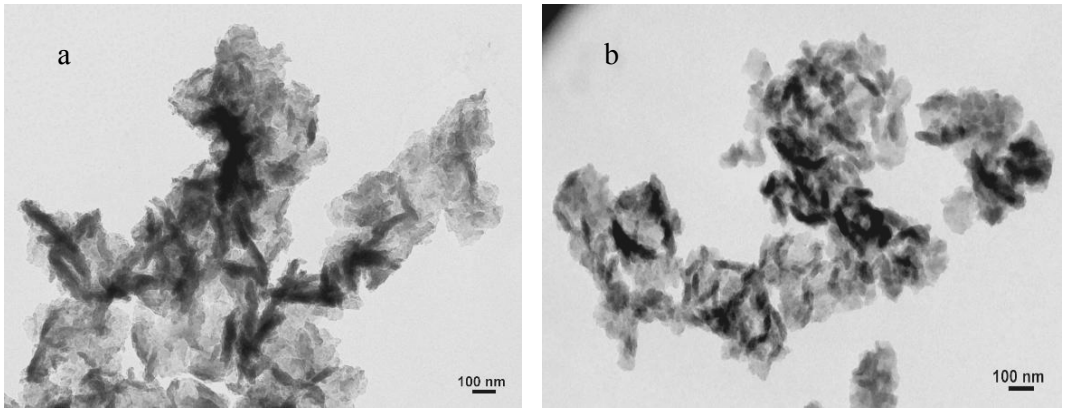

Figure II-7: TEM images of PEDOT nano-rods prepared using PEO-based stabilizers having same molar mass(51000 g/mol) but different different concentrations (a) 20 wt.% and (b) 50 wt.% in water/methanol mixture (2/3, v/v) at 85°C using $Fe^{(III)}(OTs)_3.6(H_2O)$

Run N°	Oxidant	α-EDOT-PEO $\overline{M}_n$ g/mol	α-EDOT-PEO[a] introduced wt.-%	T °C	Yield %	Particle diameter (nm)	Remarks
1	$Fe^{(III)}(OTs)_3$	51000	50	85	80	200 ± 20[b]	particles
2	$Fe^{(III)}(OTs)_3$	51000	20	85	84	260 ± 40[b]	particles
3	$Fe^{(III)}(OTs)_3$	51000	10	85	81	280 ± 30[b]	particles
4	$Fe^{(III)}(OTs)_3$	51000	20	25	0	–	–
5	$Fe^{(III)}(OTs)_3$	25000	20	85	80	264 ± 50 [b]	particles

(a) Versus the monomer (EDOT + α-EDOT-PEO), (b) Determined by Malvern Zetasizer 3000 HS_A at 25°C in methanol,

Table II-3: Synthesis of PEDOT nanoparticles by dispersion polymerization using $Fe^{(III)}(OTs)_3$ as an oxidant in water/methanol (3/2)

I.3. Dimensional and morphological characterizations of PEDOT samples

The particles obtained with the two oxidants were characterized using different techniques with the objectives (i) to confirm the presence of PEO chains attached to the PEDOT particles and (ii) to check the capacity of these materials to exhibit conductive properties. The complete solubilization of the PEDOT-PEO samples in DMF or DMSO - allowing the characterization of the material by GPC and NMR techniques- was only effective when high molar mass PEO was used as a stabilizer and ammonium persulfate as an oxidant (runs 7-11).

The presence of PEO within the samples was proved by ^{1}H NMR spectroscopy. As shown in Figure II-8 (run 10, as an example), signals corresponding to ethylene oxide units (CH_2O-) centered at 3.5 ppm and to EDOT ones (CH_2O-) at 4.3 ppm are clearly observed, allowing us to determine the wt.% of PEO contained in the particle.

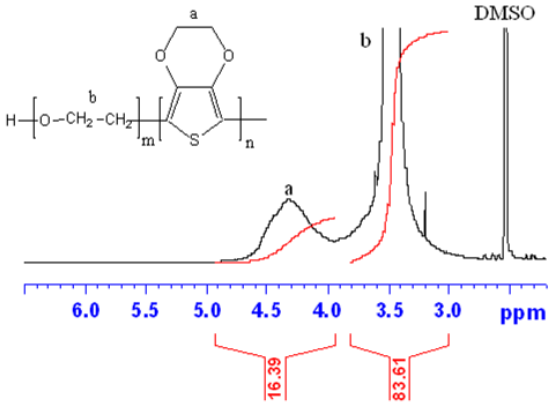

Figure II-8: ^{1}H NMR spectra of PEDOT particles in DMSO (run 10, Table II-2).

As it is indicated in Table II-4, the weight fraction of PEO was found ranging from 32% (run 11) to 75% (run 7). These data underline the higher efficiency of α-EDOT-PEO in methanol/water mixture than in pure water and also show that the particles contain relative high amount of PEO, in agreement with the low conversion of EDOT in these experimental conditions (ammonium persulfate as an oxidant).

EDOT samples were also characterized by double detection (IR and UV) GPC using DMF as a mobile phase and polystyrene as standards (see Table II-4). As it is shown in Figure II-9, the samples could be analyzed using a UV detector, proof of the presence of PEDOT segments, since PEO is not UV-absorbent. GPC traces exhibit monomodal distribution with apparent M_n values ranging from 5000 g/mol. to 11000 g/mol and low dispersity indexes ($1.3<D<1.6$). The higher the temperature, the higher the molar masses (runs 7, 9, 10).

Run N°	α-EDOT-PEO $\overline{M}_n$ g/mol	T °C	$\overline{M}_n$ of PEDOT[a] g/mol	PDI
7	25000	25	5300	1.4
8	51000	25	8400	1.3
9	51000	50	11000	1.4
10	51000	85	11500	1.6
11	51000	50	7400	1.4

a) Determined by GPC using DMF as mobile phase and polystyrene as standards at 60°C

Table II-4: Molar masses of the PEDOT prepared using ammonium persulfate as an oxidant and in the presence of α-EDOT-PEO (50 wt.-%)

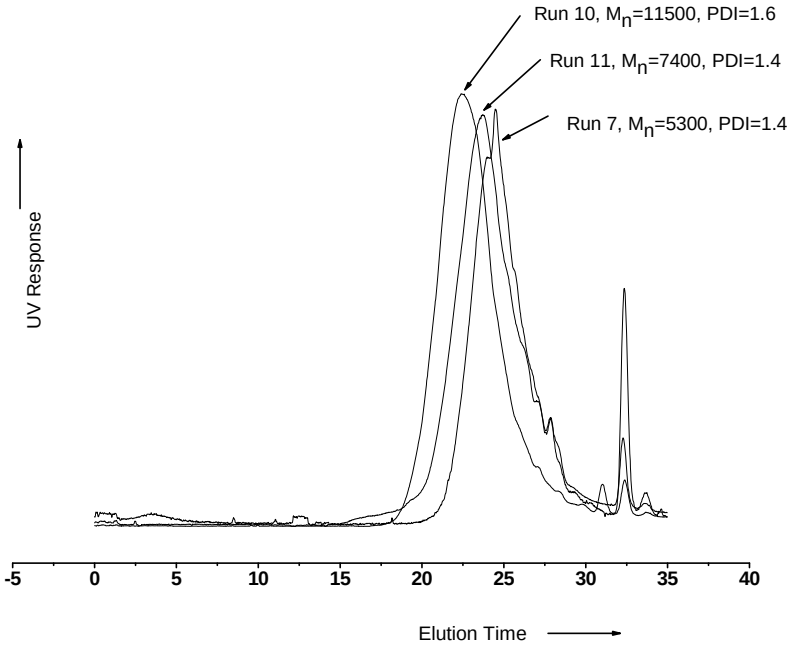

Figure III-9: GPC traces of PEDOT samples runs 7, 10 and 11 (in DMF as eluent at 60°C in the presence of LiBr salt)

It is worth mentioning that PEDOT particles prepared in the presence of $Fe^{(III)}(OTs)_3.6(H_2O)$ as an oxidant, were found insoluble both in DMF and DMSO (even after sonication), impeding a full characterization of the chains contained within the particles. This phenomenon may be attributed to a high content of PEDOT units within the particles so formed, in accord with the high yield obtained.

I.4. Conductivity measurements of PEDOT samples

The conductivity of PEDOT-PEO samples was measured using the conventional four probes technique on dried and compressed PEDOT particles under the form of disc pellets. Contrarily to experiments performed with $Fe^{(III)}(OTs)_3.6(H_2O)$ as an oxidant, addition of para-toluene sulfonic acid (PTSA) as an external doping agent was required for PEDOT samples prepared in the presence of $[(NH_4)_2S_2O_8]$. In the latter case, PTSA (0.33 eq *vs* EDOT) was added at the beginning of the polymerization. Conductivity values were found from $8x10^{-5}$ S/cm to $1.5x10^{-2}$ S/cm for PEDOT samples obtained using 50 wt% and 20 wt% α-EDOT-PEO respectively. This trend is in agreement with the insulating properties of PEO within the material. A similar result has been obtained and reported in the literature for dispersion polymerization of pyrrole.[9,10]

II. Dispersion polymerization of EDOT in the presence of α- and α, ω end-functionalized reactive PEO in methanol/water mixture

In order to optimize the morphology of the PEDOT nano-objects, we study the role of various parameters, such as the functionality, the nature of the termini and the molecular weight of the reactive PEO stabilizers. To that purpose, a series of α-functionalized and α,ω-functionalized PEO of different molecular weight, *i.e.* α-(*N*-methyl pyrrole) PEO (α-Py-PEO), α-thiophene PEO (α-Th-PEO), α-fluorene PEO (α-Flu-PEO), α,ω-(*N*-methyl pyrrole) PEO (α,ω-Py-PEO), α,ω-(thiophene) PEO (α,ω-Th-PEO) and α,ω-(fluorene) PEO (α,ω-Flu-PEO), have been synthesized and compared as steric reactive stabilizers. End groups such as pyrrole, thiophene, or fluorene moieties have been chosen so as to react by oxidative radical coupling with the growing PEDOT chains. In addition, monofunctionalized or telechelic reactive

stabilizers were investigated as they are supposed to behave differently in polymerizations in dispersed media.

II.1. Synthesis of α- and α, ω end-functionalized PEO

A series of PEO, end-capped by one or two functions such as pyrrole (Py), thiophene (Th) or fluorene (Fluo) having different molecular weight were prepared. The latter were synthesized by esterification of α,ω-OH PEO with the corresponding carboxylic acids of pyrrole, thiophene, and fluorene respectively (scheme II-5). The reaction was catalyzed by the 1:1 molecular complex of 4-(dimethylamino) pyridine with *p*-toluenesulfonic acid also known as 4-(dimethylamino)pyridinium 4-toluenesulfonate (DPTS), the role of DPTS being to favor the ester formation by suppressing the side reaction leading to the formation of *N*-acylurea.[11] The chain-end derivatization proceeds readily at room temperature which results in the formation of mono- or difunctionalized PEO depending on the amount of the carboxylic acid used. The general synthetic pathway is shown in Scheme II-4.

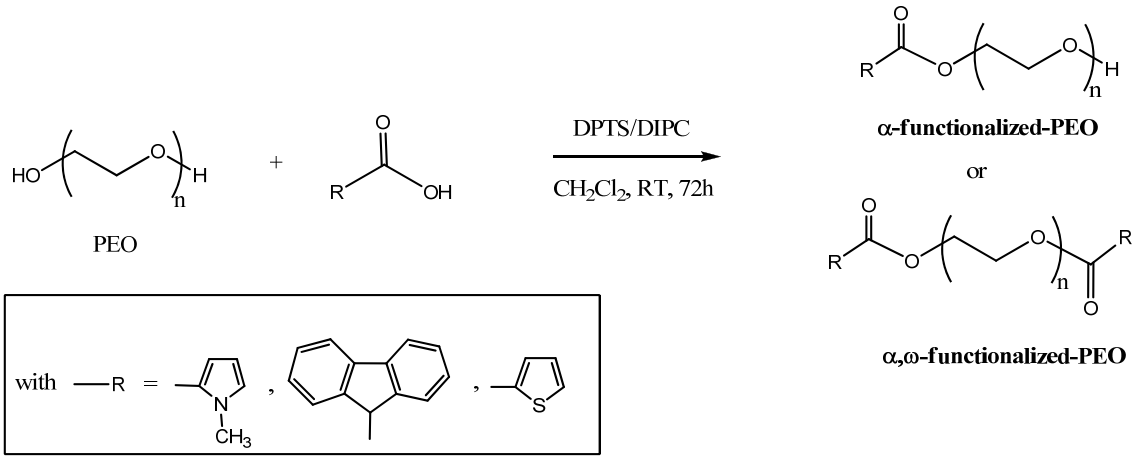

Scheme II-4: **Synthesis of end-capped PEO by esterification reaction of α,ω-OH-PEO with various carboxylic acids, *i.e.* *N*-methyl-2-pyrrolecarboxylic acid, thiophene-2-carboxylic acid and fluorene-9-carboxylic acid**

All the functionalized PEO were characterized by ^{1}H NMR spectroscopy. Three examples are shown in Figure II-10. The ^{1}H NMR spectrum in DMSO of α-Py-PEO ($\overline{M}_n$ = 10000 g.mol^{-1}) is shown in Figure II-10b (to compare with that of α,ω-OH PEO Figure II-

10a). The appearance of signals at 6.08 ppm (a), 6.83 ppm (b) and 7.09 ppm (c), due to pyrrole ring protons resonance and at 4.27 ppm (d) due to CH_2O- of the ester function confirms the presence of pyrrole moiety at the PEO chain-end. The integration values of each peak are in accordance with the presence of only one pyrrole unit per PEO chain. Similarly, the complete disappearance of signal at 4.54 ppm due to -OH function confirms the synthesis of α,ω-Py-PEO, as demonstrated on Figure II-10c.

In the same way, the disappearance of signal at 4.54 ppm (-OH group) together with the appearance of signals at 7.22 ppm–7.96 ppm due to thiophene ring protons and at 4.36 ppm due to CH_2O- of ester group respectively, are in accordance with the formation of α,ω-Th-PEO ($\overline{M}_n$ = 10000 g.mol^{-1}) (see Figure II-11a). The ^{1}H NMR spectrum of α,ω-flu-PEO was performed in $CDCl_3$ as fluorene peaks are difficult to distinguish in DMSO. The signals at 7.31 ppm-7.74 ppm due to the resonance of fluorene ring protons and at 4.31 ppm due to resonance of protons from CH_2O- of the ester group, together with the complete disappearance of –OH signal at 2.65 ppm prove the presence of fluorene moieties at both end of the PEO chain ($\overline{M}_n$ = 10000 g.mol^{-1}) (see Figure II-11b). This was confirmed by integration of the different signals. SEC traces of all these end-functionalized PEO remain monomodal and match the ones of α,ω-OH PEO precursor which confirms that the functionalization reactions did not alter the structure of the PEO chains.

The presence of aromatic functions in modified PEO chains can also be verified by UV-visible spectroscopy. UV-visible spectra of the modified and un-modified poly(ethyleneoxide) was performed in $CHCl_3$. All modified poly(ethyleneoxide) give strong absorption at about 300 nm due to aromatic rings present at the chain end while un-modified PEO does not absorb in UV-visible region (Figure II-12).

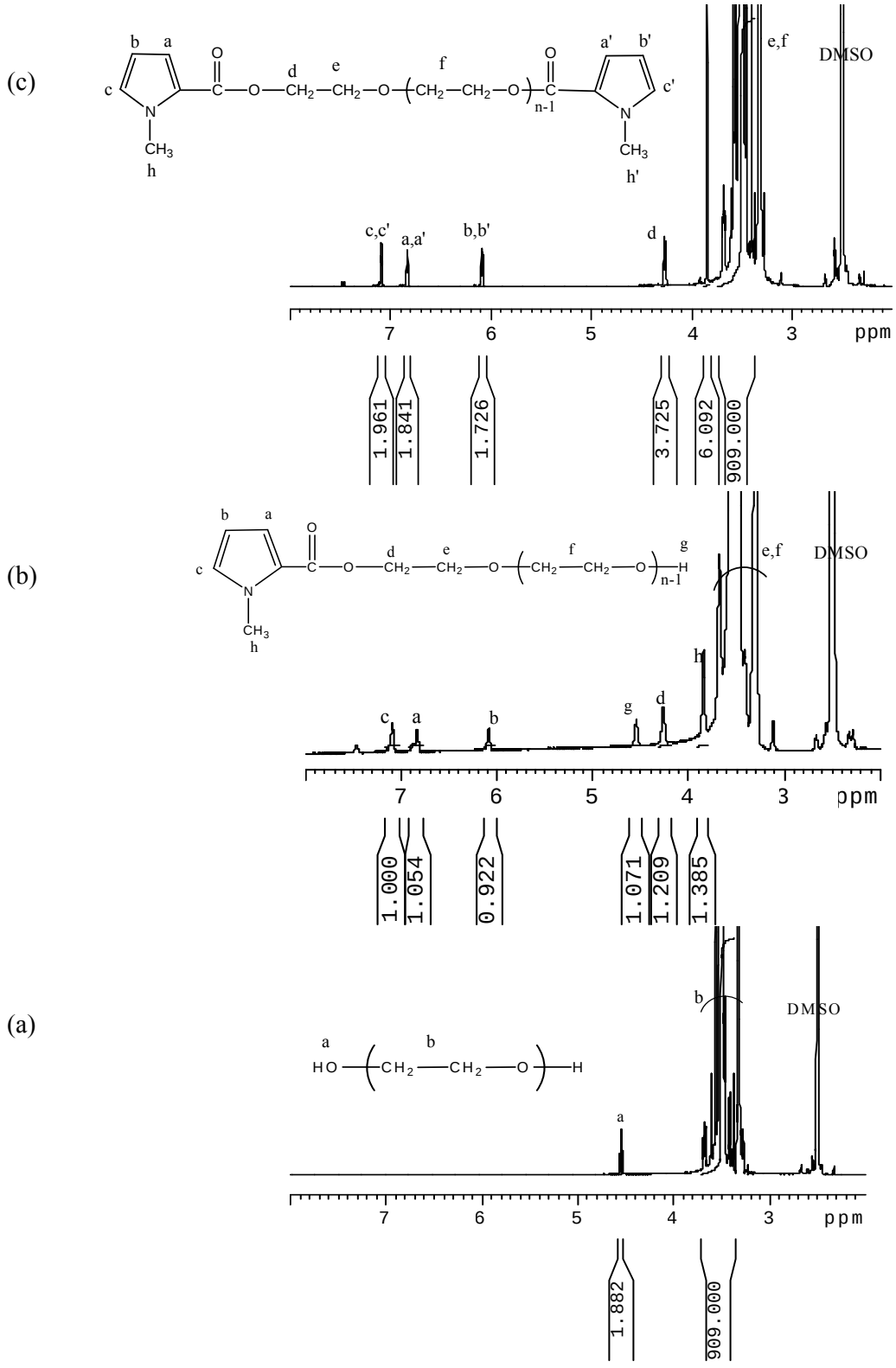

Figure II-10: ^{1}H NMR spectra of (a) Poly(ethylene oxide) (b) α-N-methyl-pyrrole poly (ethylene oxide), (c) α,ω-N-methyl-pyrrole poly (ethylene oxide) in DMSO.

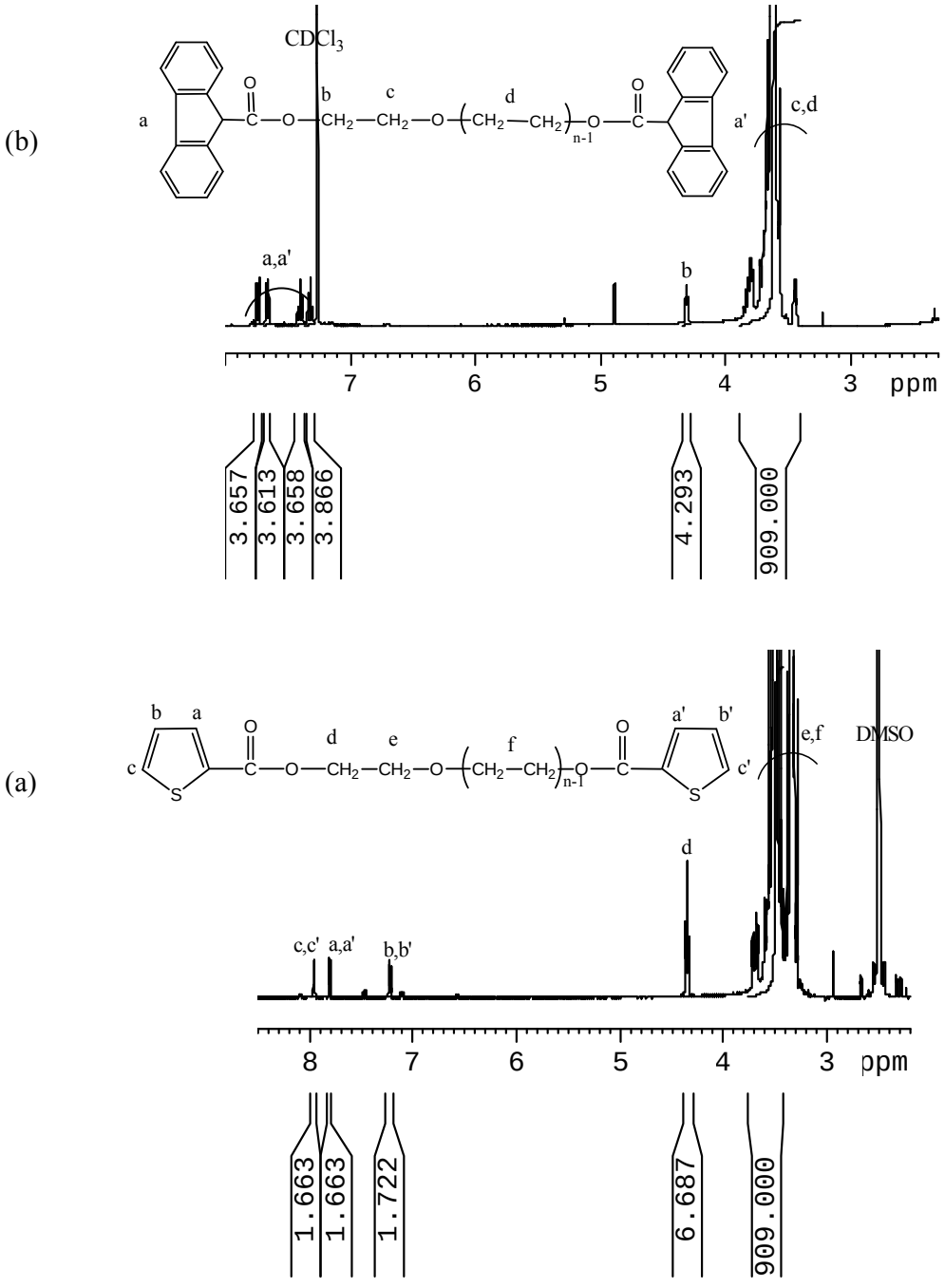

Figure II-11: ^{1}H NMR (400MHz) spectra of (a) α,ω-Th-PEO in DMSO-*d*6 and (b) α, ω -Fluo-PEO in $CDCl_3$

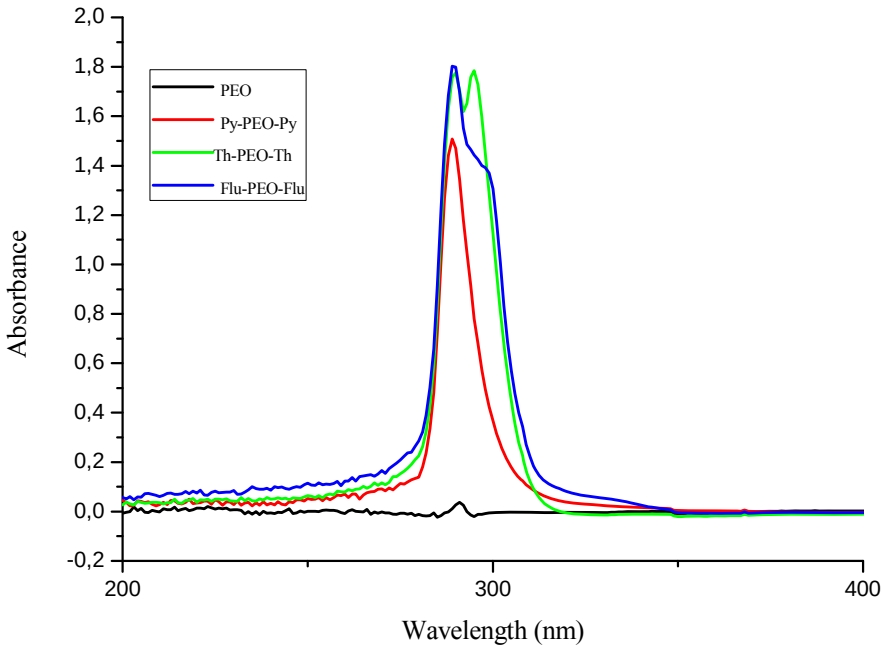

Figure II-12: UV-Visible spectra of modified and un-modified poly(ethyleneoxide) in $CDCl_3$ (5mg/mL)

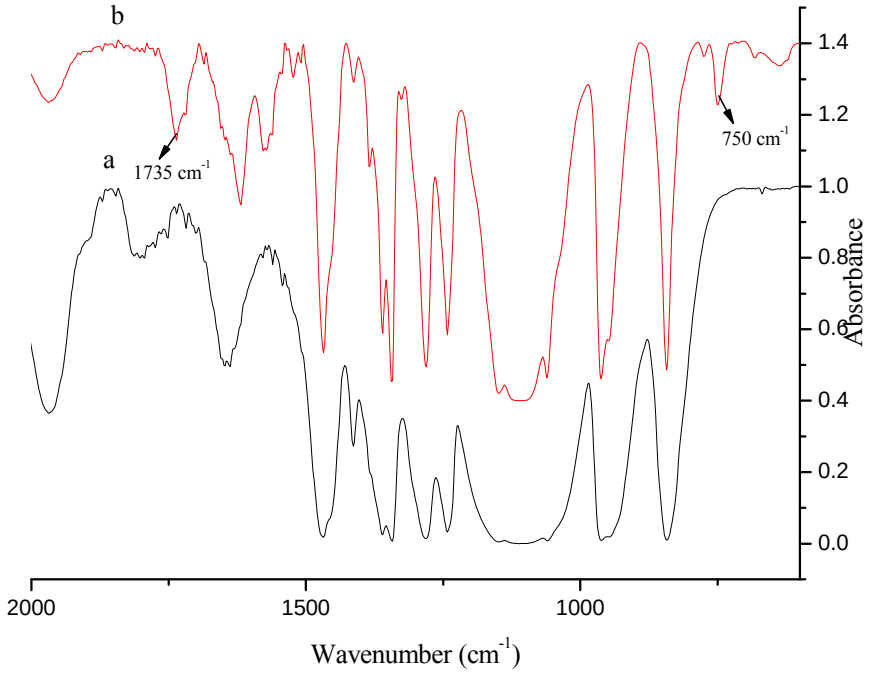

Figure II-13: FTIR spectra of (a) α,ω-OH-PEO and (b) α,ω-Flu-PEO

The functionalization of poly(ethyleneoxide) by reactive organic moieties was also confirmed by Fourier transform infrared (FTIR) spectroscopy. The appearance of peaks at 1735 cm^{-1} due to C=O stretching vibration of the ester group and at 750 cm^{-1} due to CH out of plane deformation vibration of aromatic ring confirms the functionalization of the poly(ethyleneoxide) by aromatic moieties. These features are not observed in un-modified poly(ethyleneoxide) (see Figure II-13)

II.2. Dispersion Polymerization of EDOT

As already described in the previous section, due to the limited solubility of EDOT in water,[12] the dispersion polymerization of EDOT was always performed in a mixture of methanol and water (2/3, v/v) (see Scheme II-5). The effect of the molecular weight, functionality and concentration of the reactive PEO as well as the nature and concentration of the oxidant used, on the PEDOT particle size control was investigated.

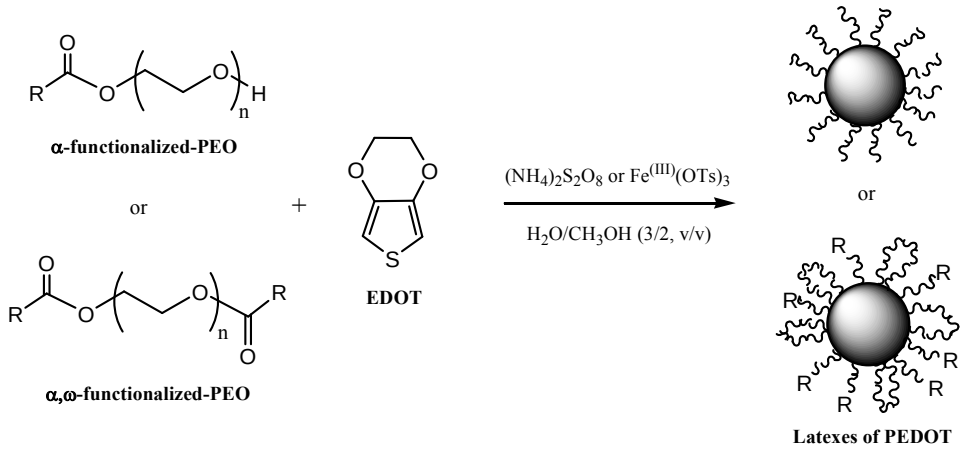

Scheme II-5: Synthesis of PEDOT latexes by dispersion polymerization in methanol/water (2:3) mixture in the presence of α-functionalized-PEO and α,ω-difunctionalized-PEO reactive steric stabilizers.

II.2.1. Use of of α-Py-PEO and α-Flu-PEO as reactive stabilizers

Dispersion polymerization data performed in the presence of α-Py-PEO and α-Flu-PEO are gathered in Table II-5. As can be seen, the size and the morphology of the PEDOT nano-objects are affected by the nature of the oxidant, the molecular weight, the concentration and the functionality of the reactive PEO.

II.2.1.1. $(NH_4)_2S_2O_8$ as an oxidant

As already noticed with α-EDOT-PEO, dispersion in the presence of low molecular weight α-Py-PEO (5000 g.mol^{-1}) (run 1) does not yield well-defined nano-objects. Coagulation generally occurs in the presence of low molecular weight reactive stabilizer. However, well-defined spherical particles could be obtained with the help of higher molecular weight reactive stabilizer (from 10000 to 35000 g.mol^{-1}) in the presence of $(NH_4)_2S_2O_8$. The particle size decreased from 550-600 nm to 350-450 nm as the molecular weight of α-Py-PEO goes from 10000 g/mol to 35000 g/mol (runs 2 & 10). This is explained by a higher surface coverage of high molecular weight stabilizer as compared to smaller one, leading to the formation of a higher number of stable primary particles at the start of the dispersion polymerization. Similar results were obtained and reported by Mandal and coll. for the dispersion polymerization of pyrrole.[13]

As a general trend,[9,10] the size of the PEDOT particles decreases with the increase in stabilizer concentration; the particle size goes from 550-600 nm to 300-350 nm as the concentration of α-Py-PEO ($\overline{M}_n$ = 10000 g.mol^{-1}) varies from 20 wt.% to 50 wt.% (see runs 2-4). Indeed, the use of higher amount of stabilizer enables a higher surface coverage and therefore leads to the formation of a larger number of stable primary particles at the beginning of the reaction. As shown by SEM images of PEDOT particles, the size distribution of the particles formed in these conditions is quite narrow, underlining the efficient role of α-Py-PEO (Figure II-14) as a steric and reactive stabilizer.

Run N°	Oxidant type	Stabilizer type	Oxidant (Mole Equivalent)[b]	stabilizer Mn (g/mol)	stabilizer Introduced (Wt.%)	Yield (%)	PEO Incorporated (determined by ^{1}H NMR (%)	Conductivity (S/cm)	Mn (and dipersity of the PEDOT samples) ($g.mol^{-1}$)	Particle size (nm)[c]	Remarks
1	$(NH_4)_2S_2O_8$	α-Py-PEO	1.6	5000	20	50	nd	nd	nd	_	Coagulum
2	$(NH_4)_2S_2O_8$	α-Py-PEO	1.6	10000	20	50	17	nd	nd	550-600	Particles
3	$(NH_4)_2S_2O_8$	α-Py-PEO	1.6	10000	35	50	22	nd	6000 (1.6)	400-500	Particles
4	$(NH_4)_2S_2O_8$	α-Py-PEO	1.6	10000	50	55	23	nd	5500 (1.7)	300-350	Particles
5	$(NH_4)_2S_2O_8$	α-Py-PEO	1.4	10000	50	55	5	5.40×10^{-6}	6000 (2.0)	600-700	Particles
6	$(NH_4)_2S_2O_8$	α-Py-PEO	2.3	10000	50	55	10	4.23×10^{-6}	5100 (1.7)	400-600	Particles
7	$(NH_4)_2S_2O_8$	α-Flu-PEO	1.6	10000	20	60	27	4.40×10^{-6}	7000 (1.8)	450-500	Particles
8	$(NH_4)_2S_2O_8$	α-Py-PEO	1.6	20000	20	50	28	4.36×10^{-6}	6000 (1.6)	200-500	Particles
9	$(NH_4)_2S_2O_8$	α-Py-PEO	1.6	20000	35	55	21	3.36×10^{-6}	5200 (1.7)	150-300	Particles
10	$(NH_4)_2S_2O_8$	α-Py-PEO	1.6	35000	20	40	12	8.38×10^{-6}	6200 (1.8)	350-400	Particles
11	$(NH_4)_2S_2O_8$	α-Py-PEO	1.6	35000	35	50	3	1.28×10^{-6}	6100 (1.7)	275-300	Particles
12[a]	$Fe(OTs)_3$	α-Py-PEO	2.6	35000	20	83	nd	1.10×10^{-2}	_	_	Desert rose
13[a]	$Fe(OTs)_3$	α-Py-PEO	2.6	35000	35	75	nd	1.90×10^{-2}	_	_	Desert rose
14[a]	$Fe(OTs)_3$	α-Py-PEO	2.6	35000	50	80	nd	1.74×10^{-3}	_	_	Desert rose

a) Reactions were carried at 85 °C
b) Versus monomer
c) More than 95 % of particles belong to the span given

Table II-5: Synthesis of PEDOT dispersions in methanol/water mixture (2:3) using mono-functionalized PEO-based reactive stabilizer at 35°C

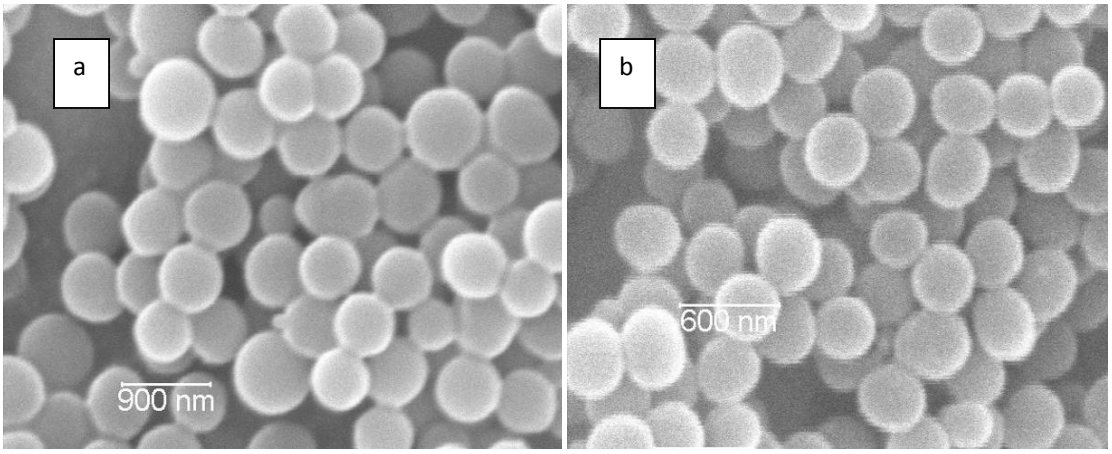

Figure II-14: SEM images of PEDOT core-shell particles prepared in the presence of (a) α-Py-PEO, 10000 g.mol^{-1}, 20 wt.%, (run 2, Table II-5) and (b) α-Py-PEO, 35000 g.mol^{-1}, 20 wt.% (run 10, Table II-5).

The substitution of pyrrole end group by fluorene function has nearly no effect on the particle size. For a given PEO molar mass and concentration (runs 2 & 10), particles with a comparable size and a narrow size distribution are obtained.

As already noticed in a previous section (Table II-2) the yield in PEDOT particles never exceeds 60% irrespective of the $(NH_4)_2S_2O_8$ concentration. This can be explained by the low efficiency of this oxidant, compared to $Fe^{III}(OTs)_3.6H_2O$ (see below). In addition, all the samples prepared using $(NH_4)_2S_2O_8$ were found soluble in DMF and DMSO, allowing the characterization of the PEDOT samples by GPC and ^{1}H NMR. As indicated in Table II-5, the molecular weights determined by GPC against polystyrene calibration remain in the range 5000-7000 g.mol^{-1} whatever the experimental conditions. A typical GPC trace is shown in Figure II-15

The wt% of PEO incorporated within the PEDOT samples could be determined by means of NMR spectroscopy by comparing integrations of peaks at 3.5 ppm and 4.4 ppm that are due to the resonances of ethylene protons of ethylene oxide and PEDOT repeating units, respectively. The PEO content within the particles is generally high (3-28 wt.%) and proportional to the amount of reactive PEO introduced at the beginning of the polymerization,

proving the effective participation of the reactive stabilizer in the whole polymerization (Figure II-16).

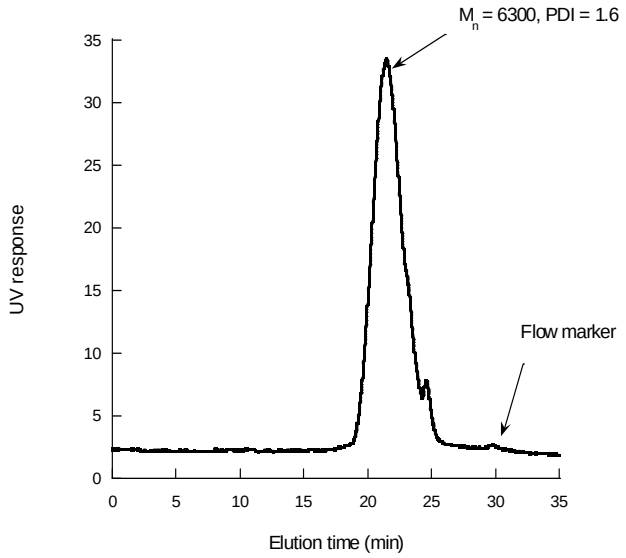

Figure II-15: GPC trace of PEDOT sample prepared using α-Py-PEO, $\overline{M}_n$ = 20000 g.mol^{-1}, 20 wt.% (Run 8, Table II-5), in DMF as eluent at 60 °C in the presence of LiBr salt.

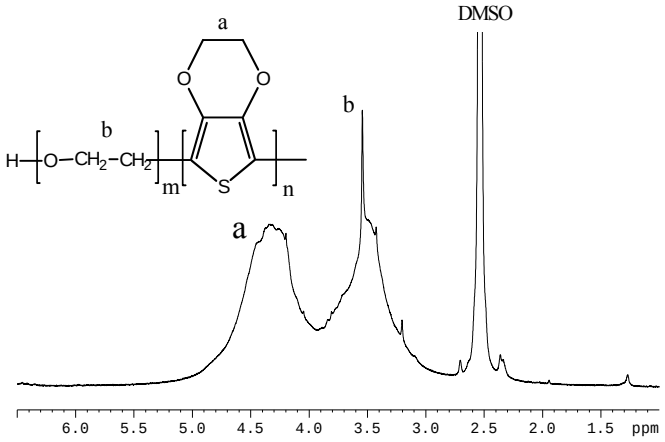

Figure II-16: ^{1}H NMR spectra in DMSO of PEDOT samples prepared using α-Py-PEO as reactive stabilizer, $\overline{M}_n$ = 20000 g.mol^{-1}, 20 wt.% (Run 8, Table II-5)

All the data highlight that α-Py-PEO and α-Flu-PEO are efficient reactive stabilizers for the synthesis of calibrated PEDOT particles in the presence of $(NH_4)_2S_2O_8$. In particular, a better control of the particle size and size distribution was systematically obtained as compared to experiments conducted in the presence of α-EDOT-PEO, for which a higher

concentration (50 wt%) was required to finally obtain rather broad particle size distribution (runs 6-8, Table II-2).

II.2.1.2. End-functionalized PEO behavior in methanol/water mixture (2/3, v/v) with respect to the end-group nature

We performed DLS analysis of α-Py-PEO and α-Flu-PEO reactive stabilizers of different molecular weights and concentrations. As previously observed for the highest molecular weight α-EDOT-PEO (Figure II-4c), one single population, corresponding to unimers with R_H in the range 4-5 nm, is observed as it is clear from relaxation time distributions [G(t)] at 90° and relaxation frequency (Γ) as a function of q^2 for α-Py-PEO and α-Flu-PEO at the concentration of 5 g/L (Figure II-17). Similar results were obtained for other concentrations at different angles (Figure II-18). Hence, we can consider that α-Py-PEO and α-Flu-PEO reactive stabilizers do not form micellar-like aggregates in this solvent mixture. Their complete solubility in the solvent mixture ensure true dispersion polymerization conditions and may explain the quite good control of the PEDOT particle size distribution and morphology.

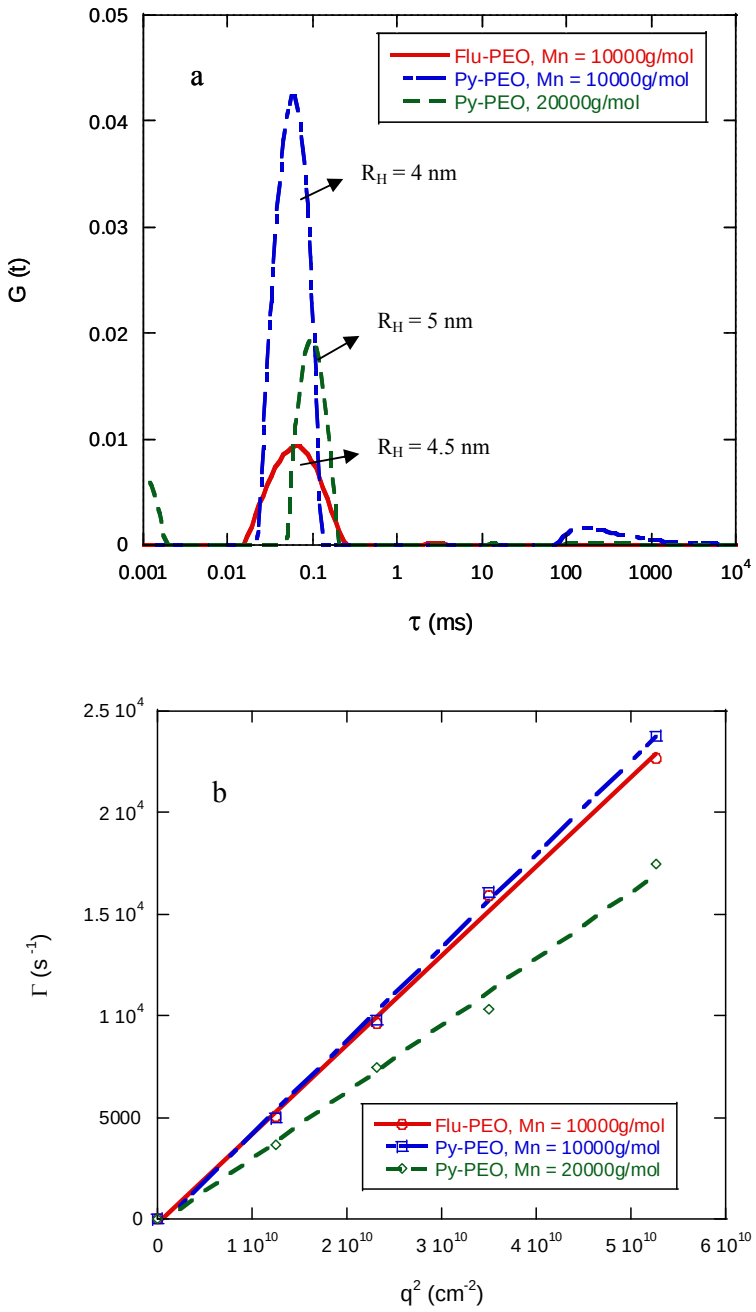

Figure II-17: (a) Relaxation time distributions G(t) at 90° and (b) relaxation frequency Γ as a function of q^2 for α-Flu-PEO ($\overline{M}_n$ = 10000 g.mol^{-1}), α-Py-PEO ($\overline{M}_n$ = 10000 g.mol^{-1}) and Py-PEO ($\overline{M}_n$ = 20000 g.mol^{-1}) at 5 g/L concentration

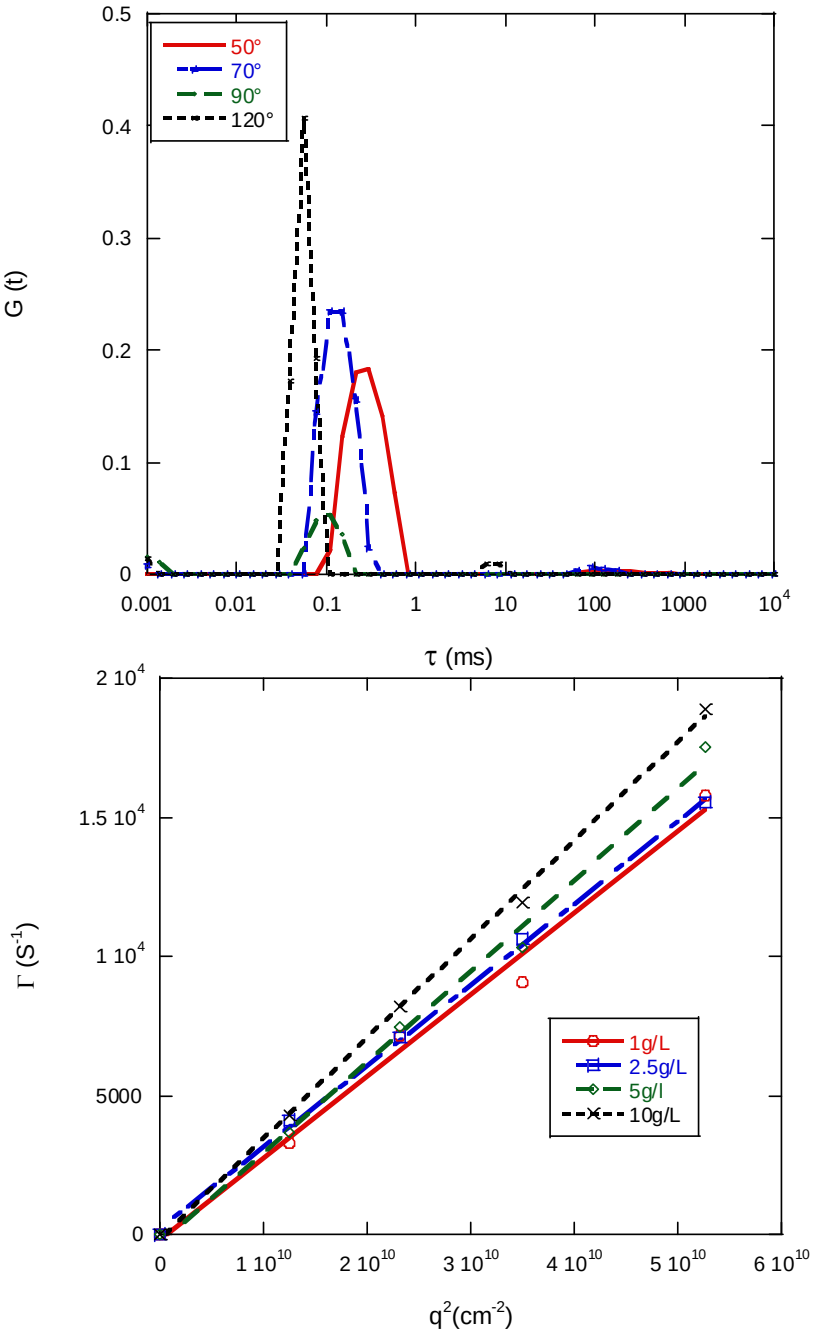

Figure II-18: (a) Relaxation time distributions G(t) at different angles and at 5 g/L, (b) Relaxation frequency Γas a function of q^2 at different concentrations for Py-PEO ($\overline{M}_n$ = 20000 g.mol^{-1})

II.2.1.3. $Fe(OTs)_3.6(H_2O)$ as an oxidant

Let us recall that very low yield is obtained at room temperature with $Fe(OTs)_3.6(H_2O)$ (run 4,Table II-3). The polymerization of EDOT was thus performed at 85 C, in the presence of α-Py-PEO. Unlike polymerizations conducted in the presence of $(NH_4)_2S_2O_8$, the solution color' change "from transparent to blue purple" is quite fast with $Fe(OTs)_3.6(H_2O)$, in accord with a higher efficiency of this latter oxidant, leading to high polymerization yields (runs 12-14). The probable high molecular weights PEDOTs within the samples impede their dissolution in any common organic solvent, limiting their characterization at the molecular level. In these experimental conditions, nano-objects with desert rose-like morphology are obtained as shown in Figure II-19. Such a morphology may be explained by the fact that α-Py-PEO is not effective enough to sufficiently stabilize the first nuclei, condition to obtain well-defined spherical particles.

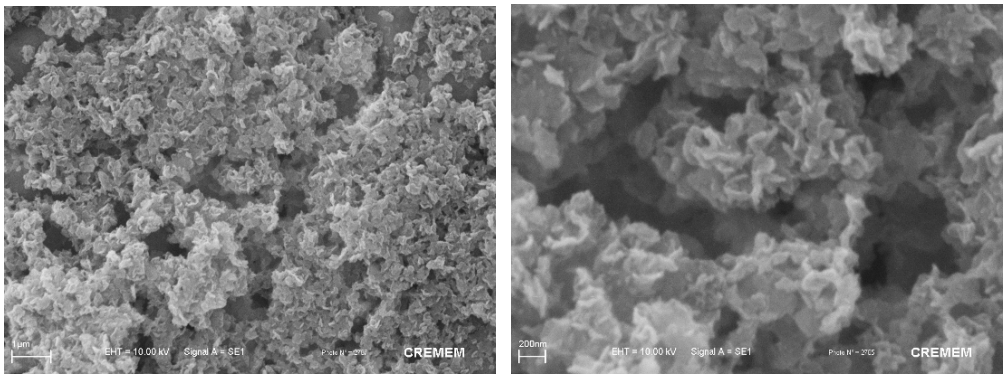

Figure II.19: SEM images of PEDOT samples prepared using α-Py-PEO reactive stabilizer ($\overline{M}_n$ = 35000 g.mol^{-1}, 20 wt.%, run 12, Table II-5) in the presence of $Fe^{(III)}(OTs)_3.6(H_2O)$ as an oxidant.

II.2.2. Dispersion Polymerization of EDOT in the presence of α,ω-difunctionalized PEO reactive stabilizers

In order to further study the effect of PEO end groups onto the control of PEDOT particles, telechelic PEO (α,ω-Py-PEO, α,ω-Flu-PEO and α,ω-Th-PEO) were used as reactive stabilizers.

II.2.2.1. $(NH_4)_2S_2O_8$ as an oxidant

The dispersion polymerization data of EDOT in the presence of α,ω-difunctionalized PEO used as reactive steric stabilizers yields very well-defined PEDOT particles, as shown in Table II-5. Alike experiments performed with monofunctional PEO, similar trend in the PEDOT particle size was observed with respect to the stabilizers molecular weight and concentration. A comparison between the different stabilizers clearly shows that the size and size distribution of PEDOT particles obtained with α,ω-Flu-PEO stabilizer (run 7; 200-250 nm) are slightly smaller than those obtained with α,ω-Py-PEO (run 4; 350-400 nm) and α,ω-Th-PEO (run 2; 250-400 nm), in similar experimental conditions. SEM and TEM images of the PEDOT particles prepared using these difunctional stabilizers are shown in Figure II.20 that demonstrates the narrow size distribution of PEDOT particles.

The PEDOT samples prepared in these conditions were soluble in DMF and DMSO and could be characterized as described above with monofunctional end-capped PEO. From these analyses, the amount of incorporated/grafted PEO could be determined. High wt % of incorporated PEO (19-40 wt %) was measured while using these difunctional PEO. This result may be logically explained by the presence of the two reactive end-groups per chain. From this investigation, it can be partially concluded that the behaviors of monofunctional- and difunctional PEO are quite comparable with respect to the control of the PEDOT morphology. However, unlike PEDOT latexes obtained with monofunctional PEO as steric stabilizer, the latexes obtained in the presence of difunctional PEO were found stable for very long time (several months without sedimentation) and were also more easily re-dispersible in the solvent mixture. This feature was explained by the higher wt % of incorporated PEO while using telechelic (difunctional) reactive stabilizer.

Run N°	Oxidant type	Stabilizer type	stabilizer M_n (g/mol)	Amount of stabilizer Introduced (Wt.%)	Yield (%)	PEO Incorporated (determined by ^{1}H NMR) (%)	M_n(and dispersity of the PEDOT samples) ($g.mol^{-1}$)	Particle diameter (nm)	Remarks
1	$(NH_4)_2S_2O_8$	α,ω-Th-PEO	10000	20	50	25	5500 (1.7)	350-400	Particles
2	$(NH_4)_2S_2O_8$	α,ω-Th-PEO	35000	35	60	29	5300 (1.6)	250-400	Particles
3	$(NH_4)_2S_2O_8$	α,ω-Py-PEO	10000	20	60	19	7000 (1.5)	500-600	Particles
4	$(NH_4)_2S_2O_8$	α,ω-Py-PEO	35000	35	60	40	5800 (1.5)	350-400	Particles
5	$(NH_4)_2S_2O_8$	α,ω-Flu-PEO	10000	20	60	40	5400 (1.4)	350-400	Particles
6	$(NH_4)_2S_2O_8$	α,ω-Flu-PEO	35000	20	55	30	7100 (1.6)	275-300	Particles
7	$(NH_4)_2S_2O_8$	α,ω-Flu-PEO	35000	35	60	30	6300 (1.6)	200-250	Particles
8	$(NH_4)_2S_2O_8$/ $FeCl_3$	α,ω-Py-PEO	20000	20	75	35	5400 (1.7)[a]	50-60	Particles
9	$(NH_4)_2S_2O_8$/ $FeCl_3$	α,ω-Flu-PEO	20000	20	75	30	5400 (1.5)[a]	50-60	Particles
10	$(NH_4)_2S_2O_8$/ $FeCl_3$	α,ω-Th-PEO	20000	20	75	33	5300 (1.8)[a]	35-40	Particles
11[b]	$Fe(OTs)_3$	α,ω-Flu-PEO	35000	35	80	nd	nd	50-80	Particles
12[b]	$Fe(OTs)_3$	α,ω-Flu-PEO	35000	50	80	nd	nd	50-60	Particles

a) Partially soluble in DMF

b) Reaction temperature was 85°C

Table II-6: Synthesis of PEDOT dispersions in methanol/water mixture (2:3) using α,ω-functionalized PEO-based reactive stabilizer

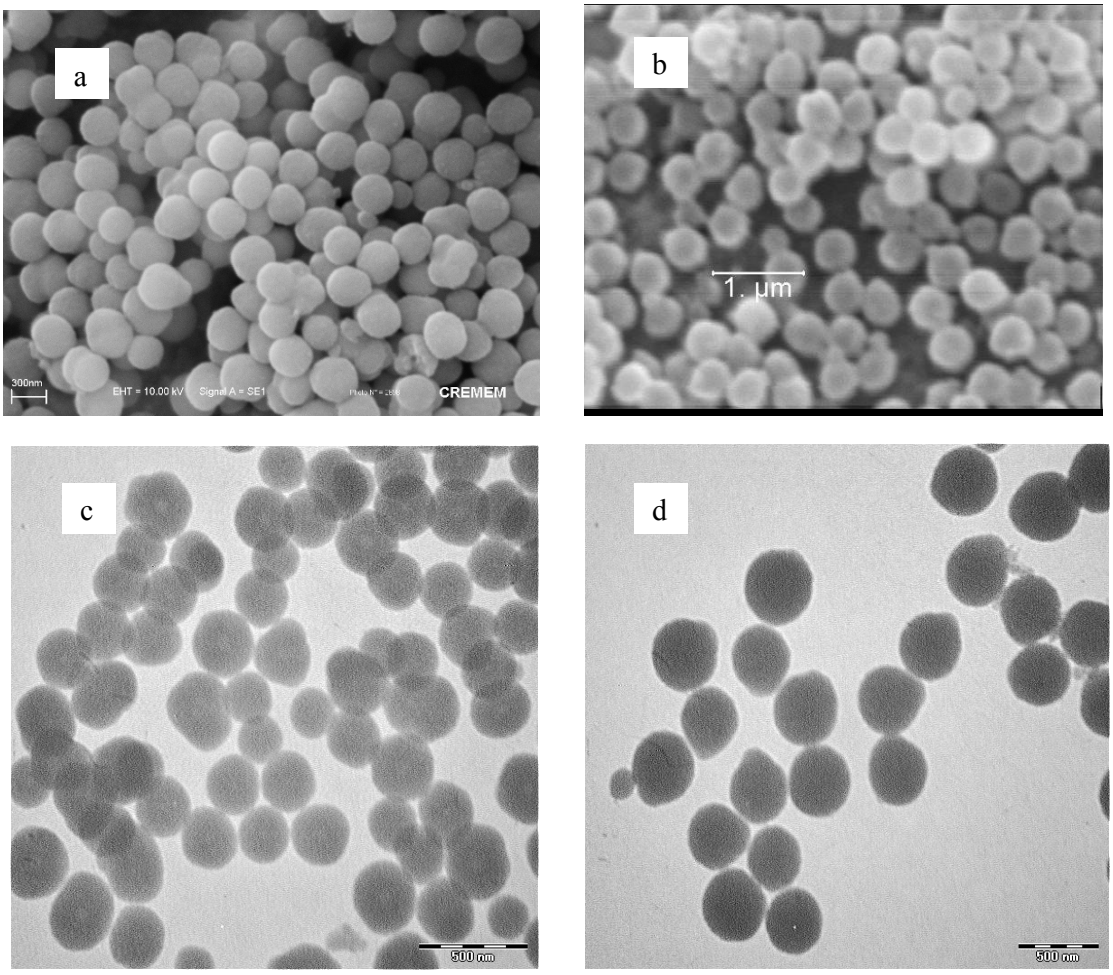

Figure II-20: (a) & (b) are the SEM images of PEDOT core-shell particles prepared using α,ω-Th-PEO (run 1, Table II-6) and α,ω-Flu-PEO (run 5, Table II-6) respectively as reactive stabilizers having same molecular weight ($\overline{M}_n$ = 10000 g.mol^{-1}) and concentrations (20 wt.%) but different end-groups and (c) & (d) are their corresponding TEM images.

We also performed DLS analysis of reactive α,ω-Py-PEO, α,ω-Th-PEO, α,ω-Flu-PEO and α,ω-OH-PEO of same molar mass (20000 g.mol^{-1}) in the water/methanol mixture. All the systems presented a very low scattering intensity that corresponds to small R_H around 4nm, typical of free chains in solution. It is worth noting that α,ω-Py-PEO, α,ω-Th-PEO and α,ω-Flu-PEO show similar behavior than hydroxytelechelic PEO in the solvent reaction mixture.

II.2.2.2. $Fe^{(III)}(OTs)_3.6(H_2O)$ and $(NH_4)_2S_2O_8/FeCl_3$ mixture as oxidants

Very small PEDOT particles with a narrow size distribution could be obtained in high yields at 85°C (runs 11, 12, Table II-6) in the presence of $Fe^{(III)}(OTs)_3.6(H_2O)$ as oxidant and α,ω-Flu-PEO as stabilizer (See SEM image, Figure II-21). The effect of the double functionality of the stabilizer must be underlined in this specific case, as only desert rose-like morphologies were obtained in the presence of α-Py-PEO in similar conditions (runs 12-14, Table II-5). This result proves the higher efficiency of difunctional stabilizer, compared to monofunctional one, with respect to the formation and the stabilization of the first nuclei formed along with the dispersion polymerization. As already mentioned, PEDOT samples prepared with this oxidant could not be dissolved in any solvent limiting their characterization, phenomenon explained by the high PEDOT content within the particles.

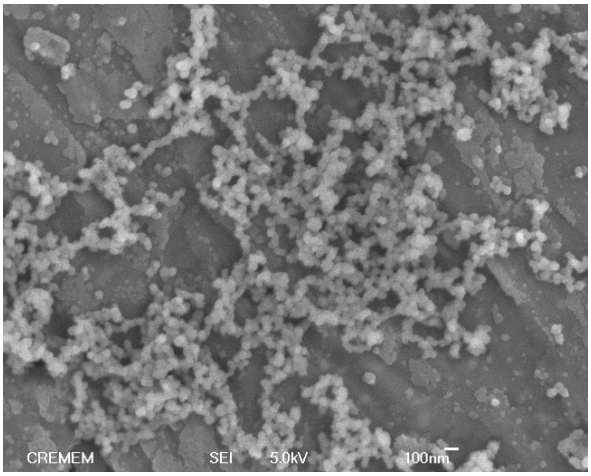

Figure II-21: SEM images of PEDOT samples prepared using α,ω-Flu-PEO reactive stabilizer ($\overline{M}_n$ = 35000 g.mol^{-1}, 50 wt.%, run 12, Table II-6) in the presence of $Fe^{(III)}(OTs)_3.6(H_2O)$ as an oxidant at 85 °C.

Interestingly, the synthesis of small PEDOT particles and low size distribution could be also achieved in the presence of mixtures of oxidants, *i.e.* $(NH_4)_2S_2O_8$ plus $FeCl_3$ (1.6:1 ; mol:mol). The small particles formed (50-60 nm) were characterized by AFM as shown in Figure II-22. In that case, the particles were partially soluble in DMF and could be analyzed by GPC and NMR. Data are collected in Table II-6 (runs 8-10).

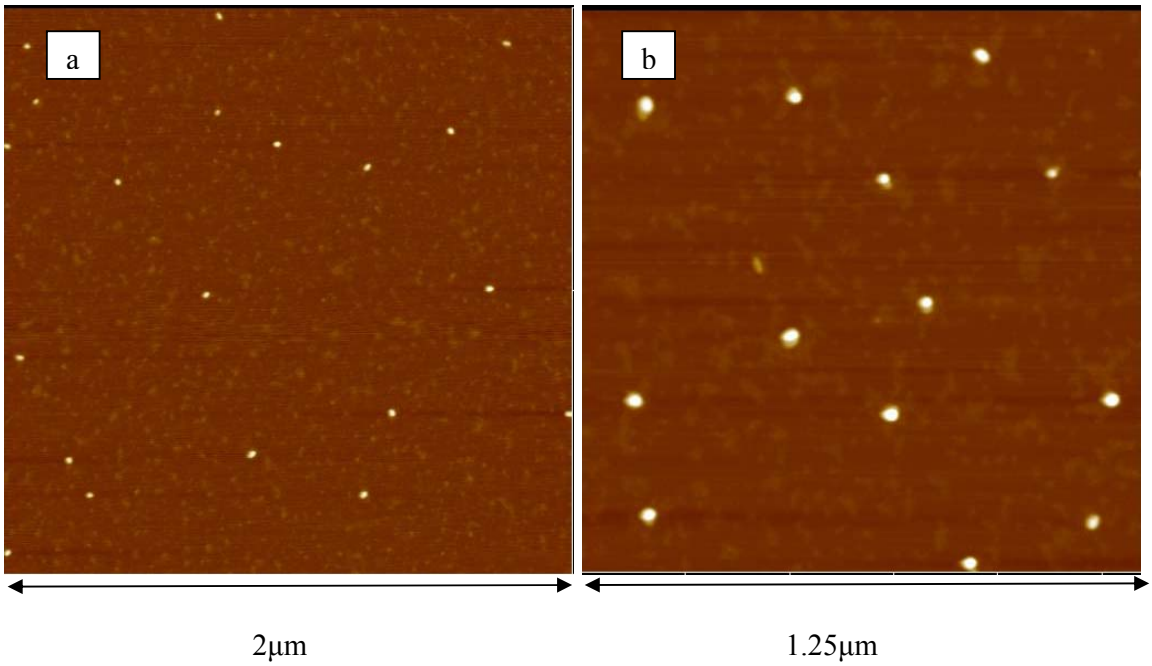

Figure II-22: AFM images of PEDOT core-shell particles prepared using different PEO-based reactive stabilizers of same molecular weight (20000 g.mol^{-1}) and concentration (20 wt.%) (a) α,ω-Flu-PEO (b) α,ω-Th-PEO.

II.3. FTIR and UV-visible characterizations of PEDOT samples

The chemical composition of PEDOT samples was studied by Fourier Transformer infrared (FTIR) spectroscopy (see Figure II-23). The presence of peaks at 1382 and1353 cm^{-1} (C-C and C=C stretching vibrations of thiophene ring), 1214 and 1095 (C-O-C stretching in ethylene oxide unit), 986 and 694 cm^{-1} (C-S bond stretching vibrations in thiophene ring)[14, 15] prove the formation of PEDOT. Moreover, due to similar nature of ethyleneoxide both in stabilizer and PEDOT, it is difficult to distinguish the peaks due to stabilizer.

UV-Visible-NIR spectrum of the PEDOT sample is shown in II-24. PEDOT samples give two absorption peaks, one weak absorption at 820 nm corresponding to polarons and bipolarons due to partial doping of PEDOT during polymerization and another at 525 nm originating from π-π* electronic transition in de-doped PEDOT[14]

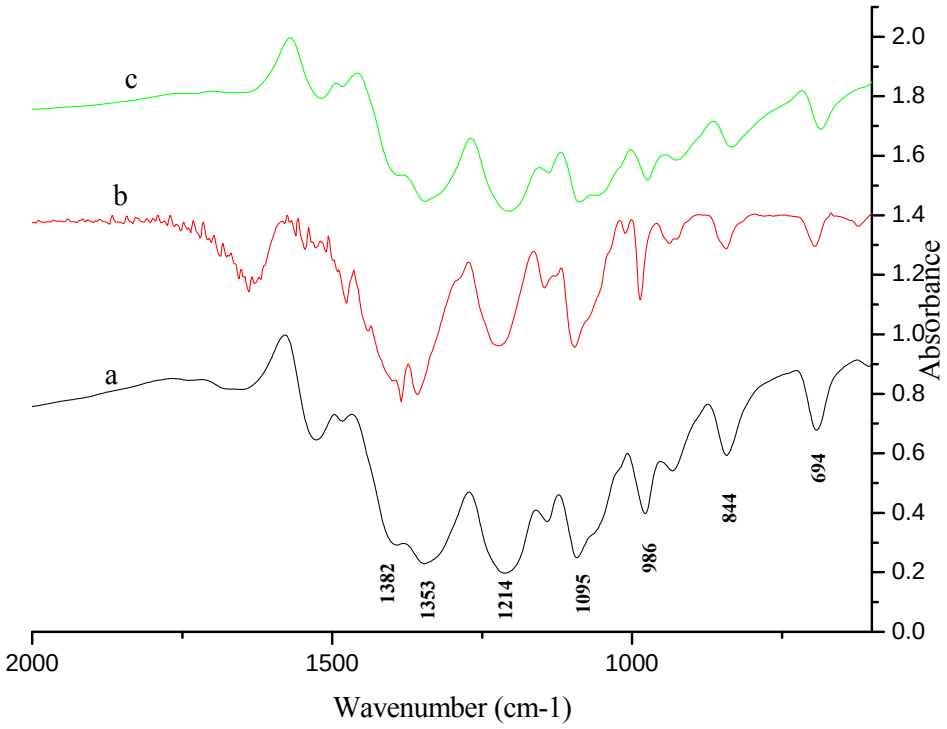

Figure II-23: FTIR spectra of (a) PEDOT bulk-powder (c) PEDOT sample prepared using $(NH_4)_2S_2O_8$ as an oxidant and (c) PEDOT sample prepared using $Fe^{(III)}(OTs)_3.6(H_2O)$ as an oxidant.

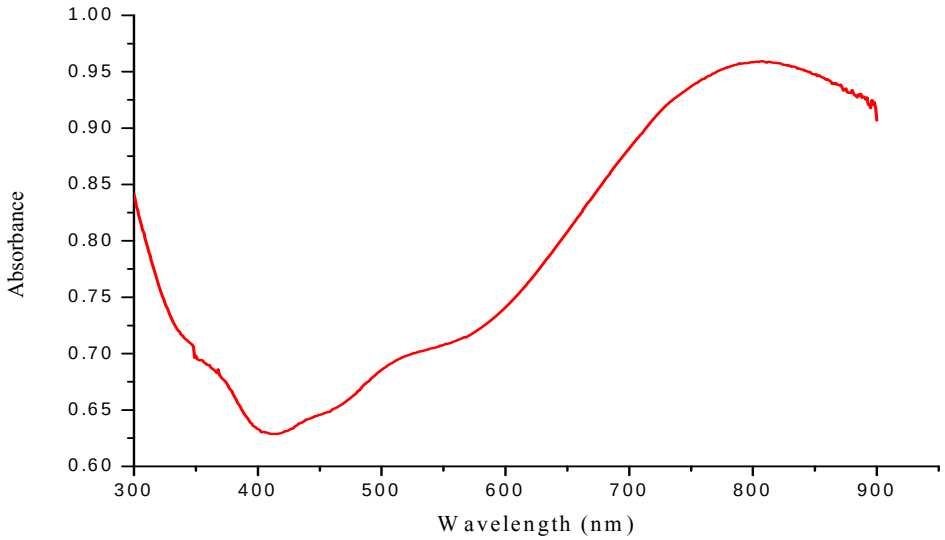

Figure II-24: UV-visible spectrum of PEDOT sample in H_2O

II.4. Conductivity measurements of PEDOT samples

The conductivity of PEDOT-PEO samples was measured using the conventional 4-probe technique on dried and compressed PEDOT particles under the form of disc pellets. Contrarily to experiments performed with $Fe^{(III)}(OTs)_3.6(H_2O)$ as an oxidant, addition of *p*-toluene sulfonic acid (PTSA) as an external doping agent is required for PEDOT samples prepared in the presence of $(NH_4)_2S_2O_8$. Conductivity values were found from 1.28×10^{-6} S/cm to 1.10×10^{-2} S/cm for PEDOT samples. Only low conductivities values were obtained in the presence of ammonium persulfate as an oxidant while high values are obtained when using $Fe^{(III)}(OTs)_3.6(H_2O)$. This characteristic is explained by the dual role played by iron derivatives that act as oxidant and dopant. The conductivity values increase from 1.74×10^{-3} S/cm to 1.10×10^{-2} S/cm as the amount of α-Py-PEO decreases from 50 wt% to 20 wt% while using $Fe^{(III)}(OTs)_3.6(H_2O)$ as an oxidant. This trend is in agreement with the insulating properties of PEO within the material. A similar result has been obtained and reported in the literature for dispersion polymerization of pyrrole.[9, 10]

III. Conclusion

In conclusion, spherical PEDOT particles with a controlled size and a narrow size distribution were prepared in the presence of specifically designed PEO-based reactive stabilizers in aqueous dispersant media. The morphology and size of the nano-objects formed were tuned by changing the functionality, molecular weight, and concentration of the PEO as well as the type of the oxidant used. The DLS analyses of these end-functionalized PEO show no organization in the solvent mixture except for α-EDOT-PEO which gives, in some cases, vesicle-like morphology. There was very less or no effect on the size and morphology of the PEDOT particles by changing the PEO end from pyrrole to fluorene or thiophene. PEDOT particles exhibiting high conductivity values were obtained in high yields in the presence of $Fe^{(III)}(OTs)_3.6(H_2O)$ as an oxidant but comparatively low yield and conductivity values were obtained using $(NH_4)_2S_2O_8$. A better understanding of the parameters that govern the synthesis of calibrated conductive PEDOT latexes allows us to extend this synthetic strategy to other π-conjugated polymers. It also opens the route to conductive inks for a large range of applications from PLEDs to flexible organic solar cells.

References

(1) Szwarc, M. *Nature* **1956**, 178, 1168.

(2) Szwarc, M.; Levy, M.; Milkovich, R. *J. Am. Chem. Soc.* **1956**, 78, 2656.

(3) Flory, P. J. *J. Am. Chem. Soc.* **1940**, 62, 1561.

(4) Feng, X.-S.; Taton, D.; Chaikof, E. L.; Gnanou, Y. *J. Am. Chem. Soc.* **2005**, 127, 10956.

(**5**) Shen, S.; D. Sudol, E.; El-Aasser, M. S. *J. Polym. Sci. Part A: Polym. Chem*. **1994**, 32, 1087.

(6) Provencher, S. W. *Comput. Phys. Commun.* **1982**, *27*, 213.

(7) Chécot, F.; Brulet, A.; Oberdisse, J.; Gnanou, Y.; Mondain-Monval, O.; Lecommandoux, S. *Langmuir* **2005**, *21*, 4308-4315.

(8) Chécot, F.; Lecommandoux, S.; Gnanou, Y.; Klok, H.-A. *Angew. Chem. Int. Ed.* **2002**, *41*, 1339.

(9) Armes, S. P.; Aldissi, M.; Angew, S. F. *Synth. Met.* **1989**, *28*, 837.

(10) Armes, S. P.; Aldissi, M.N.; Hawley, M.; Beery, J. G.; Gottesfeld, R. *Langmuir* **1991**, *7*, 1447.

(11) Moore, J. S.; Stupp, S. I. *Macromolecules* **1990**, *23*, 65.

(12) Provisional Product Information Sheet, Trial Product A14060, Bayer AG (Nov 1994).

(13) Mandal, T. K.; Mandal, B. M. *J. Polym. Chem. Part A: Polym Chem* **1999**, *37*, 3723.

(14) Yang, Y.; Jiang, Y.; Xu, J.; Yu, J. *Polymer* **2007**, 48, 4459.

(15) Kumar, S. S.; Kumar, C. S.; Mathiyarasu, J.; Phani, K. L. *Langmuir*, **2007**, 23, 3401.

Chapter III

Synthesis of PEDOT nano-objects using poly(vinyl alcohol), poly(N-vinylpyrrolidone)-b-poly(vinyl alcohol) and poly(N-vinylpyrrolidone)-co-poly(vinyl alcohol) based reactive stabilizers

Table of contents

I. Water-borne dispersion of PEDOT nano-objects using poly(vinyl alcohol)-based reactive stabilizers in aqueous dispersion

In this first part of the chapter, we discuss the synthesis in aqueous dispersion of well-defined PEDOT nano-objects with various morphologies, including particles and donuts, in the presence of pyrrole-*modified* poly(vinyl alcohol) (PVA-*mod*-Py) used as a reactive stabilizer. Ammonium persulfate and iron(III) *p*-toluene sulfonate hexahydrate [$Fe^{(III)}(OTs)_3.6(H_2O)$] were used as oxidants. The nano-objects formed show electrical conductivity up to $1.6x10^{-2}$ S cm^{-1}. The size of these nano-objects ranges from 30 to 450 nm depending upon the experimental conditions.

I.1. Synthesis of the stabilizers

In order to prepare PEDOT core-shell particles, we derivatized a series of PVA-*mod*-Py (that are used as steric reactive stabilizers) with different degrees of substitution and molecular weight by partial esterification of PVA with *N*-methyl-2-pyrrolecarboxylic acid in the presence of 4-(dimethylamino)pyridinium 4-toluenosulfonate (DPTS).[1] The general synthetic procedure is shown in Scheme III.1.

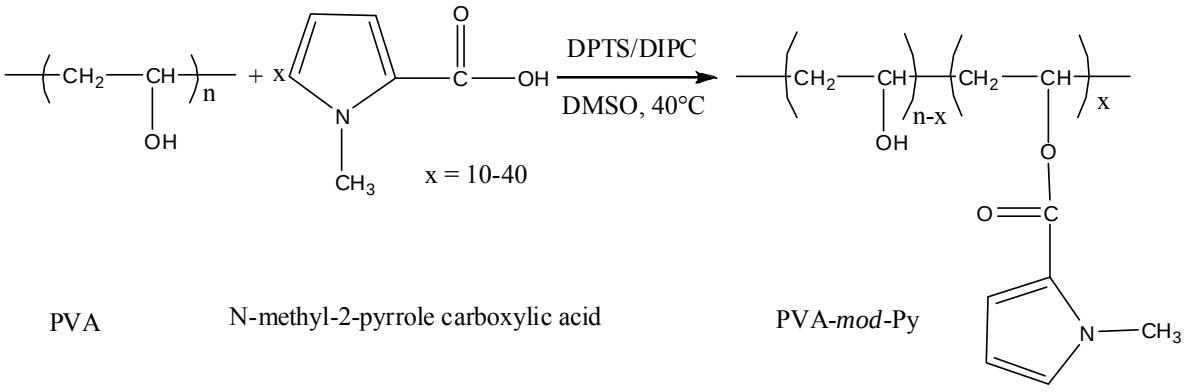

Scheme III.1: (a) Synthesis of PVA-*mod*-Py

^{1}H NMR analysis was used to evaluate the density of grafting of pyrrole units per PVA chain in particular for degree of substitution higher than 5%.^{1}H NMR spectrum in

DMSO of the PVA-*mod*-Py is shown in Figure III.1. The appearance of the signals at 7.05 (h), 6.80 (f) and 6.07 ppm (g) due to pyrrole ring resonance confirmed the functionalization of pyrrole units along the PVA backbone.

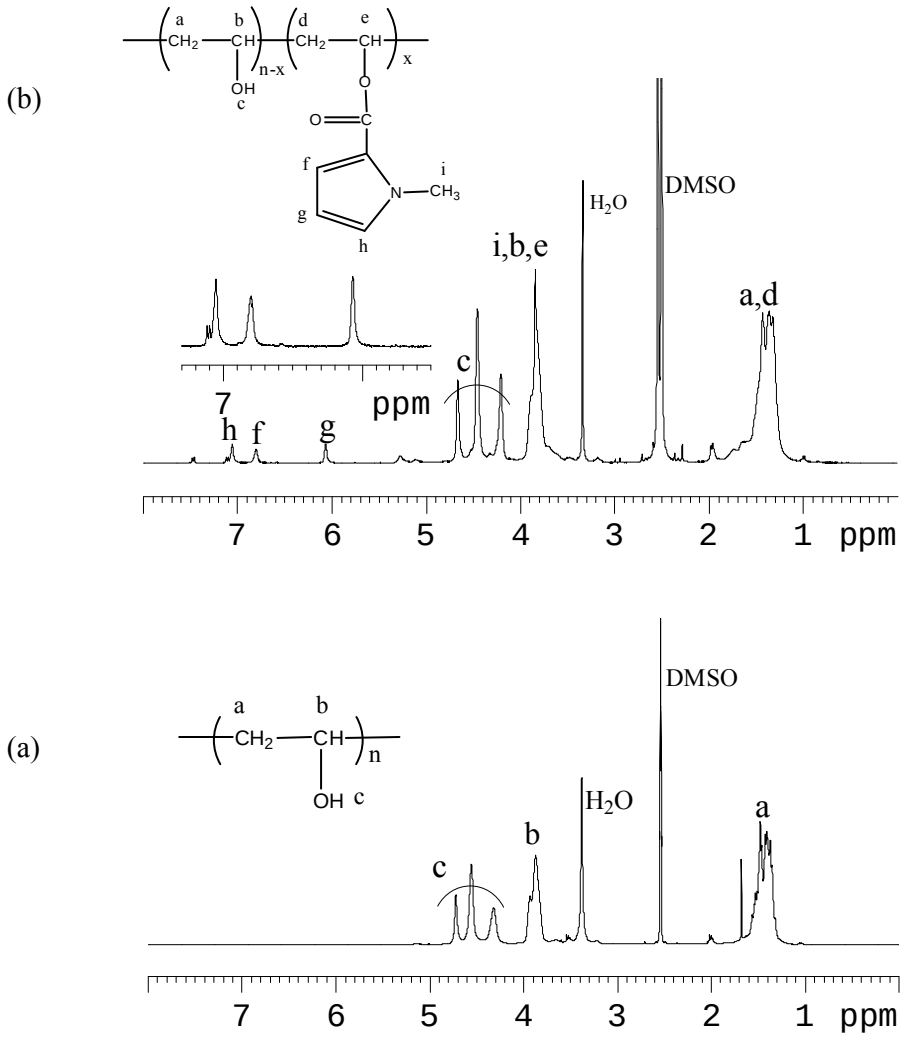

Figure III.1: ^{1}H NMR spectra of (a) PVA and (b) PVA-*mod*-Py (7.5 mol.% of pyrrole functionalization) in DMSO at room temperature

I.2. Synthesis of PEDOT nano-objects

As already described, due to bad solubility of EDOT in water, the dispersion polymerization was performed in a mixture of methanol:water (1:4). Two types of oxidants *i.e.* ammonium persulfate and $Fe^{(III)}(OTs)_3.6(H_2O)$ were used for the oxidative polymerization of EDOT. A general scheme of PEDOT nano-objects synthesis is illustrated in Scheme III.2.

The effect of the concentration, degree of substitution and the molecular weight of the PVA-*mod*-Py stabilizers on the morphology and size of the nano-objects was investigated and analyzed by dynamic light scattering (DLS). The data of EDOT dispersion polymerization in the presence of PVA-*mod*-Py are summarized in Table III.1.

I.2.1. Synthesis of PEDOT dispersions using $(NH_4)_2S_2O_8$ as an oxidant

Unlike polymerizations of EDOT performed in the presence of non-modified PVA (run 1) the functionalization of PVA hydroxyl moieties with pyrrole was shown to be essential in order to prepare PEDOT nano-objects having various morphologies (runs 2-15) (see Figure III.2)

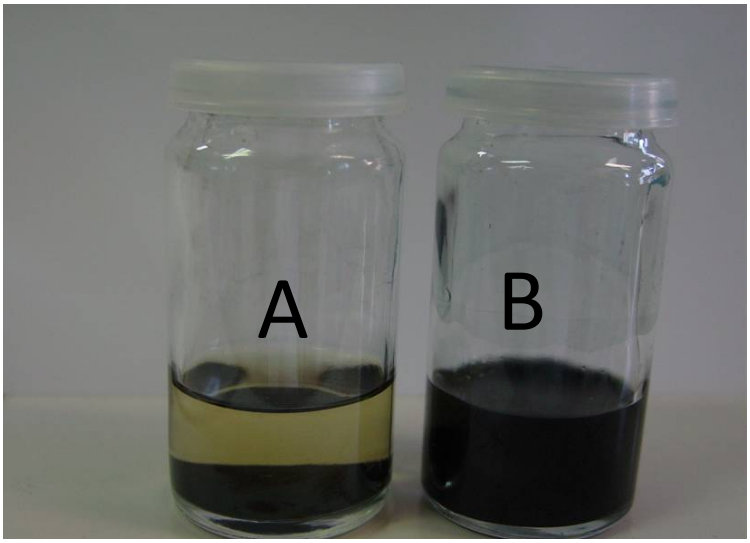

Figure III.2: PEDOT particles prepared using (A) unmodified PVA and (B) modified PVA (PVA-*mod*-Py)

Above 5 mol. %, the degree of PVA substitution ([Py]) has a little effect on the average PEDOT particle size which remains in the range 100-200 nm (Runs 5-15). However, at a very low degree of substitution (runs 3 & 4), there is an amazing formation of rings, or so-called “donuts”. Although we do not have a full explanation on the formation of donuts, there is an evident relationship between the density of pyrrole grafting onto the PVA reactive

stabilizers and the morphology of PEDOT objects. A lack of thermodynamic stability is probably the cause of the formation of hollow spheres. It is noteworthy that ring structure have been already reported by Dìez et al. in the case of synthesis of polypyrrole in aqueous media.[2] However, in this specific work the authors use templates (β-naphthalene and fluorosurfactants) for pyrrole polymerization. In our case, we have checked by DLS measurements that no particular self-organization of the PVA-*mod*-Py reactive stabilizer was formed prior polymerization. The change in PEDOT morphologies from donuts to dense particles was noticed while increasing the concentration of pyrrole units onto PVA backbone (see runs 3 & 5). Spherical particles were only obtained above a critical value of pyrrole units as it is illustrated in Figure III-3 (for broader view of donuts, see Figure III-4)

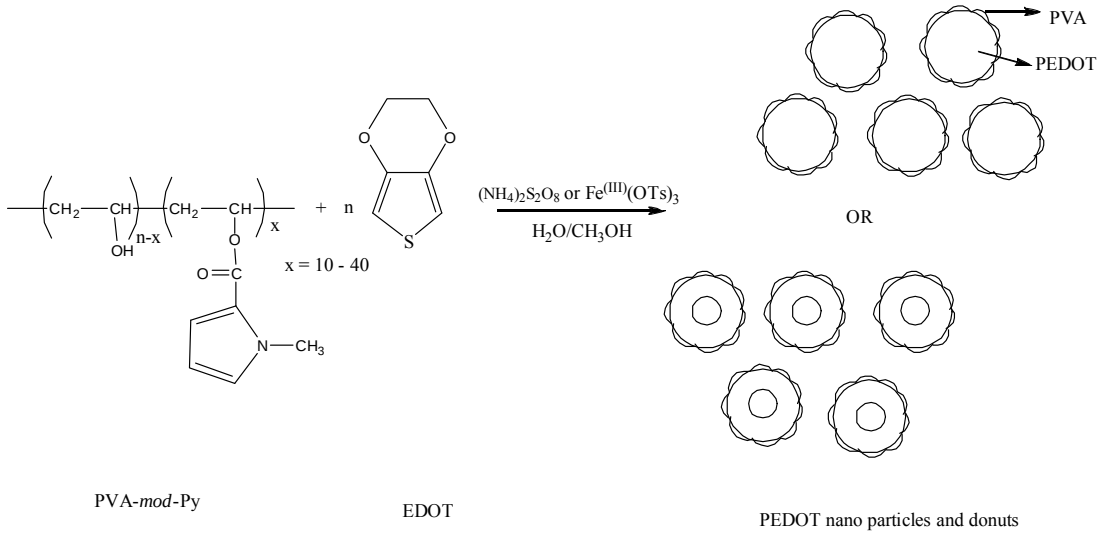

Scheme III.2: Synthesis of PEDOT particles and donuts by dispersion polymerization in the presence of PVA-*mod*-Py as a stabilizer

Run N°	Oxidant type	PVA-*mod*-Py M_w g mol^{-1}	Mol.%. of Py per chain	PVA-*mod*-Py Introduced wt.%	Yield %	Conductivity[a] S cm^{-1}	Particle Size[b] nm	Remarks
1	$(NH_4)_2S_2O_8$	18000	0	20	50	nd	_	Aggregates
2	$(NH_4)_2S_2O_8$	18000	2.5	20	55	nd	_	Aggregates
3	$(NH_4)_2S_2O_8$	18000	2.5	35	60	$3.5x10^{-6}$	300-400	Donuts
4	$(NH_4)_2S_2O_8$	18000	5.0	20	70	$3.2x10^{-6}$	400-800	Donuts
5	$(NH_4)_2S_2O_8$	18000	5.0	35	60	$7.5x10^{-5}$	180-200	Particles
6	$(NH_4)_2S_2O_8$	18000	7.5	10	55	$9.0x10^{-6}$	150-180	Particles
7	$(NH_4)_2S_2O_8$	18000	7.5	20	60	$3.6x10^{-6}$	100-140	Particles
8	$(NH_4)_2S_2O_8$	18000	7.5	35	50	$1.6x10^{-6}$	80-120	Particles
9	$(NH_4)_2S_2O_8$	18000	10.0	20	60	$7.2x10^{-6}$	150-200	Particles
10	$(NH_4)_2S_2O_8$	88000	1.0	10	60	$4.4x10^{-6}$	150-190	Particles
11	$(NH_4)_2S_2O_8$	88000	1.0	20	50	$4.0x10^{-6}$	100-170	Particles
12	$(NH_4)_2S_2O_8$	88000	5.0	10	60	nd	80-100	Particles
13	$(NH_4)_2S_2O_8$	88000	5.0	20	60	nd	50-100	Particles
14[c]	$Fe(OTs)_3$	88000	5.0	35	80	$1.6x10^{-2}$	100-140	Particles
15[c]	$Fe(OTs)_3$	18000	7.5	50	80	$1.8x10^{-3}$	50-60	Particles

a) Measured by the four probe method
b) Measured from SEM images. In all cases averages on 100 objects were made.
c) Reaction mixture kept at 85 °C for 48 h.

Table III-1: Synthesis of PEDOT particles using PVA-*mod*-Py as a reactive stabilizer in water/methanol (1:4) at 40 °C

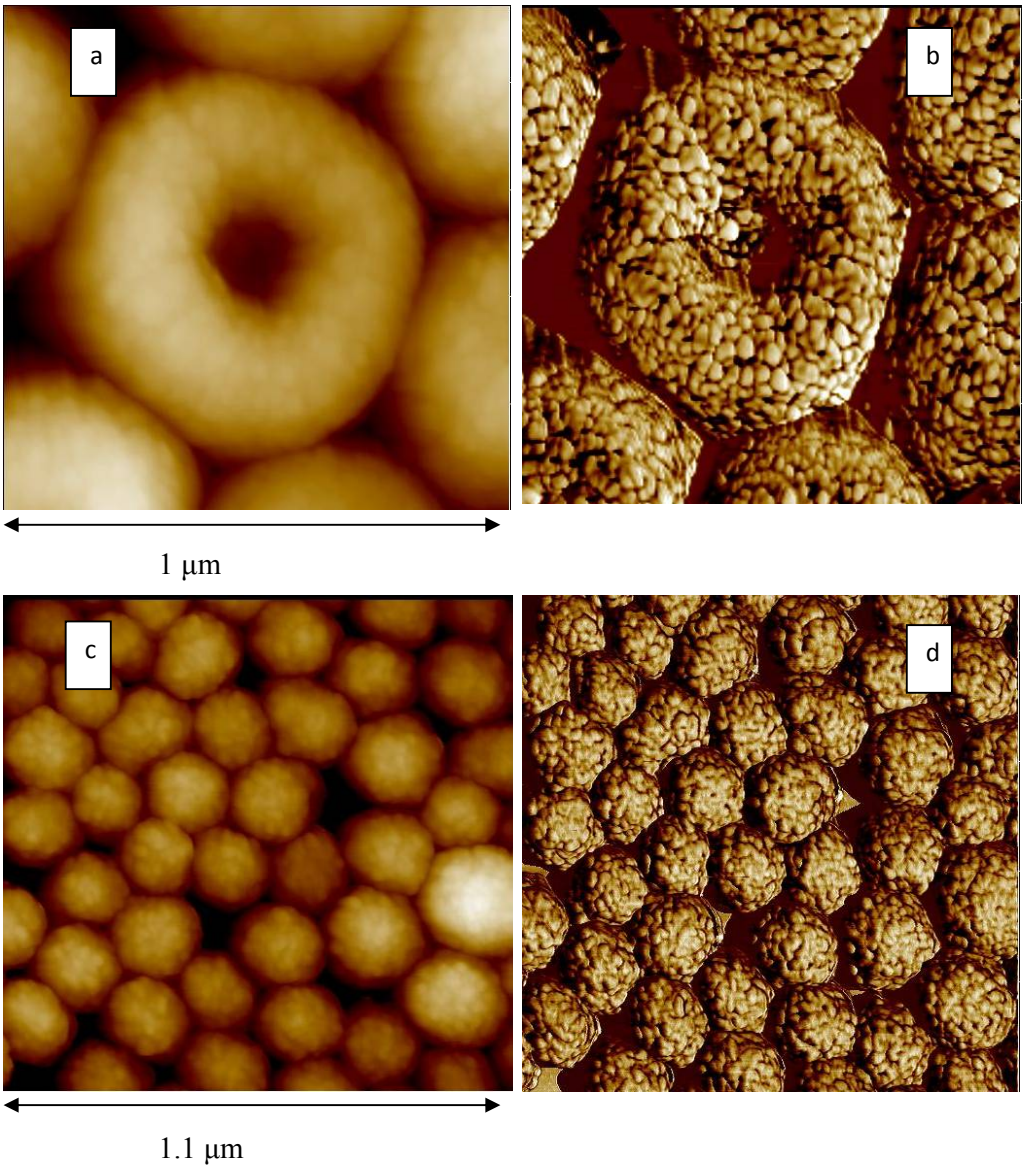

Figure III-3: AFM images of PEDOT particles and donuts prepared using PVA-*mod*-Py stabilizer having 5 mol.% of pyrrole functionalization, at different concentrations, (a&b) 20 wt.% (Run 4) and c,&d) 35 wt.% (Run 5).

In accordance with literature data,[3,4] the average size of the PEDOT particles decreases from 170 nm to 100 nm as the concentration in stabilizer increases from 10 wt.% to 35 wt.% (see runs 6-8 and 10,11). This is logically explained by a higher surface coverage in the presence of a higher amount of steric reactive stabilizer.

As expected, the molecular weight of the stabilizer also affects the size of the PEDOT particles. The latter decreases as the molecular weight of the PVA-*mod*-Py increases from 18000 g mol^{-1} to 88000 g mol^{-1}, even at low stabilizer concentrations (see runs 4, 5, 12 and 13). This is again explained by the higher surface coverage afforded by the high molecular weight stabilizer molecules, which leads to the formation of a larger number of stable, primary particles. Similar results were obtained and reported by Mandal and coll. for the dispersion polymerization of pyrrole.[5]

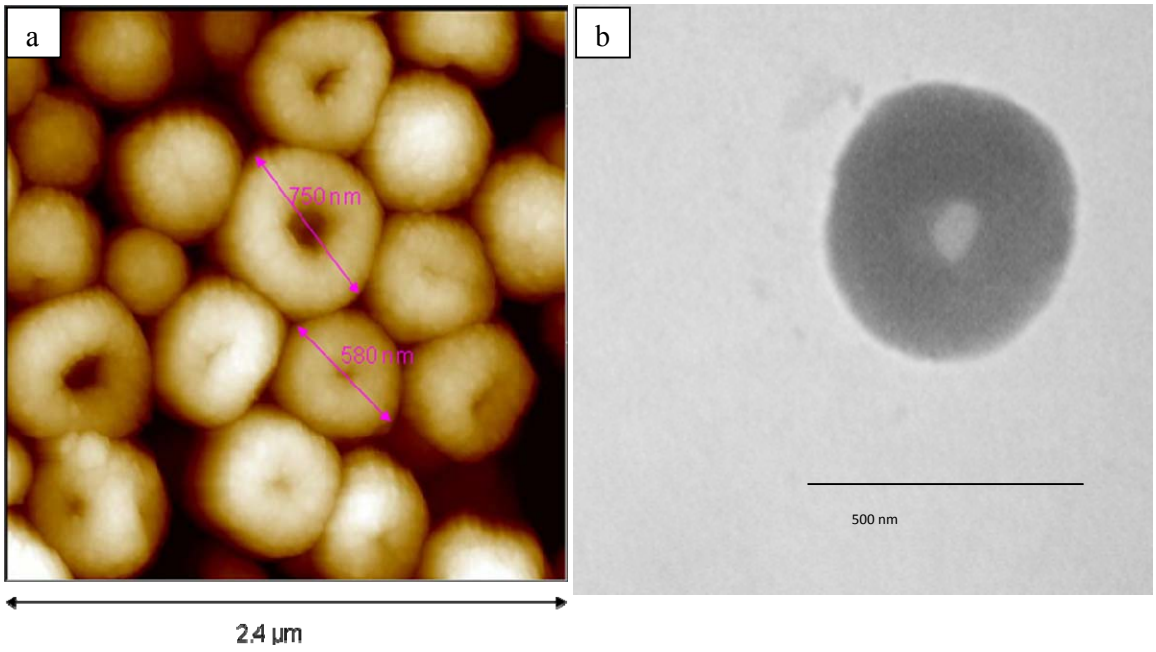

Figure III-4: (a) AFM and (b) TEM images of the PEDOT "donuts" prepared using 20 wt. % of PVA-*mod*-Py stabilizer having 5 mol. % of grafted pyrrole (run 4, Table 1)

AFM images (Figure III-3 & III-5) clearly show that each PEDOT nano-object is formed by the aggregation of very small nano-particles having a size between 20-30 nm which were also called particulates or metastable particles by Mandal and coll.[6] These results thus further strengthen the mechanism of the particle formation proposed by Paine saying that each large stable particle is formed by the combination of small metastable elementary particles.[7-9] Similar results were observed and reported later by Armes *et al.* with the help of scanning tunneling microscopy.[5]

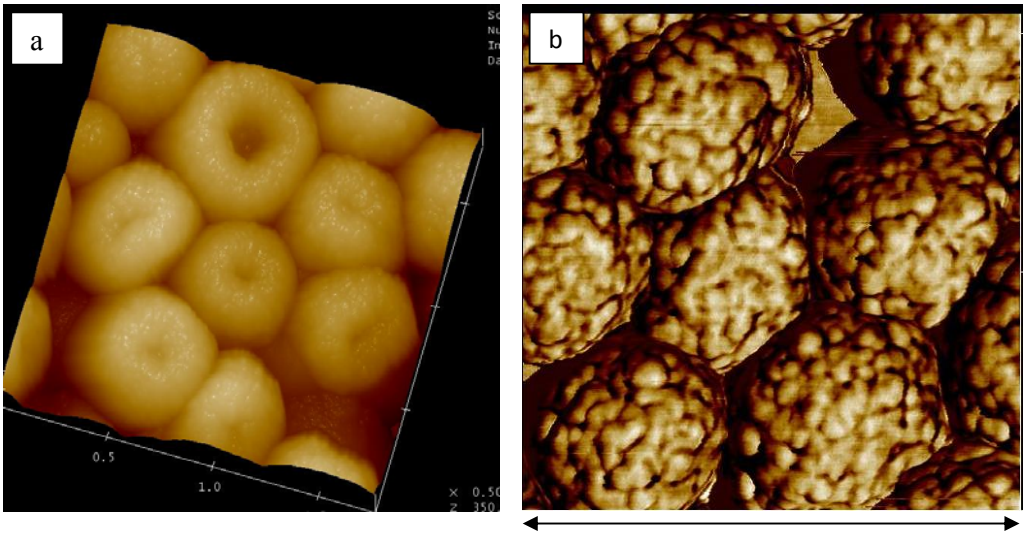

Figure III-5: AFM images of PEDOT particles, "donuts" prepared using PVA-*mod*-Py stabilizer having 5 mol.% of pyrrole functionalization, at different stabilizer concentrations, (a) 20wt.% (Run 4) and (b) 35 wt.% (Run 5).

In order to further analyze the size, size distribution and morphology of PEDOT nano-objects, dynamic light scattering (DLS) experiments of PEDOT samples were performed in methanol/water (1:4) mixture. DLS results for a PEDOT sample (run 5) are shown in Figure III-6.

The auto-correlation functions C(q,t) (Figure III-6a) and the corresponding relaxation time distributions G(t) (Figure III-6b) of a PEDOT sample measured at different angles show a single population with very narrow relaxation time distributions in each case. This confirms that PEDOT nano-objects have very narrow size distribution which was already illustrated by AFM images. The evolution of the relaxation frequency as a function of the square of the wave-vector permits us to calculate the apparent diffusion coefficient of PEDOT particles. The linear relation between relaxation frequency and square of the wave vector (Figure III-6c) confirm the homogeneous size and spherical nature of these PEDOT nano-objects. The size of these latter particles was found to be 200 nm which is in agreement with the results obtained by AFM and SEM. These DLS results further prove that these particles are monodispersed and are well separated from each other *i.e.* no aggregation occurs among final PEDOT particles.

(a)

(b)

(c)

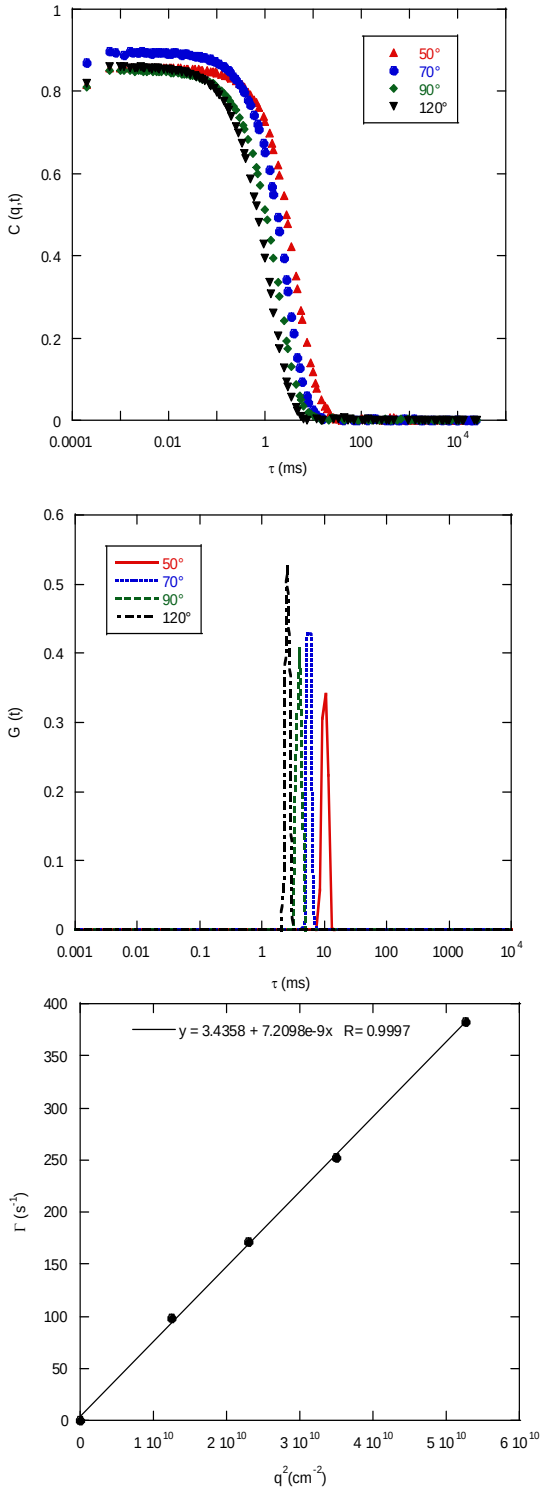

Figure III-6: (a) Auto-correlation function C(q,t), (b) Relaxation time distribution G(t) at different angles and, (c) Relaxation frequency in the function of q^2 of PEDOT sample (run 5) prepared using modified PVA ($\overline{M}_W$ = 18000 g mol^{-1}, 5 mol.% pyrrole functionalization) as a reactive stabilizer in water/methanol mixture (4:1) at 25 °C.

I.2.2. Synthesis of PEDOT using $Fe^{(III)}(OTs)_3.6(H_2O)$ as an oxidant

As already noted (see chapter II) PEDOT particles were obtained in high yield when using $Fe^{(III)}(OTs)_3.6(H_2O)$ as an oxidant at 85 °C (see runs 14 and 15 in Table III-1). This is explained by a higher efficiency of $Fe^{(III)}(OTs)_3.6(H_2O)$ in the given experimental conditions as compared to ammonium persulfate. In addition, the PEDOT particles formed in these conditions are smaller in size as compared to the ones obtained using ammonium persulfate as an oxidant for a same degree of substitution and concentration of stabilizer (see runs 5 and 14). The PEDOT samples synthesized in the presence of $Fe^{(III)}(OTs)_3.6(H_2O)$ are insoluble in any common organic solvent preventing their characterization by NMR and SEC.

I.3. Conductivity measurements

The conductivity of the PEDOT particles was measured using the conventional four probe technique on dried and compressed PEDOT powders under the form of disc pellets. PEDOT samples prepared using ammonium persulfate as an oxidant show low conductivities (up to $9.0x10^{-6}$ S cm^{-1}) while those prepared using $Fe^{(III)}(OTs)_3.6(H_2O)$ exhibit higher conductivities (up to$1.6x10^{-2}$ S cm^{-1}). This is explained by the higher content, doping level and molecular weight of PEDOT within the latter samples and also because in case of ammonium persulfate PEDOT samples can be over-oxidized.

I-4. X-ray Photoelectron spectroscopy (XPS) characterization

The core-shell nature of the formed particles *i.e.* shell of PVA onto PEDOT core was proved by x-ray photoelectron microscopy (XPS) analyses. XPS survey spectra of PEDOT core-shell particles and PEDOT bulk powder are presented in Figure III-7. Both samples show four peak signals originating from C 1s, O 1s, S 2s and S 2p. The relative intensity of the signals due to S 2s and S 2p in PEDOT core-shell particles is lower than PEDOT bulk powder. In addition, XPS analyses allowed us to estimate the surface coverage of the PEDOT particles by the PVA stabilizer as revealed for instance by the presence of the N1s signal. As anticipated, data gathered in Figure III-7c reveal an increase of the N% together with the

expected mol% of pyrrole groups per chain. For runs 3 and 5, the binding energy of the maximum at 399.9 eV is consistent with the N- methylpyrrole groups on the PVA stabilizer chains (see also Figure III-8 a&b). For run 8, the N1s maximum is located at 401.4 eV suggesting some remaining ammonium ions from $(NH_4)_2S_2O_8$ onto the particles (Figure III-8c).

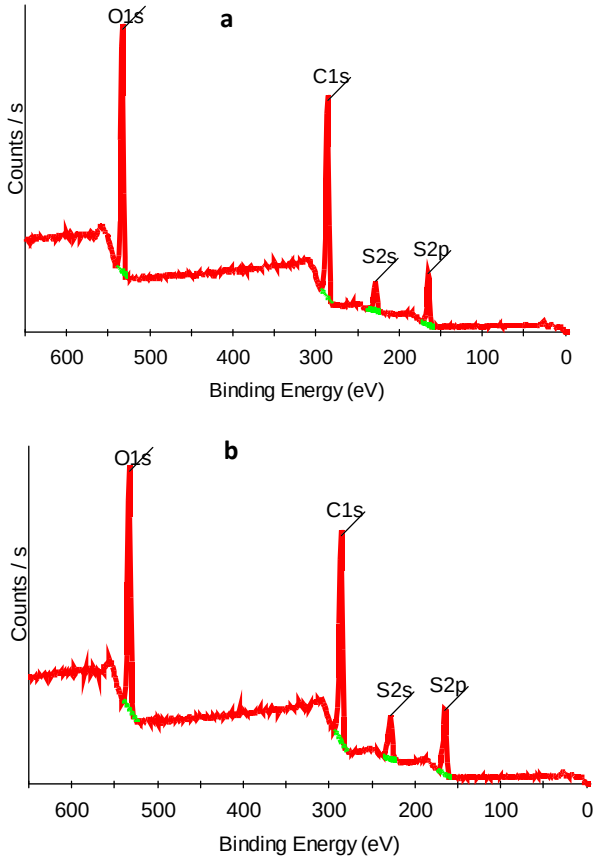

(c)

Samples	C	O	N	S
Run 3	60.7	29.2	0.4	9.7
Run 5	62.4	28.6	0.6	8.4
Run 8	60.9	29.9	1.8	7.4

Figure III-7: XPS survey spectra of (a) PEDOT core-shell particles and (b) PEDOT bulk powder; (c) table for the estimation of chemical composition on surface of PEDOT-PVA samples

In addition, Figure III-9 (a and b) shows the C 1s core-line spectra of PEDOT core-shell particles and PEDOT bulk powder. The peak at 286.4 eV position in C 1s core-line spectra of PEDOT core-shell particles correspond to C-O-H moieties in PVA. [10-12] In addition, the presence of peak at 532.6 eV (Figure III-9c) originating from O 1s is due to C-O-H and is in agreement to the data already available in the literature. [10] Such peak was not observed in O 1s core-line spectrum of PEDOT bulk powder (Figure III-9d) which confirms the presence of PVA on the PEDOT surface of PEDOT core-shell particles.

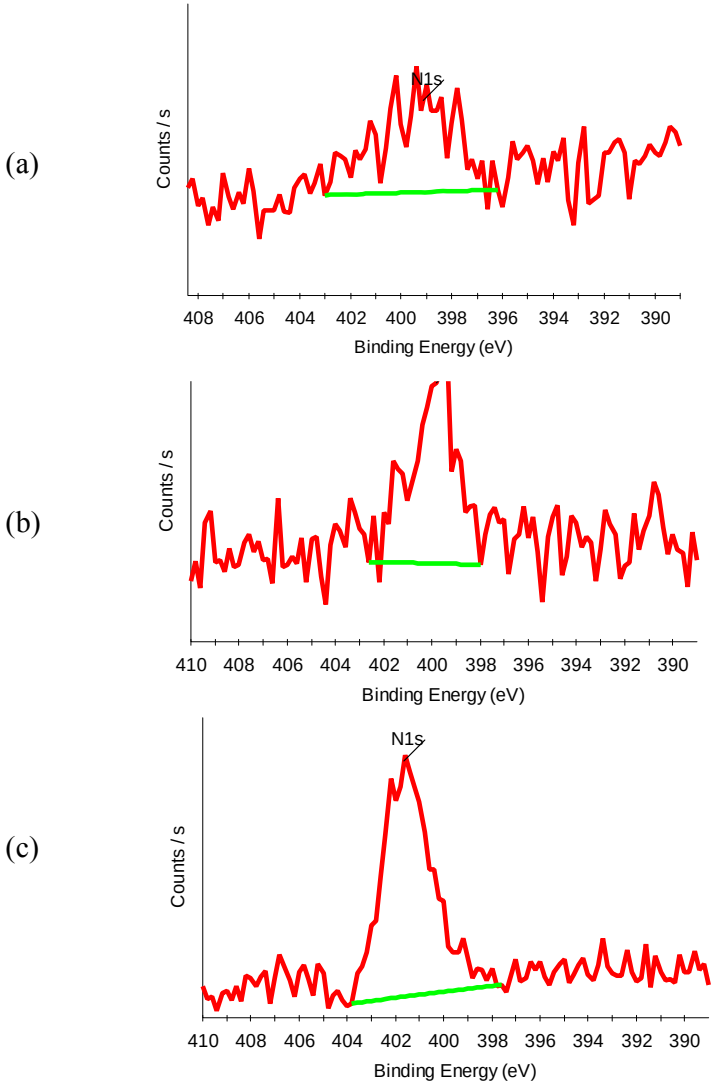

Figure III-8: XPS N1s core-line spectra for the PEDOT particles prepared using PVA-*mod*-Py stabilizers having different degree of pyrrole grafting (a) 2.5 mol.% (b) 5.0 mol.% and (c) 7.5 mol % (run 3, 5 and 8 respectively) at high resolution (Ep = 40 eV)

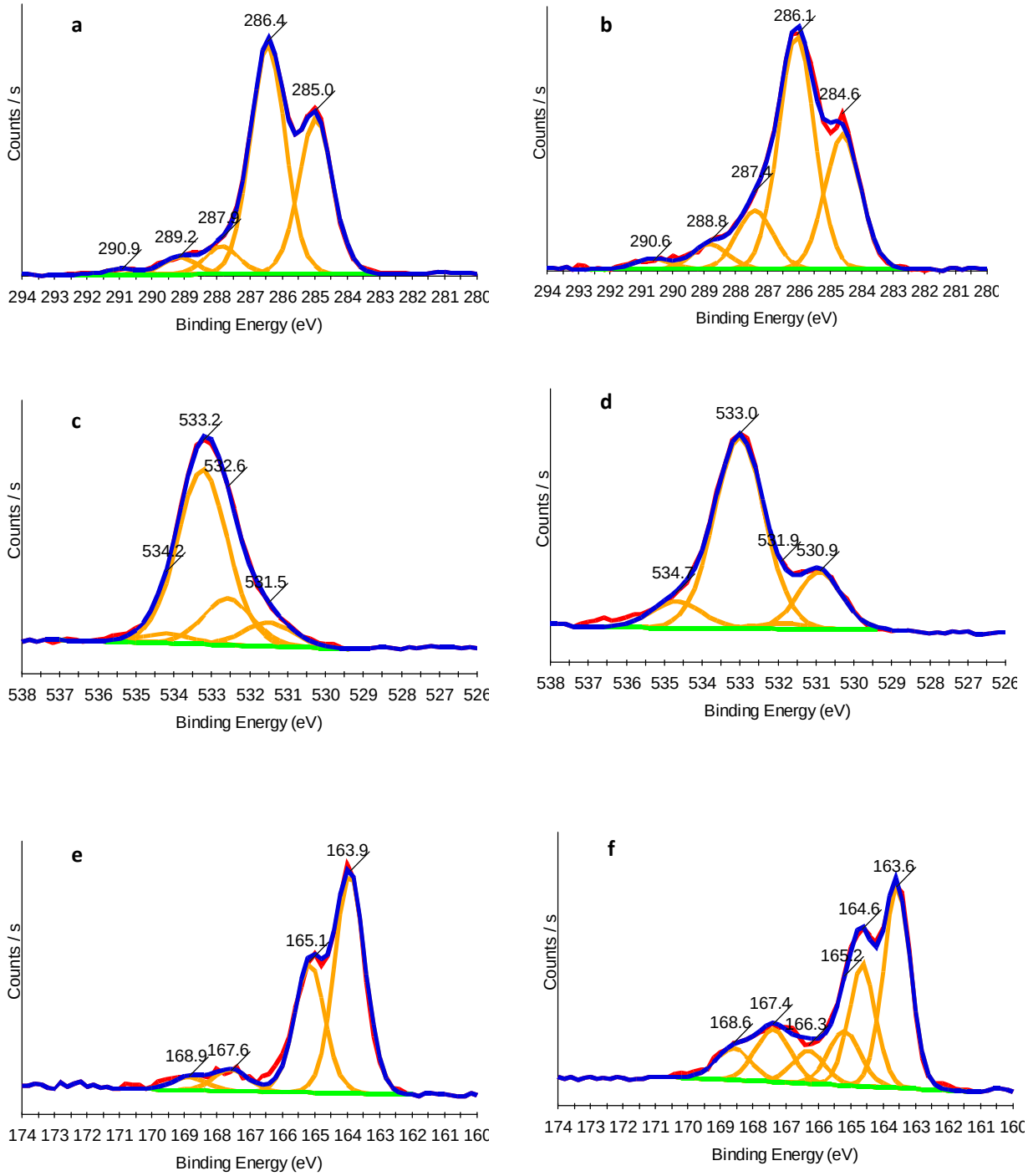

Figure III-9: XPS analyses: (a) & (b) are C 1s core-line spectra, (c) & (d) are O 1s core-line spectra and (e) & (f) are S 2p core-line spectra of PEDOT core-shell particles and PEDOT bulk powder respectively.

The S 2p core-line spectra of the samples are shown in Fig. III-9e and III-9f. The peaks at 164-165.2 eV correspond to neutral S of PEDOT backbone while the peaks at 167.6-

168.9 eV are due to sulfate anions.[13] The signals at 165.8-167.2 eV due to S^+ of PEDOT were difficult to observe in PEDOT core-shell particles probably due to the presence of the PVA shell. Finally, the amount of sulfur in the PEDOT-PVA sample was 8.5% against 12% in PEDOT bulk powder which is again in accord with the presence of PVA on the PEDOT surface.

I.5. FT-IR and UV-visible Spectroscopic characterizations

FT-IR spectra of the PEDOT bulk powder and PVA stabilized PEDOT particles synthesized using different oxidants are shown in Figure III-10. The presence of peaks at 1514 and 1344 cm^{-1} (C–C and C=C stretching vibrations of thiophene ring), the peaks absorption at 1213, 1095 and 1048 (C–O–C stretching in ethylene oxide unit), 972 and 694 cm^{-1} (C–S bond stretching vibrations in thiophene ring)[11,12] prove the formation of PEDOT. The peak at 1054 cm^{-1} due to S=O stretching confirms the presence of sulfonic groups from the dopant. [14,15] The occurrence of peaks at 3424 cm^{-1} (O–H stretching vibration) and 2950 cm^{-1} (C-H stretching vibration of CH_2 group of PVA) in PEDOT particles (Figures III-10b and III-10c) confirms the presence of PVA since such peaks are not seen in PEDOT bulk powder (Figure III-10a).

UV-Visible spectra of the PEDOT samples prepared using different oxidants are shown in Figure III-11. PEDOT samples prepared using $(NH_4)_2S_2O_8$ and $Fe^{(III)}(OTs)_3.6(H_2O$ as oxidant give two absorption peaks; one strong absorption at 790-800 nm correspond to polarons and bipolarons due to doping of PEDOT during polymerization and second weak absorption at 510-520 nm originating from π to π^* electronic transition in un-doped PEDOT[14], which clearly indicate that the PEDOT samples are nearly fully doped (see Figure III-11).

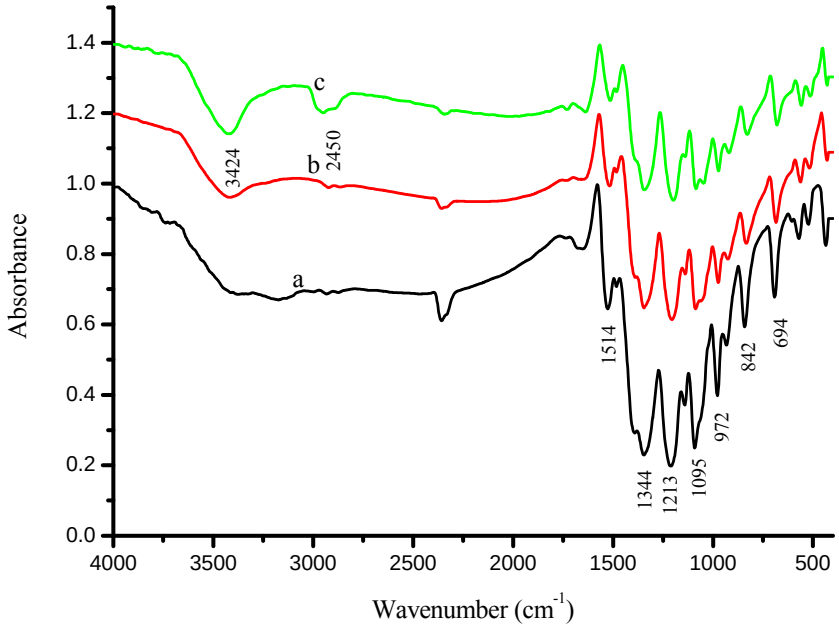

Figure III-10: FTIR spectra of (a) PEDOT bulk powder and (b) & (c) PEDOT particles prepared using $Fe^{(III)}(OTs)_3.6(H_2O)$ (run 15, Table III-1) and $(NH_4)_2S_2O_8$ (run 5, Table III-1) as oxidants respectively (measured by absorption mode using KBr pellet).

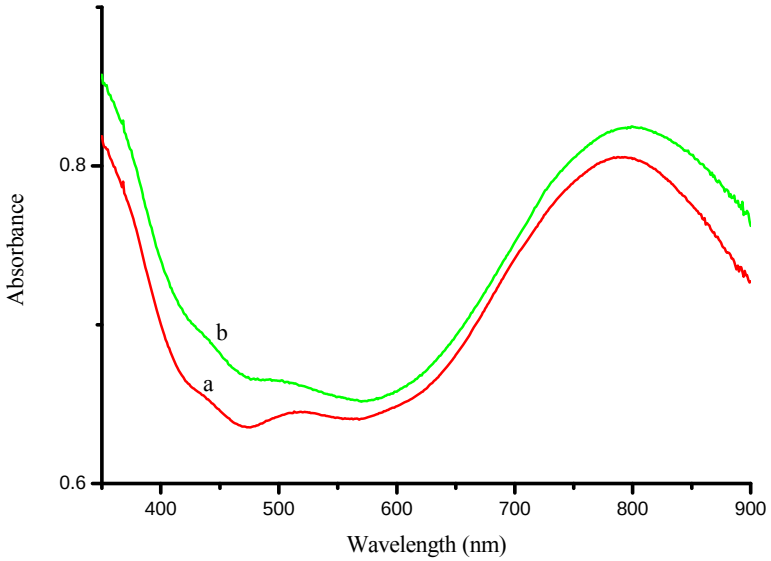

Figure III-11: UV-Visible spectra of PEDOT particles in H_2Oprepared using (a) $(NH_4)_2S_2O_8$ (run 5, table 1) and (b) $Fe^{(III)}(OTs)_3.6(H_2O)$ (run 15, table 1) as oxidants.

I.6. Thermo gravimetric analysis

The composition of the PEDOT core-shell particles was also determined by thermo gravimetric analysis (TGA). The TGA curves for PEDOT bulk powder, PVA, and PEDOT core-shell particles are shown in Figure III-12. The TGA curves for PEDOT-PVA core-shell particles is in between the ones of PEDOT bulk powder and PVA, which corroborates the presence of PEDOT and PVA in the particles. As expected, the TGA curve for PEDOT (run 12) is more close to PEDOT bulk powder as compared to PEDOT (run 13) due to greater amount of PEDOT in the former.

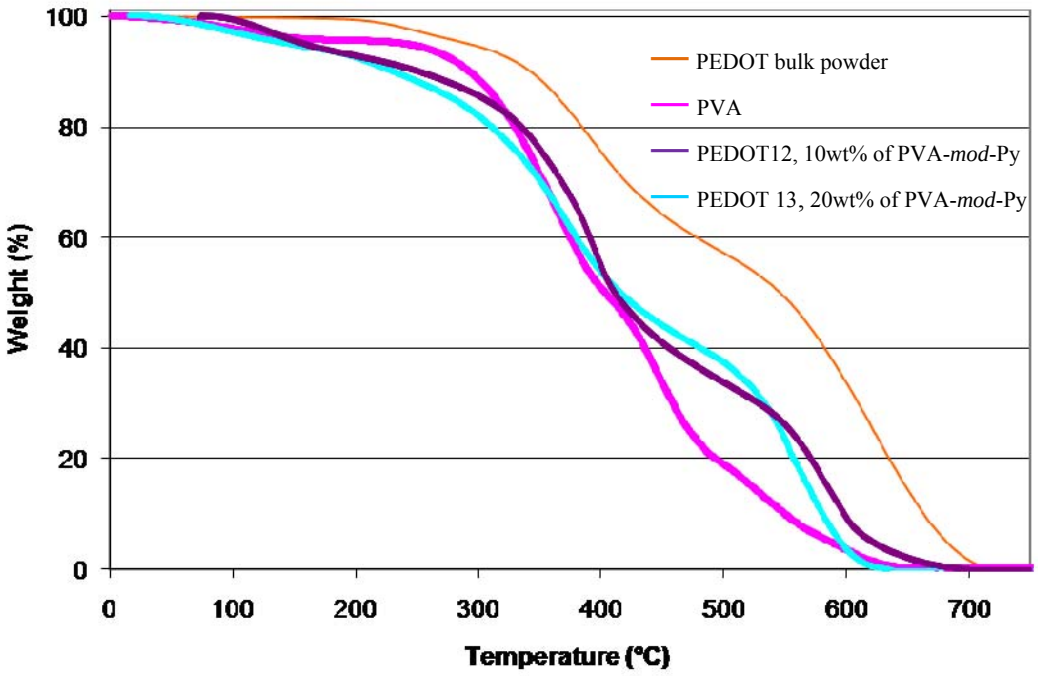

Figure III-12 : TGA traces of —PEDOT bulk powder, — PVA, —PEDOT 12 and — PEDOT 13

II. Water-borne PEDOT dispersions using PNVP-based reactive stabilizers

It is known that the addition of small amount of N-methylpyrrolidone in conducting polymer (PEDOT, PANI etc.) dispersions increase their conductivity. In this part, we have investigated the use of copolymers composed of poly(vinylpyrrolidone) (PNVP) {e.g. PNVP-*co*-PVA-*mod*-Py and PNVP-*b*- PVA-*mod*-Py} as reactive steric stabilizer for the dispersion polymerization of PEDOT. Ammonium persulfate or the mixture of ammonium persufate with $CuCl_2$ or $CuBr_2$ (1.6:0.5) were tried as oxidants.

II.1. Synthesis of PNVP-based stabilizers by cobalt-mediated controlled radical polymerization

In order to prepare PNVP-*co*-PVA and PNVP-*b*-PVA, we first synthesized PNVP-co PVAc and PNVP-*b*-PVAc precursors by cobalt mediated controlled radical polymerization (CMRP),[16-20] followed by hydrolysis. There are successful reports in the literature dealing with the synthesis of P(VAc), Poly(NVP-*co*-VAc) and Poly(NVP-*b*-VAc) by cobalt-mediated radical polymerization.[21,22] The CMRP was initiated with 2,2´-azobis(4-methoxy-2,4-dimethylvaleronitrile) (V-70) in the presence of the bis (acetylacetonate)cobalt(II) complex **A**, resulting in the formation of poly(VAc) with predetermined M_n and low dispersity. The general procedure for the cobalt-mediated mechanism is shown in Scheme III-1.

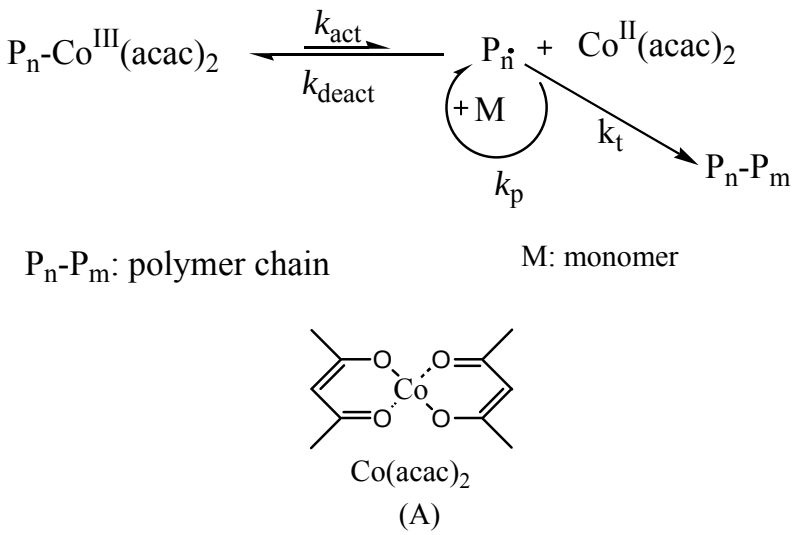

Scheme III-3: General scheme for cobalt-mediated radical polymerization (CMRP) and molecular structure of bis(acetylacetonate)cobalt(II) complex.

In the initiation step, the organic radical created by the decomposition of V-70 reacts with the monomer. Meanwhile, the cobalt(II) complex **A** can react with the propagating polymer radical to produce dormant species in the deactivation step. A spontaneous homolytic cleavage of a dormant chain end reproduces a polymer radical and a complex **A** in the activation step. The overall radical concentration in the polymerization system becomes lower when k_{deact} is much larger than k_{act}. Thus, efficient trapping of the VAc radical by complex **A** is the main requirement to establish the equilibrium between the cobalt-terminated poly(VAc) and propagating poly(VAc) radicals.

In our case, the CRMP was initiated by Azobis Isobutyro Nitrile (AIBN) in the presence of bis(acetylacetonate)Co^{II} complex at 60°C. The use of AIBN as an initiator was already described by Jérôme and co-workers for the polymerization of vinyl acetate but, in this case broad molecular weight distribution (M_w/M_n =2.0-3.5) was observed under these conditions due to high probability of irreversible chain termination.[19]

The synthesis of PNVP-*b*-PVA-*mod*-Py was carried out in four steps. First step involve the synthesis of cobalt-terminated poly(vinylacetate) macroinitiator, which then initiate the polymerization of vinylacetate to prepare PNVP-*b*-PVAc. The hydrolysis of

PNVP-*co*-PVAc gives PNVP-*b*-PVA. Finally, the esterification of PNVP-*b*-PVA with N-methylpyrrole-2-carboxylic acid gives PNVP-*b*-PVA-*mod*-Py.

II.2. Synthesis of *N*-methylpyrrole-*modified*-poly(N-vinylpyrrolidone-*block*-vinylalcohol) (PNVP-*b*-PVA-*mod*-Py)

II.2.1. Synthesis of cobalt-terminated poly(vinylacetate) macroinitiator

Cobalt-terminated poly(VAc) was prepared by bulk polymerization of VAc in the presence of Co^{II} (acetylacetonate)$_2$ using AIBN as initiator at 60°C. When the reaction mixture became enough viscous, the pink coloured poly(vinylacetate) macroradicals were directly recovered by the elimination of the residual monomer in vacuum and stored at -20°C under nitrogen atmosphere. The pink colour proves the persistence of the active cobalt at the chain end.

II.2.2. Synthesis of poly(N-vinylprrolidone)-*b*-poly(vinyl acetate)[PNVP-*b*-PVAc]

PNVP-*b*-PVAc was prepared by CMRP using cobalt-terminated poly(vinyl acetate) macroinitiator in anisole/toluene mixture (9:1) at 60°C. Whenever Co–C bond is cleaved in the presence of NVP, the released poly(vinyl acetate) radicals can initiate the NVP polymerization, whose propagation might be mediated by the cobalt complex[22]. The PNVP-*b*-PVAc samples were characterized by GPC, (^{1}H NMR) and FT-IR spectroscopy. Compared to the results already reported by Debuigne *et al*., broader molecular weight distribution were observed under these experimental conditions due to higher probability of irreversible chain termination (Table III.2).

Sample	M_n SEC g/mol;	M_w/M_n	Yield %
$PNVP_{207}$-*b*-$PVAc_{209}$	41000	2.0	70
$PNVP_{216}$-*b*-$PVAc_{47}$	28000	1.8	60

Table III-2: Characterizations of PNVP-*b*-PVAc prepared by cobalt-mediated radical polymerization using AIBN as initiator at 60°C.

The ^{1}H NMR spectrum of the PNVP-*b*-PVAc (run 2, Table III-2) in DMSO-d_6 at 25°C is shown in Figure III-13a. The peaks positioned at 4.77 ppm (C*H*-OCOCH$_3$), 1.65 ppm (-OCOCH$_3$C*H*$_2$-) and 1.93 ppm (CH-OCOC*H*$_3$) confirms the presence of PVAc block. Similarly, the peaks positioned at 3.74 ppm and 3.56 ppm (C*H*-NCO), 3.15 (C*H*$_2$-NCO-), 2.23 and 2.06 (-NCOC*H*$_2$- P*N*VP), 1.9-1.3 ppm (-N-CH$_2$-C*H*$_2$-CH$_2$-CO-) and (-C*H*$_2$-CH-NCO-) confirm the presence of PNVP in PNVP-*b*-PVAc.

The synthesis of PNVP-*b*-PVAc was also confirmed by FT-IR analysis (see Figure III-14a). The presence of main absorption peaks at 1745cm^{-1} (due to C=O stretching vibration of carbonyl group) and at 1240cm^{-1} (due to C–O stretching vibrations of ester group) prove the presence of PVAc block and absorption at 1672 cm^{-1} (due to C=O stretching vibrations of NVP) confirm the synthesis of PNVP.

II.2.3. Synthesis of poly(N-vinylpyrrolidone)-*b*-poly(vinyl alcohol) copolymer [PNVP-*b*-PVA]

The selective hydrolysis of poly(vinyl acetate) block was performed using potassium hydroxide in methanol at room temperature as PNVP resist hydrolysis under these conditions.

The full methanolysis of the PNVP-*b*-PVAc copolymer was proved by FTIR analysis (Figure III-14b). Indeed, one can observe the complete disappearance of the IR absorption bands typical of PVAc (C=O stretching at 1745 cm^{-1}, and C–O stretching at 1240cm^{-1}), where as the absorption characteristics of PNVP persists (C=O stretching at 1666 cm^{-1}). Additional evidence was found in the ^{1}H NMR of PNVP-*b*-PVA taken in the mixture of DMSO-d_6 and few drops of D$_2$O (see Figure III-13b). The complete disappearance of the PVAc signals (a-c), particularly b at 4.77 ppm (C*H*–OCOCH$_3$), the appearance of signals typical of PVA (C*H*–OH, at 3.82 ppm) and the persistence of peaks of the PNVP (d-h) confirmed the selective hydrolysis of the PVAc block.

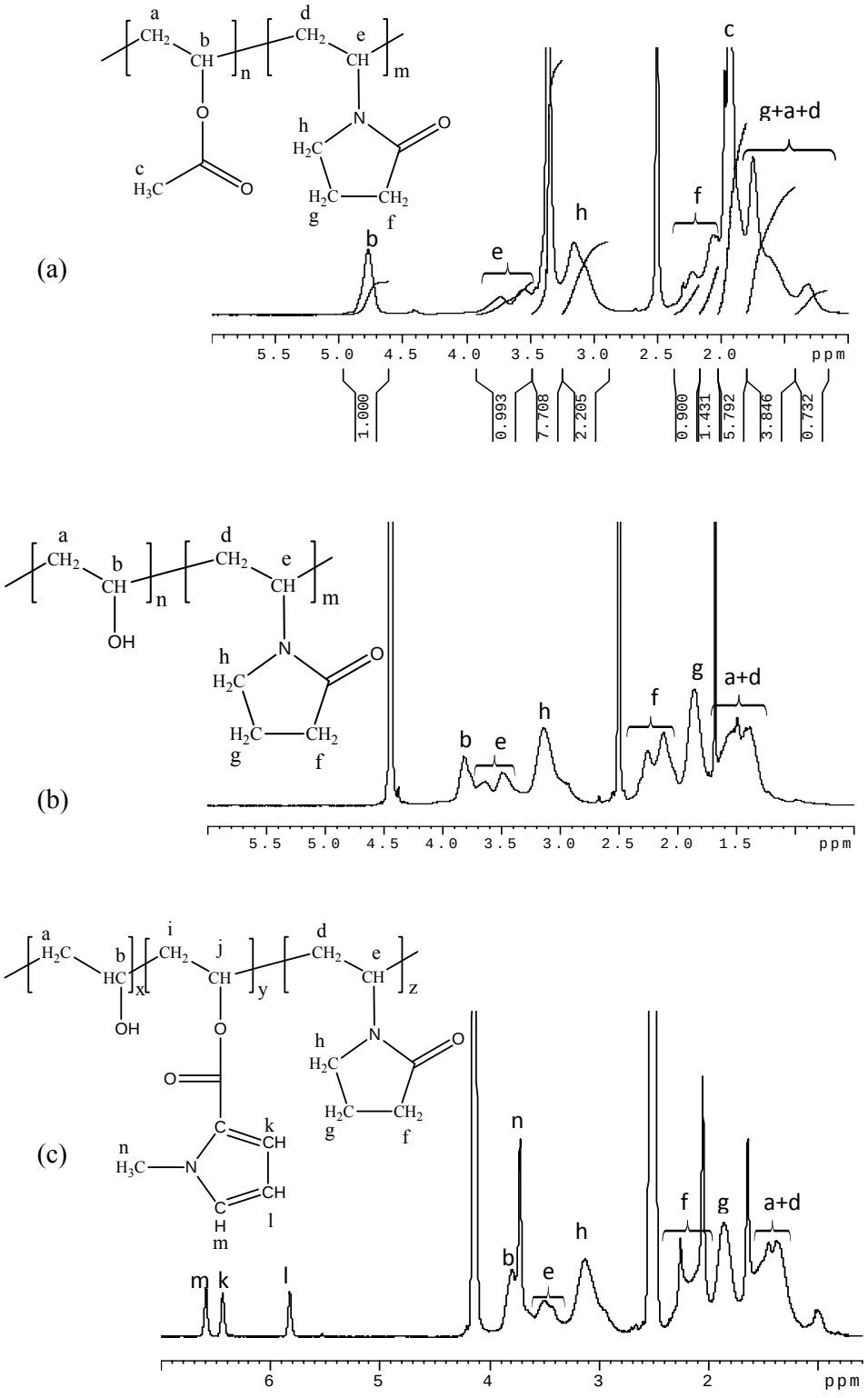

Figure III-13: ^{1}H NMR spectra of (a) PNVP-*b*-PVAc in d_6-DMSO, (b) PNVP-*b*-PVA and (c) PNVP-*b*-PVA-*mod*-Py in d_6-DMSO + few drops of D_2O at room temperature

(a)

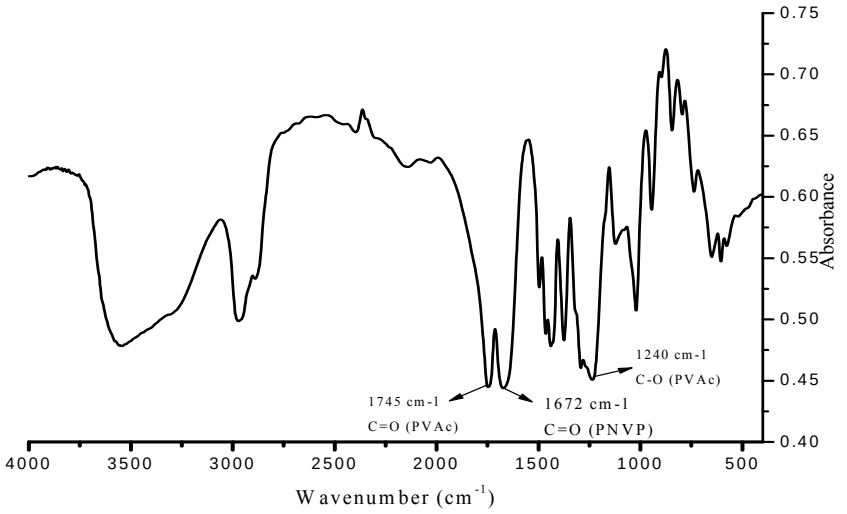

(b)

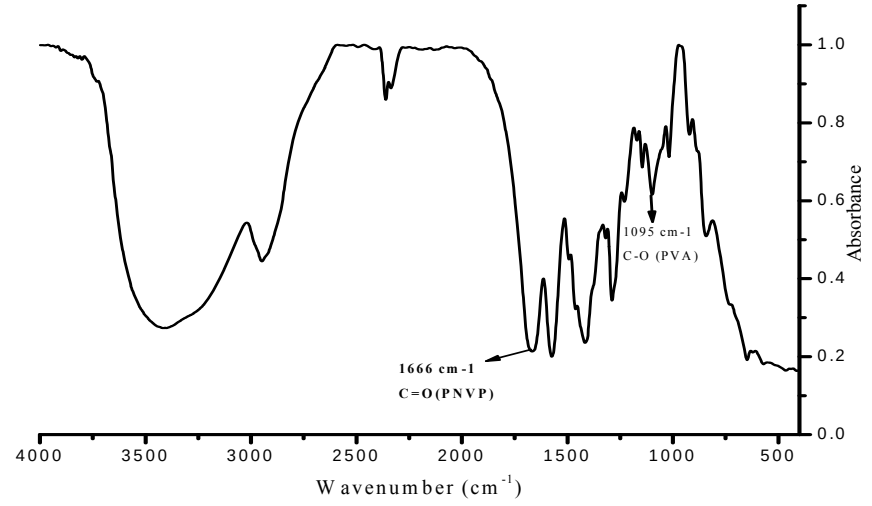

(c)

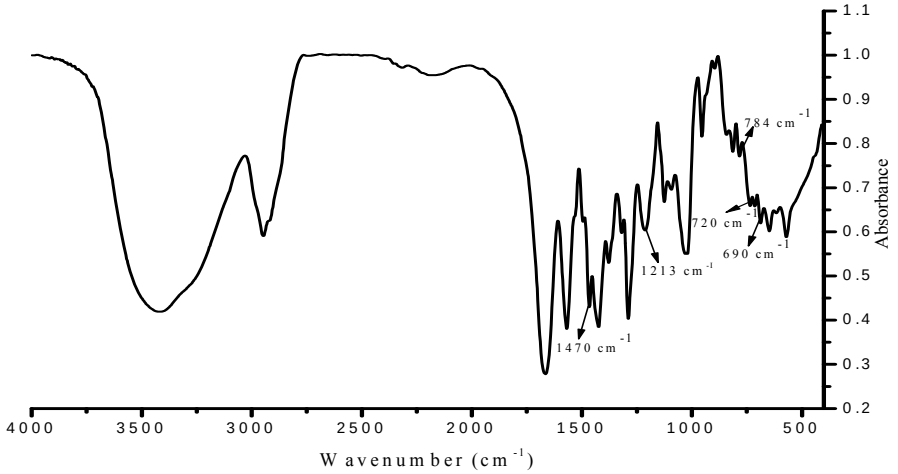

FigurIII-14: FT-IR spectra of (a) PNVP-*b*-PVAc, (b) PNVP-*b*-PVA and (c) PNVP-*b*-PVA-*mod*-Py (measured by absorption mode using KBr pellet)

II.2.4. Esterification of PNVP-b-PVA

In order to prepare PEDOT core-shell particles, PNVP-*b*-PVA-mod-Py was prepared by partial esterification (~10 mol.% with respect to PVA) of PVA block with *N*-methyl-2-pyrrolecarboxylic acid in the presence of 4-(dimethylamino)pyridinium 4-toluenesulfonate (DPTS).[1] The general synthetic procedure is shown in Scheme III.4.

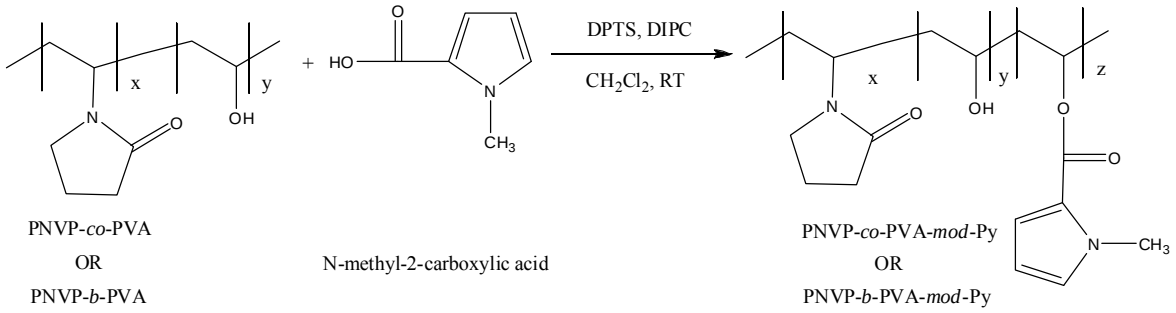

Scheme III-4: Synthesis of PNVP-*b*-PVA-*mod*-Py

The PNVP-*b*-PVA-*mod*-Py was characterized by ^{I}H NMR, FT-IR and UV-visible spectroscopy. The ^{I}H NMR of PNVP-*b*-PVA-*mod*-Py in the mixture of DMSO-d_6 and few drops of D_2O is shown in Figure III-13c. The appearance of peaks at (m) 6.59 ppm, (k) 6.44 ppm, (l) 5.82 ppm and 3.72 ppm due to N-methylpyrrole ring resonance proves the functionalization of pyrrole units along the PVA chains. The absorption peaks obtained at 1470 $cm^{-1}$and 784-690 cm^{-1}charateristics of the aromatic ring in the FT-IR spectrum of the PNVP-*b*-PVA-*mod*-Py confirm the presence of Py ring along the PNVP-*b*-PVA chains. The UV-visible spectra of PNVP-*b*-PVA and PNVP-*b*-PVA-*mod*-Py are shown in Figure III-15. A strong absorption peak at 289 nm in the UV-visible spectrum of PNVP-*b*-PVA-*mod*-Py gives an additional evidence of the presence of aromatic moieties. Comparatively weak absorption at the same area is due to the absorption of the pyrrolidone carbonyl group.

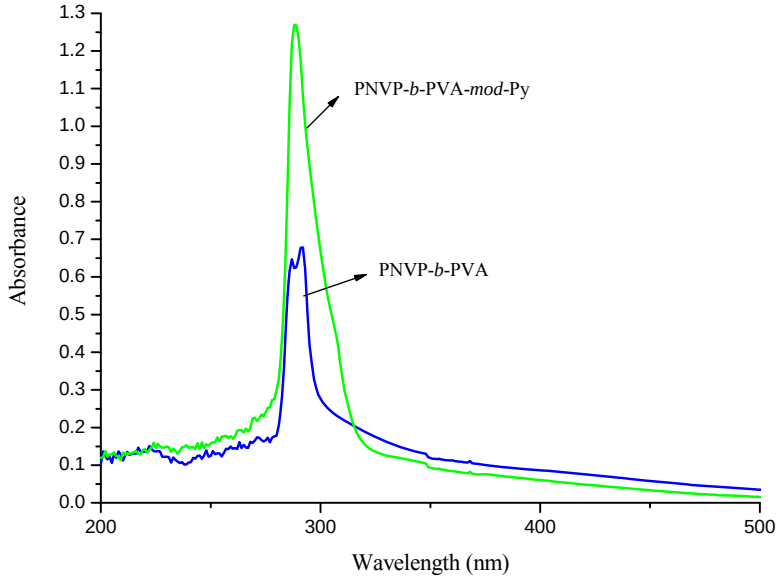

Figure III-15: UV-visible spectra of PNVP-*b*-PVA and PNVP-*b*-PVA-*mod*-Py

II.3 Synthesis of N-methylpyrrole-*modified*-poly(vinylpyrrolidone-*co*-vinyl alcohol) [PNVP-*co*-PVA-*mod*-Py]

In order to prepare N-methylpyrrole-*modified*-poly(N-vinylpyrrolidone-*co*-vinyl alcohol) copolymers, a series of Poly(NVP-*co*-VAc) were synthesized having different molecular weight and compositions (see Table III-3) by cobalt-mediated radical polymerization using AIBN as initiator in anisole/toluene mixture (9:1) at 60°C under inert atmosphere as already described in the literature.[21] The selective hydrolysis of VAc units of these samples using potassium hydroxide in methanol at room temperature produce poly(NVP-*co*-VA) copolymers. Finally, the functionalization of N-methylpyrrole units by the esterification of PNVP-*co*-PVA with N-methylpyrrole-2-carboxylic acid gave PNVP-*co*-PVA-*mod*-Py.

From Table III-3, it is clear that poly(NVP-*co*-VAc) copolymers having low molecular weight distributions are obtained when equal molar ratio of NVP to VAc was used (entry 1, and 2), while samples with high molecular weight distribution were obtained with higher NVP to VAc ratio (entry 3 and 4). This is probably explained by the much slower deactivation

caused by the reaction of NVP radical with bis(acetylacetonate)Co^{III} as compared to VAc and higher probability of irreversible chain termination in these experimental conditions.[19]

Sample	[VAc]/[NVP]/[Co]/[AIBN][a]	M_n GPC g/mol;	M_w/M_n	Yield %
PNVP-*co*-PVAc	150/150/1/2	28700	1.5	70
PNVP-*co*-PVAc	200/200/1/2	36000	1.4	80
PNVP-*co*-PVAc	50/150/1/2	10000	2.9	75
PNVP-*co*-PVAc	100/300/1/2	17000	3.0	70

(a) Initial concentrations used

Table III-3: Characterizations of PNVP-*co*-PVAc prepared by cobalt-mediated radical polymerization using AIBN as initiator at 60°C.

In order to find their compositions, PNVP-*co*-PVAc samples were characterized by ^{1}H NMR, FT-IR (For illustration see Experimental section III.1 and III-2) and UV-visible (Figure III-16) spectroscopy. Similar results were obtained as described above for the synthesis of PNVP-*b*-PVA-*mod*-Py.

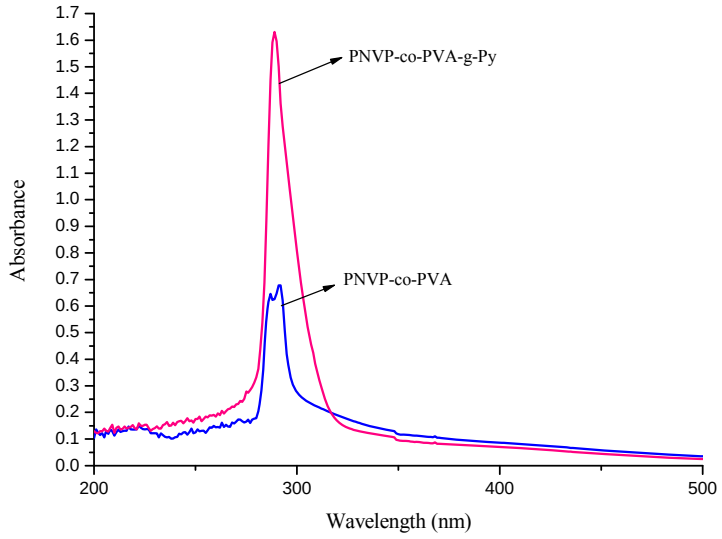

Figure III-16: UV-Visible spectra of PNVP-*co*-PVA and PNVP-*co*-PVA-*mod*-Py in water (5g/L)

II.4. Solution behavior of PNVP-*b*-PVAc, PNVP-*b*-PVA-*mod*-Py and PNVP-*co*-PVA-*mod*-Py copolymers

In order to fully investigate the behavior of stabilizers in solution and their final effect on the size and morphology of the PEDOT particles, PNVP-*b*-PVAc (M_n =28000 g/mol), PNVP-*co*-PVA-*mod*-Py (M_n =35000 g/mol) and PNVP-*co*-PVA-*mod*-Py (M_n =39000 g/mol) samples were analyzed by Dynamic Light Scattering (DLS) in the same solvent mixture used for the synthesis of PEDOT dispersions. For this purpose, solutions of each stabilizer having different concentrations (1-10 g/L) in methanol/water mixture (1/4) were prepared. These samples solutions were filtered through 0.4 µm filters and stirred for 24 hours prior to DLS analysis. The auto-correlation functions and their CONTIN analyses[23] obtained at 25°C for different stabilizers at a concentration of 5g/L are shown in Figure III-17. For PNVP-*b*-PVAc, PNVP-*b*-PVA-*mod*-Py and PNVP-*co*-PVA-*mod*-Py samples (Figures III-17a-f), one main population with hydrodynamic radii R_H respectively of 40 nm, 96 nm and 80 nm can be observed. These typical dimensions are characteristic of micellar aggregation.

Furthermore, no significant evolution of the apparent hydrodynamic radius has been observed with the change in concentrations. In addition, the linear dependence of relaxation frequency Γ as a function of the square of the wave vector q^2 confirms that the observed micellar aggregates are spherical and homogeneous in size (Figure III-18a-c). Taking into account the dimension of a unimer (about 6-7nm), such a morphology is not really consistent with a spherical micelle, but a vesicular structure is expected.[24,25]

The formation of these spherical objects was further confirmed by TEM analysis of PNVP-*co*-PVA-*mod*-Py sample (see Figure III-18d). The majority of these nanoparticles have a diameter between 150-200 nm which is very close to the value obtained by DLS analysis and the PEDOT particles obtained using this stabilizer that will be discussed later on. From these observations, one may anticipate that all above mentioned stabilizers self-assemble to form vesicular nano-objects thus leading to the formation of vesicles after EDOT polymerization.

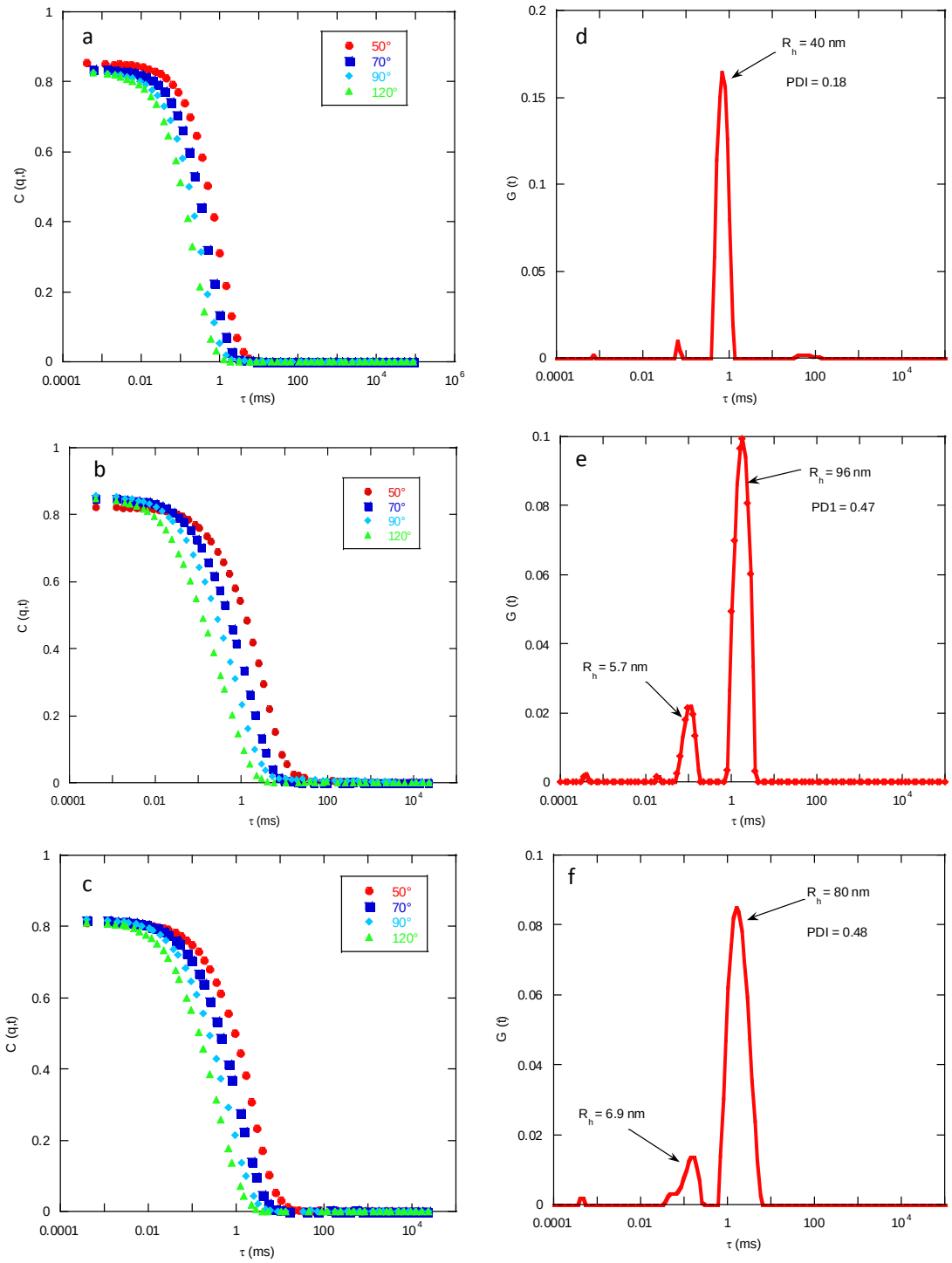

Figure III-17: Auto-correlation function C(q,t) of (a) PNVP-*b*-PVAc (M_n = 28000 g/mol), (b) PNVP-b-PVA-*mod*-Py (M_n = 35000 g/mol) and (c) PNVP-*co*-PVA-*mod*-Py (M_n = 39000 g/mol) samples (5 g/L) at different angles and (d), (e) and (f) are their respective relaxation time distribution G(t) at 90° in water/methanol mixture (4:1) at 25 °C.

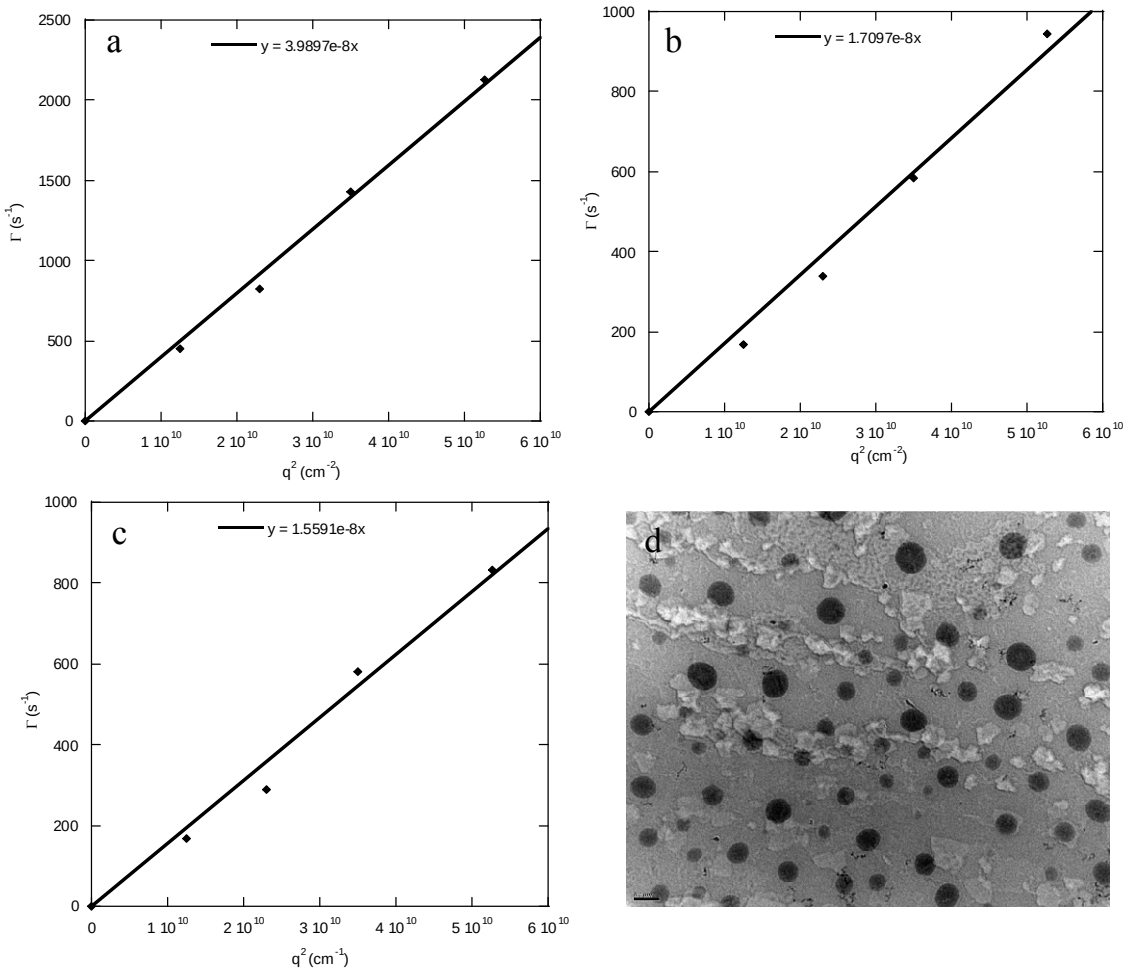

Figure III-18: Relaxation frequency in the function of q^2 for (a) PNVP-*b*-PVAc (M_n = 28000 g/mol), (b) PNVP-*b*-PVA-*mod*-Py (M_n = 35000 g/mol) and (c) PNVP-*co*-PVA-*mod*-Py (M_n = 39000 g/mol) samples (5 g/L) and (d) TEM image of PNVP-*co*-PVA-*mod*-Py reactive stabilizer (10 g/L). (Scale for Figure III-18d is 0.2 µm**)**

II.5 Synthesis of PEDOT dispersions

PEDOT dispersions were prepared in the presence of PNVP-*b*-PVA-*mod*-Py and PNVP-*co*-PVA-*mod*-Py using $(NH_4)_2S_2O_8$ or the mixture of $(NH_4)_2S_2O_8$ with either $CuBr_2$ or $CuCl_2$ (to improve the conductivity) as oxidants in water/methanol (4:1) mixture at 40°C. The effects of different parameters like molecular weight, concentration, nature and composition of stabilizer as well as the nature of the oxidants on the size, size distribution and morphology of the PEDOT particles were studied. The general scheme of dispersion polymerization of

EDOT is shown in Scheme III-4. The results of dispersion polymerization of EDOT prepared under different experimental conditions are summarized in Table III-4.

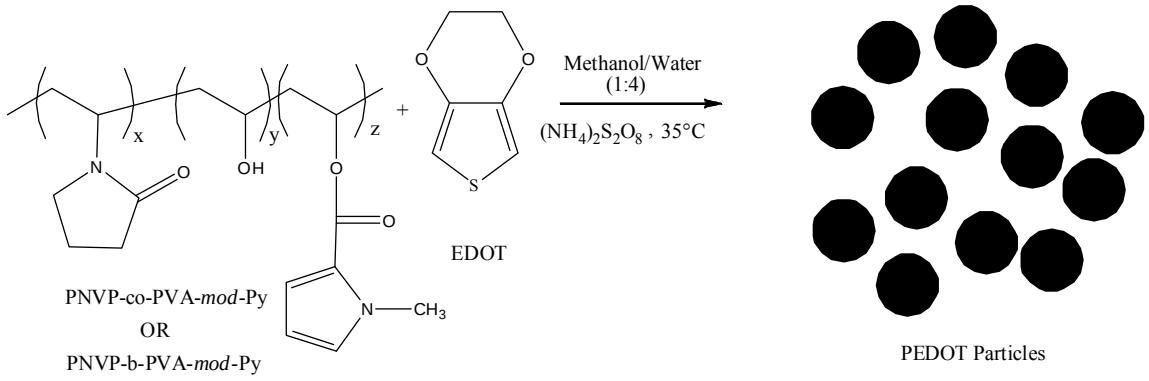

Scheme III-4: Synthesis of PEDOT dispersions in the presence of PNVP-based reactive copolymer stabilizers

II.5.1 Use of PNVP-*b*-PVA-*mod*-Py as reactive stabilizer

The dispersion polymerization of EDOT was performed using different concentrations of PNVP-*co*-PVA-*mod*-Py as a reactive stabilizer (runs 3 & 4, Table III-4). Generally very small spherical particles with narrow size distribution are obtained under these experimental conditions (see Figure III-19c-d). From the Figure III-19, it is clear that the average size of the particles decreases with the stabilizer concentration increase. The size of the particles decreases from 60-100 nm to 40-80 nm as the concentration of the stabilizer increases from 10 wt.% to 20 wt.%. This is in agreement with the previous results obtained in PEDOT dispersions using other reactive stabilizers.

S. N°	Stabilizer type	Molecular weight of the stabilizer (g/mol)	Wt.% of the stabilizer	Yield[c] %	Conductivity[d] S/cm	Particle size[e] (nm)	Remarks
1	PNVP-*b*-PVAc	28000	10	55	5.0×10^{-5}	70-100	Particles
2	PNVP-*b*-PVA	33000	20	60	4.0×10^{-6}		Vesicles
3	PNVP-*b*-PVA-*mod*-Py	35000	10	60	4.5×10^{-5}	60-100	Particles
4	PNVP-*b*-PVA-*mod*-Py	35000	20	60	2.0×10^{-5}	40-80	Particles
5	PNVP-*co*-PVA-*mod*-Py	29000	10	60	8.5×10^{-5}	150-200	Particles
6	PNVP-*co*-PVA-mod*f*-Py	29000	20	55	3.0×10^{-5}	100-120	Particles
7	PNVP-*co*-PVA-*mod*-Py	29000	35	50	7.5×10^{-6}	80-100	Particles
8	PNVP-*co*-PVA-*mod*-Py	39000	10	60	8.4×10^{-5}	200-250	Particles
9	PNVP-*co*-PVA-*mod*-Py	39000	20	60	4.5×10^{-5}	180-200	Particles
10	PNVP-*co*-PVA	35600	20	50	2.0×10^{-6}	200-300	Vesicles
11	PNVP-*co*-PVA-*mod*-Py	10000	20	55	5.3×10^{-5}	160-180	Particles
12	PNVP-*co*-PVA-mod-Py	17000	20	60	5.0×10^{-5}	160-200	Particles
13	PNVP-*co*-PVA-*mod*-Py	17000	35	60	2.5×10^{-5}	90-120	Particles
14[a]	PNVP-*co*-PVA-*mod*-Py	17000	20	70	3.0×10^{-4}	90-110	Particles
15[b]	PNVP-*co*-PVA-*mod*-Py	17000	20	65	2.0×10^{-4}	70-100	Particles

(a) A mixture of $(NH_4)_2S_2O_8$+$CuBr_2$ (1.3:1) was used as an oxidant
(b) A mixture of $(NH_4)_2S_2O_8$+$CuCl_2$ (1.3:1) was used as an oxidant
(c) obtained by gravimetric analysis
(d) measured by four probe method
(e) Measured from TEM images. In all cases averages on 100 objects were made

Table III-4: Synthesis of PEDOT particles using PNVP-*b*-PVA-*mod*-Py and PNVP-*co*-PVA-*mod*-Py as reactive stabilizers in water/methanol (1:4) at 40 °C.

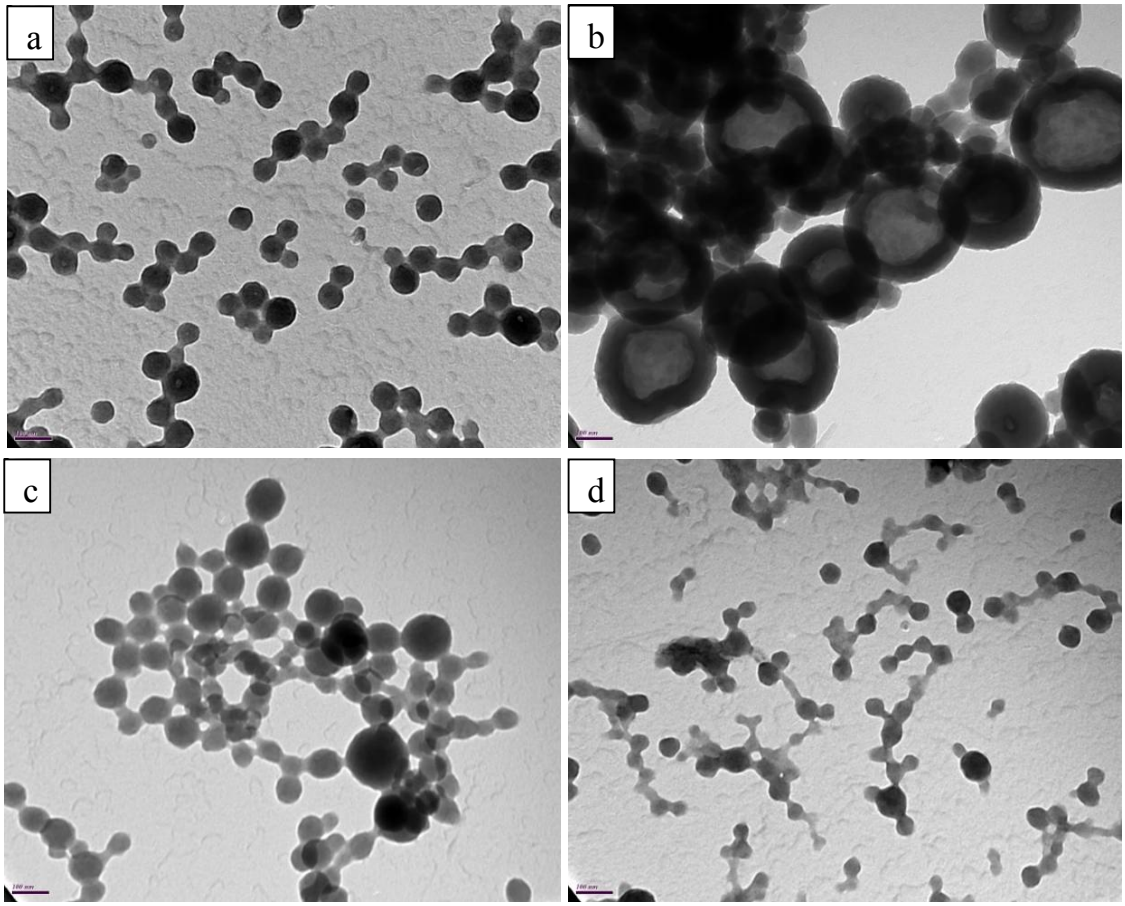

Figure III-19: TEM images of PEDOT particles prepared using different types of stabilizers and concentrations (a) PNVP-*b*-PVAc , Mn = 41000 g/mol, 10 wt.% (run 1, Table III-4), (b) PNVP-*b*-PVA, Mn = 33000 g/mol, 20 wt.%, (run 2, Table III-4), (c) PNVP-*b*-PVA-*mod*-Py, Mn = 35000 g/mol, 10 wt.% (run 3, Table III-4) and (d) PNVP-*b*-PVA-*mod*-Py, Mn = 35000 g/mol, 20 wt.% (run 4, Table III-4). (Scale for each case is 100 nm**)**

For comparison purpose, EDOT dispersion polymerization was also performed in the presence of PNVP-*b*-PVAc and PNVP-*b*-PVA as unreactive stabilizers. It should be noted that PNVP-*b*-PVAc having higher percentage of PNVP (run 2, Table III-2) was soluble in water while the one having equal percentage of PNVP and PVAc (run 1, Table III-2) was insoluble. When polymerization of EDOT was performed in the presence of soluble PNVP-b-PVAc, well-defined and small sized stable particles with homogenous size distribution were obtained (Figure III-19a). On the other hand, large size hollow particles (vesicles) were obtained using un-modified PNVP-*b*-PVA as a stabilizer (Figure III-19b).

From the above results it is clear that both unreactive and reactive stabilizers are seen to be efficient in the polymerization of EDOT, even though morphology and size are quite

different. The main reason for the formation of these nano-objects (particles and vesicles) is the self-organization of the copolymer stabilizers in the solution prior to EDOT polymerization. The EDOT polymerization probably takes place either inside or on the surface of these self-assembled nano-objects leading to the formation of particles or vesicles respectively but untill now we do not have enough data to explain further the particles or vesicles formation. More importantly, we have observed that the PEDOT dispersion prepared using reactive copolymer stabilizers are more stable as compared to unreactive ones. This is logically explained by chemical grafting of the reactive copolymer stabilizer on the surface of PEDOT during polymerization.

II.5.2 Use of PNVP-*co*-PVA-*mod*-Py as reactive stabilizer

In order to see the effect of statistical copolymer stabilizers on the morphology and size distribution of PEDOT particles, the EDOT polymerization was performed in the presence of PNVP-*co*-PVA-*mod*-Py stabilizers in similar reaction conditions. The effect of molecular weight, composition, concentration of the stabilizers and the nature of the oxidants were studied. All these factors more or less affect the size and size distribution of the particles. The results of the PEDOT dispersion prepared under different experimental conditions are shown in Table III-4 (runs 5-15). As it is clear from these data, the PEDOT particles with narrow size distribution were obtained in each case.

As expected, the size of the PEDOT particle increases as the stabilizers concentration decreases whatever the composition of the stabilizer (see runs 5-7 and 12-13, Table III-4). For example, in runs 5-7, the particle size goes from 170-200 nm to 80-100 nm as the concentration of PNVP-*co*-PVA-*mod*-Py ($\overline{M}_n$ = 29000 g.mol^{-1}) varies from 10 wt.% to 35 wt.%.(see runs 5-7). TEM images of PEDOT particles can be seen in Figures III-20 and III-21).

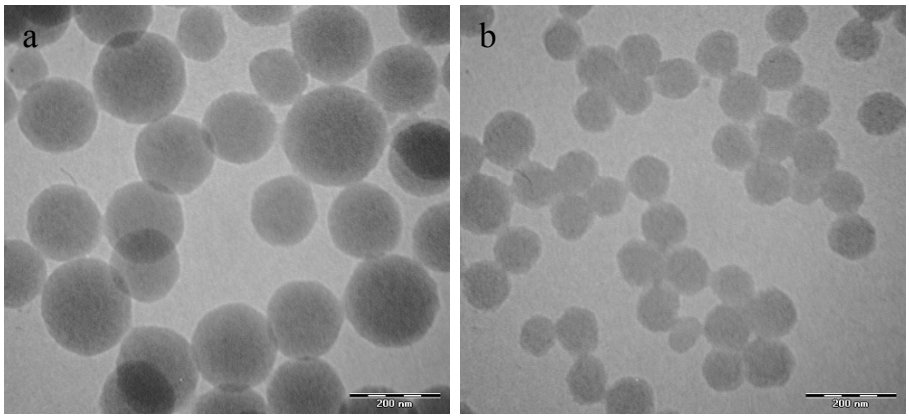

Figure III-20: TEM images of PEDOT particles prepared using different concentrations of PNVP-*co*-PVA-*mod*-Py (M_n = 29000 g/mol) (a) 10 wt.% (run 5, Table III-3), (b) 20 wt.%, (run 6, Table III-4).

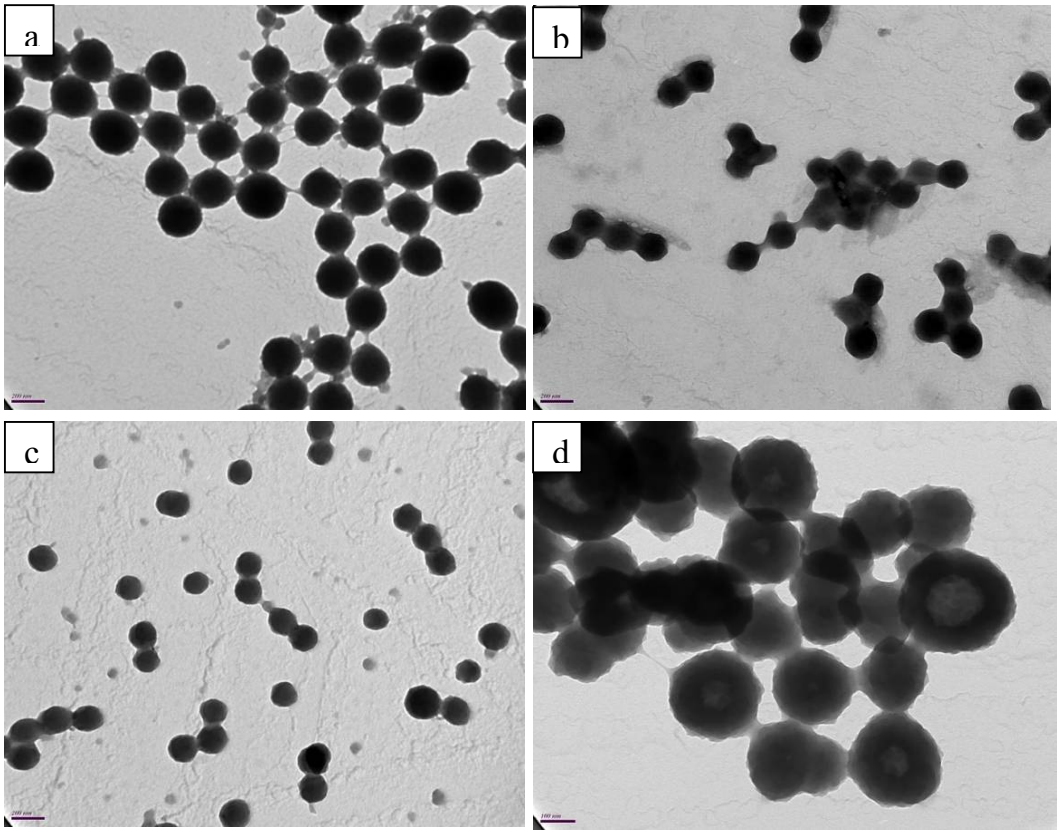

Figure III-21: TEM images of PEDOT particles prepared using different statistical copolymer stabilizers (a) PNVP-*co*-PVA-*mod*-Py , M_n = 39000 g/mol, 10 wt.% (run 8, Table III-4), (b), PNVP-*co*-PVA-*mod*-Py , M_n = 39000 g/mol, 20 wt.% (run 9, Table III-4 (c) PNVP-*co*-PVA-*mod*-Py , M_n = 10000 g/mol, 20 wt.% (run 11, Table III-4) (d) PNVP-*co*-PVA, M_n = 35600 g/mol, 20 wt.% (run 10, Table III-4) {the scale bar for (a-c) is 200 nm and for (d) is 100 nm}

From the Figures III-20 and III-21, it is clear that PEDOT particles with very narrow size distribution are obtained using PNVP-*co*-PVA-*mod*-Py reactive stabilizers. It is also clear from Table III-4 that molecular weight of the stabilizer have very less or no effect on the size of the PEDOT particles (see runs 5 & 8 and 11-12). PEDOT dispersion was also performed in the presence of non-reactive PNVP-*co*-PVA stabilizer. Similar to the results already obtained in case of non-reactive PNVP-*b*-PVA, PEDOT vesicles having size from 200 to 300 nm were obtained.

From the above discussion one can conclude that both PNVP-*co*-PVA and PNVP-*b*-PVA-based reactive stabilizers are efficient to form very stable PEDOT dispersions. It is important to note that the spherical PEDOT nano-objects with very narrow size distribution

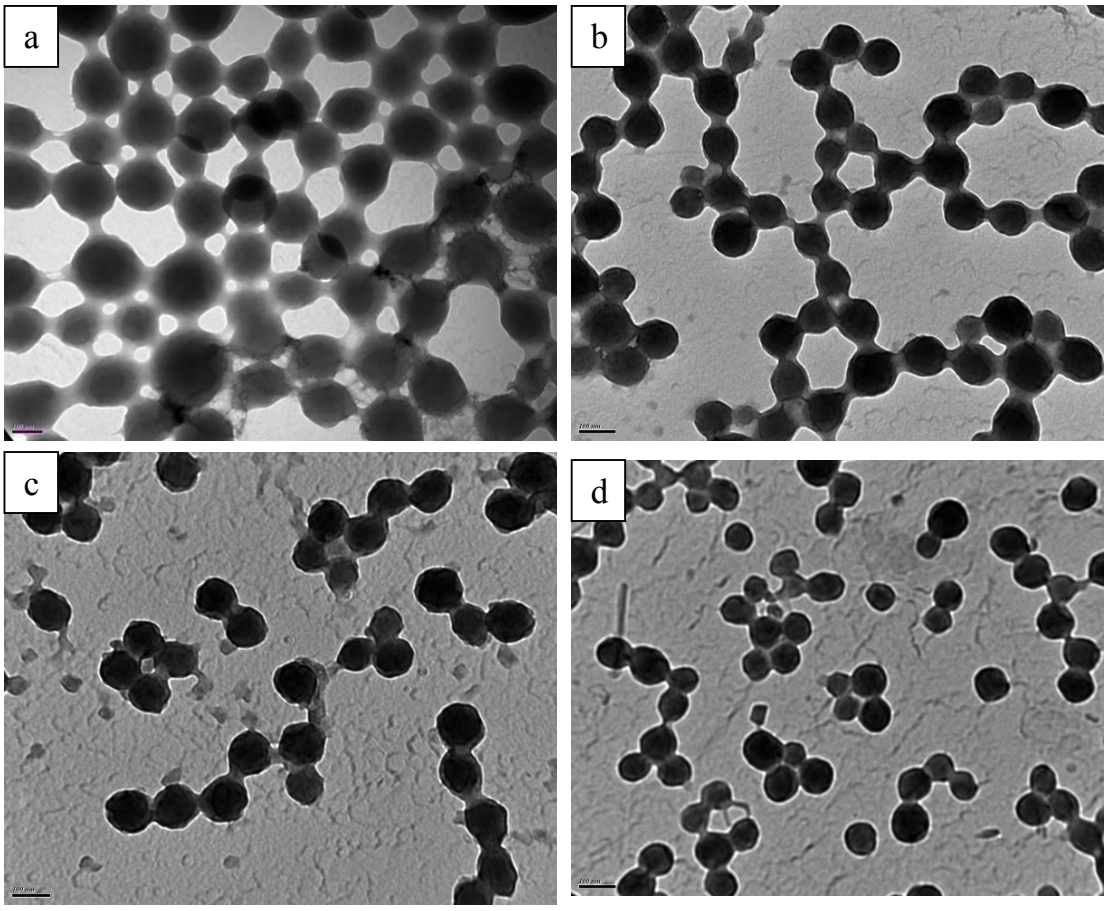

Figure III-22: TEM images of PEDOT particles prepared in the presence of PNVP-*co*-PVA-*mod*-Py (M_n = 17000 g/mol) using different oxidants (a) 20 wt.% , $NH_4)_2S_2O_8$, (run 12, Table III-4), (b), 35 wt.%, $(NH_4)_2S_2O_8$ (run 13, Table III-4 (c) 20 wt.%, $NH_4)_2S_2O_8$ + $CuBr_2$ (run 14, Table III-4 (d) 20 wt.% ,$NH_4)_2S_2O_8$ + $CuCl_2$ (run 15, Table III-4) {scale for each case is 100 nm}

are obtained using PNVP-*co*-PVA-based reactive stabilizers which makes it more efficient than PNVP-*b*-PVA-based reactive stabilizers. This behavior may be explained by well distributed reactive groups along the stabilizer chain.

In order to improve the conductivity, the dispersion polymerization of EDOT was also carried out using the mixture of $(NH_4)_2S_2O_8$ either with $CuBr_2$ or $CuCl_2$ as a oxidant. The TEM images of the particles prepared under these conditions are shown in Figure III-22c-d. In these conditions small well-defined particles are obtained in good yield. Results on conductivity will be discussed later in paragraph II.8.

II.6. XPS analysis of PEDOT core-shell particles samples

In order to investigate the core-shell nature of the PEDOT particles, XPS analysis of PEDOT samples and PEDOT bulk powder were analyzed by X-ray Photoelectron Spectroscopy (XPS). Figures III-23a and III-23 b represent the XPS survey spectra of PEDOT bulk powder and PEDOT core-shell particles (run 8, Table III-4). The presence of a peak due to N1s in survey spectrum of PEDOT core-shell particles in addition to the four main peaks originating from O1s, C1s, S2s and S2p is in favor of the presence of PNVP-*co*-PVA-*mod*-Py on the surface. Such a feature is not present in survey spectra of PEDOT bulk powder. Figures III-23c and III-23d display the high resolution C1s core-line spectra of PEDOT bulk powder and PEDOT core-shell particles. The sub peaks centered at 285.6 eV (C–N) and 287.7 eV (N–C=O)[26,27,28] prove the presence of PNVP component of the stabilizer. Similarly, the peak at 286.4 eV position in C 1s core-line spectra of PEDOT core-shell particles correspond to C-O-H moieties in PVA.[10-12] In addition, the presence of peak at 532.6 eV (Figure III-24b) originating from O 1s is due to C-O-H and is in agreement to the data already available in the literature. [10] Such peak was not observed in O 1s core-line spectrum of PEDOT bulk powder (Figure III-24a). The presence of sub peaks at 163.8-165.1 eV and 167.3-168.6 eV in S2p core-line spectrum of PEDOT-core-shell particles corresponds to the neutral S of the PEDOT and sulfate anion of the dopant respectively. The peaks due to S^+ are absent probably due to same reason as mentioned earlier.

The N1s core-line spectrum for PEDOT core-shell particles is shown in Figure III-24c. The sub peaks displayed at 399.8 eV due to the N–C=O group of the PNVP and 400.6 due to the $N–CH_3$ of N-methyl pyrrole functionalized at the PVA component of the stabilizer give

additional proof of the presence of PNVP-*co*-PVA-*mod*-Py on the surface of the PEDOT core-shell particles.

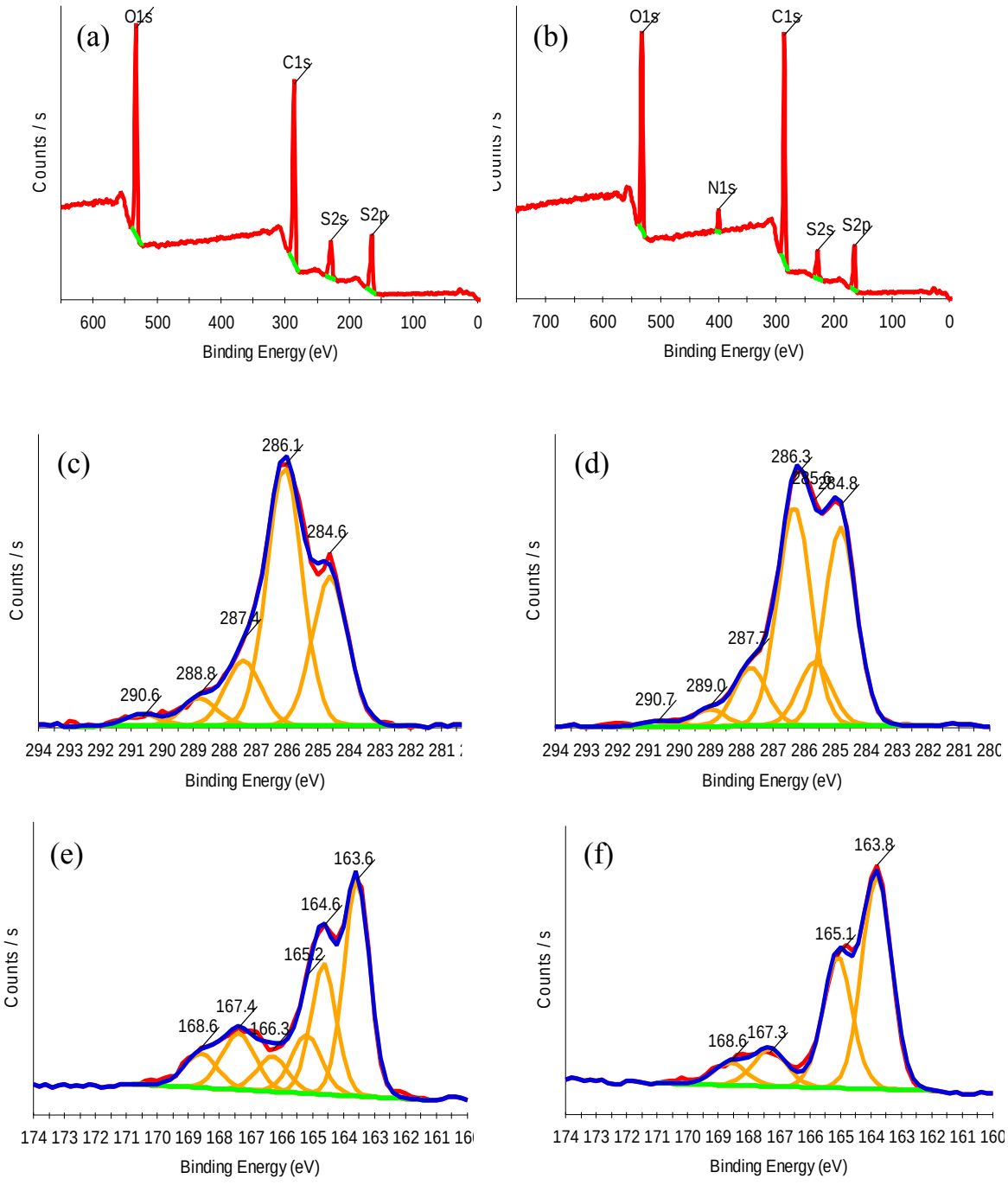

Figure III-23: (a) &(b)survey spectra of PEDOT bulk powder and PEDOT core-shell particles respectively, (c) & (d) C1s core line spectra and (e) &(f) are S2p core-line spectra of PEDOT bulk powder and PEDOT core-shell particles respectively.

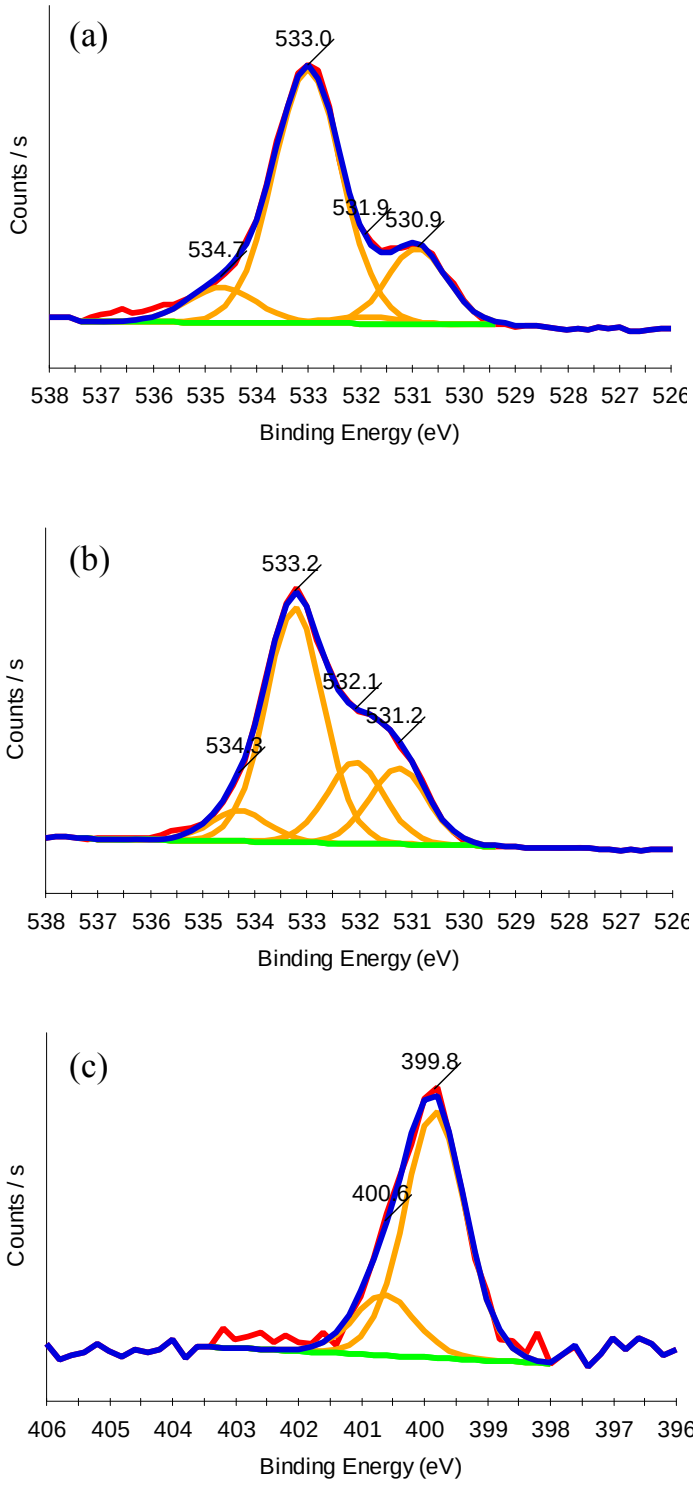

Figure III-24: (a) O1s core-line spectrum of PEDOT bulk powder, (b) &(c) are O1s core-line and N1s core-line spectra of PEDOT core-shell particles respectively.

II.7. FT-IR and UV-visible characterization of PEDOT samples

In order to find the composition of PEDOT samples, FT-IR spectra of PEDOT core-shell particles and PEDOT bulk powder were taken (Figure III-25). The presence of peaks at 692-1525 cm^{-1} confirms the synthesis of doped PEDOT materials. [11,12,14, 15] The occurrence of peaks at 1645 cm^{-1} (C=O stretching vibration of PNVP) in PEDOT particles (Figures III-25b and III-25c) confirms the presence of stabilizer since such peaks are not seen in PEDOT bulk powder (Figure III-25a). The peak intensity at 1645 cm^{-1} increases with the increase in the concentration of the stabilizer (Figures III-25b & III-25c)

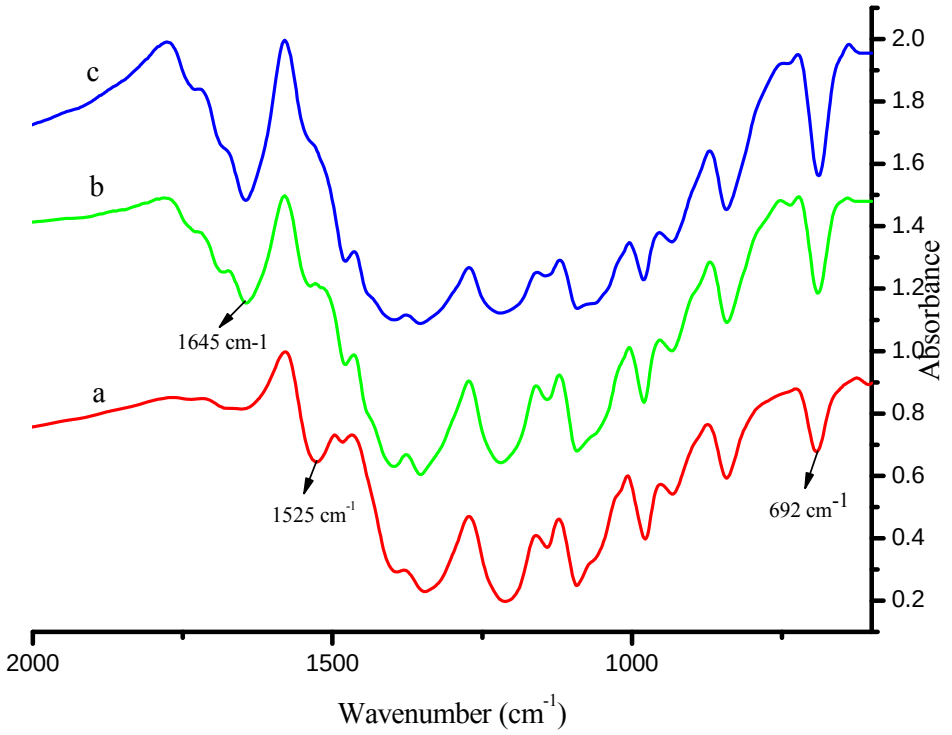

Figure III-25: FT-IR spectra of (a) PEDOT bulk powder, (b) & (c) PEDOT sample prepared in the presence of 10 wt.% and 20 wt.% of PNVP-*co*-PVA-*mod*-Py (Mn =29000 g/mol, run 5 and 6 Table III-4) respectively (measured by absorption mode using KBr pellet).

UV-Visible spectra of the PEDOT samples prepared using different oxidants are shown in Figure III-26. PEDOT samples prepared using $(NH_4)_2S_2O_8$, $(NH_4)_2S_2O_8$+$CuBr_2$ and $(NH_4)_2S_2O_8$+$CuCl_2$ as oxidants absorb strongly at 760nm, 720 nm and 750 nm, this absorption band corresponding to polarons and bipolarons due to doping of PEDOT during polymerization. The absorption at 550 nm originating from π to π* electronic transition states

in de-doped PEDOT[14], is negligible or not observed in each case which clearly indicates the fully doped PEDOT samples.

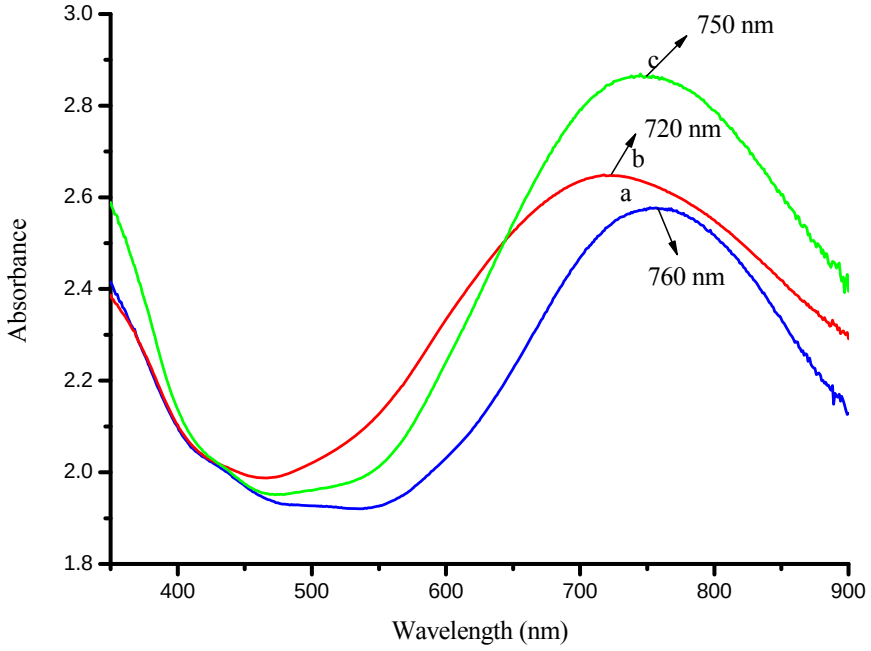

Figure III-26: UV-visible spectra of the PEDOT samples in H_2O prepared using (a) $(NH_4)_2S_2O_8$ (b) $(NH_4)_2S_2O_8$ +$CuBr_2$ and (c) $(NH_4)_2S_2O_8$ + $CuCl_2$ as oxidants.

II.8 Conductivity

As already mentioned, the conductivity of the PEDOT particles was measured using the conventional four probe technique on dried and compressed PEDOT powders under the form of disc pellets. As it is indicated in Table III-4, there was only a little increase in the conductivity was observed than our expectations. PEDOT samples prepared using PNVP-based reactive stabilizers and ammonium persulfate as an oxidant show low conductivities (up to $8.0x10^{-5}$ S cm^{-1}). These values are about 10 times higher than the conductivities obtained using PVA-based reactive stabilizers. On the other hand the PEDOT samples prepared using a mixture of $(NH_4)_2S_2O_8$+$CuBr_2$ or $(NH_4)_2S_2O_8$+$CuCl_2$ as an oxidant exhibit higher conductivities (up to 3.0×10^{-4} S cm^{-1}) probably due to higher amount of PEDOT in the samples and the presence of copper ion which act as an oxidant as well as dopant

III. Conclusion

In conclusion, in the first part of the chapter, we have shown that narrow distributed PEDOT nano-objects can be easily prepared in the presence of PVA-based reactive stabilizer. No stable PEDOT dispersions were formed using unmodified PVA while stable dispersions are formed using pyrrole-modified PVA, proving the key role played by the reactive stabilizer toward the formation of stable PEDOT dispersions. The morphology of these nano-objects can be tuned by changing the concentration of the PVA-based reactive stabilizer as well as the degree of pyrrole functions on the PVA backbone.

We have also shown that well-defined PEDOT particles with narrow size distribution can also be prepared using PNVP-*b*-PVA and PNVP-*co*-PVA based reactive stabilizers. The size of these particles can be tuned easily by changing the concentration of the stabilizers. The PEDOT particles with more narrow size distribution are obtained using PNVP-*co*-PVA-*mod*-Py which makes it more efficient reactive stabilizers than PNVP-*b*-PVA-*mod*-Py. This phenomenon can be explained by the well distributed reactive moieties along the polymer chains. Contrarily to our expectations, a small increase in the conductivity was observed using PNVP-based reactive stabilizers.

Finally, as expected, the PEDOT particles prepared using a mixture of $(NH_4)_2S_2O_8$+$CuBr_2$ or $(NH_4)_2S_2O_8$+$CuCl_2$ show higher conductivity than the samples prepared using only $(NH_4)_2S_2O_8$ as an oxidant.

References

(1) Moore, J. S.; Stupp, S. I. *Macromolecules*, **1990**, 23, 65.

(2) Díez, I.; Tauer, K.; Schulz, B. *Colloid Polym. Sci*. **2006**, 284, 1431.

(3) Armes, S. P.; Aldissi, M.; Agnew, S. F. *Synth. Met*. **1989**, 28, 837.

(4) Armes, S. P.; Aldissi, M.; Hawley, M.; Beery, J. G.; Gottesfeld, S. *Langmuir*, **1991**, 7, 1447.

(5) Mandal, T. K.; Mandal, B. M. *J. Polym. Chem. Part A: Polym Chem* **1999**, 37, 3723.

(6) Mandal, T. K. ; Mandal, B. M. *Langmuir*, **1997**, 13, 2421.

(7) Paine, A. J. *J. Colloid Interface Sci.* **1990**, 138, 157.

(8) Paine, A. J.; Luymes, W.; McNulty, J. *Macromolecules*, **1990**, 23, 3104.

(9) Paine, A. J. *Macromolecules*, **1990**, 23, 3109.

(10) Benseddik, E.; Makhlouki, M.; Bernede, J. C.; Lerfrant, S.; Proń, A. *Synth. Met***. 1995**, 72, 237.

(11) Beamon, G. and Briggs, D. *High Resolution XPS of Organic Polymers*, Wiley, Newyork, **1992**.

(12) Shakesheff, K. M.; Evora, C.; Soriano, I.; Langer, R. *J. Coll. Inter. Sci*. **1997**, 185, 538.

(13) Khan, M. A.; Armes, S. P. *Langmuir* **2000**, 16, 4171.

(14) Yang, Y.; Jiang, Y.; Xu, J.; Yu, J. *Polymer*, **2007**, 48, 4459.

(15) Kumar, S. S.; Kumar, C. S.; Mathiyarasu, J.; Phani, K. L. *Langmuir*, **2007**, 23, 3401.

(16) Wayland, B. B.; Poszmik, G.; Mukerjee, S. L.; Fryd, M. *J. Am. Chem. Soc.* **1994**, *116*, 7943-7944.

(17) Wayland, B. B.; Basickes, L.; Mukerjee, S.; Wei, M.; Fryd, M. *Macromolecules* **1997**, *30*, 8109-8112.

(18) Lu, Z.; Fryd, M.; Wayland, B. B. *Macromolecules* **2004**, *37*, 2686-2687.

(19) Debuigne, A.; Caille, J.-R.; Jerome, R. *Angew. Chem., Int. Ed.* **2005**,*44*, 1101-1104.

(20) Debuigne, A.; Caille, J.-R.; Detrembleur, C.; Jerome, R. *Angew. Chem., Int. Ed.* **2005**, *44*, 3439-3442.

(21) Kaneyoshi, H.; Matyjaszewski, K. *Macromolecules* **2006**, *39*, 2757-2763.

(22) Debuigne, A.; Willet, N.; Jrme, R.; Detrembleur, C. *Macromolecules* **2007,** *40,* 7111-7118

(23) Provencher, S. W. *Comput. Phys. Commun.* **1982**, *27*, 213.

(24) Chécot, F.; Brulet, A.; Oberdisse, J.; Gnanou, Y.; Mondain-Monval, O.; Lecommandoux, S. *Langmuir* **2005**, *21*, 4308-4315.

(25) Chécot, F.; Lecommandoux, S.; Gnanou, Y.; Klok, H.-A. *Angew. Chem. Int. Ed.* **2002**, *41*, 1339.

(26) Khan, M. A.; Armes, S. P., Perruchot, C.; Ouamara, H.; Chehimi, M. M. *Langmuir,* **2000**, *16*, 4171.

(27) Perruchot, C.; Chehimi, M. M.; Delamar, M.; Lascelles, S. F.; Armes, S. P. *Langmuir,* **1996**, *12*, 3245.

(28) Benabderrahmane, S.; Bousalem, S.; Mangeney, C.; Azioune, A.; Vaulay, M-J, Chehimi, M. M. *Polymer*, **2005**, *46*, 1339.

Chapter IV

Synthesis of Polyaniline nano-objects using PVA, PEO, and PNVP-co-PVA based reactive Stabilizers

Table of contents

II. Synthesis of Polyaniline nano-objects using PVA, PEO, and PNVP-*co*-PVA based reactive Stabilizers

In this chapter, we describe the synthesis of well-defined PANI nano-objects with different morphologies including peanuts, rice grain, needles, spheres corals and fibers. In the continuation of our previous reports on the synthesis of PEDOT latexes in aqueous media, this chapter describes the use of PEO, PVA and PNVP-*co*-PVA based reactive stabilizers for the synthesis of PANI latexes. Influence of the functionality on the PANI morphology is particularly investigated. Among functional groups attached to stabilizers, that can react with growing chains we have used aniline, fluorene and pyrrole.

I.1. Synthesis of reactive stabilizers

A series of PVA-based reactive stabilizers having different molecular weight and degree of aniline (An) or pyrrole (Py) pendant groups on to the PVA backbone were synthesized. The latter were synthesized by esterification of PVA with corresponding carboxylic acid of aniline and pyrrole respectively as already described in chapter III. The general synthetic pathway is shown in Scheme IV-1(A).

(A)

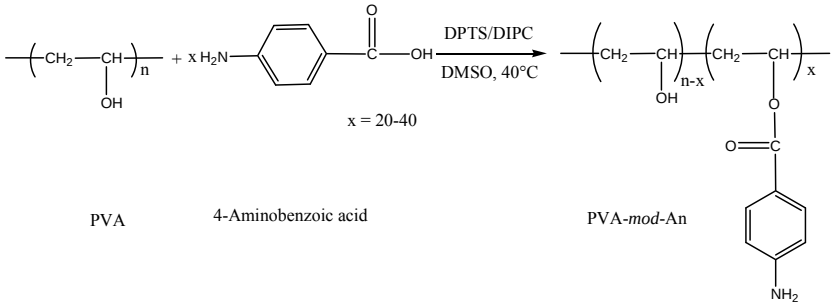

(B)

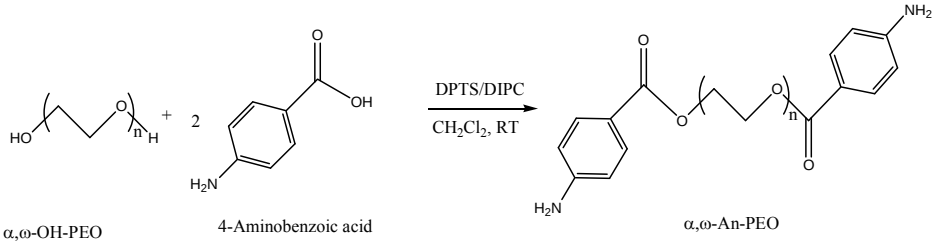

Scheme IV-1: synthetic routes to PVA-*mod*-An (A) and to α,ω-An-PEO (B).

Similarly numerous samples of PEO based reactive stabilizers with different molecular weight end-capped with aniline and fluorene (Flu) moieties were prepared by using the same methodology as describe for PVA-based stabilizers (see Scheme IV-1(B)). Another type of PVA-based stabilizer, PNVP-*co*-PVA-*mod*-Py was synthesized as described in chapter II.

All stabilizers were then analyzed by ^{1}H NMR spectroscopy. The ^{1}H NMR spectrum of PVA-g-An in DMSO is shown in Figure IV-1a. The appearance of peaks at 7.61, 6.54 ppm (f,f', g,g') confirms the functionalization of aniline moieties along PVA main chain. The peaks appeared at 7.47 and 7.11 ppm probably arises from trapped catalyst (DPTS). Similarly, the appearance of doublets (a,a', b,b') at 7.87 and 6.64 ppm in the ^{1}H NMR spectrum of aniline end capped PEO performed in $CDCl_3$ prove the attachment of aniline at the ends of PEO (Figure IV-1b). The characterizations of PVA-*mod*-Py, PNVP-co-PVA-*mod*-Py have been already given in chapter II and for α,ω-Flu-PEO in chapter III.

The presence of aniline pendant group along the PVA chain was also confirmed by taking UV-visible spectra of PVA and PVA-*mod*-An in DMSO. The appearance of a strong absorption at 310 nm in PVA-*mod*-An spectrum due to aniline moiety confirms its presence along the PVA chains. Such a feature was not observed in the spectrum of unmodified pure PVA (see Figure IV-2).

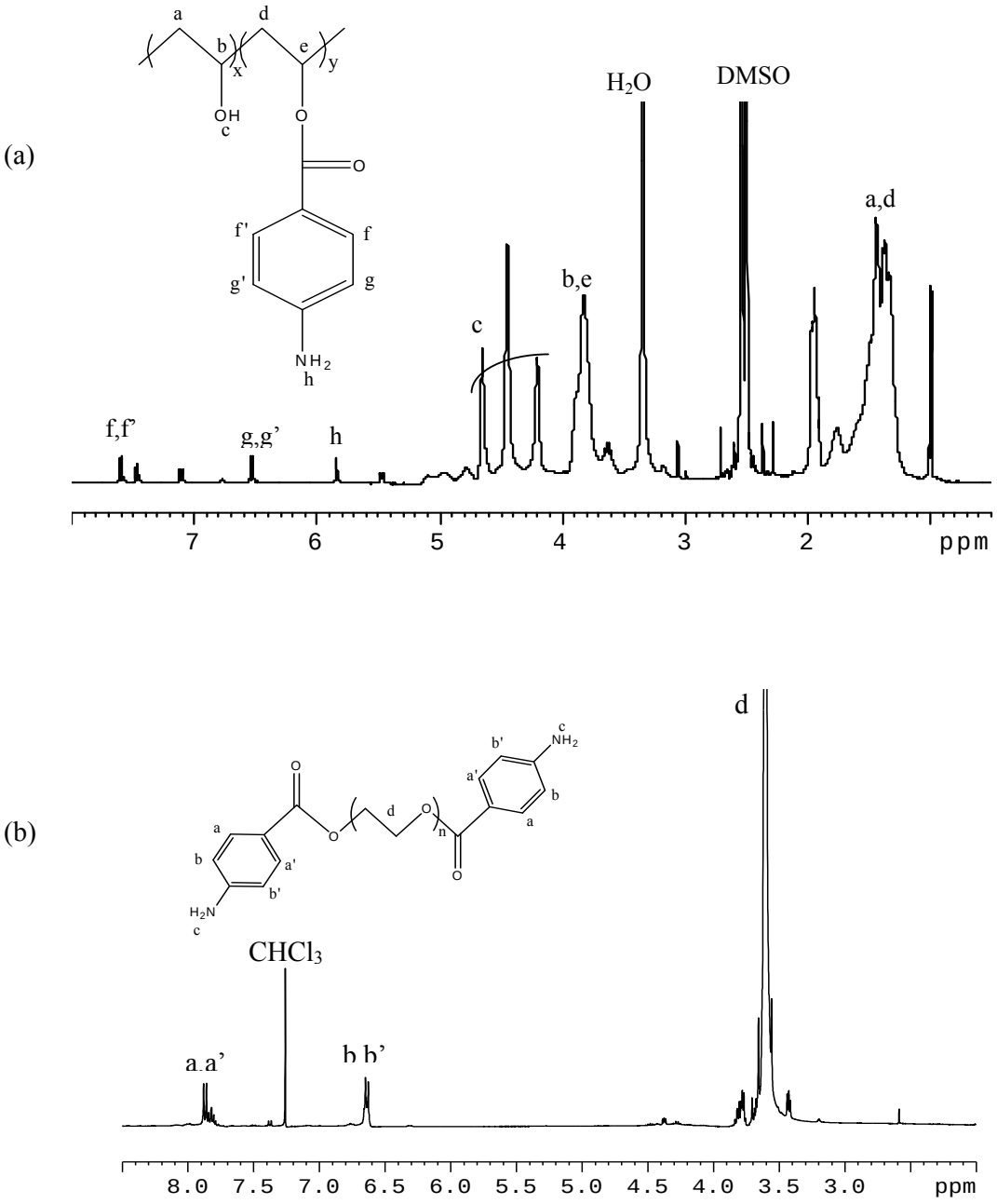

Figure IV-1: ^{1}H NMR spectra of (a) PVA-*mod*-An in DMSO and (b) α,ω-An-PEO in $CDCl_3$ (400 MHz)

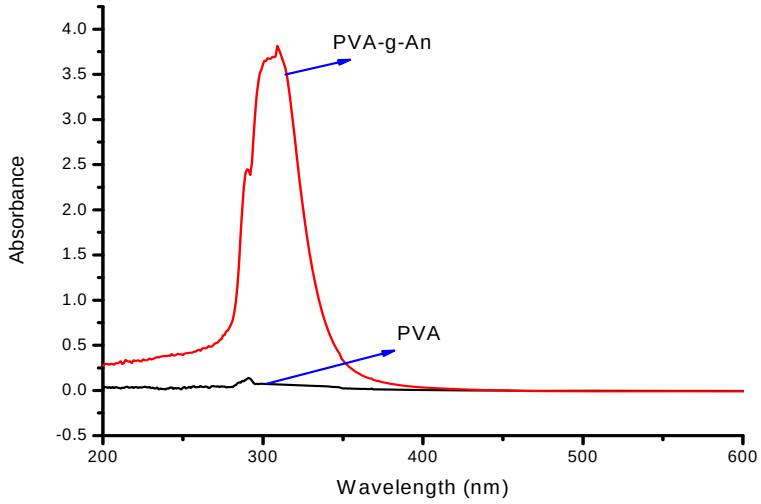

Figure IV-2: UV-visible spectra of unmodified PVA and PVA-*mod*-An

I.2. Synthesis of PANI dispersions

The oxidative polymerization of aniline was performed in 1 M HCl aqueous solution as a dispersant medium in the presence of various reactive steric stabilizers based on PEO, PVA or PNVP-*co*-PVA. The effect of the molecular weight, functionality and concentration of the reactive PEO, PVA and PNVP-*co*-PVA as well as the nature of dispersant medium on the PANI particle size and morphology was investigated

I.2.1. Use of PVA based reactive stabilizers

Numerous samples of PANI particles were prepared in 1 M aqueous HCl solution using ammonium persulfate as an oxidant in the presence of either PVA-*mod*-Py or PVA-*mod*-An. The effect of parameters such as PVA molecular weight, degree of substitution and concentration of stabilizers, co-dopants as well as the initial concentration of aniline hydrochloride on the size and morphology of the PANI particles was studied. Results of the aniline dispersion polymerizations are summarized in Table IV-1.

S.N°	Aniline hydrochloride (g)	Stabilizer type PVA functionalized with An or Py	PVA molecular weight (g/mol)	Degree of PVA substitution (Mol. %)	Amount of stabilizer (g/100 mL solvent)	Co-dopant used	Conductivity [c] (S/cm)	Particle size[d] (nm x nm) (nm)	Morphology
1	1.00	PVA-*mod*-An	18000	10	0.54	CSA	5×10^{-3}	180X120	Oval-shape
2[a]	1.00	PVA-*mod*-Py	88000	5	0.54	_		80-100	Spherical
3	1.00	PVA-*mod*-Py	88000	5	0.54	_	6×10^{-3}	120X80	Peanut-like
4	1.00	PVA-*mod*-Py	88000	5	0.54	PTSA	5×10^{-2}	120X80	Peanut-like
5	1.00	PVA-*mod*-Py	88000	5	0.54	CSA	6×10^{-3}	180X100	Peanut-like
6	1.00	PVA-*mod*-An	88000	5	0.54	_	8×10^{-3}	160X100	Peanut-like
7	1.00	PVA-*mod*-An	88000	5	0.54	PTSA	1×10^{-1}	160X90	Peanut-like
8	1.00	PVA-*mod*-An	88000	5	0.54	CSA	6×10^{-3}	150X80	Peanut-like
9	2.00	PVA-*mod*-Py	88000	10	0.50	PTSA	7×10^{-3}	150X80	Peanut-like
10	2.00	PVA-*mod*-Py	88000	10	0.50	CSA	1×10^{-2}	160X80	Peanut-like
11	2.00	PVA-*mod*-Py	88000	10	1.08	PTSA	6×10^{-2}	150X80	Peanut-like
12	2.00	PVA-*mod*-Py	88000	10	1.08	CSA	8×10^{-3}	120X70	Peanut-like
13	2.00	PVA-*mod*-An	88000	10	1.08	CSA	7×10^{-3}	1500	Needle-like
14[b]	1.00	PVA-*mod*-An	88000	5	0.54	_	2×10^{-1}	100X50	Peanut-like
15	1.00	PNVP-*co*-PVA-*mod*-Py	29000	10	0.54	_	2×10^{-1}	_	Coral-like
16[a]	1.00	PNVP-*co*-PVA-*mod*-Py	29000	10	0.54	_	1×10^{-1}	100-200	Spherical
17[b]	1.00	PNVP-*co*-PVA-*mod*-Py	29000	10	0.54	_	5×10^{-1}	_	Fibers

a) Prepared in pure deionized water.
b) prepared in a mixture of DMSO and water (2:3).
c) Measured by four probe method.
d) Average over 100 particles on TEM images.

Table IV-1: Synthesis of PANI particles in the presence of PVA based reactive stabilizer using ammonium persulfate as an oxidant in 1 molar aqueous HCl solution at 0°C.

One can note that whatever the substituent, the degree of substitution of PVA stabilizer, the concentration of the monomer and the stabilizer, nature of the co-dopant, the morphology of the PANI particles (runs 3-12, 14) adopt a peanut shape (see discussion in next sections). Two particular cases, however, were observed in runs 2 and 13 where spherical and needle like morphologies were obtained. First, spherical particles were obtained when pure deionized water was used as dispersant media (run 2) (For illustration see Figure IV-3 a-d).

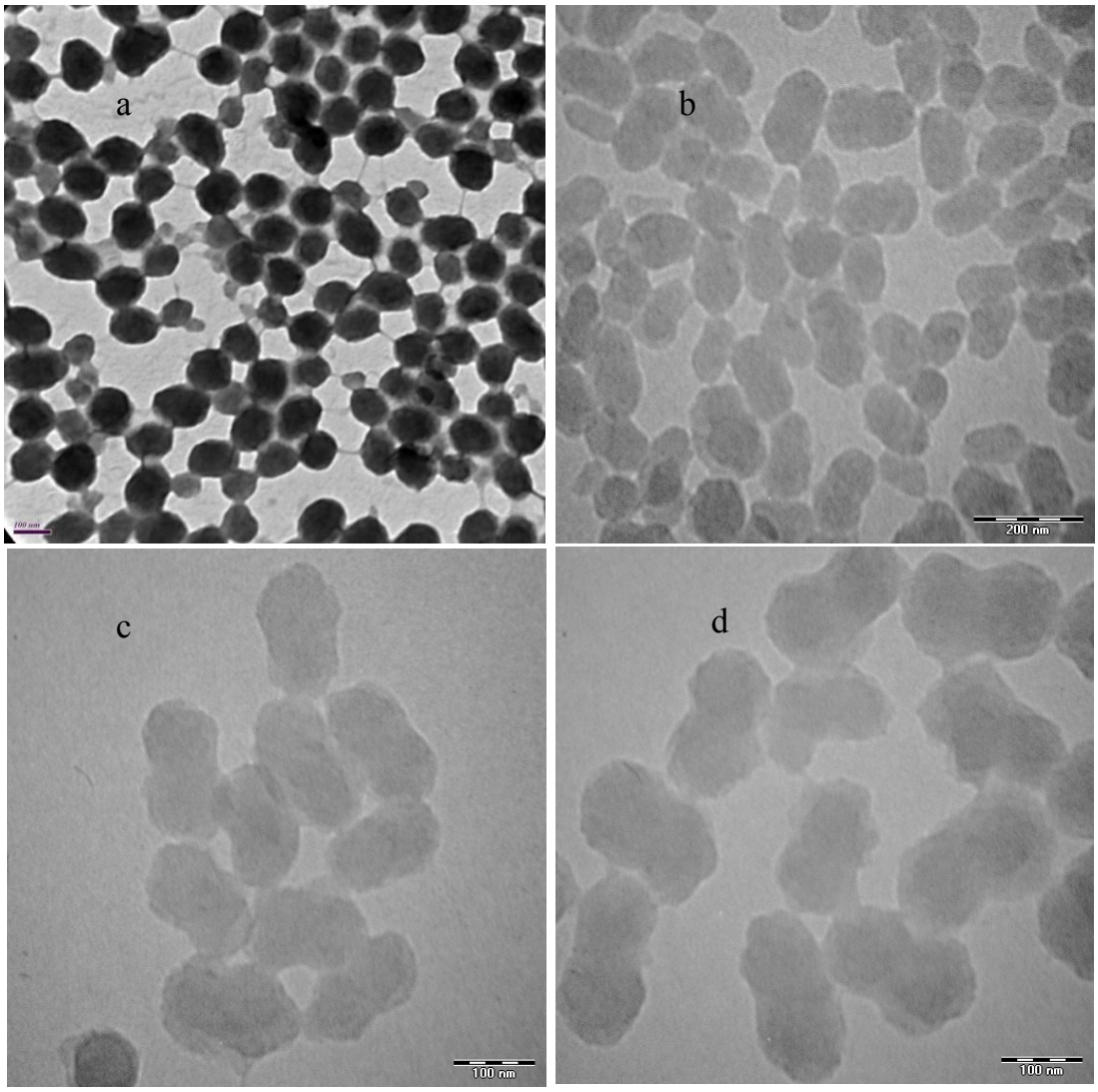

Figure IV-3: TEM images of PANI particles using 5 mol.% fuctionalized PVA-*mod*-Py as a reactive stabilizer (a) in pure deionized water (run 2, Table IV-1); (b) in 1 M aqueous HCl solution (run 3, Table IV-1) and (c) &(d) in 1 M aqueous HCl solution and using CSA and PTSA as co-dopants, respectively (run 5 & 4 Table IV-1) in the presence of $(NH_4)_2S_2O_8$ at 0 °C

Second, needle like morphology is obtained when aniline hydrochloride is polymerized in the presence of 10 mol. % aniline substituted high molecular weight PVA-*mod*-An ($\overline{M}_w$ =88000 g/mol) reactive stabilizer (Figure IV-4b) while oval shape morphology is obtained using lower molar mass stabilizer ($\overline{M}_w$ =18000 g/mol) {(run 1, Table 1) (see Figure IV-4a)}. It is worth stating that no stable dispersions were obtained using PVA-*mod*-Py ($\overline{M}_w$ =18000 g/mol) under similar experimental conditions indicating that PVA-*mod*-An is a more efficient stabilizer for PANI dispersions probably due to similar nature of the functionalized moieties with respect to the monomer that is polymerized.

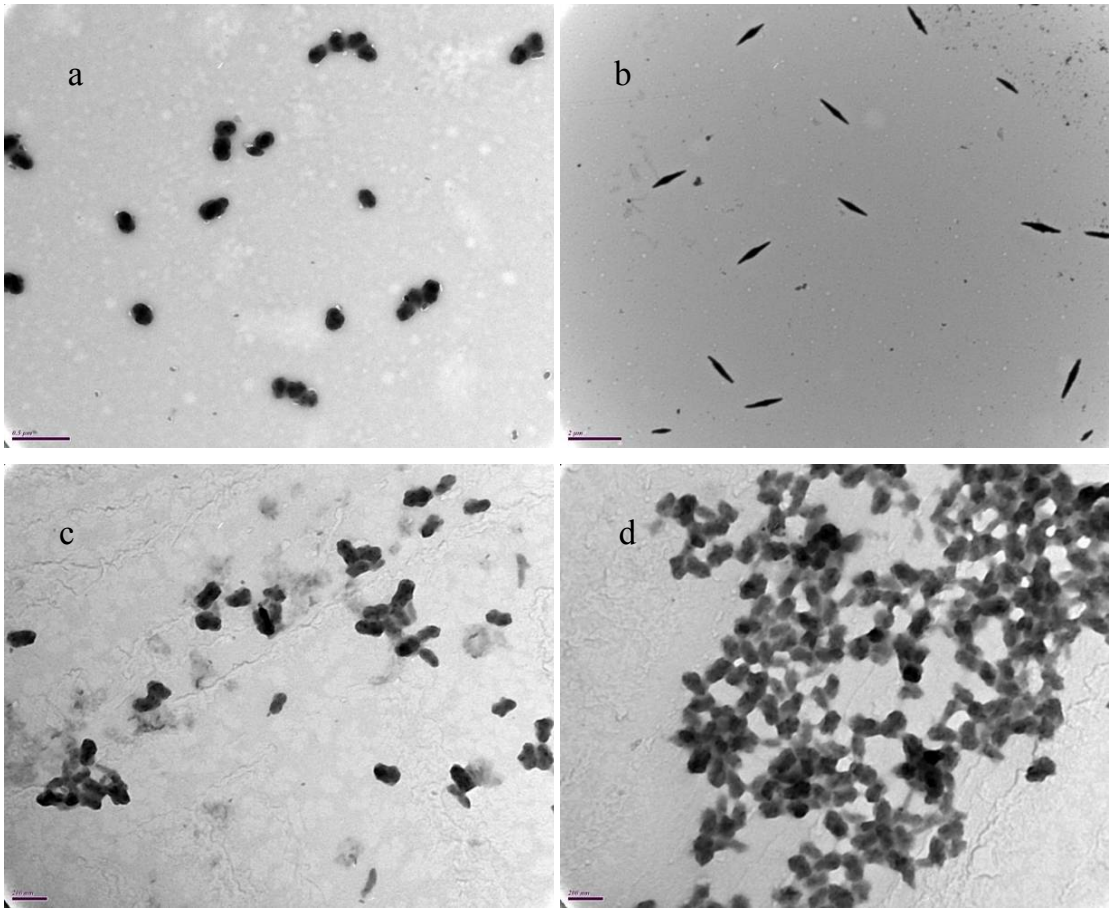

Figure IV-4: TEM images of PANI particles prepared in the presence of 35 wt.% of aniline and pyrrole modified poly(vinyl alcohol) having same degree of substitution (10 mol.%) but different molecular weight and co-dopants (a) PVA-*mod*-An, M_w = 18000 g/mol, CSA (run 1, Table IV-1), (b) PVA-*mod*-An , 88000 g/mol, CSA (run 13, Table IV-1), (c) PVA-*mod*-An , M_w = 88000 g/mol, PTSA (run 11, Table IV-1 and (d) (PVA-*mod*-Py, M_w = 88000 g/mol, CSA (run 12, Table IV-1) in 1 M aqueous HCl and using $(NH_4)_2S_2O_8$ as an oxidant at 0 °C.

As it can be noticed in Table 1, the morphology and the size of the PANI nano-objects is only slightly affected by the nature of the dispersant media *i.e.* 1 M HCl in water and 1 M HCl in the DMSO/water mixture (run 14, Table IV-1). However, in the latter case, a considerable improvement of the conductivity was observed as it is discussed in following sections. To have a closer view of the PANI nano-objects, AFM images were taken (see Figure IV-5). From the Figures, it is clear that each large particle consist of very small particles, called as particulates. Images of PANI samples confirm that the size of the "peanuts" is slightly affected by the conditions of synthesis. The length varies from 120-180 nm while width goes from 70-100 nm. Finally, nature of the co-dopants affects the conductivity of the PANI materials, as discussed below.

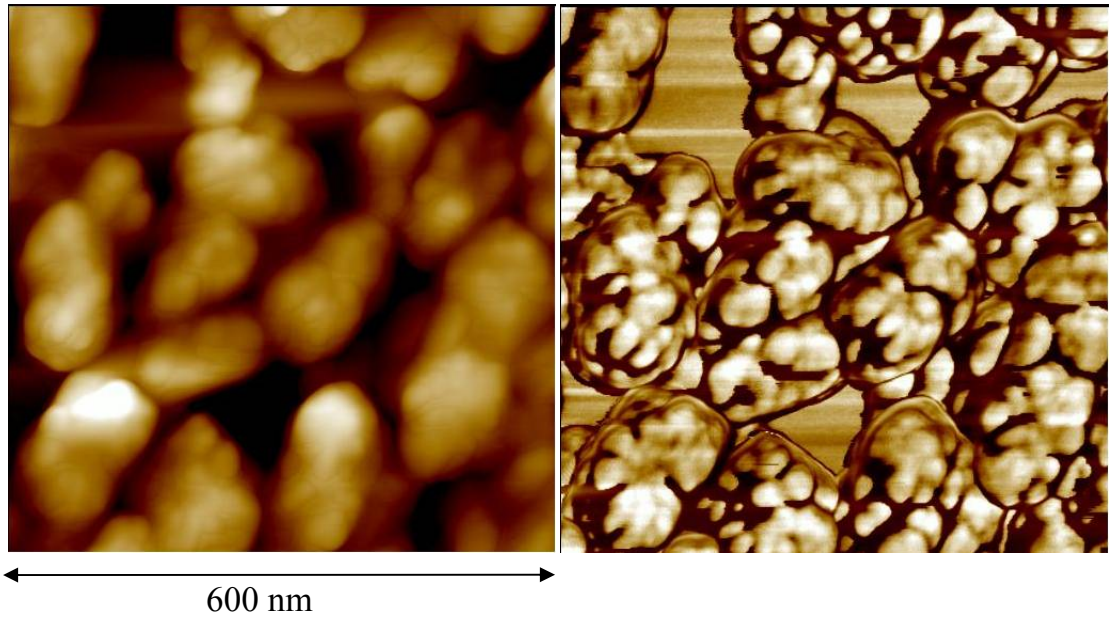

Figure IV-5: AFM images of the PANI particles using PVA-*mod*-Py as a reactive stabilizer and PTSA as co-dopant (run 11, Table IV-1) in 1M aqueous HCl at 0°C.

I.2.2. Synthesis of PANI latexes in the presence of PNVP-*co*-PVA based reactive stabilizers

It is already known from the literature that the use of high boiling solvent such as *N*-methylpyrrolidone enhances the conductivity of the PEDOT and PANI films up to several orders of magnitude.[1,2] It was also described the efficient use of high molecular weight (360 kg/mol) PNVP homopolymers as stabilizers for PANI particles formation. In this work, we decided to investigate, the effect of PNVP on to the PANI materials by using a specifically

designed statistical copolymer PNVP-*co*-PVA. Then aniline hydrochloride was polymerized in the presence of PNVP-*co*- PVA-*mod*-Py ***i.e.*** in pure water, 1 M HCl in water or in the DMSO/water mixture (2:3, v/v) {runs 15-17, Table IV-1}. In fact dispersant phase was shown to affect the morphology of the PANI samples. Coral like shapes were obtained in acidic conditions (1 M HCl in water at 0 °C) (Figure IV-6a), while spherical particles (Figure IV-6b) and fibers were formed in pure water and in DMSO/water mixture respectively. As expected, higher conductivities were measured in PANI samples synthesized with PNVP-*co*-PVA-*mod*-Py used as stabilizer.

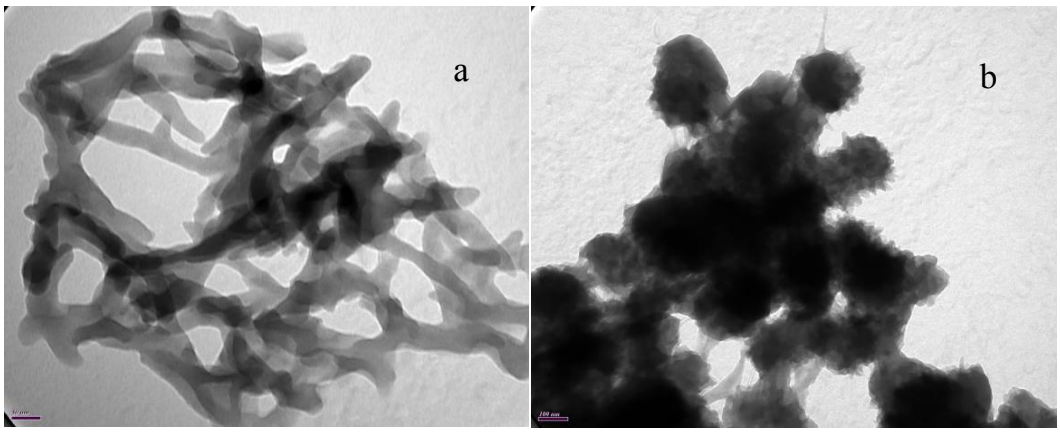

Figure IV-6: TEM images of the PANI nano-objects prepared in the presence of 35 wt.% of PNVP-*co*-PVA-mod-Py using (a) 1M aqueous HCl solution and (b) Pure deionized water as dispersant media at 0°C.

I.2.3 Synthesis of PANI latexes in the presence of PEO based reactive stabilizers

A series of PANI latexes were prepared in either pure deionized water or 1 M HCl solution at different temperatures using PEO based reactive stabilizers. Results of dispersion polymerization are summarized in Table IV-2

As can be seen in Table IV-2, the functionality of PEO reactive stabilizers (*i.e.* PEO chains α,ω- end-capped with either aniline or fluorene moieties), the reaction temperature, the concentration and the nature of the dispersant medium have considerable effects on PANI morphologies. Rice grain morphology was obtained when aniline hydrochloride was polymerized using aniline-capped PEO in 1 M HCl water solution at either 0 or 25 °C (see runs 1-4, Table IV-2, Figure IV-7) while PANI fibers were obtained using fluorene

S.N°	Stabilizer type	Stabilizer Molecular weight (g/mol)	Amount of the stabilizer[b] (w% vs. monomer)	Solvent	Reaction temperature (°C)	Conductivity[c] (S/cm)	Particle size[d] (nm x nm) (nm)	Morphology
1	An-PEO-An	35000	50	H_2O	25	8×10^{-3}	100X60	Rice-grain
2	An-PEO-An	35000	50	H_2O	0	5×10^{-2}	120X60	Rice-grain
3	An-PEO-An	35000	35	H_2O	0	2×10^{-1}	120X60	Rice-grain
4	An-PEO-An	10000	35	H_2O	0	4×10^{-2}	120X60	Rice-grain
5[a]	An-PEO-An	35000	35	H_2O	25	2×10^{-3}	80X50	Rice-grain
6[a]	An-PEO-An	35000	35	H_2O	0	8×10^{-3}	80X50	Rice-grain
7	Flu-PEO-Flu	10000	35	H_2O	0	_	_	Aggregation
8	Flu-PEO-Flu	10000	35	H_2O	25	1×10^{-1}	_	Fibers
9	Flu-PEO-Flu	10000	35	DMSO/H_2O	25	5×10^{-1}	_	Fibers

(a) Reaction was performed using only pure deionized water as a dispersant media (not in 1M HCl) and HCl was added at the end the reaction for doping PANI.
(b) Versus monomer.
(c) Measured by four probe method.
(d) Average over 100 particles on TEM images.

Table IV-2: Synthesis of PANI particles in the presence of PEO-based reactive stabilizers using ammonium persulfate as an oxidant in 1 M aqueous HCl solution.

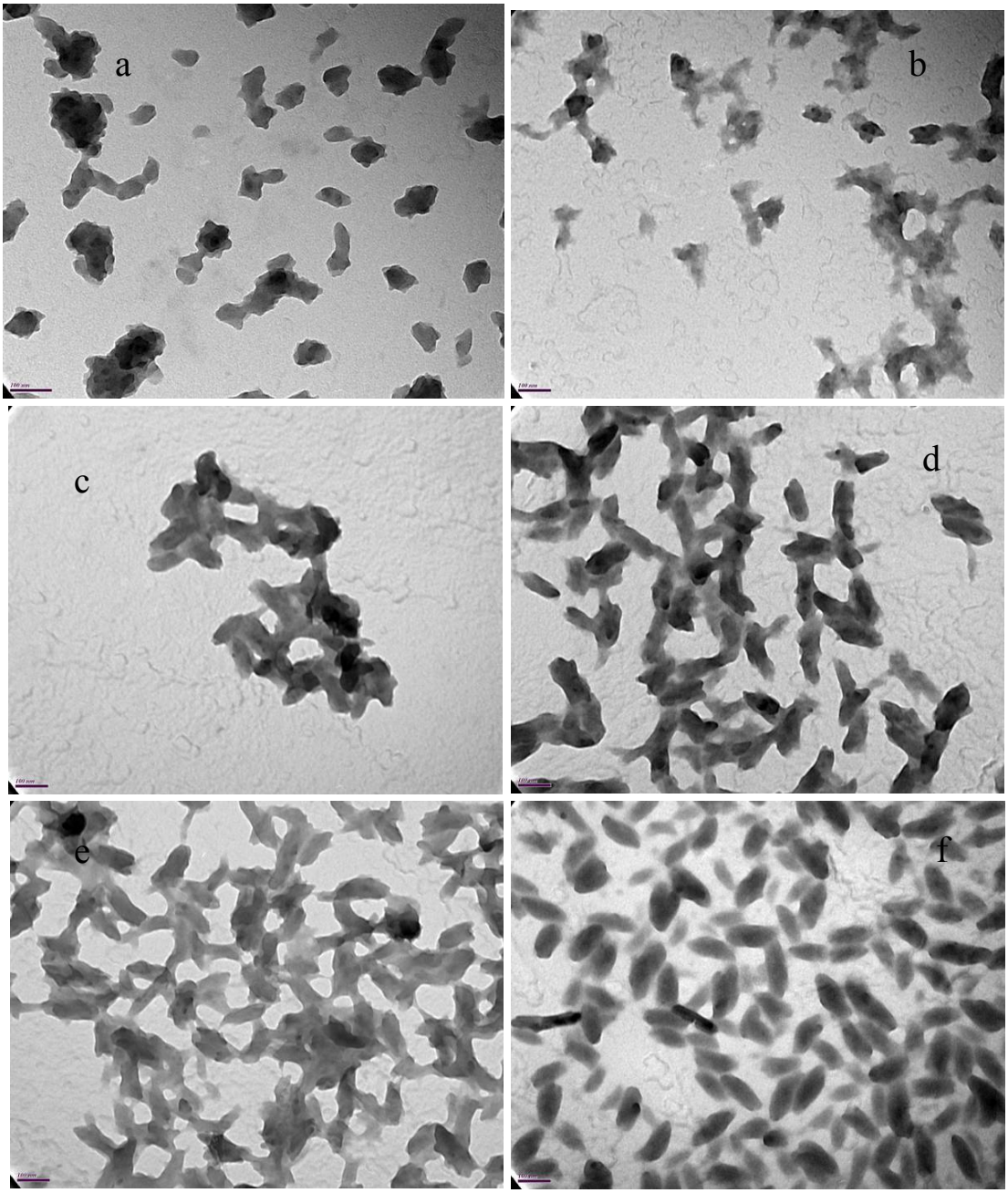

Figure IV-7: : **PANI particles prepared using α,ω-aniline-PEO reactive stabilizers having different molar mass and concentration under different experimental conditions (a) M_n =35000 g/mol, 35 Wt.% in de-ionized water at 25 °C (run 5 Table IV-2), (b) Mn=35000 g/mol, 35 Wt.% in de-ionized water at 0 °C (run 6 Table IV-2), (c) Mn=10000 g/mol, 35 Wt.% in 1M aqueous HCl solution at 0 °C (run 4 Table IV-2), (d) Mn=35000 g/mol, 35 Wt.% in 1M aqueous HCl solution at 0 °C (run 3 Table IV-2), (e) Mn=35000 g/mol, 50 Wt.% in 1M aqueous HCl solution at 0 °C (run 2 Table IV-2)and (f) Mn=35000 g/mol, 50 Wt.% in 1M aqueous HCl solution at 25 °C (run 1 Table IV-2) (**Scale bar in all images is 100 nm**).**

functionalized PEO in either 1M HCl in water or in the DMSO/water (2:3) mixture at 25 °C (Figure IV-8a-b). At 0 °C aniline end-capped PEO were shown to be more efficient in obtaining stable PANI latexes as compared to fluorene end-capped PEO. As it can be seen from Figure IV-7, the size and morphology of PANI nano-objects were not affected by increasing the molecular weight of α,ω-An-PEO from 10000 g/mol to 35000 g/mol (runs 3 & 4). Similar results were also obtained when concentration of α,ω-An-PEO increases from 35 wt.% to 50 wt.% under similar reaction conditions (see Figure IV-7d-e and runs 2&3 in Table IV-2). PANI rice grain morphologies with very smooth surfaces were obtained using 50 wt. % of α,ω-An-PEO (M_n = 35000 g/mol) at 25°C (see run 1 Table IV-2 or Figure IV-7f). However, at 0 °C, this system gave rise to ill-defined rice grain morphology (see run 2 Table IV-2 or Figure IV-7e). This phenomenon can be attributed to a transition temperature of the PEO-based stabilizer occurring between 0 and 25 °C. Poorly defined small rice-grain particles were also obtained when aniline hydrochloride was polymerized in pure deionized water at 0 or 25 °C (Figure IV-7a-b) {runs 5&6, Table IV-2}.

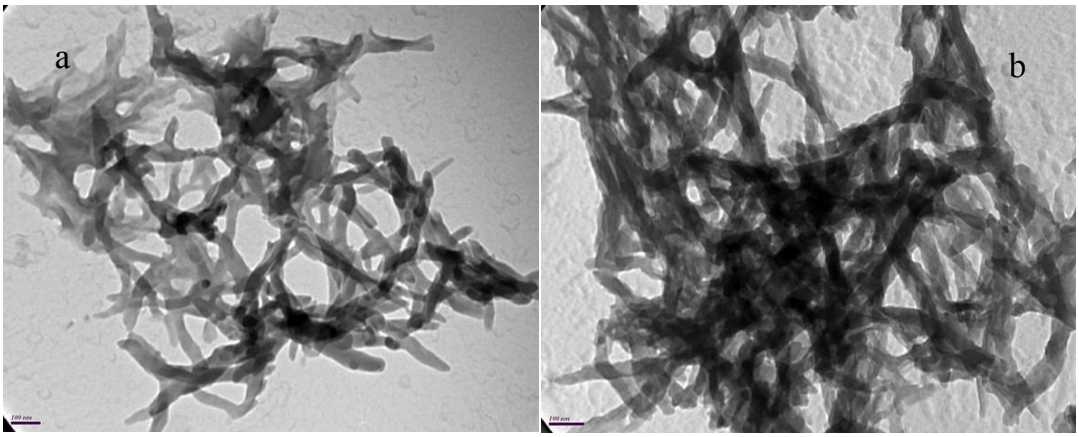

Figure IV-8: TEM images of PANI nano-corals and fibers prepared using α, ω-Flu-PEO (Mn = 10000 g/mol, 35 wt.%) as a reactive stabilizer in different solvents (a) 1M HCl solution in water and (b) 1M HCl solution in DMSO/water mixture (2:3) at 25 °C

I.3. Discussion on PANI morphologies

Unlike other conducting polymers such as PEDOT and polypyrrole, the deviation from spherical morphologies to other kind of morphologies is a common phenomenon in PANI

synthesis. This deviation is explained in detailed by Stejskal.[3] According to the author, three factors affect the formation of dispersion particles: (1) the rate at which PANI is produced; (2) the efficiency of the stabilizer attachment; and (3) the diffusion and transport processes involved in the formation of the dispersion particle from primary particles. When the primary PANI particles are produced slowly during polymerization, they can efficiently become attached to the steric stabilizer. The locally reduced concentration of the free stabilizer is compensated by the diffusion of the stabilizer from the other regions. A sufficient quantity of the incorporated stabilizer and the diffusion-controlled aggregation of primary particles lead to the formation of spherical dispersion particles.[4,5] When the rate of PANI formation is much faster than the diffusion of the stabilizer, a local depletion of the free stabilizer by primary particles may occur at PANI surfaces where the polymerization takes place. In these volume elements, the polymerization then proceeds in the absence of the stabilizer, i.e. in the precipitation mode. More and more primary particles without steric stabilizer are then produced by an auto-acceleration mechanism. The shape of the so-formed particles is likely to be affected by the polymerization features. The polymerization-controlled particle growth is expected to give rise to non-spherical morphologies.

Kinetically controlled directional polymerization of aniline may be an alternative cause of this phenomenon.[6,7] In the same way that corals naturally grow at their active ends, the PANI structures produced during the polymerization may follow a similar principle. This is supported also by the fact that wires and tubes have been produced also in the absence of a polymeric stabilizers and surfactants.[8]

In this study, spherical particles are formed when aniline hydrochloride is polymerized in the presence of pure deionized water, while peanut shape morphologies are obtained when 1 M HCl solution was used as dispersant medium keeping constant other experimental conditions (see Figures 2a and 2b). Actually, in the presence of HCl (which here acts as an accelerator), the rate of polymerization increases (which is indicated by the very rapid change of the reaction mixture from colourless to dark blue) that causes a local depletion of stabilizer near-by the particles.[9,10] As a result, the particles partially covered by the stabilizer could attach to others resulting in the formation of non spherical shapes (see Figure IV-3b-c). For example Figure IV-3b-c shows two particles attached to each other also called peanut like morphology. Beside, when the rate of polymerization is slow in the absence of HCl, the

locally reduced concentration in stabilizer is balanced by the diffusion of the stabilizer in other region. In such cases, the stabilizer more effectively deposits on the surface of the particles leading to the formation of spherical particles. Figure IV-4a-b shows oval, spherical and needle-like shapes as a function of the molecular weight of PVA-*mod*-An stabilizer. First, one can explain spherical and oval shapes by the high reactivity and high diffusivity of low molecular weight stabilizer that hampers aggregation phenomenon by more effective covering of the particles. Second, in the case of high molecular weight PVA-*mod*-An having a large number of aniline functions, the depletion of the stabilizer is not compensated due to its slow mobility, thus resulting in the formation of needle like objects formed by the aggregation of particles from their active sites (not effectively covered by stabilizer).

Similarly, the formation of PANI fibers using α,ω-Flu-PEO is due to the low reactivity (fluorene moiety *versus* aniline) and eventually slow adsorption rate of stabilizer as compared to polymerization rate. As a result, PANI surface is not fully covered by the stabilizer chains and the small primary particles joint together from their naked sites to form long fibers. Finally, α,ω-An-PEO adsorbs more quickly and reacts more efficiently than α,ω-Flu-PEO (due to the same nature between the monomer and stabilizer end groups). However, it cannot hamper the deviation from spherical morphology leading to rice grain nano-objects.

I.4. FT-IR and UV-Visible characterizations

In order to estimate the composition of PANI samples prepared using different stabilizers, FT-IR was first performed (see Experimental section, III.2 and III.3). The absorption peaks arising from 700-1570 nm proves the formation of doped PANI.[11-14] In addition, the presence of absorption peak at 1650 cm^{-1}in PANI-PVA core-shell objects arising from C=O stretching vibration of ester group indicate the presence of PVA-*mod*-Py and PVA-*mod*-An in the samples. Similarly, the peak at 1660 cm^{-1}in PANI-PNVP-*co*-PVA arising from C=O group of pyrrolidone proves the presence of PNVP-*co*-PVA-*mod*-Py in the sample.

Although it is not possible to see the PEO peaks in the spectra probably due to overlapping by the absorption peaks of PANI, the presence of PEO can be confirmed by XPS analysis as it will be discussed in following section.

The UV–visible spectra (Figure IV-9) of the PANI samples prepared using only HCl as dopant and other having CSA as co-dopant show three characteristic absorption bands at 325, 440 and 700 nm, while the sample prepared using PTSA as a co-dopant exhibits a red shift to 770 nm. The absorption peak at 325 nm region is assigned to the π–π* transition and is related to the extent of conjugation between adjacent phenyl rings in polymer chain. The peak at 440 nm results from the polaron/bipolaron transition. A broad band with an absorption maximum at 700 - 770 nm is the signature of extended conjugation. It corresponds to the transition from a localized benzenoid highest occupied molecular orbital to a quinonoid lowest unoccupied molecular orbital [15], that is, a benzenoid to quinonoid excitonic transition. [16] It also indicates the high conductivity shown by the samples prepared using PTSA as co-dopant. When UV-visible spectra were taken in DMSO, the peak absorption maximum underwent a blue shift to 640 nm (Figure IV-10), which may be due to the partial conversion of emeraldine salt to emeraldine base indicated by the change in colour from green in water to blue in DMSO.

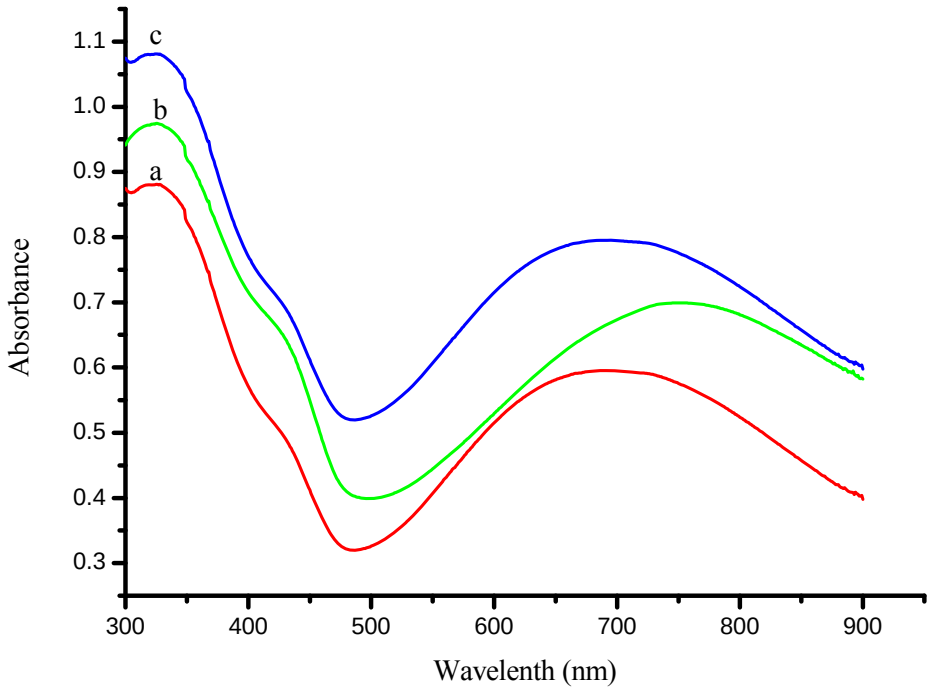

Figure IV-9: UV-visible spectra of (a) PANI-PVA-HCl-CSA, (b) PANI-PVA-HCl-PTSA (c) PANI-PVA-HCl in water

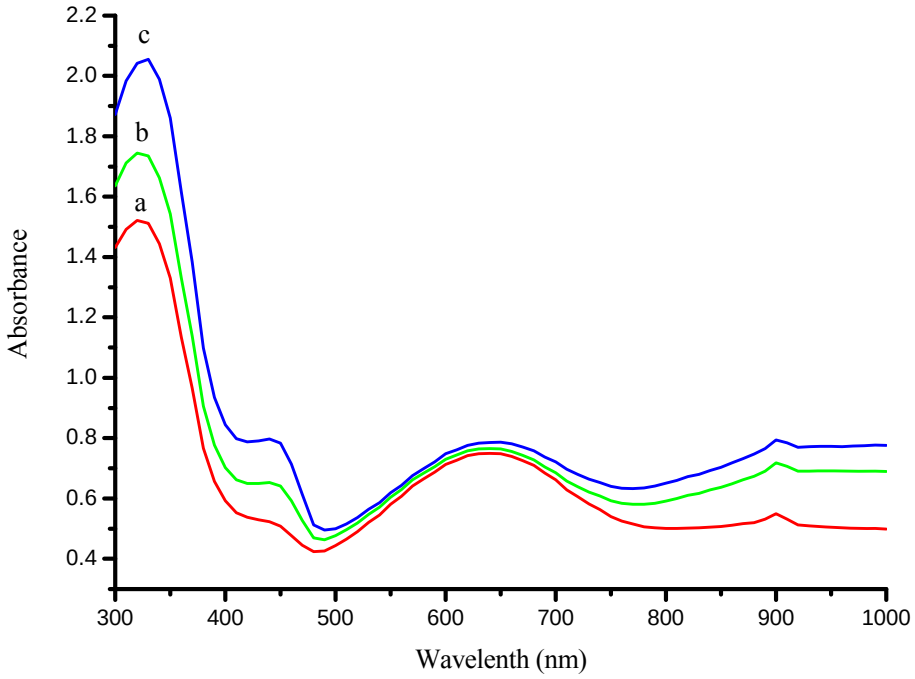

Figure IV-10: UV-visible spectra of (a) PANI-PVA-HCl-CSA, (b) PANI-PVA-HCl-PTSA (c) PANI-PVA-HCl in DMSO

I.5. XPS characterization of PANI samples

I.5.1. PANI-PVA composites

XPS survey spectra and core line spectra of individual elements of PANI bulk powder and PANI samples prepared using PVA-based reactive stabilizers are shown in Figures IV-11-13.

As it is shown in Figure IV-11, XPS survey spectra of PANI bulk powder and PANI-PVA samples consist of five main peaks corresponding to O1s, N1s, C1s, Cl2p and S2p components respectively.

The sharp increase intensity of O1s signal and decrease intensity of N1s in PANI-PVA samples as compared to PANI bulk powder clearly indicates the presence of PVA on the surface of the composites.

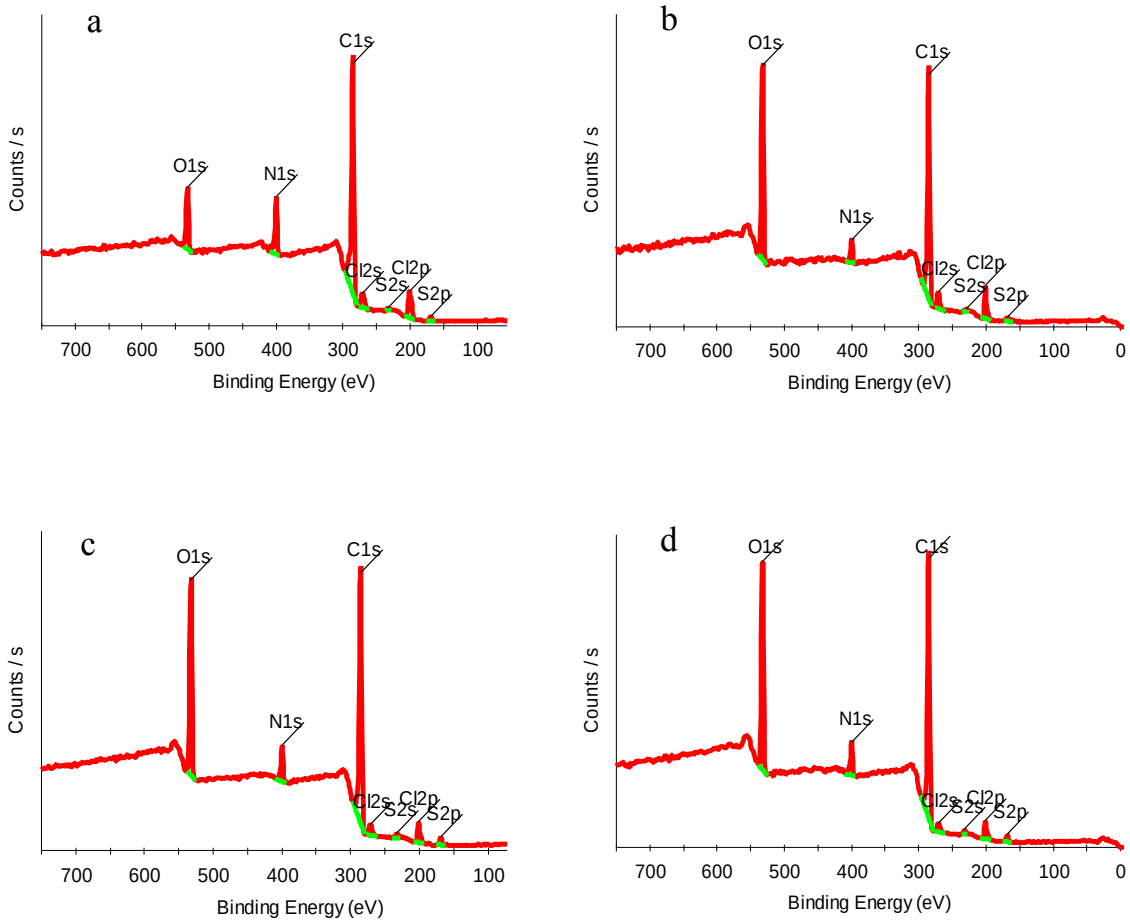

e

Sample	C	O	N	Cl	S
PANI-bulk	73.0	10.5	10.0	5.4	1.1
PANI-PVA-3	66.8	22.4	5.2	4.1	1.4
PANI-PVA-4	69.5	20.9	5.6	2.7	1.3
PANI-PVA-5	69.9	21.0	5.6	2.5	1.0

Figure IV-11: XPS survey spectra of (a) PANI bulk powder, (b) PANI-PVA-HCl (Run 3, Table IV-1), (c) PANI-PVA-CSA-HCl (Run 5, Table IV-1), (d) PANI-PVA-PTSA-HCl (Run 4, Table IV-1) and (e) Table for the elemental surface composition of PANI samples

Figure IV-12 represents the N1s core-line spectra of PANI bulk powder and PANI-PVA composites. The doping level of PANI can be determined by deconvoluted N1s core-line spectra of protonated imine and amine functionalities. [17] The maximum doping level of PANI was found to be 43.1%. XPS peaks were deconvoluted into Gaussian component peaks[18] at 399.2, 400.5, and 401.8 eV for, benzenoid amine (–NH–), protonated amine (–NH_2^+–), and protonated imine (=NH^+–) of PANI samples respectively. Kumar et al. [19,20] assigned the last two peaks to the presence of polarons (radical cations) and bipolarons (dications).

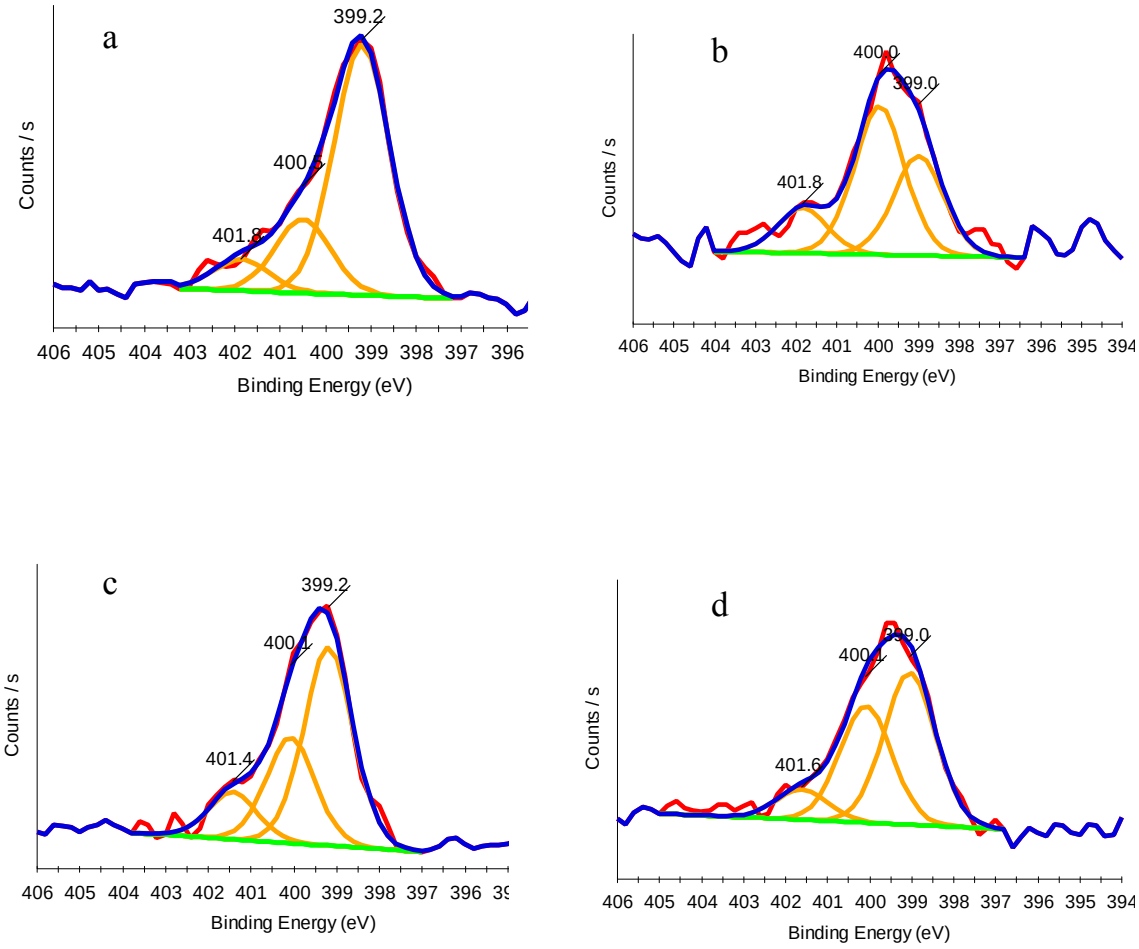

Figure IV-12: XPS N1s core line spectra of (a) PANI bulk powder, (b) PANI-PVA-HCl (Run 3, Table IV-1), (c) PANI-PVA-CSA-HCl (Run 5, Table IV-1) and (d) PANI-PVA-PTSA-HCl (Run 4, Table IV-1)

The ratio of the sum of relative areas of these two N1s components at 400.5 and 401.8 eV (positively charged nitrogens) to the total area of Gaussian fit can be considered as a direct estimation of the doping level of PANI. The doping levels calculated by the integration of

relative intensities of these peaks are 30.0%, 65%, 43.5% and 49.5% for PANI bulk powder, PANI-PVA-HCl, PANI-PVA-HCl-CSA and PANI-PVA-HCl-PTSA respectively. These data indicate that PANI-PVA-HCl is over doped while sample prepared using PTSA as a co-dopant (PANI-PVA-HCl-PTSA) is completely doped in agreement with its high conductivity (Run 4, Table 1) and UV-Visible spectrum (Figure IV-9b).

A very intense peak at 532.2 eV in O1s core-line spectra arising due to C–O–H of PVA in PANI-PVA composites (Runs 3,4,and 5, Table IV-1, for illustration see Experimental section III.4) indicate the presence of PVA in the samples. [21]

The features in C 1s core-line spectra of PANI bulk powder and PANI-PVA samples (Runs 3, 4 and 5, Table 1) demonstrate the formation of conducting PANI composite materials.[22] The peak positions at 284.6 and 286.4 are due to $–CH_2–$ and C–O–H group respectively in PVA, proving the presence of stabilizer on PANI surface.[23] The peaks positioned at 285.7 eV is due to C–N bond and peaks attributed at 287.6 and 289 eV are due to polarons and bipolarons, respectively (see Experimental section III.5).

The Cl 2p core-line spectra are shown in Figure IV-13. The degree of protonation of polyaniline prepared using ammonium persulfate is normally based on the chlorine content that is determined by elemental analysis. The two peaks positioned at 200.2 and 201.8 eV have been assigned in the literature to C1 $2p^{1/2}$ and C1 $2p^{3/2}$respectively.[24] Two additional peaks at 197 and 198 eV are probably attributed to the chloride ions from ammonium chloride formed as by-product during polymerization and trapped inside. As it is clear from the table of the elemental composition of PANI samples (Figure IV-11), the amount of chlorine is roughly half with respect to nitrogen in each case, in accord with 50% doping level of PANI prepared in our case.

The presence of two peaks arising at 166.7 and 168.4 in S2p core-line spectra of PANI-PVA-HCl-CSA (Experimental section III.6c) and 167.3 and 168.7 eV in PANI-PVA-HCl-PTSA (Experimental section 6d) are due to the $–SO_3$ group of CSA and PTSA respectively and confirm their presence as co-dopants.

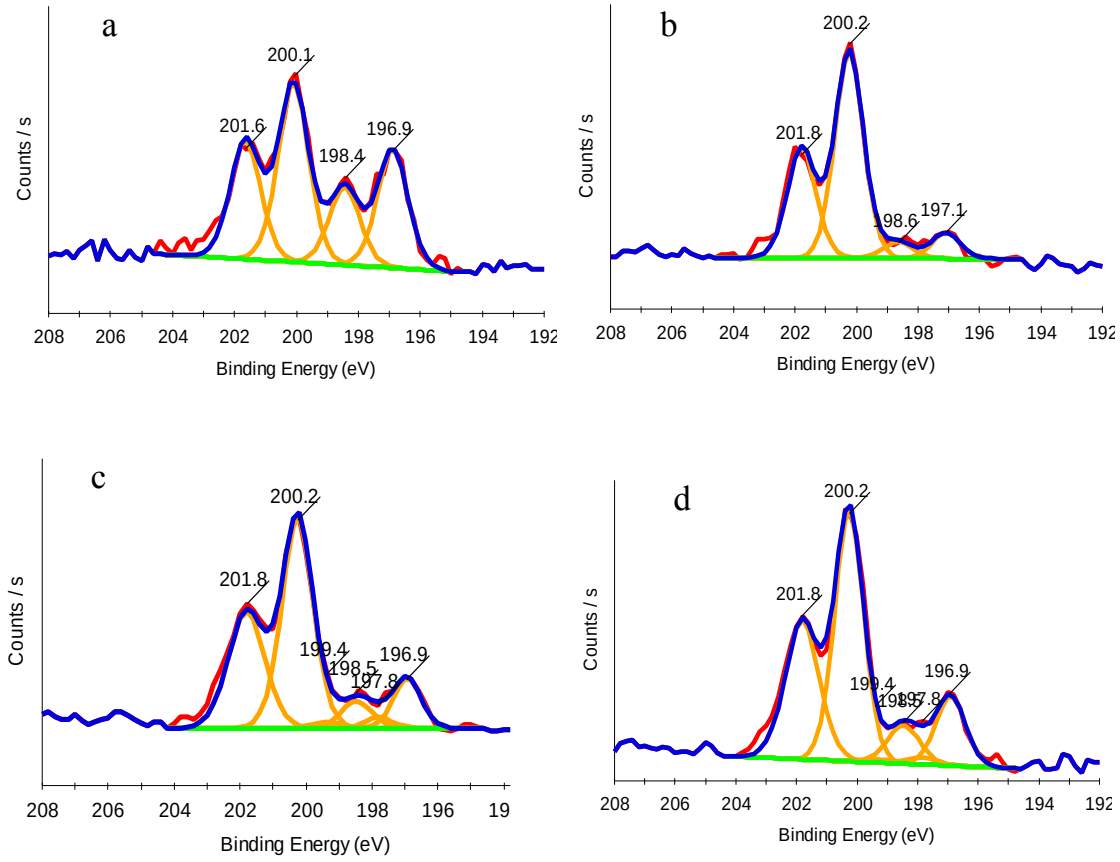

Figure IV-13: XPS Cl 2p core line spectra of (a) PANI bulk powder, (b) PANI-PVA-HCl (Run 3, Table 1), (c) PANI-PVA-CSA-HCl (Run 5, Table 1) and (d) PANI-PVA-PTSA-HCl (Run 4, Table 1)

I.5.2. PANI-PEO and PANI-PNVP-*co*-PVA composites

As for the PANI-PVA particles, XPS survey spectra of PANI prepared using PEO and PNVP-*co*-PVA based reactive stabilizers also show five main peaks originating from C 1s, O 1s, N 1s, Cl 2p and S 2p of the composites (Figure IV-14 a-b). Three signals from N1s at 398.6, 399.6 and 401.1 eV in PANI-PNVP-*co*-PVA correspond to neutral imine (=N–), amine (–NH–) and protonated imine ($=N^{+}–$) respectively (Figure IV-14c). The doping level calculated by the integration of these peaks is very low (10.43%), therefore not in agreement with the conductivity shown by this sample (Run 15, Table IV-1). Beside, the peak positions for PANI-PEO (Figure IV-14d) are exactly similar to PANI-PVA samples and show 38% doping level. C1s core line spectrum of PANI-PNVP-*co*-PVA is shown in Figure IV-14e. The

peaks assigned at 285.3, 286 and 287.5 eV are due to C–C/C–H, C–N and N–C=O respectively and indicate the presence of PNVP-*co*-PVA-*mod*-Py in the sample.[22] Similarly the presence of an intense peak at 286.2 eV for C1s (Figure IV-14f) and 532.5 for O1s (Experimental section III.7b) prove the presence of PEO on the surface of PANI-PEO.[23]

Cl 2p and S 2p core-line spectra of PANI-PNVP-*co*-PVA-*mod*-Py and PANI-PEO (Experimental section III.7c-d) arising from dopant anions are exactly similar to the spectra obtained for PANI-PVA and indicate their doping levels. As it is clear from the table of the surface composition (Figure IV-14), the amount of chlorine is almost half with respect to nitrogen in PANI-PNVP-*co*-PVA-*mod*-Py, indicating 50% doping level which is in accord with the high conductivity shown by this sample (Run 15, Table IV-1). In addition, low doping level (~33%) were observed for PANI-PEO sample (Run 1, Table IV-2) that are in agreement with both the low conductivity measured and high content of PEO within the sample (~50%).

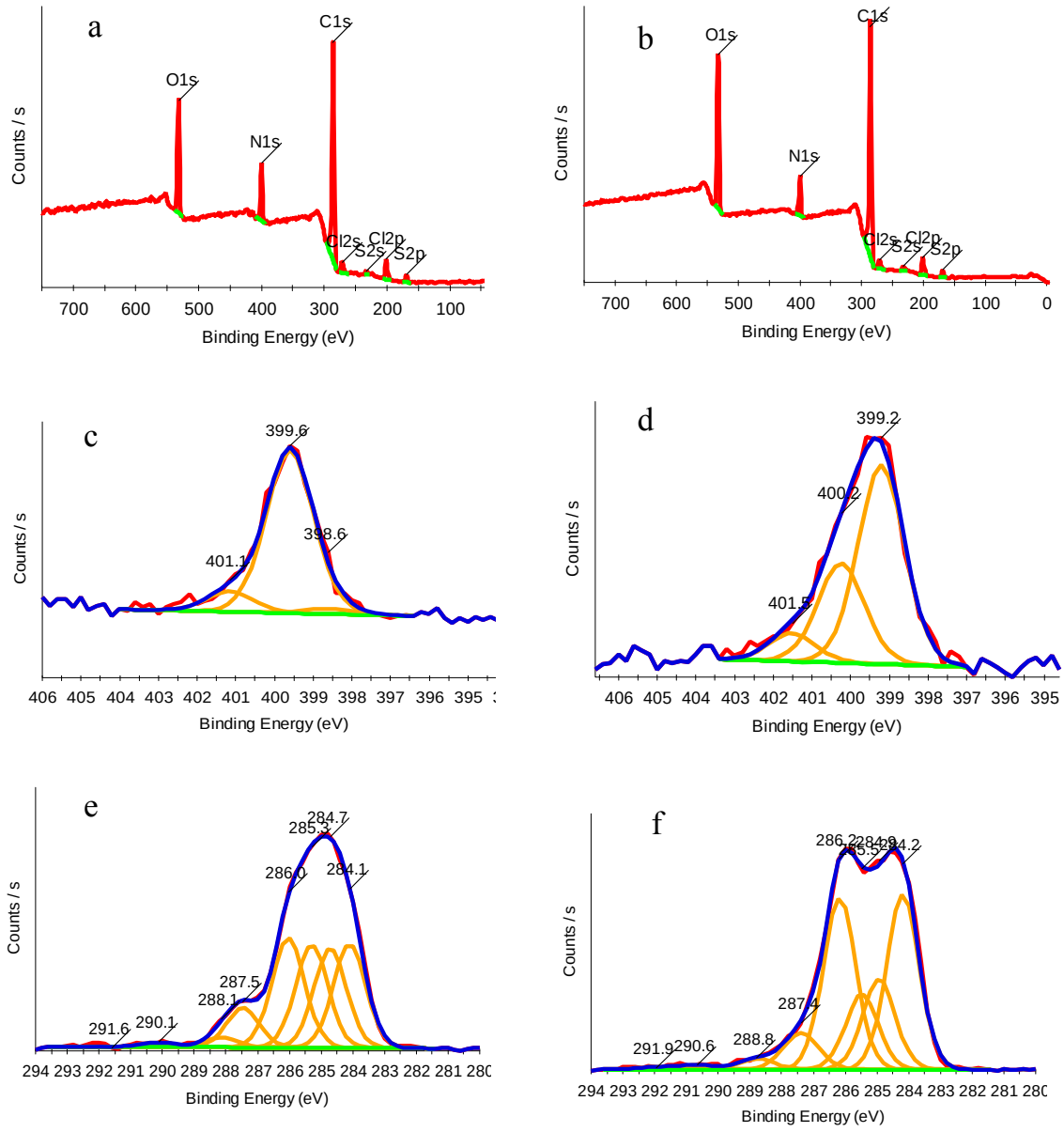

Sample	C	O	N	Cl	S
PANI-PNVP-PVA-g-Py-1	65.3	17.1	10.8	4.7	2.0
PANI-PEO-4	70.6	18.34	7.3	2.4	1.2

Figure IV-14: (a) & (b) XPS survey spectra of PANI-PNVP-*co*-PVA-*mod*-Py (Run 15, Table IV-1) and PANI-PEO (Run 1, Table IV-2), (c) & (d) XPS N 1s core line spectra of PANI-PNVP-*co*-PVA-*mod*-Py (Run 15, Table IV-1) and PANI-PEO (Run 1, Table IV-2) and (e) & (f) XPS C 1s core line spectra of PANI-PNVP-*co*-PVA-*mod*-Py (Run 15, Table IV-1) and PANI-PEO (Run 1, Table IV-2) respectively, (g) Table for the surface composition of PANI-PNVP-*co*-PVA-*mod*-Py and PANI-PEO.

I.6. DSC and TGA characterizations of PANI samples

Figure VI-15 shows the results of DSC for PVA-*mod*-An, PANI-bulk powder and PANI-PVA composites. Glass transition temperature of the samples generally appears at nearly 70-80 °C, which overlap with moisture released endotherm showing a broad signal at around 100°C. Melting point endotherm of PVA is around 200°C followed by dehydration and cross-linking of polymer near 300 °C producing polyene structures and volatile products.[25] Ultimately PVA decomposes into carbon and hydrocarbons on heating above 400°C. PANI bulk powder shows a broad endotherm that can be attributed to the release of HCl and moisture at 70-100°C followed by strong endotherm corresponding to cross-linking reaction[26] at elevated temperatures. Above 350 C, PANI degrades. In PANI-PVA composites, the moisture and dopant release retain its position at around 100 °C as well as the melting endotherm at near 200 °C. The dehydration endotherm of PVA and the endothem due to changing morphology near 300 °C is absent in composites which show their good thermal stability as compared to their precursors. From the DSC data, it is clear that composites exhibit combine physical properties of both components.

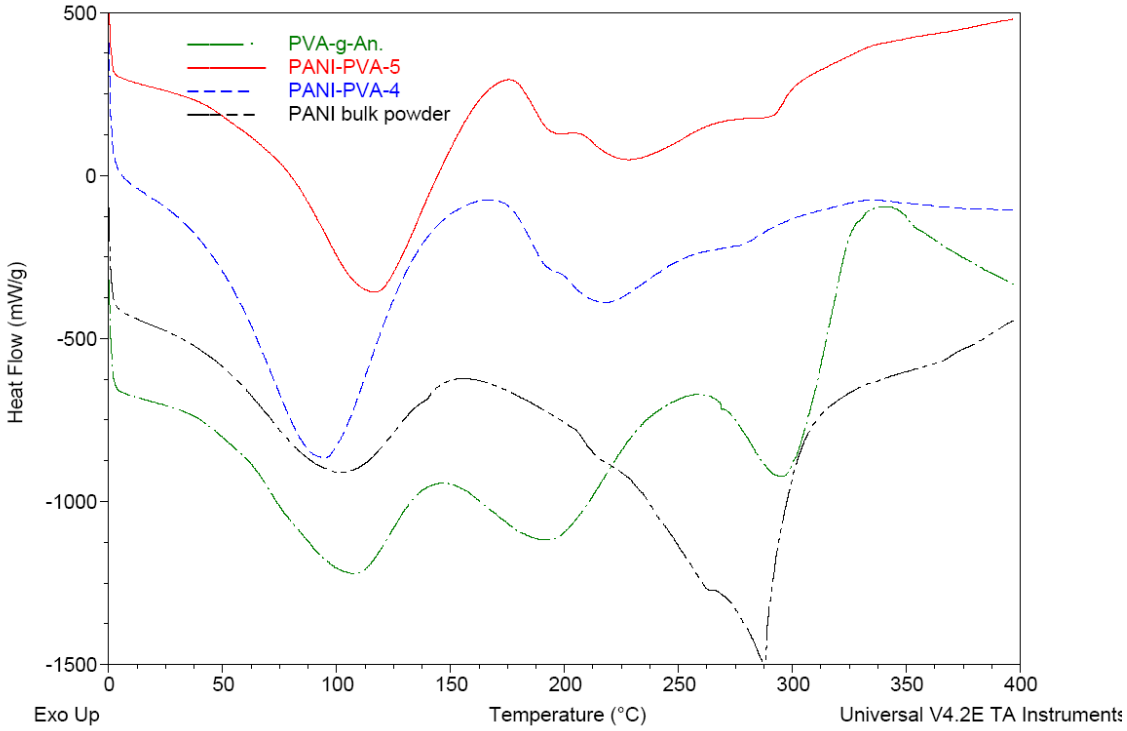

Figure IV-15: DSC curves of (—) PANI-PVA-5 (Run 5, Table 1) (– – –) PANI-PVA-4 (Run 4, Table 1), (— – —) PANI bulk powder, and (—•) PVA-*g*-An

The TGA curves for PANI bulk powder, PVA and PANI-PVA composites are shown in Figure IV-16. The thermal stability of PANI bulk powder is poor and it is found to loose HCl and moisture above 40 °C as it is shown in the slow mass loss region over 40-120 °C. Above 120 °C, it does not show any remarkable loss except for large scale thermal degradation above 300 °C. Moreover, all TGA curves due to PANI-PVA composites fall in between PANI bulk powder and PVA, confirming both the composition of the composites and their good stability.

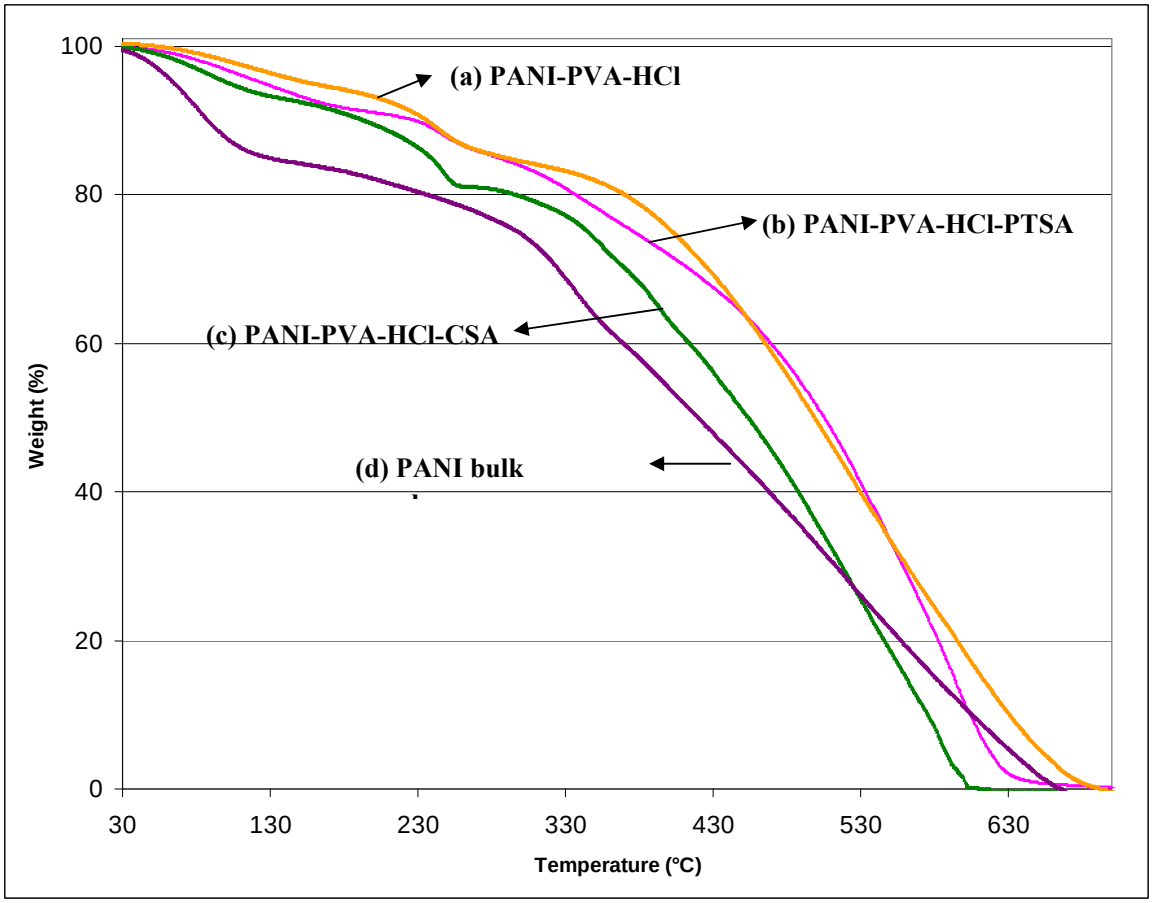

Figure IV-16: TGA curves for (a) PANI-PVA-HCl (Run 3, Table IV-1), (b) PANI-PVA-PTSA-HCl (Run 4, Table IV-1) (c) PANI-PVA-CSA-HCl (Run 5, Table IV-1) and (d) PANI bulk powder,

Similarly, the TGA curves for PANI bulk powder, PEO and PNVP-*co*-PVA-*mod*-Py stabilized nano-objects are shown in Figure IV-17. PEO reactive stabilizer does not exhibit weight loss until 400 °C. Above this temperature, there is sudden mass loss due to rapid thermal degradation of the polymer. On the other hand, there is three steps mass loss in PANI bulk powder and PANI-PEO and PANI-PNVP-*co*-PVA-*mod*-Py composites. As described above, it is attributed to loss of HCl, bound water and large scale thermal degradation of polymers above 400 °C except for PANI bulk powder where it starts at around 300 °C. It is interesting to note that PANI composites show more thermal stability than raw PANI powder materials.

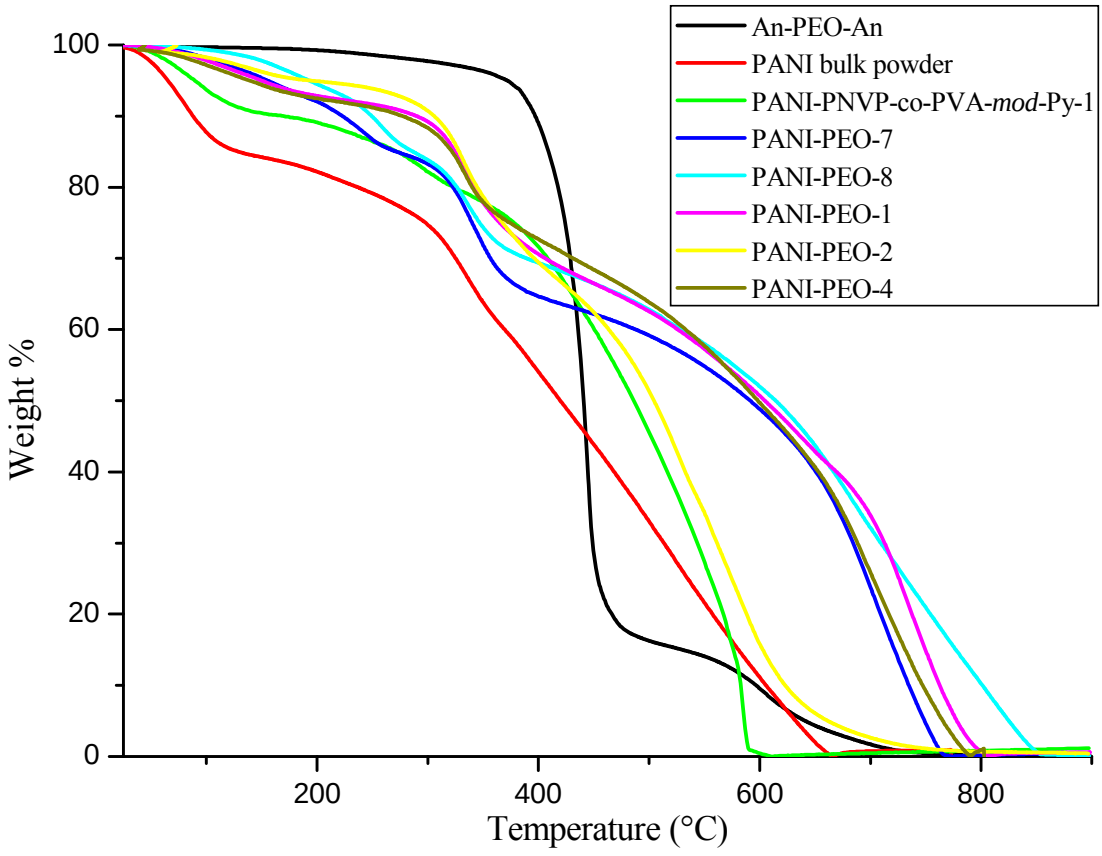

Figure IV-17: TGA curves for α,ω-An-PEOP, PANI bulk powder , PANI-PEO and PANI-PNVP-*co*-PVA-*mod*-Py composites. (The digits on left side of the name of each sample correspond to the run number in Table IV-2 except PANI-PNVP-*co*-PVA-*mod*-Py-1 which corresponds to Run 15 in Table 1)

I.7. Conductivity

Conductivity of the PANI nano-objects was measured on pressed pellets using the four probe method. As it is clear from Table IV-1, the conductivity of the PANI –PVA samples is affected by the dispersant media and type of the dopant used. Thus, interestingly rather high conductivity values were observed when DMSO/water (2:3) mixture was used as a dispersant medium and when PTSA was used as co-dopant (Runs 4, 7 and 11), which is also evident from the XPS and UV-Visible results discussed above. The increase in conductivity with the change in dispersant medium is probably due to an increase in PANI molecular weight. Indeed, as PANI is partially soluble in DMSO, the polymer chains remain in solution for longer time and as a result chain growth continues and high molecular weight PANI is produced before precipitation. Unfortunately, the insolubility of the final polymer in most solvent hampers determination of their molecular weight by GPC techniques. In most of the cases, high conductivities were shown for PANI samples prepared using PEO and PNVP-*co*-PVA based reactive stabilizers under similar experimental conditions. Indeed, from Table IV-2, it is clear that experimental parameters such as concentration of the stabilizer, reaction temperature, doping time, and reaction medium have considerable effect on conductivity. For example, the conductivity decreases from 0.15 S/cm to 0.045 S/cm as the concentration of the stabilizer increase from 35 wt.% to 50 wt.% (Runs 2&3, Table IV-2). The decrease in conductivity (5×10^{-2} to 8×10^{-3} S/cm) was also observed when the temperature of the medium increases from 0 to 25 °C (Runs 1-2, Table IV-2) probably due to the possibility of cross-linking between PANI chain at higher temperature. Higher conductivity was shown by the samples in which polymerization was performed in 1 M HCl than the PANI samples where HCl was added at the end of the reaction (runs 5-6, Table IV-2). In this latter case, the PANI is doped only from the surface while former is doped as a whole. Finally, similarly to the results obtained in the case of PANI-PVA, rather high conductivity values of 5×10^{-1} S/cm were obtained when dispersions were prepared in DMSO/water mixtures (Run 17, IV-1 and Run 9, Table IV-2).

II. Conclusion

PANI nano-objects with well-defined morphologies like peanuts, rice grain, corals, spheres and fibers were successfully prepared as a function of the nature and characteristics of

PVA, PEO and PNVP-*co*-PVA based reactive stabilizers. These nano-objects show conductivities as high as 0.5 S/cm in spite of the stabilizer insulator content within the materials. The presence and quantity of a protective thin layer composed with the stabilizer used onto the PANI samples was investigated by XPS. XPS was found to be an important tool to evaluate the doping level either by comparing the peak areas ratio of protonated imine and amine nitrogen to the neutral imine and amine or by directly measuring the amount of the dopant within the sample. The values thus obtained were found increased with the conductivities shown by PANI samples. Finally, DSC and TGA analysis revealed that PANI composites show better thermal stability than their pure PANI counterparts.

References

(1) Louwet, F.; Groenendaal, L.; Dhaen, J., Manca, J.; Luppen, J. V.; Verdonck, E.; Leenders, L. *Synth. Met*. **2003**, 135-136, 115.

(2) Kim, J. Y.; Jung, J. H.; Lee, D. E.; Loo, J. *Synth. Met*. **2002**, 126, 311.

(3) Stejskal, J. *J. Polym.Mater*. **2001**, 18, 225.

(4) Vincent, B.; Waterson J. *J. Chem. Soc., Chem. Commun*. **1990**, 683.

(5) Chattopadhyay, D.; Mandal, B. M. *Langmuir*, **1996**, 12, 1585.

(6) Stejskal, J.; Špírková, M.; Riede, A.; Helmstedt, M.; Mokreva, P.; Prokeš, J. *Polymer,* **1999**, 40, 2487.

(7) Chattopadhyay, D.; Chakraborty, M.; Mandal, B.M. *Polym. Int.* **2001**, 50, 538.

(8) Huang, K.; Wan, M. *Langmuir*, **2002**, 14, 3486.

(9) Stejskal, J.; Šírková, M.; Kratochvíl, P. *Acta Polym*. **1994**, 45, 385.

(10) Sapurina, I.; Stejskal, J. *Polym. Int*. **2008**, 57, 1295.

(11) Trchová, M.; Šeděnková, I.; Tobolková, E. Stejskal, J. *Polym. Degradation and Stability* **2004**, 86, 179.

(12) Quillard, S.; Louam, G.; Buisson, J. P.; Boyer, M.; Lapkowski, M.; Pron, A.; Lefrant S. *Synth. Met*. **1997**, 84, 805.

(13) Chiang, J. C.; MacDiarmid, A. G. *Synth. Met*. **1986**,13, 193.

(14) Socrates G. Infrared characteristic group frequencies. Chichester: Wiley, **1980**.

(15) Stejskal, J.; Trchova, M.; Prokeš,J.; Sapurina, I. *Chem. Mater*. **2001,** 13, 4083

(16) Lu, X.; Yu, Y.; Chen, L.; Mao, H.; Zhang, W. Wei, Y. *Chem. Commun*. **2004**, 1522.

(17) Barthet,C.; Guglielmi, M.; Baudry. P. J. *Electroana. Chem.* **1997**, 431, 145.

(18) Zhou, Y. K.; He, B. L.; Zhou, W. J.; Li, H.L. *J. Electrochem. Soc*. **2004**, 151, A1052.

(19) Kumar, S. N.; Bouyssoux, G.; Gaillard, F. *Surf. Interface Anal*. **1990,** 15, 531.

(20) Kumar, S. N.; Gaillard, F.; Bouyssoux, G.; Sartre, A. *Synth. Met.* **1990**;36:111.

(21) Benseddik, E.; Makhlouki, M.; Bernede, J. C.; Lerfrant, S.; Proń, A. *Synth. Met***. 1995**, 72, 237.

(22) Barthet, C.; Armes, S. P.; Chehimi, M. M.; Bilem, C.; Omastova, M. *Langmuir*, 1998, 14, 5032.

(23) Shakesheff, K. M.; Evora, C.; Soriano, I.; Langer, R. *J. Colloid Interface Sci*.**1997**, 185, 538.

(24) Wagner, C. D.; Riggs, W. M.; Davis, L. E.; Moulder, J. F.; Muilenberg, G. E. *Handbook of X-ray Photoelectron Spectroscopy*; Perkin-Elmer Corp.: Eden Prairie, MN, **1979**

(25) Tubbs, R. K.; Wu, T. K.; in: Finch, A. A. (Ed.) *Poly Vinyl Alcohol: Properties and Applications,* Wiley, New York, **1973**, 167-181.

(26) Ding, L.; Wang, X.; Gregory, R. V. *Synth. Met.* **1999**, 104, 73.

Chapter V

Synthesis of PEDOT- and PANI-metal composites particles in aqueous dispersion media

Table of contents

I. Synthesis of PEDOT and PANI-metal composites particles in aqueous dispersant media

With the objective to improve the electrical conductivity and optical properties of PEDOT and PANI materials and consequently their performances in optoelectronic devices, the synthesis of PEDOT and PANI nanocomposite was investigated. PEDOT- and PANI-based composites with gold, silver and copper metals have been prepared by aqueous dispersion polymerization in the presence of the following reactive stabilizers: Aniline-*modified*-poly(vinyl alcohol) (PVA-*mod*-An), pyrrole-*modified*-poly(vinyl alcohol) (PVA-*mod*-Py), α,ω-aniline-poly(ethyleneoxide) (An-PEO-An) or α,ω-fluorene-poly(ethyleneoxide) (Flu-PEO-Flu) (discussed in the previous chapters).

I.1. Synthesis of adequate stabilizers based on PEO or PVA

In order to prepare stable PEDOT-metal composites, the reactive stabilizers PNVP-*co*-PVA-*mod*-Py (M_n = 29000 g/mol, 10 mol.% of grafted pyrrole), PVA-*mod*-Py (M_n = 88000 g/mol, 5 mol.% of grafted pyrrole), PVA-*mod*-An (M_w = 88000 g/mol, 5 mol.% of aniline functionalization), α, ω-An-PEO (M_n = 35000 g/mol) and α, ω-Flu-PEO (M_n = 10000 & 35000 g/mol) were used. their synthesis was described in chapters II, III and IV.

I.2. Synthesis of PEDOT-metal composites

The composites of PEDOT with silver (Ag), gold (Au) and copper (Cu) were prepared by dispersion polymerization of EDOT in the presence of ammonium persulfate using silver nitrate ($AgNO_3$), hydrogen tetrachloroaurate ($HAuCl_4$) and copper sulfate pentahydrate ($CuSO_4.5H_20$) as co-oxidants respectively in aqueous media at room temperature. Similarly, PANI-Ag, and PANI-Au were prepared using $AgNO_3$ and $HAuCl_4$ in 1M HCl at 0°C.

I.2.1. Synthesis of PEDOT-Ag composites

In order to optimize the synthesis of PEDOT-Ag composites, the effects of the nature and concentrations of the stabilizers as well as the addition time of the co-oxidant have been studied. Data are given in Table V-1.

I.2.1.1. PEDOT-Ag prepared using PVA-based reactive stabilizers

PEDOT-*PVA*-Ag composite particles of 80-140 nm were obtained irrespective of the reactive stabilizer concentration (PVA-*mod*-Py or PVA-*mod*-An, 20-50wt.%, runs 1-3, Table V-1). Reversibly, the higher the concentration of the stabilizer, the higher the number of Ag particles deposited onto the particle surface (Figure V-1a-b). This trend shows that the stabilizer helps the Ag particles to attach on the PEDOT particles surface. In all cases, the Ag particles size on the PEDOT surface was found to be about 20 nm. It is also clear from Table V-1 that the nature of the pendant group on the stabilizer has no detectable effect on the size and morphology of PEDOT-*PVA*-Ag nanocomposites (runs 1 and 3).

I.2.1.2. PEDOT-Ag prepared using PEO-based reactive stabilizer

When EDOT was polymerized in the presence of Flu-PEO-Flu, PEDOT-*PEO*-Ag particles and vesicles were obtained depending upon the addition time of the co-oxidant. Small sized (50-80 nm) spherical PEDOT-*PEO*-Ag composite particles were obtained when $AgNO_3$ was added after 30 minutes reaction (run 4, Table 1). Reversibly, vesicles (250-300 nm) were observed when the co-oxidant was added after 24hours (runs 5, Table V-1). In the latter case, we could show that α,ω-Flu-PEO (M_n = 35000 g/mol) and PTSA self-assemble as vesicles that serve as templates during polymerization of EDOT. The phenomenon of the self-assembly of Flu-PEO-Flu in the presence of PTSA will be described in detail below in the same section. It is important to recall that only PEDOT particles were obtained when EDOT was polymerized without the addition of PTSA (see chapter II). From TEM images, on can observe Ag particles of about 10 nm all-around the surface of the PEDOT particles (Figure V-1c) and Ag particles of about 5 nm around the PEDOT-*PEO*-Ag vesicles (Figure V-1d).

S. No.	Stabilizer type	Molecular weight of the stabilizer (g/mol)	Amount of the stabilizer wt.%	Oxidant type	Co-oxidant	Addition time of co-oxidant	Amount of the co-oxidant (vs monomer)	Conductivity[b] (S/cm)	Particles size[c] (nm)	Remarks
1	PVA-*mod*-An	88000	50	$(NH_4)_2S_2O_8$	$AgNO_3$	30 min	1eq	8.0×10^{-1}	80-100	Particles
2	PVA-*mod*-Py	88000	20	$(NH_4)_2S_2O_8$	$AgNO_3$	30 min	1eq	1.0×10^{-1}	80-140	Particles
3	PVA-*mod*-Py	88000	50	$(NH_4)_2S_2O_8$	$AgNO_3$	30 min	1eq	9.0×10^{-1}	90-120	Particles
4	Flu-PEO-Flu	35000	50	$(NH_4)_2S_2O_8$	$AgNO_3$	30 min	1eq	1.0×10^{-1}	50-80	Particles
5[a]	Flu-PEO-Flu	35000	35	$(NH_4)_2S_2O_8$	$AgNO_3$	24 h	1eq	4.0×10^{-1}	250-300	Vesicles
6	PNVP-*co*-PVA-*mod*-Py	29000	35	$(NH_4)_2S_2O_8$	$AgNO_3$	30 min	1eq	1.5×10^{-1}	80-100	Particles
7	PNVP-*co*-PVA-*mod*-Py	29000	35	$(NH_4)_2S_2O_8$	$AgNO_3$	24 h	1eq	1.0×10^{-1}	150-170	Particles
8	PNVP-*co*-PVA-*mod*-Py	29000	35	$(NH_4)_2S_2O_8$	$AgNO_3$	30 min	0.5eq	6.0×10^{-1}	70-90	Particles
9	PNVP-*co*-PVA-*mod*-Py	29000	35	$AgNO_3$	APS	30 min	0.5eq	9.0×10^{-1}	60-70	Particles

(a) PTSA was added as dopant at the beginning of the reaction
(b) Measured by the four probe method
(c) Measured from TEM images. In all cases averages on 100 objects were made.

Table V-1: Synthesis of PEDOT-Ag nanocomposites in aqueous dispersant media.

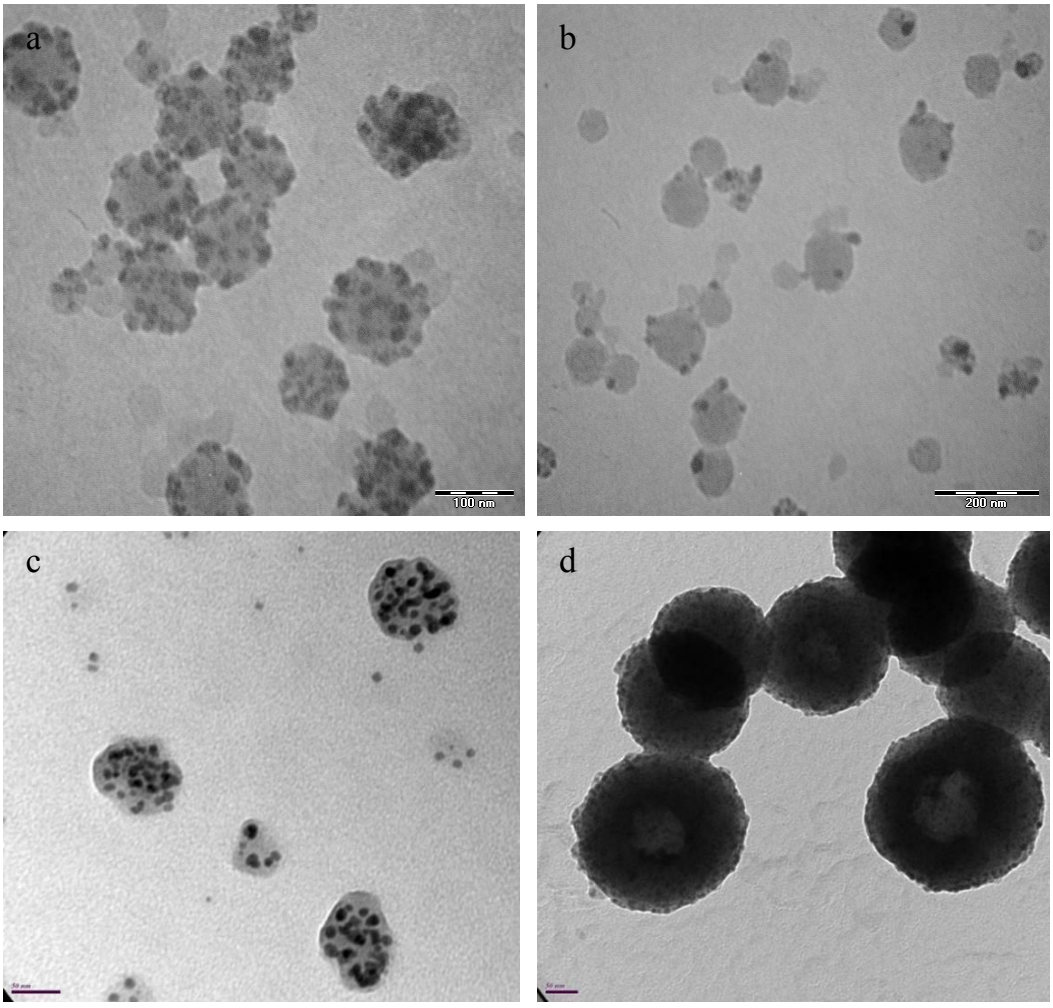

Figure V-1: TEM images of PEDOT-Ag nanocomposites prepared using different concentration and nature of stabilizers and addition time of co-oxidant(a) PVA-*mod*-Py, 50 wt.%, 30 min (run 3, Table V-1), (b) PVA-*mod*-Py, 20 wt.% , 30 min (run 2, Table V-1), (c) Flu-PEO-Flu, 50 wt.% 30 min (run 4, Table V-1), (d) Flu-PEO-Flu, 35 wt.%, 24 h (run 5, Table V-1), {Scale for c & d is 50 nm **}**

In order to fully understand, the behavior of α,ω-Flu-PEO in the presence of PTSA in solution and the effect on the size and morphology of the PEDOT composite particles, α,ω-Flu-PEO (M_n =35000 g/mol) solution in the presence of PTSA was analyzed by Dynamic Light Scattering (DLS). For this purpose, a solution of the stabilizer and PTSA at the concentration of 5.4 g/L and 7g/L respectively in methanol/water mixture (1/4) was prepared. The solution was filtered through 1 μm filter and stirred for 24 hours prior to DLS analysis. The auto-correlation function at different angles and their CONTIN analyses at 90°obtained at 25°C for α,ω-Flu-PEO/PTSA mixture are shown in Figure V-2a-b. For α,ω-Flu-PEO/PTSA mixture, one main population with a hydrodynamic radius, $R_{H,}$ of 130 nm is obtained. This

size is characteristic of micellar aggregation and is in good agreement with the PEDOT-Ag/Au vesicles obtained in our study.

In addition, the linear dependence of relaxation frequency Γ as a function of the square of the wave vector q^2 confirms that the observed micellar aggregates are spherical and homogeneous in size (Figure V-2c). Taking into account the dimension of a unimer (about 10nm), such a morphology is not really consistent with a spherical micelle, but more to a vesicular structure. The formation of vesicles was also confirmed by TEM analysis (See Figure V-2d) The TEM image shows vesicular objects with size about 100 nm. The decrease in size is probably due to the shrinkage of the vesicles in dry state.

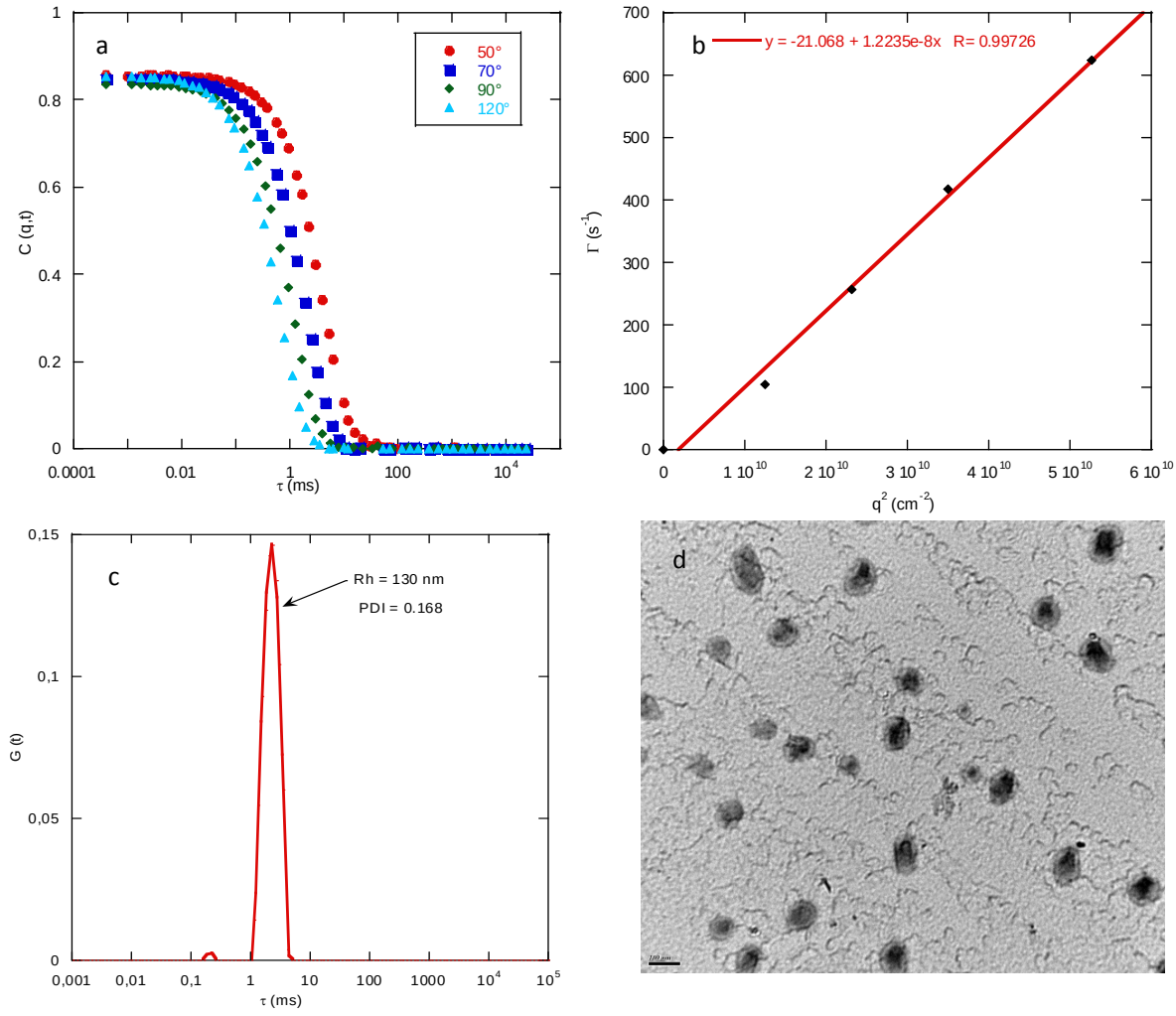

Figure V-2: (a)Auto-correlation functions C(q,t), at different angles (b) Relaxation frequency in the function of q^2 (c) relaxation time distribution G(t) at 90° for α,ω-Flu-PEO/PTSA mixture in water/methanol mixture (4:1) at 25 °C and (d) TEM images of the α,ω-Flu-PEO/PTSA mixture. {Scale for figure V-6d is 100 nm}

From this DLS data it is clear that α,ω-Flu-PEO self-assemble in the presence of PTSA to form vesicles that lead to the formation of PEDOT vesicles during the dispersion polymerization of EDOT. It is important to note that such self-assembly was not observed in α,ω-Flu-PEO solution (without PTSA) by DLS analysis (see chapter II). It could be interesting to investigate the solution behavior of α,ω-Flu-PEO of different molecular weights and their effect on the size and morphology of PEDOT composites.

I.2.1.3. PEDOT-Ag prepared using PNVP-*co*-PVA-based reactive stabilizer

In the case of EDOT polymerization performed in the presence of PNVP-*co*-PVA-*mod*-Py and $AgNO_3$ as a co-oxidant, spherical PEDOT-*PNVP-co-PVA*-Ag composite particles are formed independent of the addition time of the co-oxidant (runs 6-9, Table V-1)). However, the particles size is affected by the addition time of $AgNO_3$. The smallest particles (60-100 nm) were obtained when $AgNO_3$ was added at the beginning of the reaction (after 30 minutes, runs 6, Table V-1, Figure V-3). This phenomenon can be explained by the higher

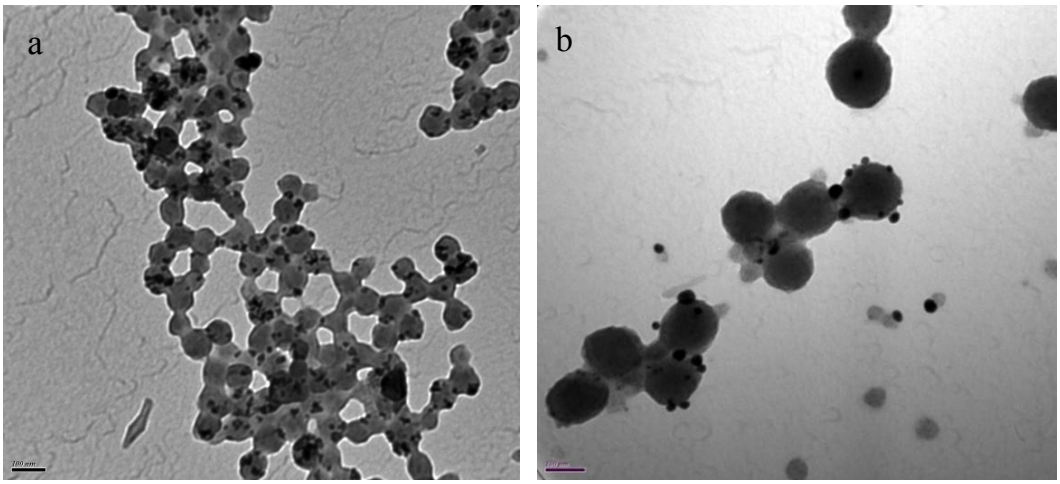

Figure V-3: TEM images of PEDOT-Ag nanocomposites prepared using same concentration of PNVP-*co*-PVA-*mod*-Py stabilizer but different addition time of co-oxidant (a) 30 min (run 8, Table IV-1) and (b), 24 h (run 7, Table V-1). {Scale for a & b is 100 nm}

reactivity of the oxidant mixture as compared to pure $(NH_4)_2S_2O_8$, that probably leads to the formation of a higher concentration of nuclei at the beginning of the reaction. Similar results were obtained when EDOT was polymerized in the presence of the mixture of ammonium persulfate and iron(III) chloride as oxidant (see chapter II). Furthermore, the size and morphology of the PEDOT-*PNVP-co-PVA*-Ag composite particles remain is little affected by

the addition order of the oxidants (run 8 & 9, Table V-1). While in this study, the stabilizers at the concentration ranging from 20 - 50 wt.% were used, it will be interesting to check the effect of lower amount of stabilizers on the formation and morphology of the nanocomposite particles.

I.2.2. Synthesis of PEDOT-Au composites

As already indicated, PEDOT-Au composite particles were prepared by dispersion polymerization using $HAuCl_4$ as a co-oxidant. Au^{+3} ion is reduced to Au^0 either by EDOT monomer or PEDOT and is then stabilized on the surface or inside the PEDOT particle. The effects of different reactive stabilizers and the addition time of the co-oxidant on the size and morphology of PEDOT-Au composite were also studied. The results of the PEDOT-Au composites prepared in different experimental conditions are summarized in Table V-2 (runs 1-5).

As it can be seen in Table V-2, the smallest particles in the range 40-80 nm are obtained when the co-oxidant is added in one dose at the beginning of the reaction; irrespective of the nature of the stabilizer used (runs 1, 2 and 5). The smallest particles (40-50 nm) were obtained using PVA-*mod*-Py (M_w = 88000 g/mol) as reactive stabilizer (see Figure V-4e). The formation of such small particles is logically explained by a good coverage offered by high molecular weight PVA-*mod*-Py to the growing PEDOT-Au composite particles.

As already seen in case of PEDOT-*PEO*-Ag nanocomposites, the nano-vesicles were obtained when $HAuCl_4$ was added after 24h in the reaction medium with Flu-PEO-Flu as a reactive stabilizer and PTSA as a doping agent while spherical nano-particles were obtained when the co-oxidant was added at the beginning of the reaction. The formation of nano-vesicles result of the self-assemblage of Flu-PEO-Flu in the presence of PTSA as described above in the previous section.

In the case of PNVP-*co*-PVA reactive stabilizer, the small gold nano-particles self-assembled to sub-micrometer sized (400-500 nm) gold particles, when the co-oxidant $HAuCl_4$ was added slowly (in about 5 minutes) drop-wise in the reaction mixture (for illustration see Figure V-4c). Similar results were obtained by Li *et al.*[1] who studied the reduction of $HAuCl_4$

S. No.	Stabilizer type	Molecular weight of the stabilizer (g/mol)	Amount of stabilizer Wt.%	Oxidant type	Co-oxidant	Amount of the co-oxidant	Addition time of co-oxidant	Conductivity[b] (S/cm)	Particles size[c] (nm)	Remarks
1	PVA-*mod*-Py	88000	50	$(NH_4)_2S_2O_8$	$HAuCl_4$	0.33eq	30 min	8.0×10^{-2}	40-50	Particles
2	Flu-PEO-Flu	35000	50	$(NH_4)_2S_2O_8$	$HAuCl_4$	0.33eq	30 min	3.0×10^{-1}	50-80	Particles
3[a]	Flu-PEO-Flu	35000	35	$(NH_4)_2S_2O_8$	$HAuCl_4$	0.33eq	24 h	4.2×10^{-2}	200-250	Vesicles
4	PNVP-*co*-PVA-*mod*-Py	29000	35	$(NH_4)_2S_2O_8$	$HAuCl_4$	0.33eq	30 min	1.0×10^{-1}		Particles
5	PNVP-*co*-PVA-*mod*-Py	29000	35	$HAuCl_4$	—	—	—	1.25	70-80	Particles

(a) PTSA was added as dopant at the beginning of the reaction
(b) Measured by the four probe method
(c) Measured from TEM images. In all cases averages on 100 objects were made.

Table V-2: Synthesis of PEDOT-Au nanocomposites in aqueous dispersant media.

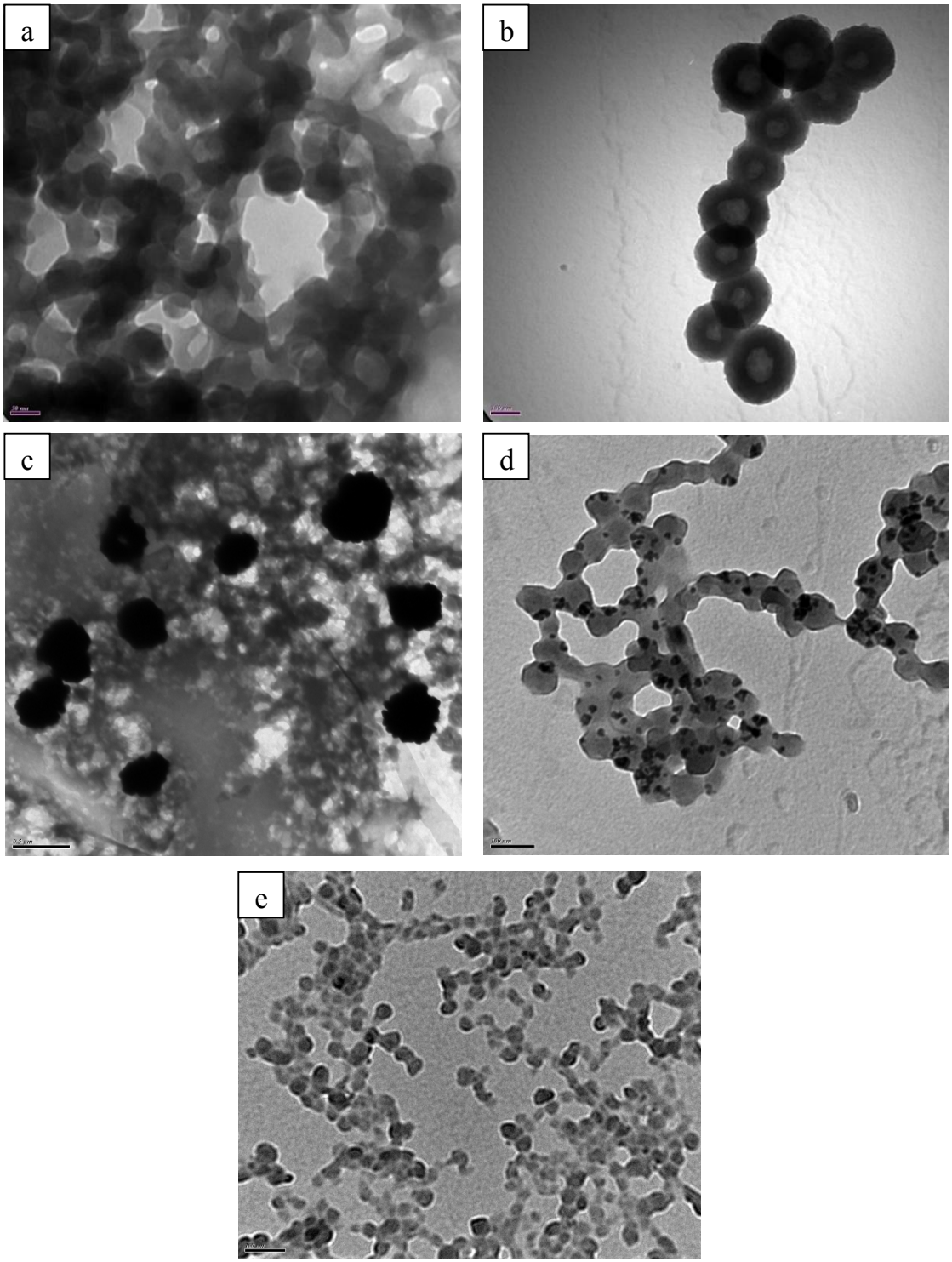

Figure V-4: TEM images of PEDOT-Au nanocomposites prepared using different concentration and nature of stabilizers and addition time of co-oxidant (a) Flu-PEO-Flu, 50 wt.%, 30 min (run 2, Table V-2), (b) Flu-PEO-Flu, 50 wt.%, 24 h (run 3, Table V-2), (c) PNVP-*co*-PVA-*mod*-Py, 35 wt.%, 30 min (run 4, Table V-2), (d) PNVP-*co*-PVA-*mod*-Py, 35 wt.% (run 5, Table V-2) and (e) PVA-*mod*-Py, 50 wt.%, 30 min (run 1, Table V-2). {Scale for b, d, & e is 100 nm and a and c is 50 and 500 nm respectively}

by EDOT, in THF solution, using dioctylamine as a stabilizer at 120°C. Reversibly, gold coated PEDOT composite particles were obtained when $HAuCl_4$ (the only oxidant i.e. without any co-oxidant) was added drop-wise in the reaction medium ((Figure V-4d). Although, in some cases, it is difficult to see Au nano-particles on the PEDOT surface by TEM, the presence of Au could be confirmed by XPS analysis, as it will be discussed in later sections.

I.2.3. Synthesis of PEDOT-Cu composites

PEDOT-Cu composites were prepared using $CuSO_4$ solution (in 5N NH_4OH) as a co-oxidant. The addition of ammonium hydroxide eases the dissolution of $CuSO_4$ in aqueous media and facilitates the reduction of Cu^{+2} to Cu^0. The results of PEDOT-Cu composites are shown in Table V-3 (runs 1-3). PEDOT-Cu vesicles are obtained in the presence of PVA-*mod*-Py (Figure V-5a) while spherical nano-particles are obtained in the presence of PNVP-*co*-PVA-*mod*-Py (Figure V-5b-c). PTSA was added after few minutes of the co-oxidant addition in order to neutralize and dope the PEDOT formed (run 2) while few mL of concentrated HCl was added in the reaction mixture of run 3 after 24h in order to neutralize the added base. As it is clear from TEM images, the best results, in terms of morphology were obtained in the latter case (run3, Figure V-5c). The reason for the formation of vesicular objects using PVA-*mod*-Py as a reactive stabilizer is currently unknown.

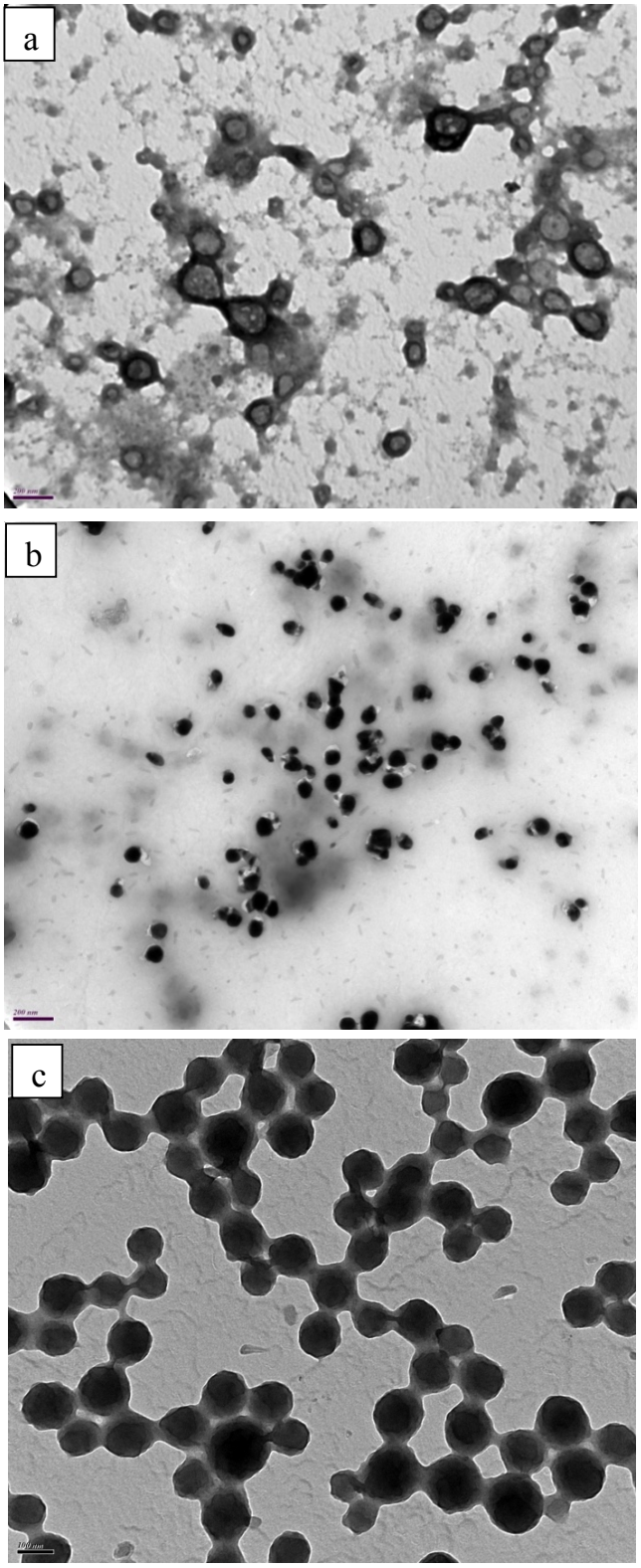

Figure V-5: TEM images of PEDOT-Cu nanocomposites prepared using different stabilizers and experimental conditions (a) PVA-*mod*-Py , 50 wt.%+ NH_4OH (run 1, Table V-3), (b) PVA-*mod*-Py , 50 wt.%+ NH_4OH+PTSA (run 2, Table V-3) and (c) PNVP-*co*-PVA-*mod*-Py , 35 wt.%+ NH_4OH+HCl, (run 3, Table V-3) { Scale for a & b is 200 nm and c is 100 nm**}**

S. No.	Stabilizer type	Molecular weight of the stabilizer (g/mol)	Amount of stabilizer wt.%	Oxidant	Co-oxidant	Amount of co-oxidant (vs monomer)	Addition time of co-oxidant	Conductivity[d] (S/cm)	Particle size[e] (nm)	Remarks
1[a]	PVA-*mod*-Py	88000	50	$(NH_4)_2S_2O_8$	$CuSO_4$	0.5eq	30 min	—	120-200	Vesicles
2[a,b]	PVA-*mod*-Py	88000	50	$(NH_4)_2S_2O_8$	$CuSO_4$	0.5eq	30 min	3.6×10^{-2}	70-100	Particles
3[a,c]	PNVP-*co*-PVA-*mod*-Py	29000	35	$(NH_4)_2S_2O_8$	$CuSO_4$	0.5eq	30 min	8.0×10^{-2}	100-130	Particles

(a) CuSO4 was dissolved in 5ml of 5N NH_4OH and added after 10 minutes of the start of the reaction
(b) PTSA was added to neutralize the NH_4OH at the beginning of the reaction
(c) 5 ml concentrated HCl was added in order neutralize the NH_4OH at the end of the reaction
(d) Measured by the four probe method
(e) Measured from SEM images. In all cases averages on 100 objects were made.

Table V-3: Synthesis of PEDOT-Cu nanocomposites in aqueous dispersant media.

I.3. XPS characterization of PEDOT-metals composites

In order to investigate the composition of the PEDOT-metals composite particles, XPS analysis of PEDOT samples and PEDOT bulk powder were analyzed by X-ray Photoelectron Spectroscopy (XPS). Figures V-6 and V-7 represent the XPS survey and high resolution spectra of PEDOT composite samples respectively. The presence of peaks due to Ag 3d, Au 4f and Cu 2p in survey spectra of PEDOT-metal composites in addition to the four main peaks originating from O1s, C1s, S2s and S2p confirms the presence of silver, gold and copper respectively in the composite materials. Such features are not present in survey spectra of PEDOT bulk powder.

Examination of the peak-fitted Au 4f core-line spectra for PEDOT-Au composite (see Figure V-7b) reveals two strong signals due to Au $4f_{5/2}$ and $4f_{7/2}$ electrons, respectively. Each signal is adequately peak-fitted with only one component, clearly showing that only one gold species is present. The $4f_{7/2}$ peak is centered at 84 eV, and the accompanying $4f_{5/2}$ peak at 87.6 eV. This doublet is characteristic of zero-valent Au.[2] In addition, there is no sign of any signal due to Au(III) (the $4f_{7/2}$ peak would be expected at *ca.* 86 – 87 eV). These data prove unambiguously that reduction of Au(III) to Au(0) has indeed taken place, and is in close agreement with the work of Kang and co-workers.[3,4] From the high resolution spectra of Ag 3d (Figure V-7a), the binding energy for Ag $3d_{5/2}$ and Ag $3d_{3/2}$ were found to be 368.34 and 374.50 eV, respectively. The S $2p_{3/2}$ core-level spectra of Ag/PEDOT nanocomposites peaks at 161.3-162.4 eV has been assigned to sulfur of –C–S–Ag [5-7] (Figure V-9b). Therefore, it can be suggested that there is a significant chemical interaction between the Ag and sulfur atom of thiophene ring. The characteristic Cu 2p peak at 932 eV[8-10] in Figure V-7c confirms the reduction of Cu^{+2} to Cu^{0}.

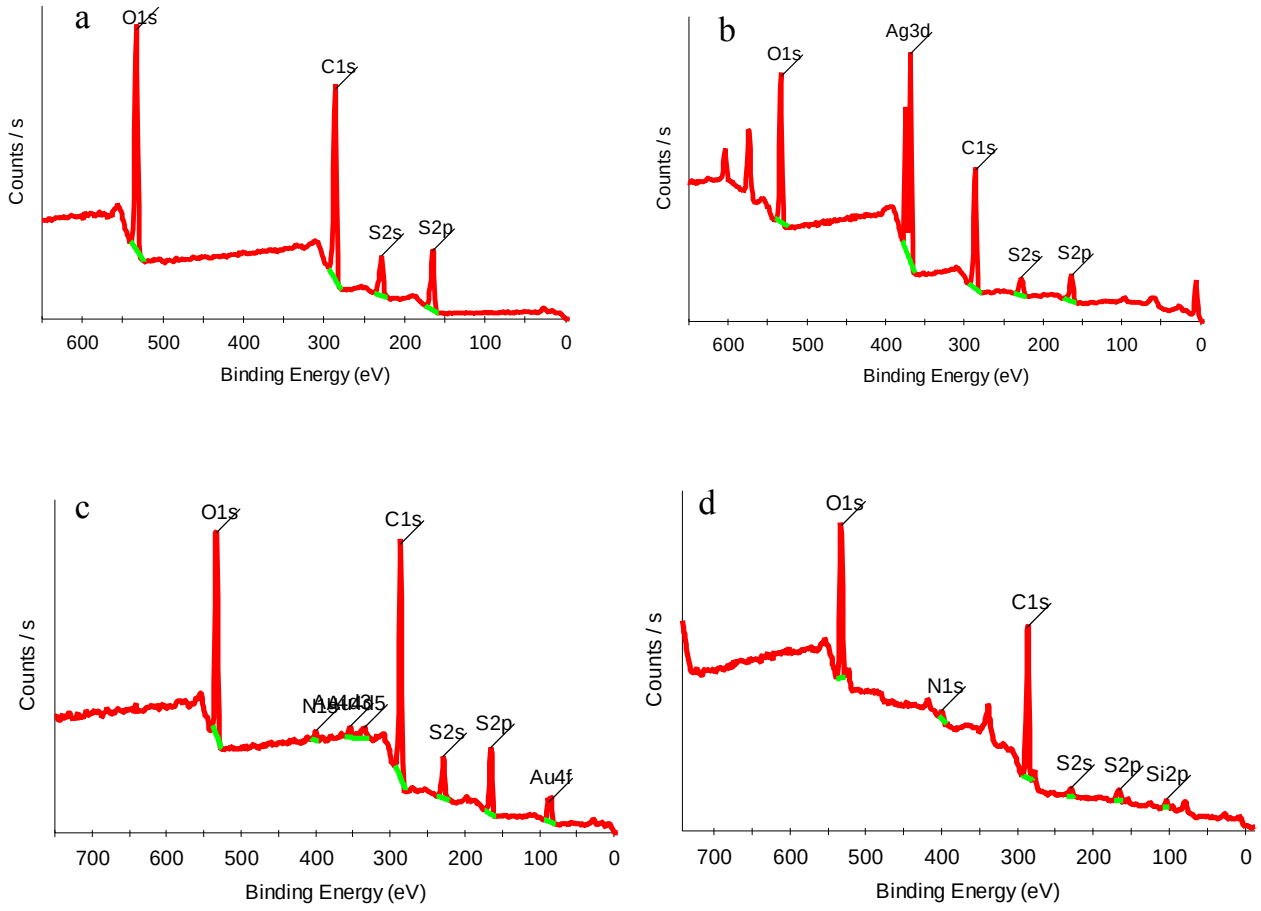

Figure V-6: XPS survey spectra of (a) PEDOT bulk powder, (b) PEDOT-*PVA*-Ag composite (run 3, Table V-1), (c) PEDOT-*PVA*-Au composite (run 1, Table V-2) and (d) PEDOT-Cu composites (run 1, Table V-3)

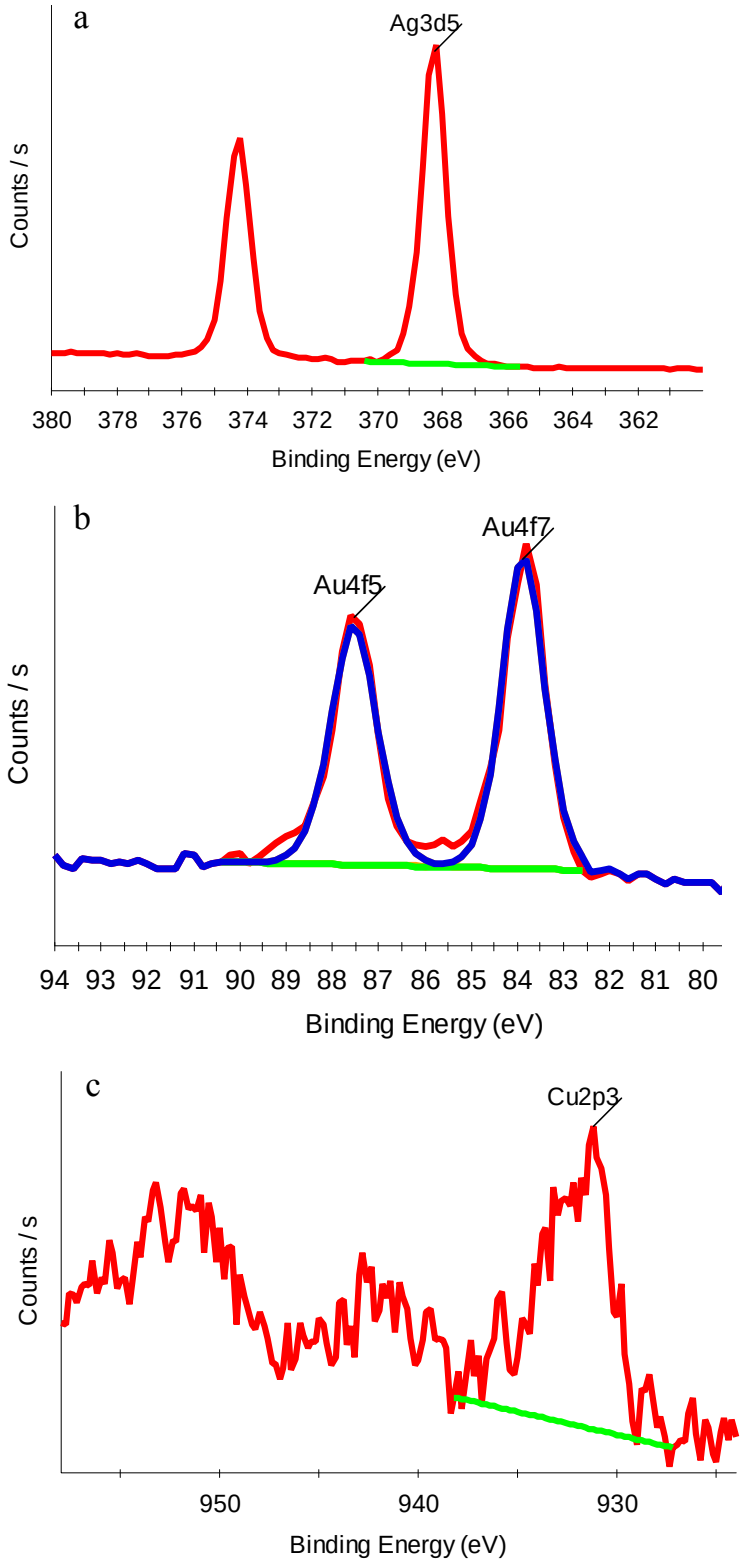

Figure V-7: XPS high resolution spectra of Ag 3d (run 3, Table V-1), (b) Au 4f (run 1, Table V-2) and (c) Cu 2p (run 1, Table V-3).

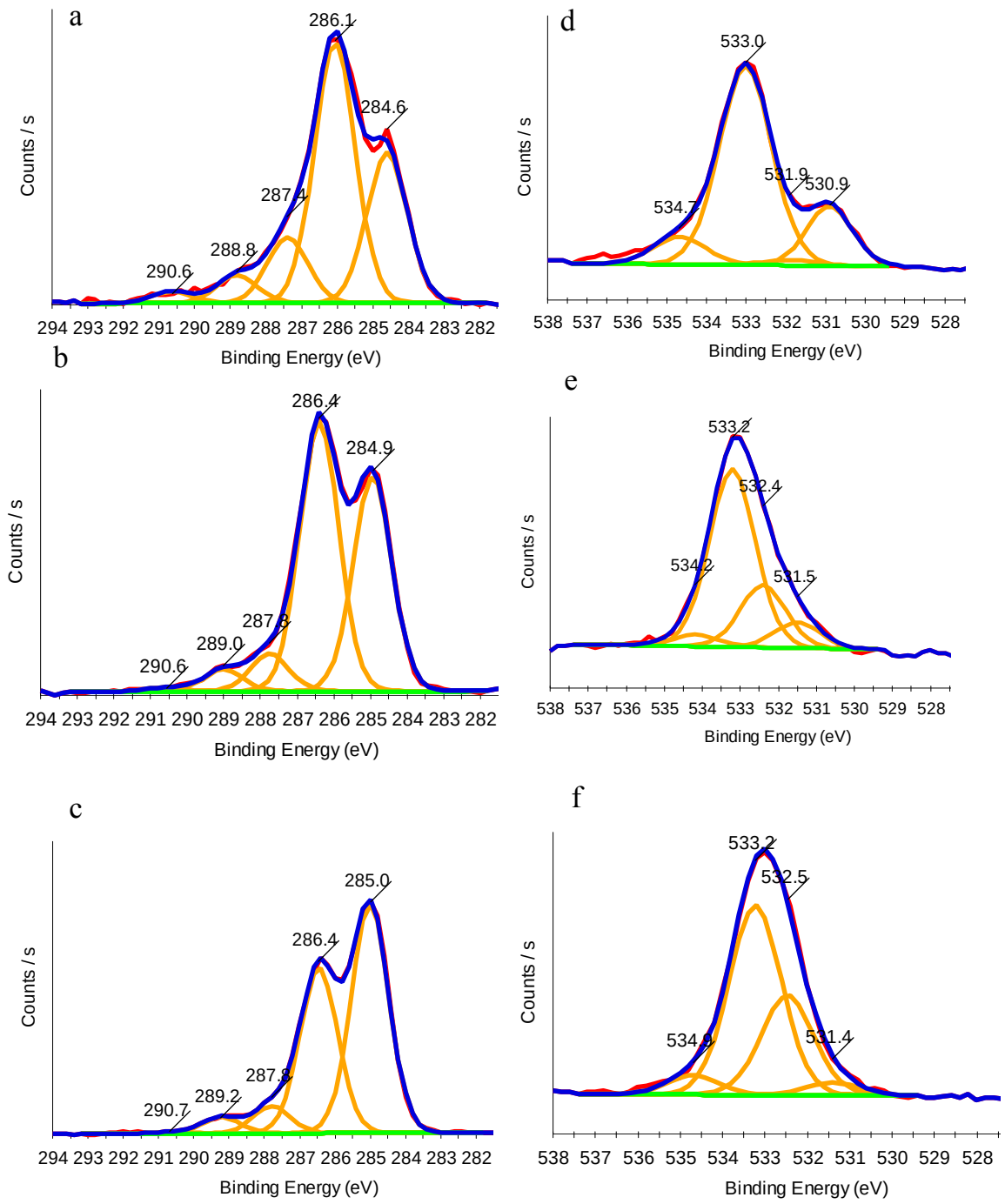

Figure V-8: C1s core-line spectra of (a) PEDOT bulk powder, (b) PEDOT-*PVA*-Ag composite run 3, Table V-1), (c) PEDOT-*PVA*-Au composite (run 1, Table V-2) and (d), (e) & (f) are their corresponding O1s core-line spectra respectively

Figure V-8a-f displays the high resolution C 1s and O 1s core-line spectra of PEDOT bulk powder and PEDOT-metals composite particles. The peak positioned at 286.4 eV in C 1s

core-line spectra of PEDOT composites samples correspond to C-O-H moieties in PVA.[11-13] In addition, the presence of peak at 532.6 eV (Figure V-9e&f) originating from O 1s is due to C-O-H and is in agreement to the data already available in the literature. [11] Such peak was not observed in O 1s core-line spectrum of PEDOT bulk powder (Figure V-8d). From these results it is clear that PVA is present on the surface of the PEDOT particles and is responsible for the stability of the nano-composites.

Figure V-9a-d represents the S 2p core-line spectra of PEDOT bulk powder and PEDOT metal composites. In each case (except for PEDOT-Cu) the main peak has been fitted with three components: neutral S (163.8 - 165.1 eV) and cationic S^+ (165.2 - 167.4 eV) associated with the PEDOT backbone and highly oxidized SO_4^- (167.4 - 169.5 eV) of the

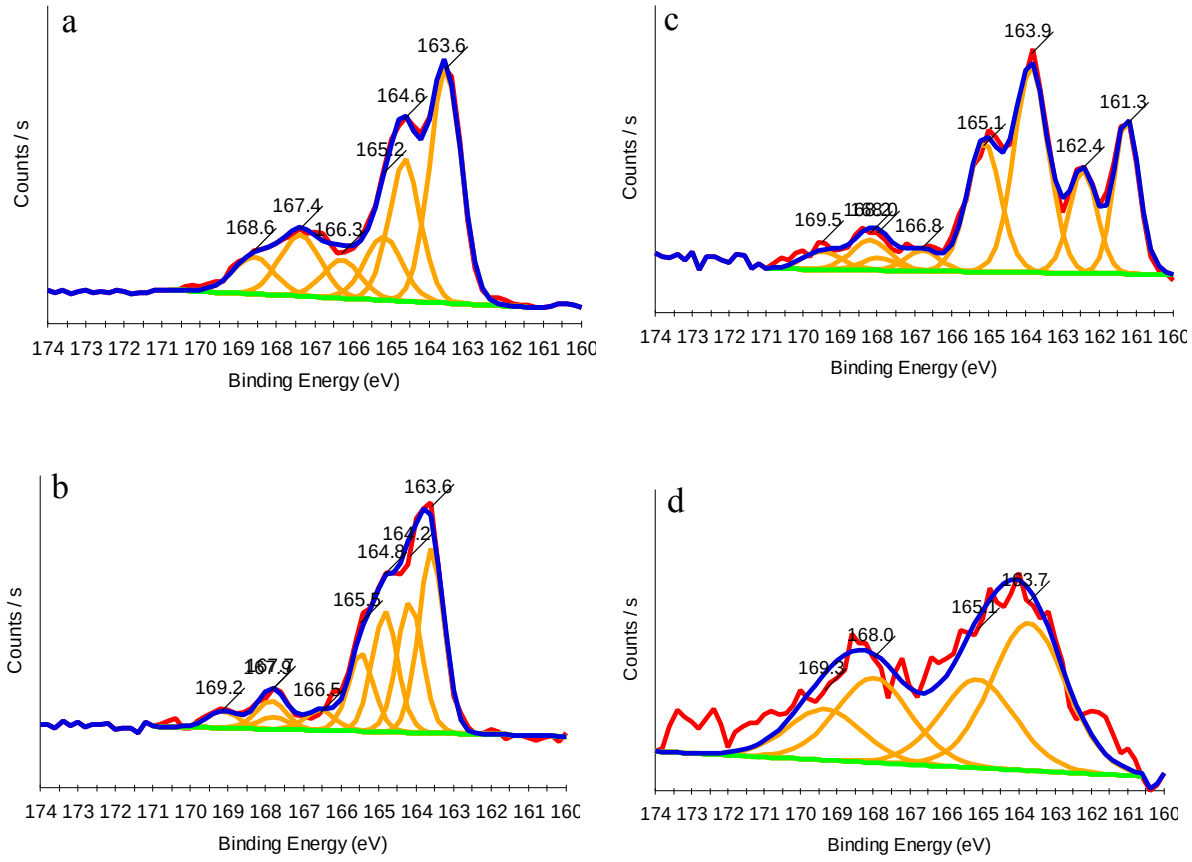

Figure V-9: XPS S2p core-line spectra of a) PEDOT bulk powder, (b) PEDOT-*PVA*-Ag composite run 3, Table V-1), (c) PEDOT-*PVA*-Au composite (run 1, Table V-2) and (d) PEDOT-PVA-Cu composite (run 1, Table V-3).

dopant. Each of these components is represented by two peaks arising from the $2p_{1/2}$ and $2p_{3/2}$ electrons, resulting in a total of six peaks. The sub-peak due to S^+ cation is absent in the S2p core-line spectrum of PEDOT-Cu composite due to its neutral nature because of added ammonium hydroxide at the beginning of the reaction (run 1, Table V-3).

From the above discussion it is obvious that PEDOT core-shell particles decorated with silver, gold and copper are successfully prepared in one pot synthesis by dispersion polymerization techniques. It paves the way to new composite materials based on semi-conducting organic polymers and metals…

I.4. TGA analysis of PEDOT-metals composites

TGA of the PEDOT composite materials was performed in order to know their thermal stability and to evaluate their composition. The TGA traces of PEDOT-metals composites and PEDOT bulk powder are shown in the Figure V-10. From the Figure it is

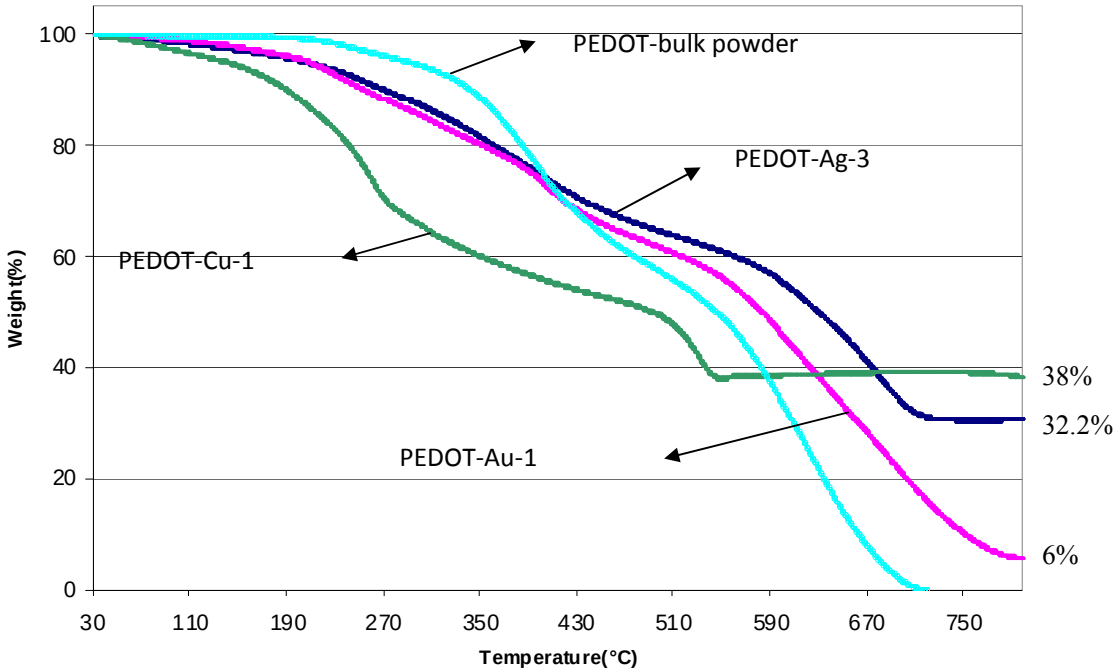

Figure V-10: TGA curves of — PEDOT bulk powder, — PEDOT-PVA-Ag (run 3, Table V-1), — PEDOT-PVA-Au (run 1, Table V-2) and — PEDOT-PVA-Cu (run 1, Table V-3)

clear that PEDOT-Ag and PEDOT-Au composites show higher thermal stability as compared to the PEDOT bulk powder while PEDOT-Cu shows lower thermal stability. The reason for the lower stability shown by PEDOT-Cu composite is not known. TGA traces can be used to estimate the amount of metals in the composites assuming that remaining incombustible materials are gold, copper and silver respectively. The amount of gold, silver and gold was found to be 6%, 32.2 %and 38% in PEDOT-Au-1 (run 1, Table V-2), PEDOT-Ag-3 (run 3, Table V-1) and PEDOT-Cu-1 (run 1, Table V-3) respectively. These values are rather good in agreement with the amount of metal added at the beginning of the polymerization.

I.5. Synthesis of PANI-metal composites

PANI-Ag and PANI-Au composites were prepared using aniline or PANI as a reducing agents by dispersion polymerization in the presence of α,ω-An-PEO (M_n = 35000 g/mol), PVA-*mod*-An (M_n = 88000 g/mol) and PNVP-*co*-PVA-*mod*-Py (M_n = 29000 g/mol) as reactive stabilizers. The results of the dispersion polymerization of aniline using metal salts as co-oxidants are shown in Table V-4.

I.5.1. Synthesis of PANI-Ag composites

PANI-Ag composites were prepared using $AgNO_3$ as a co-oxidant during dispersion polymerization of aniline hydrochloride in which Ag^{+1} ions reduced to Ag^0 by aniline or PANI. Ag particles thus formed deposit on the surface as well as inside the growing PANI particles.

As can be seen from Figures V-10a and V-10b, the nature of the stabilizers has no effect on the size and final morphology of PANI-Ag composite particles. In both cases, nearly spherical PANI-Ag nano-particles in the range of 80-150 nm are formed when the co-oxidant is added at the beginning of the reaction while PANI peanut and fibers are obtained in the presence PVA-*mod*-An and PNVP-co-*PVA-mod*-Py respectively without using co-oxidant (see chapter IV).

S. No.	Stabilizer type	Molecular weight of the stabilizer (g/mol)	Amount of stabilizer[a] Wt.%	Oxidant	Co-oxidant	Amount of co-oxidant[b]	Conductivity[d] (S/cm)	Remarks
1	PVA-*mod*-An	88000	50	$(NH_4)_2S_2O_8$	$AgNO_3$	1eq	1.0×10^{-1}	Particles
2	PNVP-*co*-PVA-*mod*-Py	88000	50	$(NH_4)_2S_2O_8$	$AgNO_3$	1eq	6.28×10^{-2}	Particles
3	PVA-*mod*-An	88000	50	$(NH_4)_2S_2O_8$	$HAuCl_4$	0.33eq	5.0×10^{-2}	Particles
4[c]	An-PEO-An	35000	50	$(NH_4)_2S_2O_8$	$HAuCl_4$	0.33eq	8.0×10^{-1}	Particles

(a,b). Versus monomer

(c). Co-oxidant was added after washing and re-dispersing of PANI dispersion

(d) Measured by the four probe method

Table V-4: Synthesis of PANI-metal nanocomposites in aqueous dispersant media

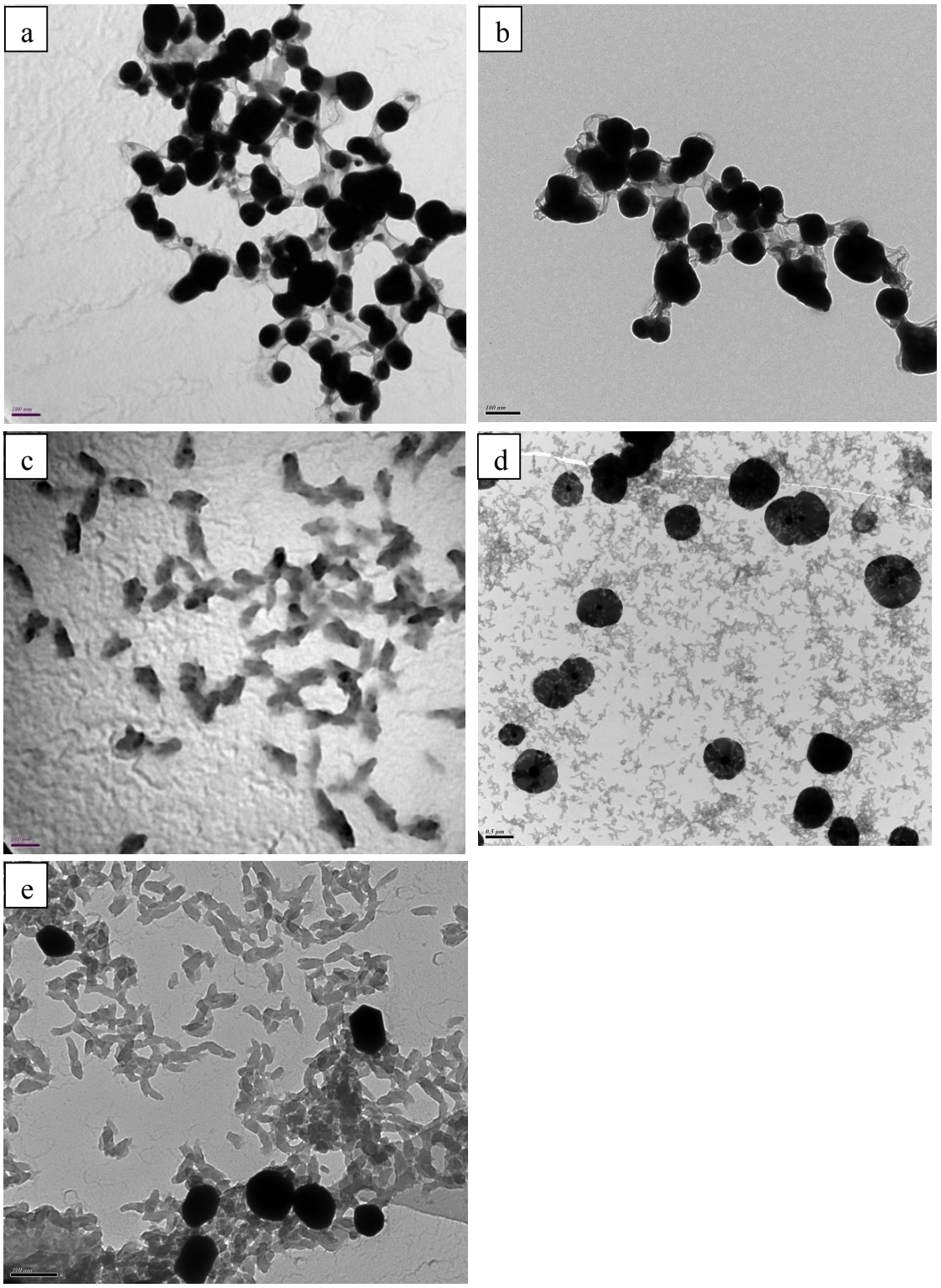

Figure V-10: TEM images of PANI-metals composites prepared using ammonium persulfate as oxidant and metal salts as co-oxidants in the presence of different stabilizers (a) PVA-*mod*-An, 50 wt.% +AgNO3 as a co-oxidant (run 1, Table V-4), (b) PNVP-*co*-PVA-*mod*-Py, 50 wt.% +$AgNO_3$ as a co-oxidant (run 2, Table V-4), (c) PVA-*mod*-An, 50 wt.% +$HAuCl_4$ as a co-oxidant (run 3, Table V-4) and (d) & (e) An-PEO-An, 50 wt.% +$HAuCl_4$ as a co-oxidant (run 4, Table V-4) { Scale for a, b & c is 100 nm and d & e are 500 and 200 nm respectively}

I.5.2. Synthesis of PANI-Au composites

As described above for the synthesis of PANI-Ag composites, PANI-Au composites were also prepared using $HAuCl_4$ as an oxidant. $HAuCl_4$ was added as a co-oxidant during dispersion polymerization of aniline hydrochloride or it was added in cleaned PANI dispersion, the latter acting as a reducing agent and converting Au^{+3} to Au^0. There is considerable effect of the addition time on the final PANI-dispersion. Rice grain morphology of gold coated PANI particles was obtained when $HAuCl_4$ was added at the beginning of the reaction (see Figure V-10c). Self-assembled (spheres and cubes) sub-micrometer sized gold particles dispersed in PANI matrix were obtained when $HAuCl_4$ was added in already washed PANI dispersion (Figure V-10d-e). The formation of these assemblies probably results from the crystalline nature of the gold particles.

I.6. XPS characterization of PANI-metal composites

XPS survey spectra of PANI-*PVA*-Ag (run 1, Table V-2) and PANI-*PVA*-Au (run 3, Table V-4) composite samples contain peaks due to Ag 3d and Au 4f, in addition to four main peaks corresponding to O1s, N1s, C 1s, and Cl 2p components respectively, which indicate the presence of gold and silver metal in the composites (see Figure V-11).

The doublet in the high resolution core-line spectrum of Au 4f (Figure 11d) arises from Au $4f_{5/2}$ and $4f_{7/2}$ electrons, respectively. Each signal is adequately peak-fitted with only one component, clearly showing that only one gold species is present. The $4f_{7/2}$ peak is centered at 83.84 eV, and the accompanying $4f_{5/2}$ peak at 87.51 eV which are the characteristic of zero-valent gold. Similarly doublet appearing in high resolution spectrum of Ag 3d (Figure V-11c) at 367.2 eV and 373.5 eV arise due to Ag $3d_{5/2}$ and Ag $3d_{3/2}$ electrons and prove the presence of atomic Ag in the composite. From these results it is clear that Ag^+ and Au^{+3} ions are completely reduced to their zero-valent state during dispersion polymerization of aniline, the latter being of interest in term of conductivity.

The C1s core-line spectrum of PANI-*PVA*-Au composite (run 3, Table V-2) is shown in Figure V-12a). The peak position at 284 eV is attributed to =CH– of aromatic ring. The peak positions at 284.68 and 286.4 are due to $–CH_2–$ and C–O–H group respectively in PVA,

proving the presence of stabilizer on PANI surface.[13] The peak position at 285.61 eV is due to C–N bond and peaks attributed at 287.73 and 288.9 eV are due to polaron and bipolaron respectively which proves the synthesis of doped PANI during dispersion polymerization of aniline.

O1s core-line spectrum of PANI-*PVA*-Au composite sample is shown in Figure V-12b). A very intense peak at 532.2 eV due to C–O–H of PVA in the composite proves the presence of PVA.[11]

Three signals from N1s at 399.2, 400.4 and 401.7 eV in PANI-*PVA*-Au correspond to neutral imine (=N–), amine (–NH–) and protonated imine (=N^+–) respectively (Figure V-12 c). The peak at 398.1 due to quinonoid imine (–N=) is absent, which means that quinonoid group is completely converted into protonated imine (=NH^+–). The doping level calculated by the integration of these peaks is 35.48% which is lower than the PANI samples prepared without using $AgNO_3$ (see chapter IV) but the conductivity shown by PANI-Ag composites is higher than the latter probably due to contribution from Ag metal.

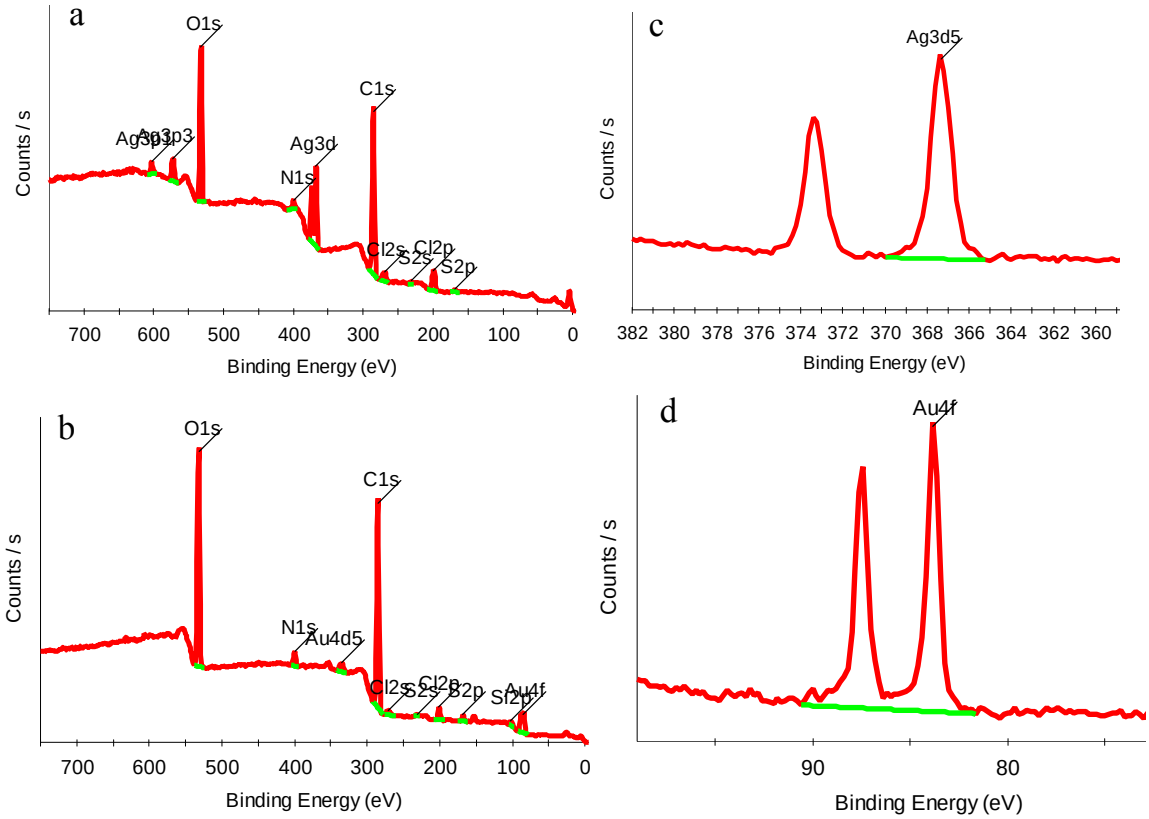

Figure V-11: XPS survey spectra of (a) PANI-*PVA*-Ag composite (run 1, Table V-4), (b) PANI-*PVA*-Au composite (run 3, Table V-4), (c) and (d) are their high resolution Ag3d and Au4f spectra respectively.

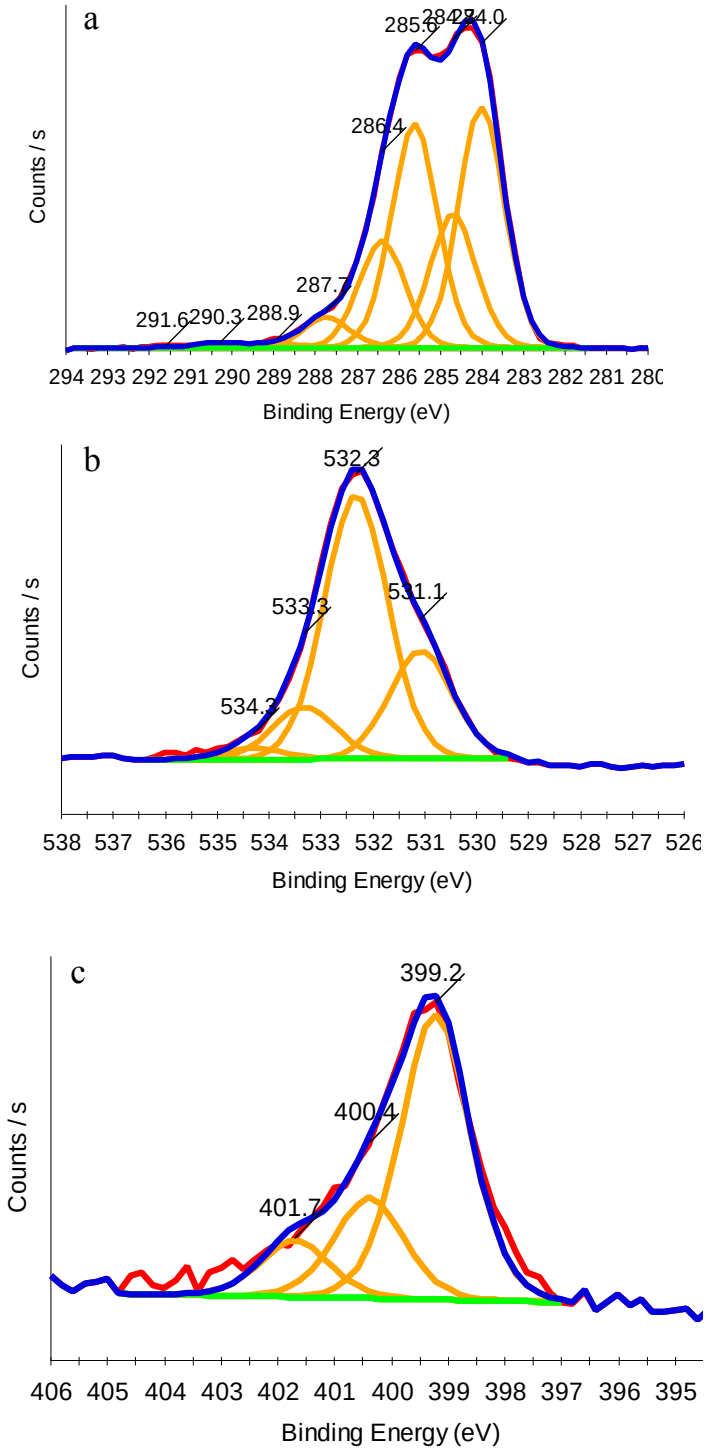

Figure V-12: (a) C1s core-line spectrum, (b) O1s core-line spectrum (c) N1s core-line spectrum of PANI-*PVA*-Ag composite (run 1, Table V-4)

I.7. Conductivity

The conductivities of the PANI and PEDOT-metals composites were measured by pressed pellet method using the four probe technique. As indicated in Table V-1, four to five fold increase in the conductivity of PEDOT-metals composite material are observed as compared to PEDOT samples without metals (see chapters 2 and 3). Conductivities values in the range 1.25 to 3.6×10^{-2} S/cm were obtained. The best conductivity value is obtained for the PEDOT-Au composite prepared using $HAuCl_4$ as an oxidant probably due to higher amount of gold inside (run 5, Table V-2) while insulator composite material was obtained when ammonium hydroxide was added in order to dissolve the copper sulfate and facilitate the reduction of copper ion to copper metal.

In the case of PANI-metals composites, upto two fold increase in conductivity was observed as compared to the PANI samples without metals (see chapter V-4). The best conductivity value (0.8 S/cm) was obtained for PANI-Au composite prepared using Flu-PEO-Flu as a reactive stabilizer probably due to the electrolyte nature of the latter.

These results show that the conductivity of both the PEDOT and PANI particles can be easily increased up to several orders of magnitude by incorporation of metal particles during dispersion polymerization which is high enough for several useful applications in the field of opto-electronics, main objective of this work.

II. Conclusion

In conclusion, PEDOT-metal and PANI-metal nanocomposites can be easily prepared by dispersion polymerization using EDOT, PEDOT, aniline and PANI as reducing agents. The addition time of the co-oxidant has considerable effect on the size and morphology of final composite particles. PEDOT-composites with reasonable high conductivity are obtained which make them good candidate typically as electrode material for use in organic light emitting devices. These composites can also be used to catalyze some reaction, for example the reduction of nitro group to amine.

References

(1) Li, X.; Li, Y.; Tan, Y.; Yang, C.; Li, Y. *J. Phys. Chem. B* **2004**, 108, 5192.

(2) Briggs, D.; Seah, M. P. *Practical Surface Analysis Vol. 1* (Second Edn), Wiley, Chichester **1990**.

(3) Ting, Y.P.; Neoh, K. G.; Kang, E. T.; Tan, K. L. *J. Chem. Tech. Biotechnol*. **1994**, *59*, 31.

(4) Neoh, K. G.; Tan, K. K.; Goh, P. L.; Huang, S. W.; Kang, E. T.; Tan, K. L. *Polymer* **1999**, *40*, 887.

(5) Lee, C. J.; Karim, M. R.; Lee, M. *Mater. Lett.* **2007**, 61, 2675.

(6) Li, Y.; Vamvounis, G.; Holdcroft, S. *Macromolecules* **2002**, 35, 6900.

(7) Laiho,T.; Leiro,J.A.; Heinonen, M.H.; Mattila, S.S.; Lukkari, J. *J. Electron Spectrosc. Relat. Phenom.* **2005**, 142, 105.

(8) Cho, M.S.; Kim, Nam, S.Y.; J.D.; Lee Y. *Synth. Met.* **2008**, 158, 865.

(9) Wu, S.-H.; Chen, D.-H. *J. Colloid Interface Sci.* **2004**, 273, 165.

(10) Toshima, N.; Wang, Y. *Langmuir* **1994**, 10, 4574.

(11) Benseddik, E.; Makhlouki, M.; Bernede, J. C.; Lerfrant, S.; Proń, A. *Synth. Met.* **1995**, 72, 237.

(12) Beamon, G. and Briggs, D. *High Resolution XPS of Organic Polymers*, Wiley, Newyork, **1992**.

(13) Shakesheff, K. M.; Evora, C.; Soriano, I.; Langer, R. *J. Coll. Inter. Sci*. **1997**, 185, 538.

Chapter VI

Experimental Section

Table of contents

I. Materials and synthesis

I.1. Materials

N-methyl-2-pyrrolecarboxylic acid, thiophene-2-carboxylic acid and fluorene-9-carboxylic acid, Aniline hydrochloride, and 4-aminobenzoic acid were purchased from Aldrich and used without further purification. Dimethylsulfoxide (DMSO) was distilled over CaH_2. 3,4-ethylenedioxythiophene (Aldrich) was first distilled over CaH_2 and then distilled over dibutyl magnesium. N,N-dimethylformamide (Aldrich, 98.8%) was distilled over dibutyl magnesium. Ethylene oxide (Fluka, 99.8 %) was first stirred over sodium at -30°C for 3h and then cryodistilled. Tetrahydrofuran (THF) (JT Baker) was first distilled over CaH_2 and then distilled over sodium benzophenone. Diethyl ether (JT Baker) was first distilled over CaH_2 and then cryodistilled over polystyryl lithium. Methanol was distilled over magnesium. Dichloromethane was distilled over CaH_2. *N*-vinylpyrrolidone (NVP) and vinylacetate were purchased from aldrich and distilled under reduced pressure prior to use. Hydrogen tetrachloroaurate ($HAuCl_4$), silver nitrate ($AgNO_3$) and Copper sulfate pentahydrate ($CuSO_4.5H_2O$), ammonium persulfate [$(NH_4)_2S_2O_8$], iron (III) p-toluenesulfonate hexahydrate [$Fe(OTs)_3$ $6(H_20)$] of technical grade, PVA { $\overline{M}_w$ = 13000-23000 g/mol, 98% hydrolyzed} and p-toluenesulfonic acid (98.5%) were purchased from Aldrich and used as received.

I.2. Synthesis

I.1.1. Synthesis of 2-methylol-3,4-ethylenedioxythiophene (EDOT-CH_2OH)

The synthesis of 2-methylol-3,4-ethylenedioxythiophene (EDOT-CH_2OH) was performed in two steps. In a first step, 2-formaldehyde-3,4-ethylenedioxythiophene (EDOT-CHO) was synthesized as follows: EDOT (1.3 mL, 12 mmol) was dissolved in ether (100 mL) in a three necked flask. n-BuLi (8.4 mL, 13.44 mmol) was added drop-wise at -40°C. The reaction mixture was stirred for 1h. This solution was then transferred in another flask containing DMF (1.21 mL, 15.6 mmol) mixed with diethyl ether (10 mL) at 0 C. The reaction mixture was stirred for 20h then transferred in cold water (200 mL) for hydrolysis. EDOT-

CHO was extracted from the reaction mixture with ether and then purified by passing through a silica gel column (eluent = dichloromethane/pentane 2/1) giving white crystals of EDOT-CHO in 70 % yield.

^{1}H NMR ($CDCl_3$): δ (ppm) = 9.90 (s, 1H, CHO), 6.79 (s, 1H, CH) 4.36, 4.27 (m, 4H, OCH_2CH_2O).

In a second step, the reduction of EDOT-CHO produced EDOT-CH_2OH. $NaBH_4$ (0.322 g, 8.46 mmol), used as the reducing agent, was dissolved in methanol (36 mL). This solution was transferred in another three necked flask containing EDOT-CHO (0.48 g, 2.82 mmol) dissolved in dichloromethane (36 mL). The reaction mixture was stirred for 20h then hydrolyzed by aqueous solution of NaOH (90 mL, 1M). The reaction product was extracted with dichloromethane to give white crystals of EDOT-CH_2OH in 80% yield.

^{1}H NMR ($CDCl_3$): δ (ppm) = 6.28 (s, 1H, CH), 4.66 (d, 2H, CH_2O) 4.20 (m, 4H, OCH_2CH_2O), 1.06 (t, 1H, OH)

I.1.2. Synthesis of α-EDOT-PEO

The following anionic polymerization procedure was adopted to synthesize α-EDOT-PEO. EDOT-CH_2OH (320 mg, 1.86 mmol) was introduced in a flame dried three necked round bottom flask (500 mL) under nitrogen. After lyophilization, THF (230 mL) was added over EDOT-CH_2OH. Diphenyl methyl potassium (DPMK) (1.60 mmol, 86 mol% *vs* initiator) was then added drop-wise; the color of the solution turned orange-yellow. Ethylene oxide (3.72 g, 4.22 mL) was then introduced slowly by keeping the temperature of the flask at -15 °C. Polymerization was allowed to proceed for 72h at 45°C. The reaction mixture was then deactivated using a 10% solution of HCl in methanol. Solvent was evaporated and the polymer was precipitated in cold ether.

^{1}H NMR (DMSO d_6): δ (ppm) = 4.53 (s, 2H, CH_2O), 4.33 (s, 4H, OCH_2CH_2O), 3.55 (m, 4H, CH_2CH_2O)

I.1.3. Synthesis of PEDOT particles

In a typical procedure, PEDOT particles were prepared by dispersion polymerization as the following: EDOT (1 g, 7 mmol) was charged in the flask equipped with a mechanical stirrer and containing a solution of reactive stabilizer (*e.g.* α-EDOT-PEO; 1g; $\overline{M}_n$ = 5200g/mol) in 80 mL of a mixture of methanol and water (3/2, v/v). A solution of ammonium persulfate (4.36 g dissolved in 20 mL of the methanol-water mixture) was then introduced at once. The reaction mixture was stirred for 72h at room temperature. The resulting blue dispersion was centrifuged at 10000 rpm at 5°C for 30 minutes. The supernatant was carefully decanted and the dark blue sediment was re-dispersed in methanol+water. This re-dispersion-centrifugation cycle was repeated three times in order to ensure the complete removal of inorganic material such as ammonium sulfate and eventual unattached reactive stabilizer.

Similarly, PEDOT samples were prepared in high yield using $Fe(OTs)_3$ as an oxidant and heating the reaction mixture at 85 C for 48h. These samples were then washed as described above.

I.1.4. Synthesis of α,ω-*N*-methyl-2-pyrrole poly(ethylene oxide) (α,ω-Py-PEO) and α-*N*-methyl-2-pyrrole poly(ethylene oxide) (α-Py-PEO)

α,ω-OH poly(ethylene oxide) (5 g, 0.5 mmol, $\overline{M}_n$=10000 g.mol^{-1}), *N*-methyl-2-pyrrole carboxylic acid (0.313g, 2.5 mmol) and 4-(dimethylamino)pyridinium 4-toluene sulfonate (DPTS) (0.148 g, 0.50 mmol) were introduced in a 250 mL flame dried three necked round bottom flask under nitrogen. CH_2Cl_2 (60 mL) was then added and finally, diisopropylcarbodiimide (DIPC) (0.50 mL, 3.25 mmol) was introduced by syringe. Stirring under nitrogen at room temperature was continued for 60h. The solution was filtered to remove diisopropylurea. The solvent was evaporated and the α,ω-Py-PEO was precipitated in cold ethyl ether (yield = 98%).

^{1}H NMR (DMSO-*d6*): δ (ppm) = 7.09 (s, 2H, CH), 6.83 (s, 2H, CHN), 6.08 (s, 2H, CH), 4.27 (s, 4H, CH_2O), 3.84 (s, 6H, NCH_3), 3.50 (m, 4H, CH_2CH_2O)

Similarly, α-N-methyl-2-pyrrole poly(ethylene oxide) (α-Py-PEO) was prepared using 2.3 equivalents of *N*-methyl-2-pyrrolecarboxylic acid with respect to PEO ; (the addition of

only 1 equivalent of *N*-methyl-2-pyrrole carboxylic acid versus PEO was not sufficient to obtain the complete monofunctionalization) (yield = 97 %).

^{1}H NMR (DMSO-*d*6): δ (ppm) = 7.09 (s, 1H, CH), 6.83 (s, 1H, CHN), 6.08 (s, 1H, CH), 4.54 (s, 1H, OH), 4.27 (s, 2H, CH_2O), 3.84 (s, 3H, NCH_3), 3.50 (m, 4H, CH_2CH_2O)

I.1.5. Synthesis of α, ω-thiophene poly(ethylene oxide) (α, ω-Th-PEO)

The procedure described for the above experiment was repeated using 5 equivalents of thiophene-2-carboxylic acid (yield = 97 %).

^{1}H NMR (DMSO-*d*6): δ ppm = 7.96 (d, 2H, CH), 7.81 (d, 2H, CHS), 7.22 (t, 2H, CH), 4.36 (t, 4H, CH_2O), 3.50 (m, CH_2CH_2O)

I.1.6. Synthesis of α, ω-fluorene poly(ethylene oxide) (α, ω-Flu-PEO)

The method of preparation was the same as described above for the synthesis of α,ω-Py- PEO with the addition of 5 equivalents of fluorene-9-carboxylic acid (yield = 96 %).

^{1}H NMR ($CHCl_3$): δ ppm = 7.73 (d, 4H, CH), 7.66 (d, 4H, CH), 7.39 (t, 4H, CH), 7.32 (t, 4H, CH), 4.31 (t, 4H, CH_2O), 3.62 (m, CH_2CH_2O)

I.1.7. Synthesis of poly (vinyl alcohol) based reactive stabilizers

I.1.7.1 Synthesis of PVA-*mod*-Py

In a particular case, poly(vinyl alcohol) (PVA) based reactive stabilizer was prepared by the partial esterification of PVA with *N*-methyl-2-pyrrolecarboxylic acid as follows: PVA (3 g, $\overline{M}_w$ =18000g/mol) was introduced in a flame dried 250 mL three necked flask under nitrogen. The DMSO (30 mL) was added in the flask and the temperature was raised to 70 °C in order to dissolve the PVA. After complete dissolution of the PVA, the temperature of the system was lowered to 40 °C and then *N*-methyl-2-carboxylic acid (0.627 g), diisopropyl carbodiimide (1.02 mL) and 4-(dimethylamino)pyridinium 4-toluenesulfonate (0.294 g) were

added under the current of nitrogen. The reaction mixture was stirred for 72 h and then cooled to room temperature. The reaction mixture was concentrated by distillation of the excess solvent and precipitated in CH_2Cl_2 in order to get pure PVA-*mod*-Py as a final product.

^{1}H NMR (DMSO-d_6): δ (ppm) = 7.05 (s, 1H, CH), 6.80 (s, 1H, CHN), 6.07 (s, 1H, CH), 4.66, 4.46, 4.21 (s, 1H, OH), 3.84 (s, 1H, CH) and 1.40 (m, 2H, CH_2)

I.1.7.2. Synthesis of PVA-*mod*-An

In a particular case, poly(vinyl alcohol) (PVA) based reactive stabilizer was prepared by the partial esterification of PVA with 4-amino benzoic acid as follows: PVA (3 g, $\overline{M}_w$ =18000g/mol) was introduced in a flame dried 250 mL three-necked flask under nitrogen. The DMSO (30 mL) was added in the flask and the temperature was raised to 70 °C in order to dissolve the PVA. After complete dissolution of the PVA, the temperature of the system was lowered to 40 °C and then 4-amino benzoic acid (0.914 g), diisopropyl carbodiimide (1.34 mL) and 4-(dimethylamino)pyridinium 4-toluenesulfonate (0.392 g) were added under the current of nitrogen. The reaction mixture was stirred for 72 h and then cooled to room temperature. The reaction mixture was concentrated by distillation of the excess of solvent and precipitated in CH_2Cl_2 in order to get pure PVA-*mod*-An as a final product. (Yield = 95 %)

^{1}H NMR (DMSO-d_6): δ (ppm) = 7.60 (d, 2H, CH), 6.52 (d, 2H, CH), 4.66, 4.46, 4.21 (s, 1H, OH), 3.84 (s, 1H, CH) and 1.40 (m, 2H, CH_2)

I.1.8. Synthesis of α,ω-aniline poly(ethylene oxide) (α,ω-An-PEO)

α,ω-OH poly(ethylene oxide) (5 g, 0.5 mmol, $\overline{M}_n$ =10000 g.mol^{-1}), 4-amino benzoic acid (0.343 g, 2.5 mmol) and 4-(dimethylamino)pyridinium 4-toluenesulfonate (DPTS) (0.148 g, 0.50 mmol) were introduced in a 250 mL flame dried three-necked round bottom flask under nitrogen. CH_2Cl_2 (60 mL) was then added and finally, diisopropylcarbodiimide (DIPC) (0.50 mL, 3.25 mmol) was introduced by syringe. Stirring under nitrogen at room temperature was continued for 60 h. The solution was filtered to remove diisopropylurea. The solvent was evaporated and the α,ω-Py-PEO was precipitated in cold ethyl ether (yield = 98 %).

^{1}H NMR ($CDCl_3$): δ (ppm) = 7.87 (d, 2H, CH), 6.64 (d, 2H, CH), 3.60 (m, 4H, CH_2CH_2O)

I.1.9. Synthesis of Polyaniline dispersions

In a typical procedure, PANI dispersion was prepared as following: poly(vinyl alcohol) grafted pyrrole units [(PVA-*mod*-Py) (270 mg, $\overline{M}_w$ = 88000g/mol)] was introduced in 250 mL flask equipped with a mechanical stirrer. HCl solution (1 M, 40mL) was then added and the temperature of the system was raised up to 60°C in order to dissolve the stabilizer. The temperature was then lowered to 0°C by putting the flask in an ice bath and Aniline.HCl (0.5 g,) was charged in the flask in one shot. A solution of ammonium persulfate (1.30 g dissolved in 10 mL of water) was then introduced in a single dose. The reaction mixture was stirred for 8 h at same temperature. The colour of the solution turns dark blue at the beginning of the reaction, proof of the formation of PANI- base and finally changes to dark green, a sign of PANI salt formation. The resulting dark green dispersion was centrifuged at 10000 rpm at 5°C for 30 minutes. The supernatant was carefully decanted and the dark blue sediment was re-dispersed in de-ionized water. This re-dispersion-centrifugation cycle was repeated three times in order to ensure the complete removal of inorganic material such as ammonium sulfate and eventual unattached reactive stabilizer.

I.1.10. Synthesis of PEDOT- and PANI metal composite particles

In a typical procedure, PEDOT-metal nanocomposites particles were prepared by dispersion polymerization as follows: EDOT (500 mg, 3.5 mmol) was charged in the flask equipped with a mechanical stirrer and containing a solution of reactive stabilizer (PVA-*mod*-Py, M_w= 88000 g.mol^{-1}, 500 mg) in 40mL of a mixture of methanol and water (1/4, v/v). A solution of ammonium persulfate (4.36g dissolved in 10 mL of the methanol-water mixture) was then introduced in on shot. Finally, the solution of metal salt ($AgNO_3$, $HAuCl_4$ or $CuSO_4.5H_2O$) was introduced after 30 minutes or 24h. The reaction mixture was stirred for 26h at room temperature. The resulting blue dispersion was centrifuged at 10000 rpm at 5 C for 30 min. The supernatant was carefully decanted and the dark blue sediment was re-dispersed in the mixture of methanol and water (1/4, v/v). This re-dispersion-centrifugation

cycle was repeated three times in order to ensure the complete removal of inorganic material such as ammonium sulfate and eventual unattached reactive stabilizer.

Similarly, PANI-Au and PANI-Ag were prepared in IM aqueous HCl by addition of $HAuCl_4$ and $AgNO_3$ after 30 minutes of the reaction.

II. Characterization

- ^1H NMR spectra were recorded using a Bruker AC-400 NMR spectrometer.
- Size Exclusion Chromatography (SEC) of the stabilizer was performed using a JASCO HPLC pump type 9012, PL aquagel-OH MIXED 8 μm columns and a Varian (series RI-4) refractive index detector with water as mobile phase. SEC for soluble PEDOT samples was performed using two PLgel 5 μm MIXED-C (300x7.5 mm) columns, one PLgel 5 μm (50x7.5 mm) guard column and a JASCO 875-UV detector with DMF as mobile phase, at 60°C in the presence of LiBr salt.
- SEM images of the PEDOT samples were taken using JEOL JSM-5200 and JEOL 6700F scanning microscopes.
- TEM images of the PEDOT samples were taken using a JEOL 2000FX transmission electron microscope. Atomic force microscopy (AFM) images were recorded in air with a Nanoscope IIIa microscope operating in tapping mode (TM). The probes were commercially available as silicon tips with a spring constant of 42 N m^{-1}, resonance frequency of 285 kHz, and a typical radius of curvature in the 10-12 nm range. Both the topography and the phase signal images were recorded with a resolution of 512 * 512 data points. Samples for AFM were prepared by solvent casting at room temperature from water/methanol solutions. Typically, 100 μl of a dilute solution (0.1wt.%) was cast on a 1×1 cm^2 freshly cleaved mica.
- Dynamic Light Scattering (DLS) measurements were performed using ALV Laser goniometer, which consists of a 22 mW HeNe linear polarized laser with a 632.8 nm wavelength, and an ALV-5000/EPP Multiple tau digital correlator with 250 ns initial sample time. The samples were kept at a temperature of 25°C. The accessible scattering angle range is from 40° up to 150°. However, most of the dynamic measurements were performed at 90°. The solutions were introduced into 10 mm diameter glass cells. The data acquisition was obtained with the ALV-Correlator

Control Software. Solutions used for DLS were prepared using the following method: water/methanol mixture used as a solvent was preliminary filtered through a 0.22 μm PTFE membrane and added to end-capped PEO. The solutions were then left under stirring for several days at 25±1 °C.

- Conductivity measurements of the PEDOT and PANI samples (pressed pellets) were performed using a Keithley 2400 Source Meter four probe instrument.
- TGA measurements were taken using PERKIN ELMER Thermogravimetric Analyzer (TGA 7).
- XPS measurements were made using an ESCALAB 220-iXL spectrometer (Thermo-Electron, VG Company). Photoemission was stimulated by a monochromatized Al Kα radiation (1486.6 eV). An area of about 250 μm diameter was analyzed for each sample. Surveys and high resolution spectra were recorded, and then fitted with an Avantage processing program provided by ThermoFisher Scientific.
- UV-visible spectra were recorded with a Spectramax-M2 spectrometer.
- Fourier Transformer Infrared measurements (FTIR) spectra were performed on a Bruker Tensor 27 spectrometer.

III. ^{1}H NMR, FTIR and UV-visible spectra

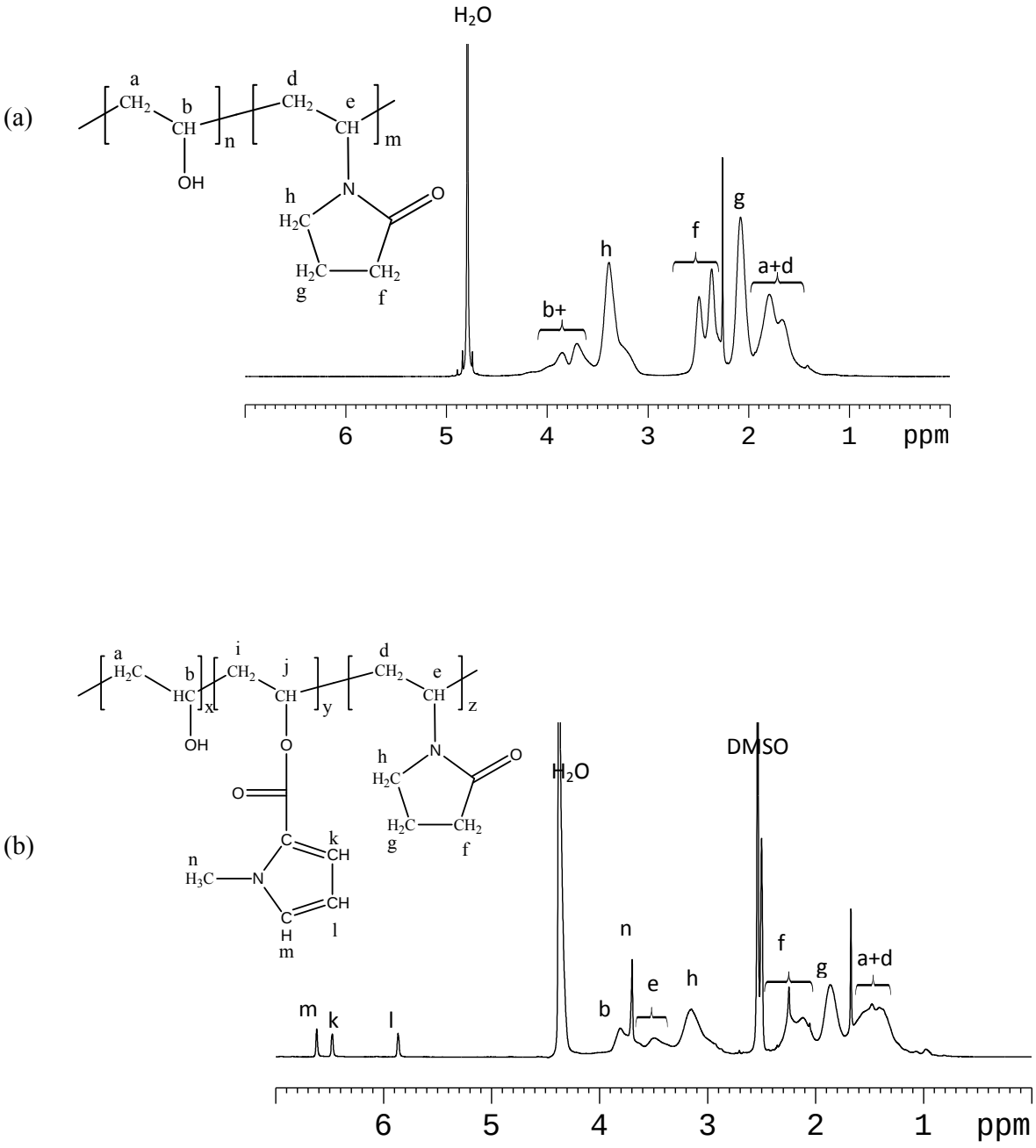

III.1. ^{1}H NMR spectra of (a) PNVP-*co*-PVA and (c) PNVP-*co*-PVA-*mod*-Py in d_6-DMSO + few drops of D_2O at room temperature

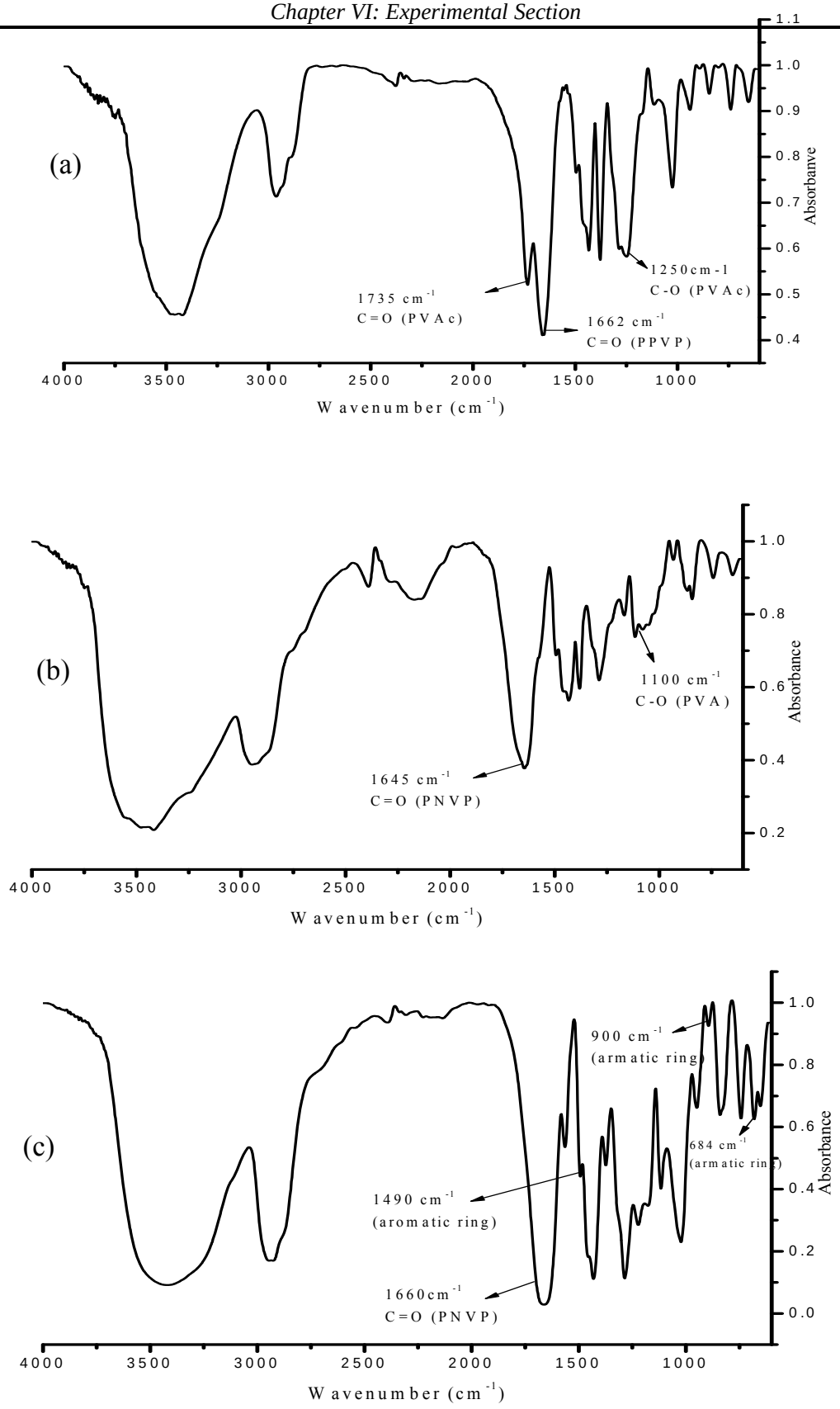

III.2. FT-IR spectra of (a) PNVP-co-PVOAc, (b) PNVP-co-PVA and (c) PNVP-*co*-PVA-*mod*-Py

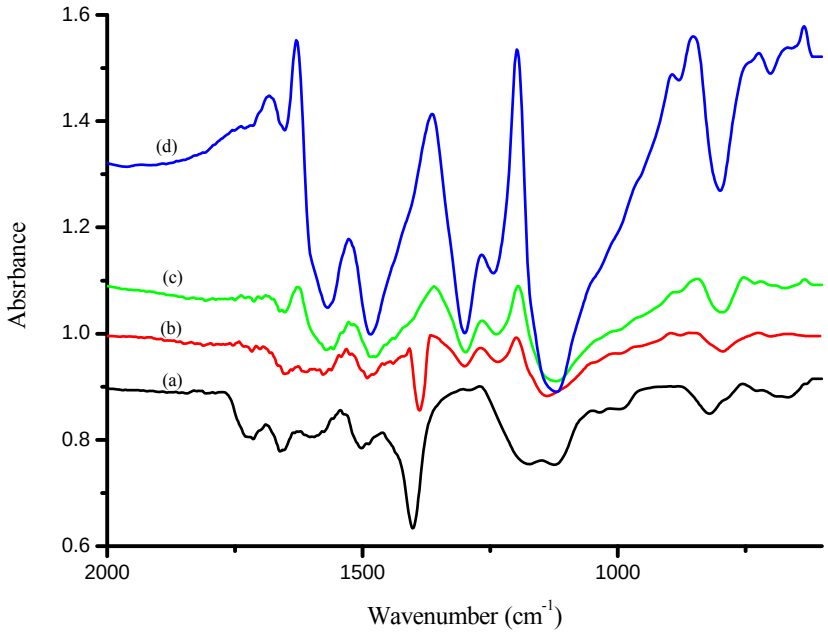

III.2. FT-IR spectra of (a) PVA, (b) PANI prepared using PVA-*mod*-Py (run 2, table IV-1) and PANI prepared using PVA-*mod*-An in the presence of different dopants (c) HCl (d) HCl-PTSA,

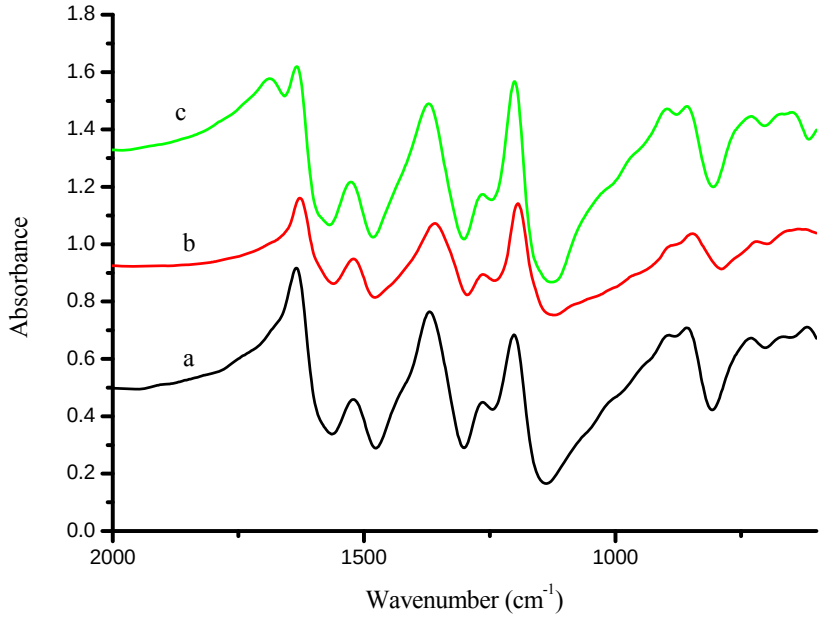

III.3. FT-IR spectra of (a) PANI bulk powder, (b) PANI prepared using An-PEO-An (run 1, table 2) and (c) PANI using PNVP-*co*-PVA-*mod*-Py (run 6, Table IV-2,) as reactive stabilizers

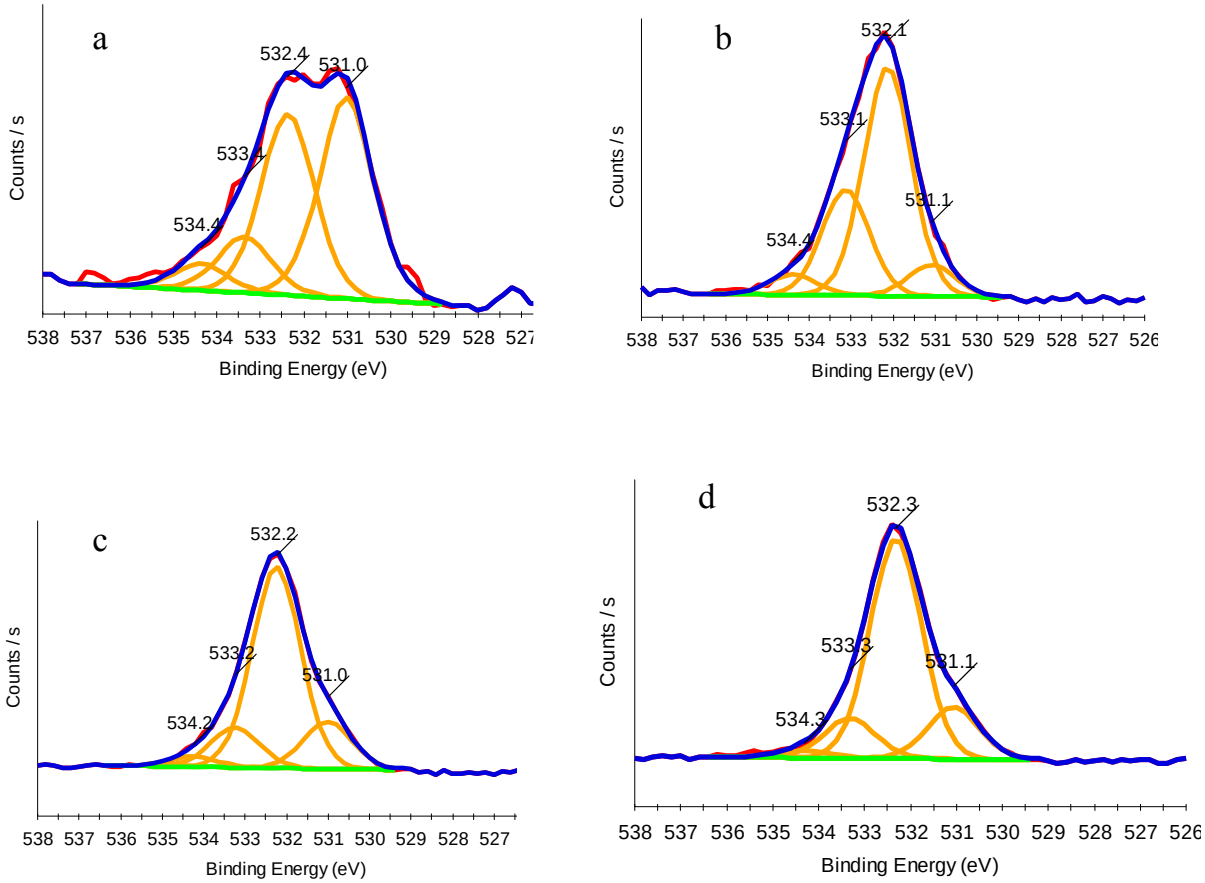

III.4. XPS O1s core line spectra of (a) PANI bulk powder, (b) PANI-PVA-HCl (Run 3, Table IV-1,), (c) PANI-PVA-CSA-HCl (Run 5, Table IV-1,) and (d) PANI-PVA-PTSA-HCl (Run 4, Table IV-1)

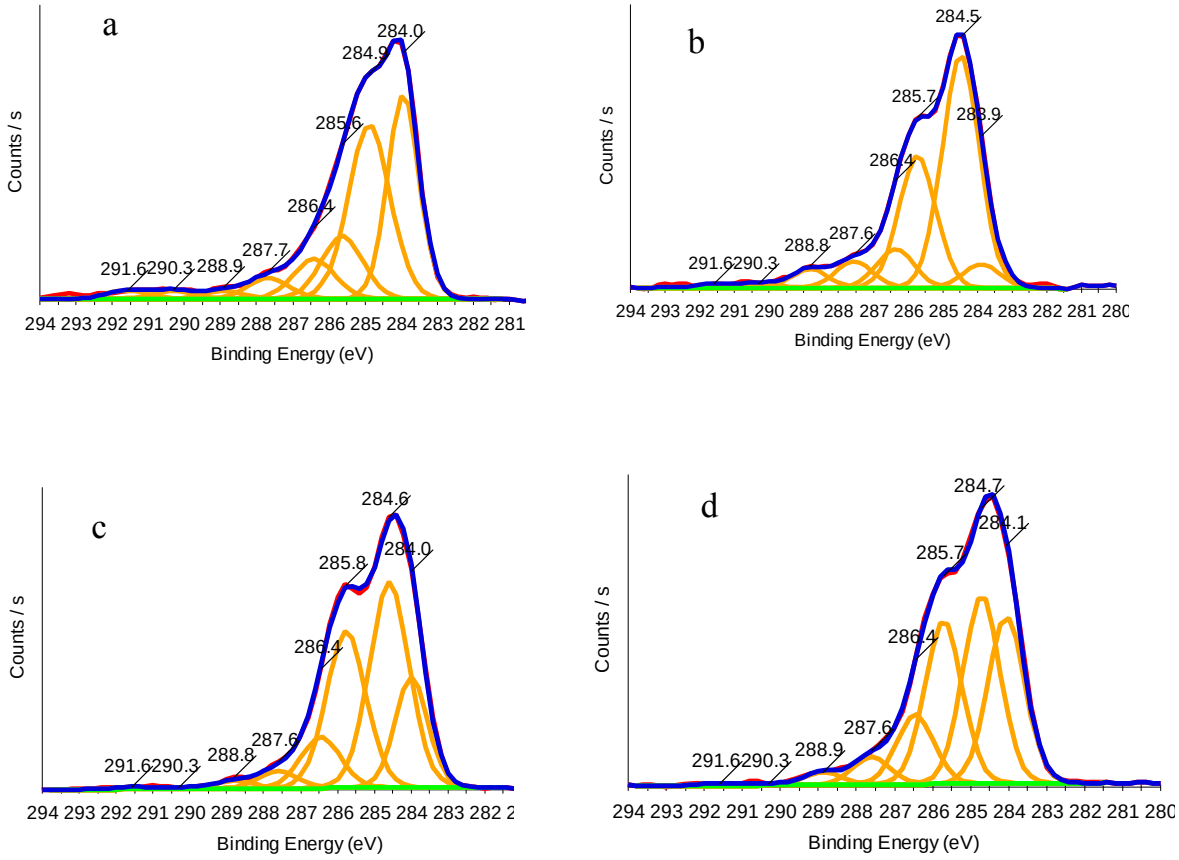

II.5. XPS C1s core line spectra of (a) PANI bulk powder, (b) PANI-PVA-HCl (Run 3, Table IV-1), (c) PANI-PVA-CSA-HCl (Run 5, Table IV-1) and (d) PANI-PVA-PTSA-HCl (Run 4, Table IV-1)

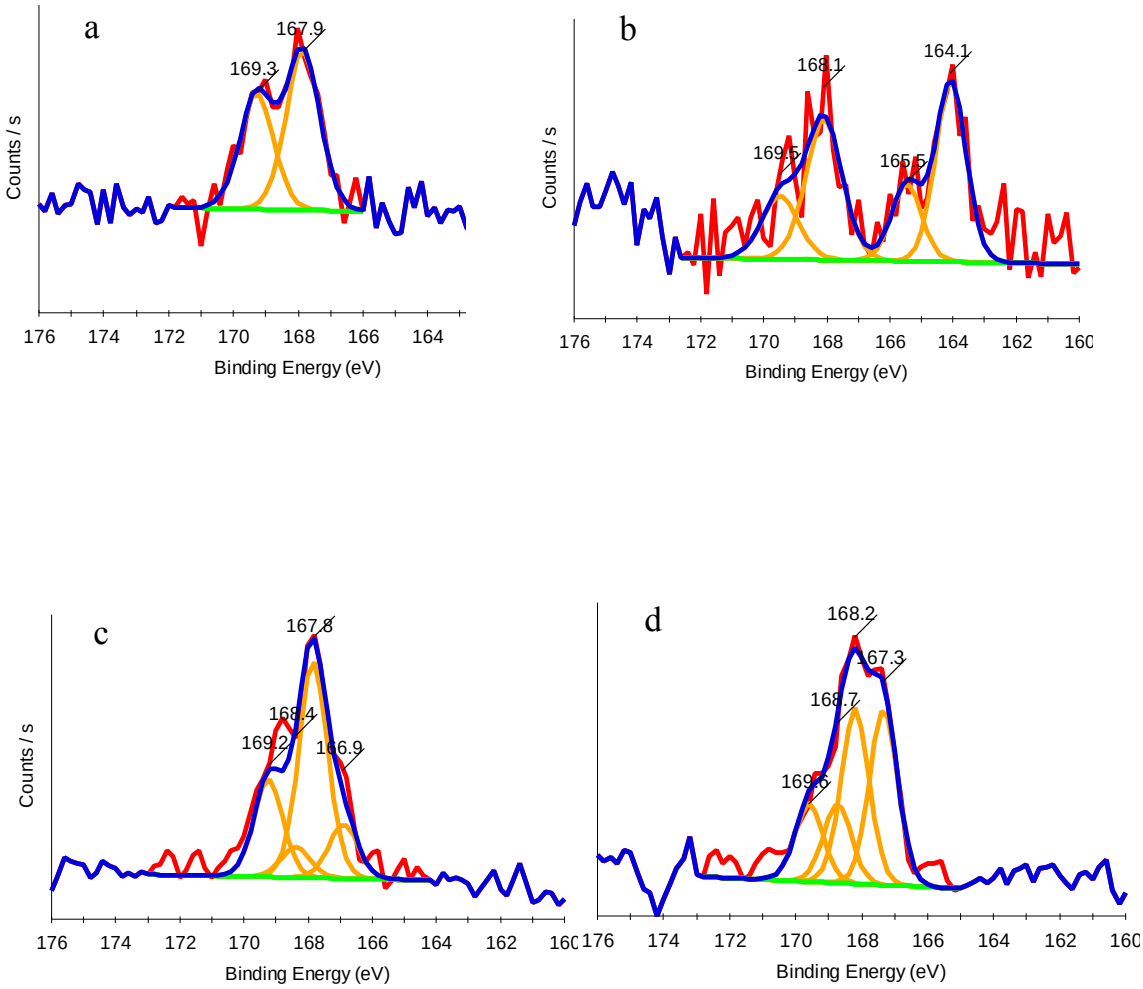

III.6 : XPS S 2p core line spectra of (a) PANI bulk powder, (b) PANI-PVA-HCl (Run 3, Table IV-1), (c) PANI-PVA-CSA-HCl (Run 5, Table IV-1) and (d) PANI-PVA-PTSA-HCl (Run 4, Table IV-1)

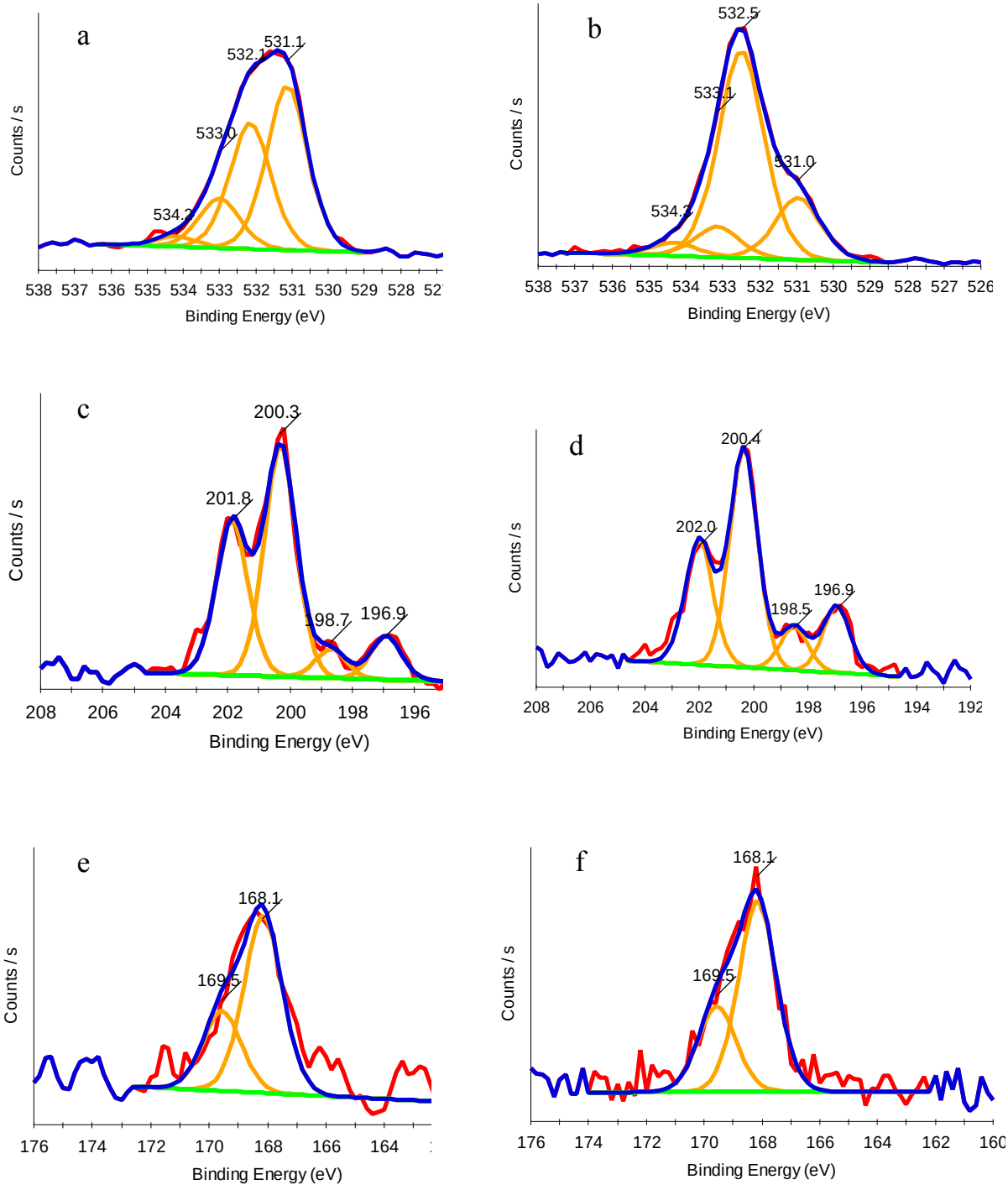

III.7. (a) & (b) XPS O 1s core line spectra of PANI-PNVP-co-PVA-*mod*-Py (Run 1, Table IV-2) and PANI-PEO (Run 4, Table IV-2 and (c) & (d) XPS Cl 2p core line spectra of PANI-PNVP-co-PVA-*mod*-Py (Run 1, Table IV-2) and PANI-PEO (Run 4, Table IV-2) and XPS S 2p core line spectra of PANI-PNVP-co-PVA-*mod*-Py (Run 1, Table IV-2) and PANI-PEO (Run 4, Table IV-2) respectively.

General Conclusions

Easily processable semi-conducting polymers under the form of inks are desired in the view of large scale development of organic electronics and photovoltaics. The main objective of this study was thus to synthesize PEDOT and PANI latexes constituted of nano-objects of well-defined and tuneable morphologies. Indeed, PEDOT and PANI nano-objects were prepared by alcohol-aqueous dispersion polymerization of the respective monomers in the presence of specifically designed reactive stabilizers based on PEO and PVA.

First, spherical PEDOT particles with controlled sizes and narrow size distribution were prepared in the presence of PEO-based stabilizers end-capped in α (or in α, ω) position by a reactive moiety such as EDOT, pyrrole, thiophene and fluorene. Two oxidants, respectively $(NH_4)_2S_2O_8$ and $Fe(III)(OTs)_3 \cdot 6(H_2O)$ were tested, the latter yielding the higher polymerization yields (85 % compared to 35% obtained by former). The size of the spherical PEDOT particles (ranging from 35 nm to 600 nm) could be tuned by changing the molecular weight and concentration of the reactive PEO as well as the type of the oxidant used. As expected, the higher the concentration and molecular weight of the reactive stabilizer, the lower the size of the particles. Reversibly, the size and the morphology of the PEDOT particles were not really affected by the PEO end-group, except in case of α-EDOT-PEO (50wt.%, M_n = 25000 g/mol) for which a vesicle-like morphology was obtained. The morphology (particles or vesicles) of PEDOT could be attributed to the behaviour of the reactive stabilizer as shown by DLS analysis of the different end-functionalized PEO in the polymerization solvent. In most cases, the α- or α, ω end-capped PEO stabilizers were found soluble in the solvent mixture and did not exhibit any specific self-assembly, conditions

required for a true dispersion polymerization. In these experimental conditions, spherical PEDOT particles were readily formed. However, a self-assembly of α-EDOT-PEO (M_n = 25000 g/mol) under a vesicle morphology was observed at the concentration of 50 wt.% which gave rise to the formation of PEDOT vesicles. It is worth noting that no stable PEDOT dispersion could be obtained using non-functionalized PEO as stabilizer, highlighting the crucial role played by the reactive termini. All the PEDOT particles exhibited conductivity values ranging from 1.3×10^{-6} to 1.9×10^{-2} S/cm, the higher values being obtained with $Fe(III)(OTs)_3\cdot6(H_2O)$ as the oxidant.

Second, the former study opened the route to considering the use of multifunctional reactive stabilizers and to analyze the effect on the size, the morphology and the stability with time of the PEDOT nano-objects. For this purpose, poly(vinyl alcohol)-based reactive stabilizers were chosen as they can be easily functionalized on pendant OH groups. PVA-*mod*-Py, PNVP-*co*-PVA-*mod*-Py and PNVP-*b*-PVA-*mod*-Py having multiple reactive moieties along the polymer backbone were synthesized and used for EDOT dispersion polymerization. In comparison to dispersions performed in the presence of α-ended PEO, smaller (ranging from 40 nm to 200 nm) and better defined PEDOT nano-objects were obtained in the presence of PVA-based reactive stabilizers. The high effectiveness of this stabilizer, explained by the large number of reactive end-groups functionalized on its backbone, was also proved by its low concentration (10 wt %) required to get stable PEDOT dispersion. Interestingly, the morphology of PEDOT nano-objects (spherical particles, donuts, etc.) could be controlled by the degree of pyrrole moities functionalized on the PVA backbone. Best results in terms of morphology and size distribution were obtained in the presence of PNVP-*co*-PVA and PNVP-b-PVA-based stabilizers. Even better results were obtained using PNVP-*co*-PVA-*mod*-Py as reactive stabilizers probably due to well distributed reactive moieties along the stabilizer chain. It is noteworthy that PEDOT vesicles were obtained when EDOT polymerization was performed in the presence of unreactive PNVP-*co*-PVA and PNVP-*b*-PVA stabilizers thanks to the self-assemblies of these stabilizers in the reaction medium as indicated by DLS analysis. Interestingly, PEDOT particles prepared in the presence of PNVP-*b*-PVA and PNVP-*co*-PVA based reactive stabilizers revealed higher conductivities (x 10) in comparison to the ones prepared using PVA-based reactive stabilizers. Similarly, the use of oxidant mixtures $(NH_4)_2S_2O_8$+$CuBr_2$ or $(NH_4)_2S_2O_8$+$CuCl_2$ enabled to increase the PEDOT conductivity (3.0×10^{-4} S/cm) compared to $(NH_4)_2S_2O_8$ used as the only oxidant (8.0×10^{-5} S/cm).

In a third approach, the different reactive stabilizers discussed above, were tested for the synthesis of PANI dispersions. PANI nano-objects with various morphologies like peanuts, rice grain, corals, spheres and fibers could be successfully prepared by tuning the reaction conditions as well as the characteristics of the PVA-, PEO- and PNVP-*co*-PVA-based reactive stabilizers**.** In spite of the stabilizer insulator content within the materials, the nano-objects thus-formed showed conductivities as high as 0.5 S/cm. PANI samples were investigated by XPS which confirmed the core-shell nature of the PANI particles. The XPS technique was also found to be an important tool for evaluating the doping level either by comparing the peak areas ratio of protonated imine and amine nitrogen to the neutral imine and amine in the sample or by the amount of the dopant in the sample. These values thus obtained by XPS were found in good agreement with the conductivities measured on PANI samples. Finally, DSC and TGA analyses revealed that PANI composites show better thermal stability than their pure PANI counterparts.

In the last part of the work, PEDOT-metal and PANI-metal nanocomposites were prepared by dispersion polymerization using EDOT/PEDOT and aniline/PANI as reducing agents, respectively. We could demonstrate that the addition time of the co-oxidant had a considerable effect on the size and morphology of the final composite particles. When α,ω-Fluorene-PEO (α,ω-Flu-PEO) was used as a stabilizer in the presence of *p*-toluenesulfonic acid (PTSA), PEDOT–Au and PEDOT-Ag vesicles were obtained. Thanks to DLS and TEM analyses, we could demonstrate that α,ω-Flu-PEO (35 wt.%, M_n = 35000 g/mol) in the presence of PTSA self assembles as vesicles that serve as templates for the formation of vesicular PEDOT-Ag and PEDOT-Au nanocomposites. These PEDOT-composites with reasonable high conductivities (upto 1.25 S/cm) make them as good candidates as electrode materials for organic electronics and photovoltaics.

In terms of perspectives, we could think to an extension of this methodology to prepare even smaller semi-conducting nano-objects and their metal composites. With the objective to prepare large scale inks of semi-conducting polymers, tools of formulation can be used. A better understanding of the relationship between the process, the morphology and the final optoelectronic characteristics would therefore be a prerequisite. Finally, as most of the work was performed in aqueous media, for some applications it would be interesting to carry

out same approach in different dispersant phases such as in organic media or in supercritical carbon dioxide.

Appendix

I. X-ray Photoelectron Spectroscopy

I.1. Introduction

Electron spectroscopy is the study and analysis of emitted low energy electrons (*ca*. 20 – 2000 eV). X-ray photoelectron spectroscopy (XPS), in particular, is concerned with the analysis of electrons emitted from the core-levels of an atom due to incident x-rays of energy hν (see Figure IV.1).

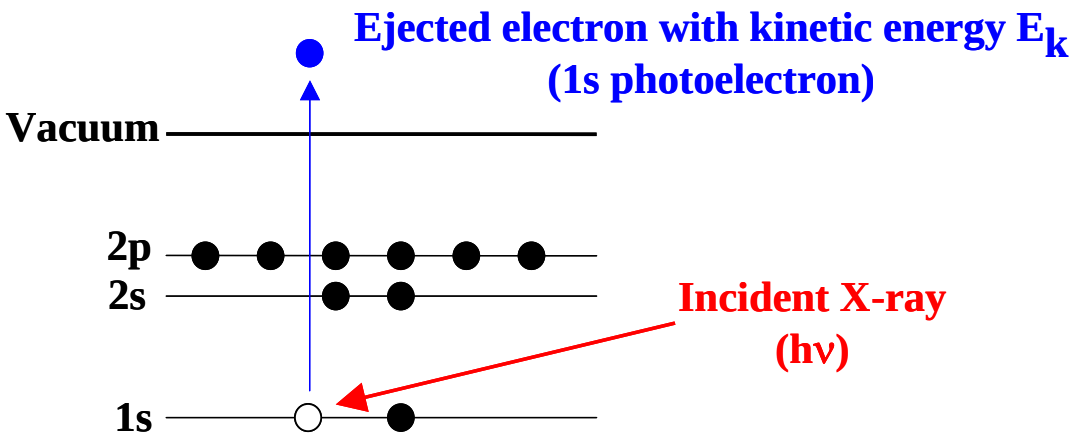

Figure IV.1: Schematic representation of core electron emission as a result of incident x-rays.

I.2.Theory[1]

The kinetic energy, E_k, of the ejected electron can be measured by the spectrometer, but depends on the nature of the x-ray source employed. Thus it is not an intrinsic material property. It is the binding energy, E_b, of the electron which can identify the electron, and the element, from which it is originated. E_b can be calculated using Equation 1:

$$E_b = h\nu - E_k - W \qquad (1)$$

Where W is the work function of the spectrometer, which is specific to each instrument. Since hν, E_k and W are all known or measurable, it is a simple matter to calculate E_b. Characterisation of samples usually begins with a survey spectrum being recorded over 0 –

1000 eV, providing strong peaks for all elements present (except hydrogen). Electrostatic charging of insulating or semi-conducting samples can result in a reduction of E_k, which corresponds to an apparent increase in E_b. Such discrepancies are best overcome by accurate referencing of the spectrum to a standard peak, such as 285.0 eV for the C 1s peak.

The binding energy of an electron is characteristic of the specific element and the particular atomic level from which it is originated. However, differences in the chemical environment or oxidation state of an atom, ion or molecule can result in slight differences in this binding energy. These changes are known as the XPS chemical shift. It is not possible for XPS spectrometers to resolve chemical shifts, but it is possible to deconvolute (or peak-fit) signals obtained from high-resolution XPS analysis to account for different environments and/or oxidation states of atoms. High resolution analysis consists of recording a spectrum over a specific region corresponding to the elemental peak observed in the survey spectrum. Databases are readily available for matching chemical shifts to different chemical states[2,3]

XPS is a surface-specific technique and, although the sampling depth of analysis varies with the kinetic energies of the electrons under consideration and the x-ray source, it is typically in the range 2 – 10 nm. Quantitative measurements of the surface composition can be made, in which the fractional concentration of a particular element A (%A) is calculated using Equation B.2:

$$\%A = [(I_A/s_A)/\sum_i(I_i/s_i)] \times 100 \qquad (2)$$

In which I and s are the integrated peak areas and sensitivity factors, respectively. Sensitivity factors are related to the probabilities of different elements emitting electrons when bombarded with x-rays. The sensitivity factors are published[2,3] or can be determined in-house by analysing compounds of accurately known elemental stoichiometries. The main assumption made when using Equation 2 is that the volume sampled by the spectrometer is homogeneous. Although this is rarely achieved in practice, good comparisons can nevertheless be made between samples which are similar in nature.

I.3. Instrumentation

In simple terms, the electron spectroscopy set-up consists of an x-ray source which irradiates the sample, and an electron analyser which detect emitted photoelectrons. These components are all contained within a chamber under ultrahigh vacuum (UHV), typically less than 10^{-9} mbar. XPS must be carried out under UHV for two reasons: firstly, low energy electrons are readily scattered by residual gas molecules and become lost in the increased noise level of the spectrum. Secondly, monolayers of adsorbed gas on the surface of the sample must be avoided. The origin of primary radiation for XPS is normally soft x-rays produced by either an AlKα ($h\nu$ = 1486.6 eV) or a MgKα ($h\nu$ = 1253.6 eV) source. Emitted photoelectrons are transported and focussed by an electrostatic lens at the entrance to the electron analyser. For solid state XPS the sample need satisfy only one condition; it must have a sufficiently low vapour pressure to be stable in the UHV regime. The XPS area of analysis is typically 10 mm^2.

I.4. Uses and Limitations[4,5]

XPS is one of the most widely used analytical techniques for studying polymer surfaces. Many organic polymers comprise a small number of elements and therefore often yield apparently simple spectra (generally C 1s plus one or more peaks from O 1s or N 1s, for example). Since many functional groups can give rise to similar 'shifts', obtaining useful information from the peak-fitted C 1s signals can sometimes be difficult. During the initial pioneering work carried out on XPS of polymers, several workers attempted to overcome these problems by using specific derivatising agents which react with a particular functional group, providing a distinctive elemental label. However, with the development of the ESCA300 spectrometer in the late 1980's, and subsequent improvements, sensitivity and spectral resolution were improved greatly and such derivatisation is no longer commonly employed.

For insulating materials such as the majority of organic polymers, sample-charging may cause line broadening and lead to shifts in the apparent binding energy. This can be overcome by accurate referencing of the spectrum as described in Section 2. In addition, techniques have been developed to minimise charging effects, such as spin-casting a thin film

of the polymer from solution onto a conducting substrate. Provided the film thickness is comparable to the XPS sampling depth, secondary electrons from the substrate can pass through the film and neutralise any positive charge developed by the x-ray beam. More commonly, an electron gun is focused over the sample during analysis. It thus follows that conducting polymers are ideally suited to analysis by XPS, as charging problems are largely absent, and much work has been carried out in this area[6-18] Moreover, conducting samples are far less prone to damage by the x-ray beam.

References

(1) Watts, J. F. *An Introduction to Surface Analysis by Electron Spectroscopy*, Oxford University Press, **1990**.

(2) See for example, Moulder, J. F., Stickle, W. F.; Sobol, P. E.; Bomben, K. D. *Handbook of X-ray Photoelectron Spectroscopy*, Chastain, J., Ed., Perkin-Elmer Corp., Minnesota, **1992**.

(3) NIST XPS Database, see internet address http://srdata.nist.gov/xps.

(4) Briggs, D.; Seah, M. P. *Practical Surface Analysis Vol. 1* (Second Edn), Wiley, Chichester **1990**.

(5) Beamson, G.; Briggs, D. *High Resolution XPS of Organic Polymers*, Wiley, Chichester **1992**.

(6) Neoh, K.G.; Kang, E. T.; Tan, K. L. *J. Polym. Sci. Part A : Polym. Chem.* **1991**, *29*, 759.

(7) Kang, E. T.; Neoh, K. G.; Ong, Y. K.; Tan, K. L.; Tan, B. T. G. *Macromolecules* **1991**, *24*, 2822.

(8) Kang, E. T.; Neoh, K. G.; Khor, S. H.; Tan, K. L.; Tan, B. T. G. *J. Chem. Soc., Chem. Commun*. **1989**, 695.

(9) Hagiwara, T.; Yamaura, M.; Iwata, K. *Synth. Met*. **1988**, *25*, 243.

(10) Kang, E. T.; Neoh, K. G.; Tan, K. L. *Polym. J.* **1989**, *21*, 873.

(11) Neoh, K. G.; Kang, E. T.; Tan, K. L. *J. Phys. Chem*. **1992**, *96*, 6777.

(12) Tan, K. L.; Tan, B. T. G.; Kang, E. T.; Neoh, K. G. *J. Mater. Sci.* **1992**, *27*, 4056.

(13) Kang, E. T.; Tan, K. L.; Neoh, K. G.; Chan, H. S. O.; Tan, B. T. G. *Polym. Bull.* **1989**, *21*, 53.

(14) Chan, H. S. O.; Ng, S. C.; Sim, W. S.; Tan, K. L.; Tan, B. T. G. *Macromolecules* **1992**, *25*, 6029.

(15) Toshima, N.; Tayanagi, J. *Chem. Lett*. **1990**, 1369.

(16) Abel, M.; Chehimi, M. M. *Synth. Met*. **1994**, *66*, 225.

(17) Nakajima, T.; Harada, M.; Osawa, R.; Kawagoe, T.; Furukawa, Y.; Harada, I. *Macromolecules* **1989**, *22*, 2644.

(18) Snauwaert, P. H.; Lazzaroni, R.; Riga, J.; Verbist, J. J. *Synth. Met*. **1986**, *16*, 245.